

AD A152 368

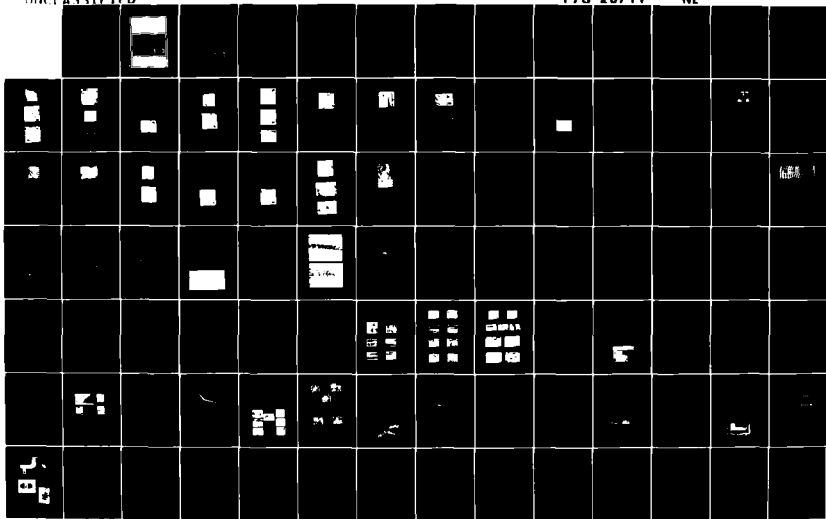
FATIGUE CRACK TOPOGRAPHY(U) ADVISORY GROUP FOR  
AEROSPACE RESEARCH AND DEVELOPMENT NEUILLY-SUR-SEINE  
(FRANCE) 1984 AGARD-CP-378

1/3

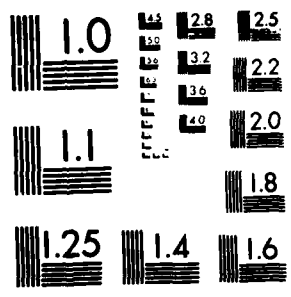
UNCLASSIFIED

F/G 20/11

NL



p



MICROCOPY RESOLUTION TEST CHART  
NATIONAL BUREAU OF STANDARDS-1963-A

2

14  
AGARD-CP-376

AD-A152 368

# AGARD

ADVISORY GROUP FOR AEROSPACE RESEARCH & DEVELOPMENT

7 RUE ANGELE 92200 NEUILLY SUR SEINE FRANCE

AGARD CONFERENCE PROCEEDINGS No.376

## Fatigue Crack Topography

**DISTRIBUTION STATEMENT A**  
Approved for public release  
Distribution Unlimited

DTIC  
ELECTE  
MAR 11 1985  
S B

DTIC FILE COPY

NORTH ATLANTIC TREATY ORGANIZATION



DISTRIBUTION AND AVAILABILITY  
ON BACK COVER

85 08 04 042

AGARD-CP-376

NORTH ATLANTIC TREATY ORGANIZATION  
ADVISORY GROUP FOR AEROSPACE RESEARCH AND DEVELOPMENT  
(ORGANISATION DU TRAITE DE L'ATLANTIQUE NORD)

AGARD Conference Proceedings No.376

FATIGUE CRACK TOPOGRAPHY

DTIC  
ELECTE  
MAR 11 1985  
S D  
B

**DISTRIBUTION STATEMENT A**  
Approved for public release  
Distribution Unlimited

Papers presented at the 58th Meeting of the Structures and Materials Panel  
in Sienna, Italy, on 1-6 April 1984.

## THE MISSION OF AGARD

The mission of AGARD is to bring together the leading personalities of the NATO nations in the fields of science and technology relating to aerospace for the following purposes:

- Exchanging of scientific and technical information;
- Continuously stimulating advances in the aerospace sciences relevant to strengthening the common defence posture;
- Improving the co-operation among member nations in aerospace research and development;
- Providing scientific and technical advice and assistance to the North Atlantic Military Committee in the field of aerospace research and development;
- Rendering scientific and technical assistance, as requested, to other NATO bodies and to member nations in connection with research and development problems in the aerospace field;
- Providing assistance to member nations for the purpose of increasing their scientific and technical potential;
- Recommending effective ways for the member nations to use their research and development capabilities for the common benefit of the NATO community.

The highest authority within AGARD is the National Delegates Board consisting of officially appointed senior representatives from each member nation. The mission of AGARD is carried out through the Panels which are composed of experts appointed by the National Delegates, the Consultant and Exchange Programme and the Aerospace Applications Studies Programme. The results of AGARD work are reported to the member nations and the NATO Authorities through the AGARD series of publications of which this is one.

Participation in AGARD activities is by invitation only and is normally limited to citizens of the NATO nations.

*The content of this publication has been reproduced directly from material supplied by AGARD or the authors.*

Published November 1984  
Copyright © AGARD 1984  
All Rights Reserved

ISBN 92-835-1480-7



*Printed by Specialised Printing Services Limited  
40 Chigwell Lane, Loughton, Essex IG10 3TZ*

## INTRODUCTION

During the last few years the concept of Damage Tolerance for Aircraft Structures has become widely accepted throughout the Aerospace community. For the application of this concept, knowledge of crack growth rates has become of primary importance. The crack growth that has occurred in tests can sometimes be determined from fractographic features of the crack surface, such as growth bands and striations.

Various means have been proposed to create recognizable markings on the fracture surface, including the introduction of so-called marker loads. However, these means are not always successful and moreover may themselves have an influence on the crack growth rates obtained.

The meeting brought together specialists in the field of Fracture Surface Analysis and Structural Test Engineering with the following objectives:

- To review available methods for determining the growth rate of cracks from their topography.
- To note any shortcomings in these methods and to recommend further research and development where necessary.

The Meeting consisted of four sessions. The first three were devoted to "Phenomenological Aspects of Fatigue Fractures", to "Methods and Means of Crack Front Marking" and to "Fracture Surface Analysis Techniques" respectively.

Each of these sessions started with an overview of approximately 40 minutes duration, followed by a number of short presentations of about 10 minutes each. This arrangement proved to be very satisfactory as it permitted the exchange of a large quantity of information in a very short time. These conference proceedings include the overview papers plus the complete texts of the briefly presented contributions. The fourth and final session included a "General Discussion" introduced and led by Prof. J.Schijve of Delft University of Technology. A review of this General Discussion has been included in the Proceedings.

The general opinion of all participants was that this Specialists Meeting has presented a valuable state-of-the-art review and that useful suggestions with regard to future research have come up during often quite lively discussions.

Ir. J.B. de JONGE  
(Meeting Chairman)  
National Aerospace Laboratory NLR  
P.O. Box 153  
8300 AD Emmeloord  
The Netherlands

Accession For	<input checked="" type="checkbox"/>
NTIS CRA&I	<input type="checkbox"/>
DTIC TAB	<input type="checkbox"/>
Unannounced	<input type="checkbox"/>
Justification	
By	
Distribution	
Availability Codes	
Dist	
A-1	



## CONTENTS

	Page
INTRODUCTION	iii
	Reference
<u>SESSION I – PHENOMENOLOGICAL ASPECTS OF FATIGUE FRACTURES</u>	
Overview paper ESSENTIAL FEATURES IN FATIGUE FRACTURES AND REMARKABLE PHENOMENA IN FATIGUE CRACK GROWTH by H.Klinge	1
Paper 2 not available at time of printing	
FATIGUE FRACTURE TOPOGRAPHY by P.J.E.Forsyth	3
Paper 4 not available at time of printing	
FATIGUE CRACK PROPAGATION AND FRACTURE IN 7050 AND 7091 ALUMINIUM ALLOY FORGINGS by R.J.H.Wanhill, H.J.Kolkman and L.Schra	5
<u>SESSION II – METHODS AND MEANS OF CRACK FRONT MARKING</u>	
Overview paper TWO RECENT CASES OF MARKER LOAD APPLICATIONS ON CARGO/FIGHTER AIRCRAFT FATIGUE TESTS by D.R.Erskine and J.L.Hopkins	6
EFFECT OF FLIGHT SEQUENCES IN COMPLEX LOAD HISTORIES ON CRACK FRONT MARKING by A.Liberge and C.Bleuzen	7
GENERATION OF MARKER LINES BY MEANS OF MARKER LOADS by K.Hoffer and R.Hillbrecht	8
GENERATION OF MARKER LINES ON FATIGUE FRACTURE SURFACES by M.Kalweit	9
PERIODIC LOADING SEQUENCES FOR THE SYSTEMATIC MARKING OF FATIGUE CRACK FRACTURE SURFACES by J.C.Ekvall, L.Bakow and T.R.Brussat	10
MODIFICATIONS OF FLIGHT-BY-FLIGHT LOAD SEQUENCES TO PROVIDE FOR GOOD FRACTURE SURFACE READABILITY by H.H. van der Linden	11
ON THE USE OF MARKER LOADS AND REPLICAS FOR MEASURING GROWTH RATES FOR SMALL CRACKS by M.H.Swain and J.C.Newman, Jr.	12
ON THE USE OF MARKER LOADS FOR FATIGUE CRACK GROWTH MEASUREMENTS by B.Palmberg	13
FATIGUE CRACK TOPOLOGY AND CRACK GROWTH ANALYSIS by J.M.Potter, W.R.Garver, K.M.Koepsel and B.G.W.Yee	14

Reference

SESSION III – FRACTURE SURFACE ANALYSIS TECHNIQUES

Overview paper APPLICATION OF OPTICAL AND ELECTRON MICROSCOPIC TECHNIQUES IN THE FRACTOGRAPHIC DETERMINATION OF FATIGUE CRACK GROWTH RATES by R.V.Dainty	15
NEW ANALYSIS ASPECTS OF THE FATIGUE CRACK PROPAGATION BEHAVIOUR BY SEM-IN SITU MICROSCOPY by K.Schulte, K.H.Trautmann and H.Nowack	16
CRACK PROPAGATION UNDER CONSTANT AND VARIABLE STRESS AMPLITUDES: A COMPARISON OF CALCULATIONS BASED ON THE STRIATION SPACING AND TESTS by J.Foth and W.Schütz	17
Paper 18 not available at time of printing	

SESSION IV – GENERAL DISCUSSION

REVIEW OF SESSION IV: GENERAL DISCUSSION by J.B. de Jonge and J.Schijve	D
--	---

Essential Features in Fatigue Fractures and Remarkable Phenomena in Fatigue Crack Growth  
 -----  
 Dr.-Ing. H. Klingele, Institute for Scanning Electron Microscopy, München, Germany.

Fracture, i.e. the breaking apart, is a phenomenon that applies only to solid bodies. Liquids or gases cannot break. All solid bodies in the universe, even those on other celestial bodies, are susceptible to breaking. Fatigue fracture, as a special form of fracture is not limited to metals; every solid material that shows even the smallest amount of remaining deformation before breaking can be separated by fatigue fracture. Fatigue fractures can occur in bones, in wood, in plastics and even in rubber. It follows therefore, that fatigue fractures must also occur in the mineral layers of our earth or in the rock on other stars. The alternating stresses that trigger these fatigue fractures are caused by the alternating temperatures and other sources.

Fatigue fracture is defined as the separation of material in small steps with the least possible consumption of energy. The following characteristics of fatigue fractures can therefore be derived:

1. Fatigue fracture attempts to propagate in a plane. Compared with other fractures, fatigue fractures are plane over large areas (Fig. 1).
2. Fatigue crack fronts are curved and concentric. Angular crack fronts would be immediately equalized by the effect of stresses. Such forms of fatigue fractures as shown in Fig. 2 are not possible.
3. Fatigue fracture striations are parallel and cannot cross each other (Fig. 1).

Fatigue fracture always begins in the point of minimum strength, and avoids regions of high strength as well as obstacles. This characteristic of fatigue fracture is caused by the effect of stresses. The total component or specimen is permeated by the stress field. The alternating stresses are effective until the weakest point yields and forms a crack. To get a feeling for this process, you can imagine that the stressed article is made of rubber. Or one can imagine the stress fields made visible by means of photoelastic investigation.

In order to understand the distinguishing marks that fatigue fracture produces in solid bodies three models can be used. Fatigue fracture works:

1. like the flexible blade of a saw,
2. like a wave front
3. like a current.

Fatigue fractures can occur in non-metallic materials. First, wood from the beech tree. Fatigue fracture was produced by reversed bending and therefore started on both sides of the cross-section. On the front surface the fatigue fracture begins along a manufacturing groove in the same manner as can be observed in metals (Fig. 3). On the reverse side, several fatigue cracks began in various planes thus forming a pattern of steps or battlements (Fig. 4). Despite the cell structure of the wood, the characteristics of fatigue fracture are clearly visible: the fracture is plane in comparison with the cleft overload fracture in the background, and it has a curved front.

Fatigue fracture in bone is also plane and shows some details that will be dealt with later: paths, separated from each other by steps, furthermore, striations and beach markings perpendicular to the propagation paths (Fig. 5).

In rubber, the characteristic signs of fatigue fracture can also be seen: propagation in a plane, curved front (Fig. 6).

The last example of fatigue fracture in nonmetallic materials is SAN, styrene-acrylonitrile copolymer (Fig. 7). The features of this fatigue fracture are very similar to those observed in metals.

#### 1) Fatigue Fracture Origin

-----

Due to the already mentioned invisible effect of the alternating stress field, the fatigue fracture from the start selects the weakest point. This, as a rule, is a weak point in the external surface. All surface defects can qualify as points of origin for fatigue fracture: the impact points of foreign bodies, shrinkage porosities, pores, inclusions, etched or blasted surfaces, molten areas and of course, cracks caused by other reasons, for example, by stress corrosion cracking or by too heavy grinding. In fact, due to the great number of these possibilities, usually several points of origin of fatigue fracture exist, of which, however, only a few, or sometimes only one propagates. The main fracture serves to eliminate local stresses and the large number of incipient cracks in the surface remain in the initial state. These stopped incipient cracks can be seen near the center of the fatigue fracture. Furthermore, old secondary cracks form a pattern of steps or battlements at the origin of the fatigue fracture. This also serves to indicate the center of the fatigue fracture (Fig. 8).

If the material has no surface defects, fatigue fracture originates in a shear-fatigue fracture or stage I fatigue fracture (Fig. 9). These stage I cracks can sometimes be identified as narrow initial zones on fracture surfaces after failure. They can easily be misinterpreted to mechanical damage that occurred after crack propagation. It must also be noted, that large areas, i.e. extending over several grains, as stage I cracks are exceptions to the rule, and occur only in high strength nickel-based and cobalt-based alloys (Fig. 10 and 11).

It is often very important to find the exact point of origin of a fatigue fracture not only in broken machine components, but also in laboratory specimens. In addition to the already mentioned characteristic signs, other features can also be used: Due to the division into many small paths that are separated by steps, the concentric propagation of the crack results in a radial pattern. The center of this pattern is the exact point of origin of the fatigue fracture (Fig. 12, 13 and 14).

If the fatigue fracture surface is totally destroyed, there is another method of finding the crack origin. The external surface of the material or laboratory specimen must be inspected for secondary fatigue cracks and for plastic deformation (Fig. 1). Near the overload fracture the surface shows severe plastic deformation indicated by deep secondary fatigue cracks, slip lines, serpentine glide, necking and contraction in small areas, orange peel patterns and ductile micro-cracks, especially around inclusions (Fig. 15). The initial point of fatigue fracture on the other hand, can be recognised by the complete lack of plastic deformation on the surface, even under the scanning electron microscope. The intrusions and extrusions that should theoretically exist before the fatigue crack starts cannot be seen on technically worked surfaces.

## 2) Direction of Propagation

-----

How does a fatigue fracture propagate in microscopical areas? The answer to this question can be easily obtained by observing the secondary cracks. These dead ends of fatigue fracture are visible under the scanning electronic microscope only if the viewing direction corresponds to the direction of fracture propagation. The tilted specimen must be rotated under the SEM until the dark secondary cracks become visible. As a control test, rotate the specimen about 180 degrees - the secondary cracks must disappear (Fig. 16).

Further characteristic features that can be used in finding the direction of propagation are the convex curvature of the striation pattern and the fan-shaped patches or paths of propagation (Fig. 17). Even in microscopical areas it is impossible to have a fatigue fracture that starts in a broad front, becoming narrower and narrower, and finally ends in a point. As an example, once again the fatigue fracture in Ti-6Al-4V (Fig. 18).

It is possible that striation patterns and secondary cracks do not exist in the origin areas of fatigue fractures. Furthermore, the propagation paths can be so tiny and smooth, that at a first glance, one can get the impression of a brittle overload fracture or of stress corrosion cracking. There are however fundamental differences between the crack propagation in a brittle overload fracture, i.e. also in stress corrosion cracking, and crack propagation in a fatigue fracture. The basic pattern of a fatigue fracture is a fan-shaped area, a fan-shaped path; opposed to this, the basic shape of a brittle overload fracture is that of a feather or a leaf (Fig. 19). This comparison even holds true when considering the subdivision of a leaf by veins. The leaf pattern is serrated like a maple leaf. The direction of propagation runs from the stalk to the tip of the leaf, and from the central vein along the secondary veins towards the edge of the leaf. These characteristics are caused by the basic character of the cleavage which functions like a chisel or a wedge. As an example, stress corrosion cracking in an AlZnMg-alloy (Fig. 20). The feather or leaf patterns of cleavage can also be observed in other solid bodies, for example, in brittle polymers or in ceramics.

## 3) End of Fatigue Fracture

-----

In the practice of SEM investigations, it is generally of advantage to begin with the end of the fracture, this is especially so in the case of the quantitative evaluation of striations. The overload fracture can generally be recognised easily, because it is cleft and shaped like a ridge, and is well separated from the fatigue fracture. In most cases the end of a fatigue fracture is in the best condition as it is the least aged portion of the fracture surface. Additionally, the micro-characteristic signs for a ductile or brittle overload fracture (dimples and cleavage facets) can, of course, be found in the overload fracture area.

#### 4) How to Select the Measuring Line for Quantitative Evaluation

---

Actually, the fatigue fracture should be inspected completely from the point of origin to the end, i.e. move along the direction of propagation and count striation by striation. This procedure is not possible in practice. One would select a measuring line that points from the point of origin towards the end of the fracture. It is sometimes necessary however, to deviate from the main direction (Fig. 21). This is necessary in the case of plastically smeared fractures and also for components with complicated cross sections (Fig. 22). The quantitative evaluation of fatigue striations is generally reduced to a limited number of points. The evaluation can be performed directly on the SEM display. The crack arrest lines and the fatigue striations are aligned at right angles to the direction of the electron collector. The areas of examination (i.e. the distance from the origin of the crack) are set precisely with the aid of the micrometer screw on the specimen holder.

A number of successive striations,  $n$  (as large as possible) is counted, the corresponding length,  $l$  in mm in the direction of crack propagation and the magnification,  $V$ , are noted. This data is used to calculate the crack propagation velocity

$$\frac{n \cdot V}{l}$$

directly in load cycles per mm of crack propagation. Taking measurements at as many areas as possible makes it possible to determine the course of the fracture over the whole cross section, and thus, the total number of load cycles during crack propagation (Fig. 23).

#### 5) How to Select the Proper Areas for Quantitative Evaluation

---

Only large areas with uniform striations are suitable for quantitative evaluation.

The following sketches and SEM pictures illustrate features of the fatigue fracture that are not suitable for quantitative evaluation. First, a hard zone in the material (Fig. 26). On approaching the hard zone, the fatigue fracture is retarded, but after the hard region, it is accelerated. Both zones are not suited for evaluation; it is necessary to deviate around such inhomogeneties.

Next example, a hard inclusion. As the fracture propagates continuously on both sides of the inclusion, it is stopped completely for a number of load cycles at the inclusion. After climbing up the inclusion, the fracture catches up to the main fracture in large steps (Fig. 27 and 28).

Due to the lack of material, a pore has the effect of accelerating the fatigue fracture; after the pore, the fatigue fracture is retarded (Fig. 29 and 30).

Secondary cracks are not suitable for quantitative evaluation, as they will retard and finally stop fatigue fractures (Fig. 31).

Striations on a step are only suitable if they lie on crystallographically oriented planes (Fig. 24 and 25) or if they cross the step and the neighbouring areas in unbroken lines.

If a fatigue fracture surface is plastically smeared in large areas, it is necessary to use the steps between the paths of propagation for quantitative evaluation. The development of another fatigue fracture perpendicular to the main plane of fracture is shown between two fatigue fracture levels (Fig. 32). Fig. 33 shows the result: because of the catch up effect in the step, the striations are coarser than in the neighbouring areas. Striations in steps are only suitable for quantitative evaluation, if they are connected in unbroken lines with the neighbouring areas (Fig. 33 and 34).

Sometimes the influences of the microstructure do not permit a quantitative evaluation. Some special effects can be found in eutectic lamellar structures. If the fatigue fracture propagates locally normal to the lamellae, it can jump from lamella to lamella, especially if brittle lamellae are involved. In such cases, the striation pattern shows the width of the lamellae and not the real propagation pattern. As an example, the pearlite structure in cast iron (Fig. 35 and 36).

Coarse striations at the end of a fatigue fracture are normally of low importance. In spite of this, I will cover some of the features at the end of a fatigue fracture.

Sometimes separated fatigue fractures originate at a certain distance in front of the main fatigue fracture as the result of high alternating stress. Ellipses of striations are formed especially around inclusions. These striations are subsequently overtaken by the main fatigue fracture (Fig. 37 and 38).

Normally, the fatigue fracture is followed by overload fracture (Fig. 39). A sequence of tensile-overload fracture steps and fatigue fracture areas can however also occur (Fig. 40). In this case, all striations must be counted, the subsequent dimple area however, as only one step of fracture (Fig. 41).

Another frequently occurring special case is that of tensile overload steps (Fig. 42). Although these few load cycles are normally of low importance for quantitative evaluation, they can be very important in cases of in-service fractures, or fractures caused by accidents (Fig. 43 and 44).

Sometimes serpentine glide patterns in overload fracture ends look very similar to a fatigue striation pattern (Fig. 45).

#### 6) Estimation of Invisible Striations

Quantitative evaluation of fatigue fracture surfaces is limited by the resolution of the SEM (5-10 nm) and by the spacing of atoms in the metal lattice (some tenths of a nm). A striation pattern can only form if the striation width is in the order of some lattice spacings, i.e. in the region of some nm. It is however possible, that several load cycles are necessary for the fatigue crack to progress one lattice spacing. In this case, of course, no striation pattern can form. Nevertheless it is possible to estimate a theoretical striation width (Fig. 17):

The smallest paths are determined. They can only be formed by tiny steps of fatigue crack. It is therefore possible to draw a proper striation pattern and use this to calculate a propagation rate.

#### 7) Destroyed Fatigue Fracture Surfaces

In spite of plastic smearing, there are possibilities to find at least the order of magnitude of the fatigue fracture propagation rate:

- 1) Patiently search for striation in protected areas, for instance in steps and depressions.
- 2) Try to open the largest of the secondary cracks.
- 3) Striations in small secondary cracks can be used without opening the crack; the spacing in these striations is however smaller than outside the secondary crack, due to the retarding effect of the secondary cracks.

In spite of chemical attack or rust, it is sometimes possible to find conserved areas of fatigue fracture that were protected by oxide layers or coatings of oil or grease. Furthermore, chemical action develops the deep reaching zones of plastic deformation that are more resistant than the adjacent material. These relics permit an estimation of the former striation pattern.

#### 8) Fatigue Fractures in the Earth's Crust

I am certain that there are fatigue fractures in the earth's crust.

In Germany there is a well-known fracture line, the Rhine-trench. The crack visible on the earth's surface clearly shows steps or battlements as features of fatigue fracture (Fig. 46), viewing direction from south west to north east (7). Near Mainz a round hard obstacle can be seen. In my opinion this is an impact point of a meteorite or the relic of a volcano. I am sure that there are many other fatigue fractures on the continents, for instance the battlement line Nile - Lake Albert - Lake Tanganyika - Lake Malawi in Africa.

The second example are all ocean ridges, for instance, the Mid-Atlantic Ridge (Fig. 47, (8)). As a special form, fatigue fracture is open like a book. It shows a battlement pattern caused by several incipient cracks, fracture paths and striations. The fatigue fracture propagates from the surface towards the centre of the earth. Iceland is a residue from a meteorite impact and effects the fatigue fracture in the same manner as a hard inclusion; there are no fatigue cracks and therefore no striation patterns around Iceland (Figure 48, (8)). A cross section through the Mid-Atlantic Ridge shows a deep central crack (Fig. 49).

Quantitative evaluation of the earth striations may be done by geologists. My model is that of a solid floe between thin layers with volcanos (Fig. 50). Alternating stresses are caused by magma motion and other sources.

## Bibliography.

- 1) L. Engel, H. Klingele et al., An Atlas of Polymer Damage.  
Wolfe, London, Hanser, Munich, Vienna, 1981.
- 2) L. Engel, H. Klingele, An Atlas of Metal Damage.  
Wolfe, London, Hanser, Munich, Vienna, 1981.
- 3) J. C. Grosskreutz, ASTM STP 495. Philadelphia 1971.  
p. 31. Courtesy, J. Schijve.
- 4) Metals Handbook, Vol. 9, ASM, Ohio 1974, p. 167.
- 5) Metals Handbook, Vol. 9, ASM, Ohio 1974, p. 121.
- 6) Henry, M. F. Ph.D. thesis, Rensselaer Polytechnic Institute N.Y., 1974 (ASTM  
STP 600, Philadelphia 1976)
- 7) Deutschland aus dem All.  
Bild der Wissenschaft, Deutsche Verlagsanstalt Stuttgart, 1978.
- 8) World Ocean Floor. National Geographic Magazine, Washington 1981.
- 9) Welt und Umwelt, Ausgabe B, R. Oldenbourg Verlag und Georg Westermann Verlag,  
München, Braunschweig 1984.

## Acknowledgments:

The author thanks the following persons for kindly supplying materials and pictures:

Faun Frisch Baumaschinen GmbH, Kissing,  
Mr. Langanke

Orthopädische Klinik München,  
Mr. Plitz

Motoren-und-Turbinen-Union GmbH, München,  
Mrs. Borchert  
Mr. Beulke  
Mr. Esslinger  
Mr. Hansen  
Mr. Huff  
Mr. Kraus  
Mr. Lechner  
Mr. Olbrich  
Mr. Rossmann  
Mr. Schmid  
Mr. Scholz

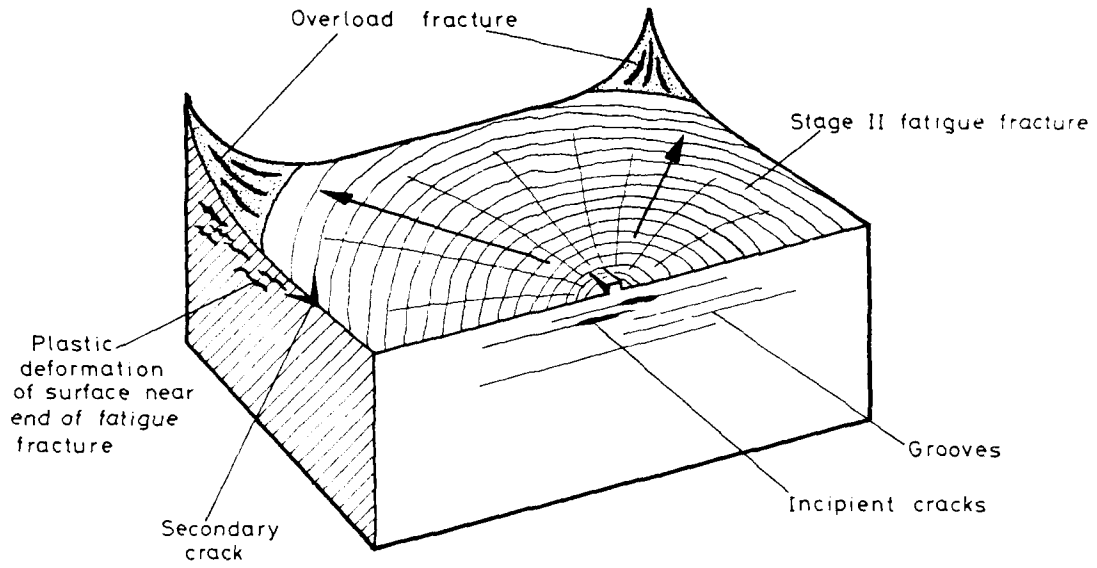


Fig. 1. Fatigue fractures are plane, and have a radial pattern with concentric striations and beach markings. Often there are several crack nuclei in the centre of a fatigue fracture.

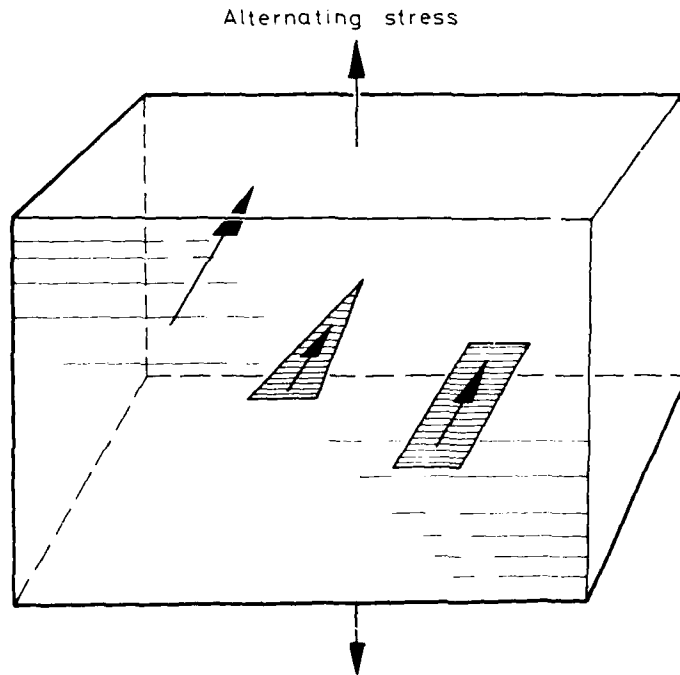


Fig. 2. Impossible forms of fatigue fracture.

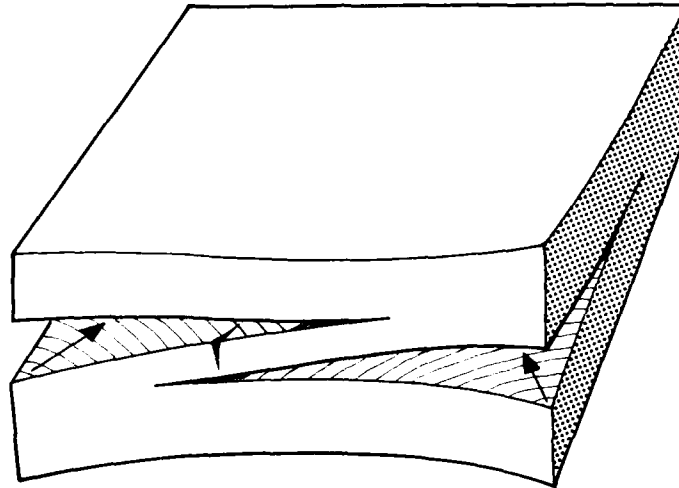


Fig. 32. A secondary fatigue crack situated between two parallel fatigue planes forms a step perpendicular to the main fatigue plane.

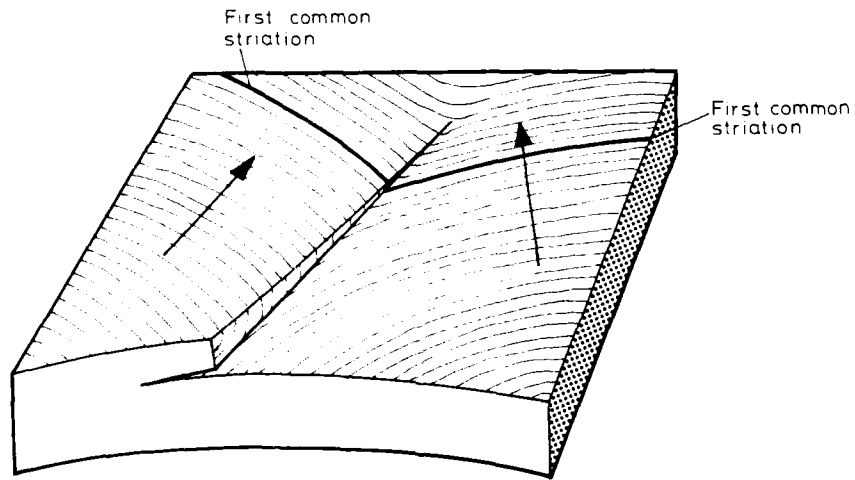


Fig. 33. Striations in steps perpendicular to main fatigue plane may only be used for quantitative evaluation if there are common striations in adjacent paths.



Fig. 30. Low-carbon iron containing a high percentage of oxygen, fractured in fatigue at room temperature. a large oxide inclusion has been nearly completely disengaged from its original pocket. Fatigue striations detour around, or extend into the pocket. Crack propagation was from bottom to top (4).

Please note that the depth of deformation is visible inside the hole by slip lines.

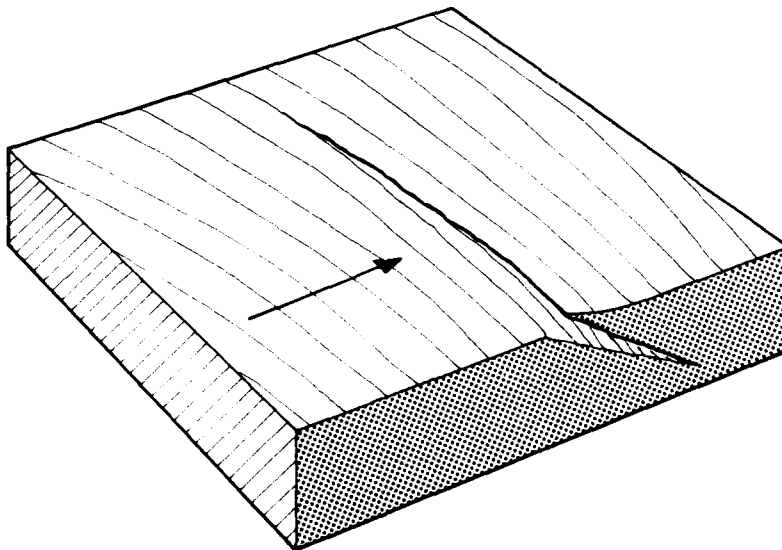


Fig. 31. Narrow striations inside a secondary crack are not appropriate for quantitative evaluation.



Fig. 28. Fatigue fracture surface of 7075-T6 aluminum showing the striations produced by a program consisting of severe overload followed by 10 constant amplitude load cycles. The lower part of the photograph shows the separation of the crack into three adjacent paths. TEM photograph from replica (3).

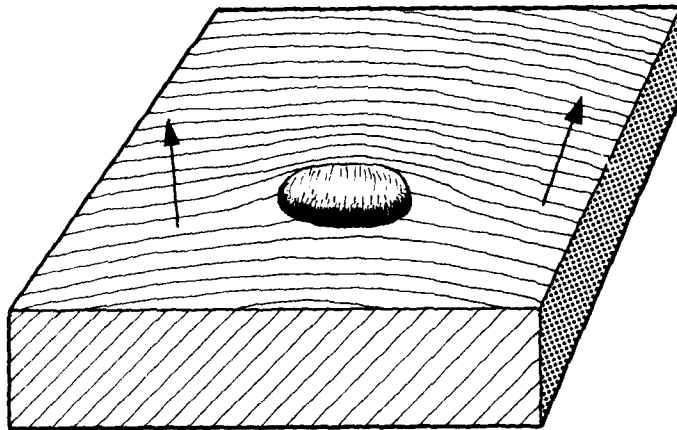


Fig. 29. When a fatigue fracture comes to a pore, it is accelerated. Behind the pore, the fatigue fracture is retarded. Quantitative evaluation of striations only in large regions with constant spacing (width) of striations.

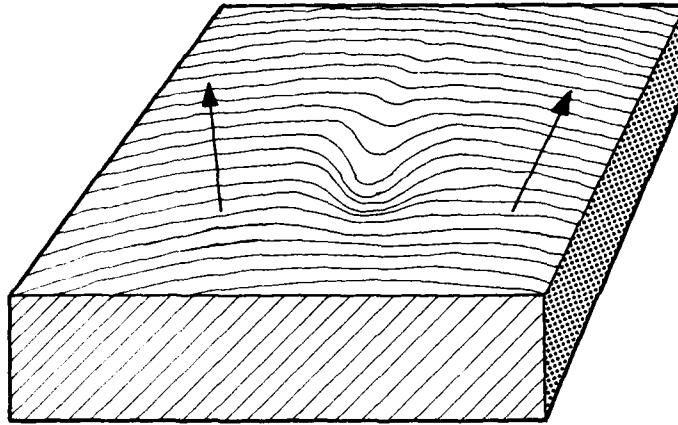


Fig. 26. In a hard region the fatigue crack is retarded, i.e. the width of the striations is smaller than on either side. Behind the hard region the crack steps are larger than on either side. Quantitative evaluation of striations only in large regions with constant spacing (width) of striations.

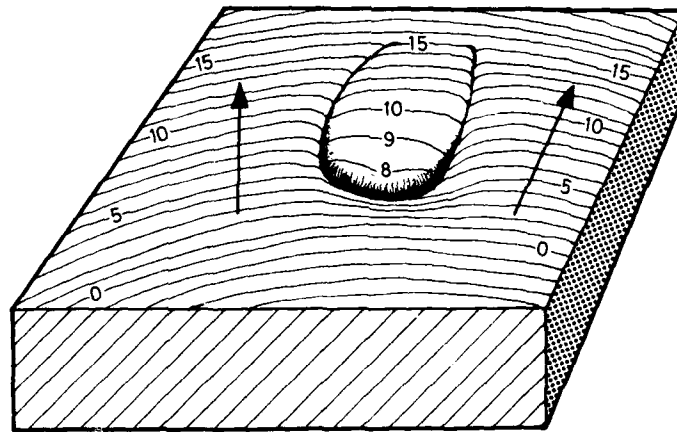


Fig. 27. Hard region (obstacle) separates the fatigue crack front into three adjacent paths with different propagation rates. Within the hard region there is no propagation for some load cycles. Quantitative evaluation of striations should be done only in large regions with constant width of striations.

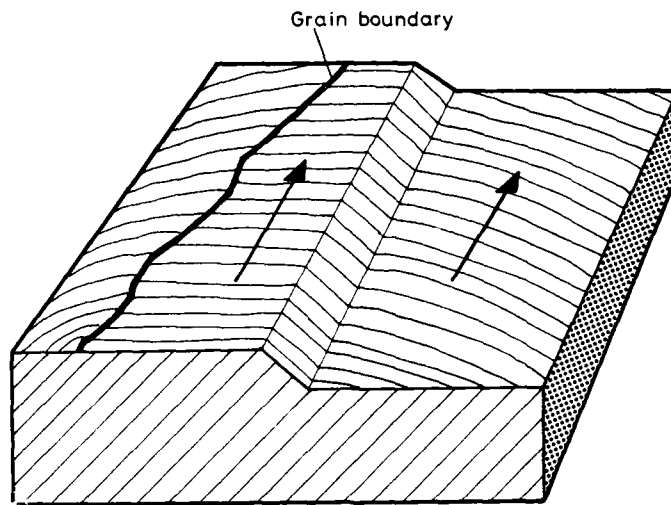


Fig. 24. Crystallographic step in fatigue fracture (e.g. in a Nickel-base alloy) is appropriate for quantitative evaluation of striations (when the rest of the fracture surface is smeared).



Fig. 25. Crystallographically oriented fatigue striations on a fatigue fracture surface (Stage II) from a laboratory tested nickel-based alloy (Inconel 718) tested at 600 °C (2).

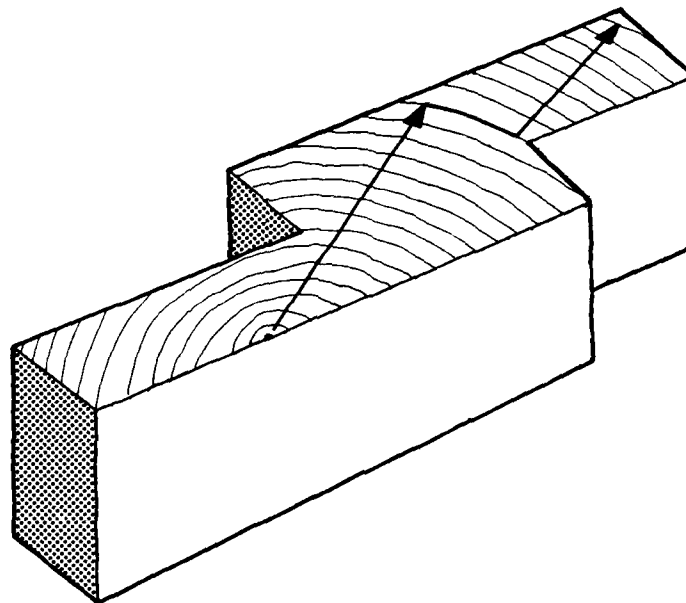


Fig. 22. Broken measuring line for quantitative evaluation of striations.

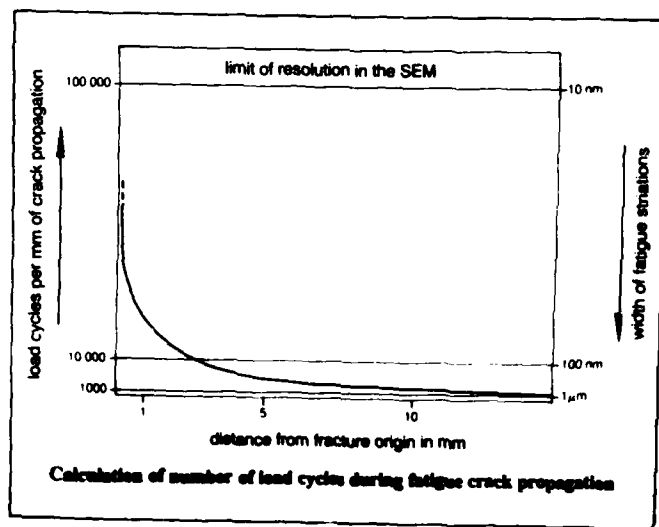


Fig. 23. Quantitative evaluation of striations (2).



Fig. 20. Stress corrosion cracking in the wrought alloy AlZnMg3. Areas of transcrystalline fracture have a feather-like appearance (2).

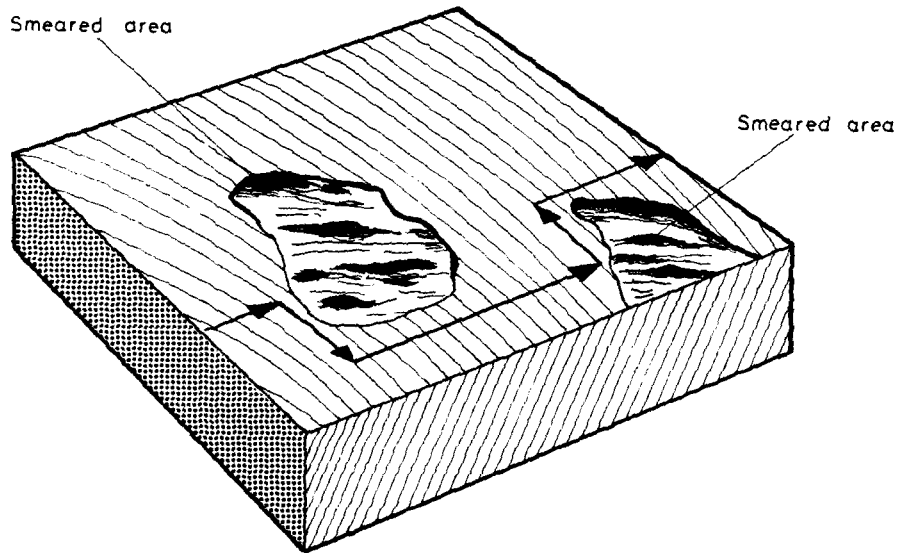


Fig. 21. Broken measuring line for quantitative evaluation of striations.



Fig. 18. Fatigue fracture in Ti-6Al-4V.

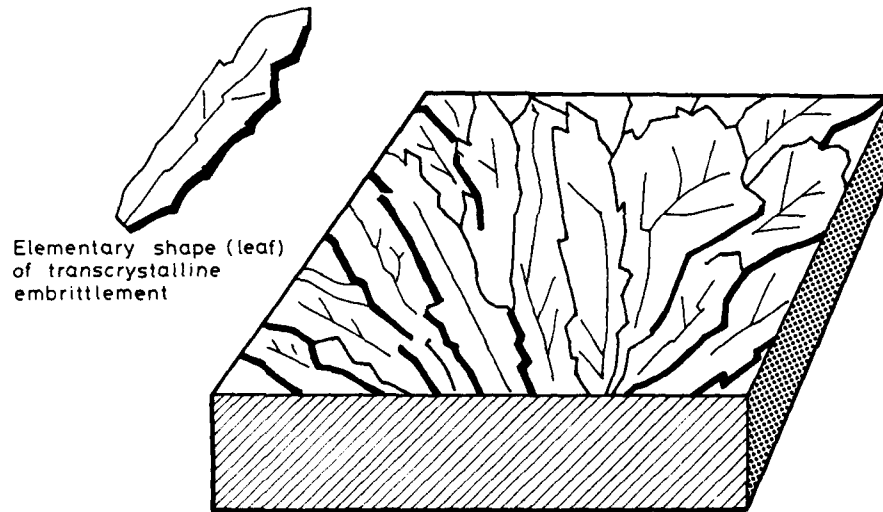


Fig. 19. Intercrystalline embrittlement (e.g. stress corrosion cracking) forms leaf-shaped areas with pointed ends and branching veins (feather marks).



Fig. 16. Fatigue fracture in Ti-6Al-4V. Many secondary cracks are visible.

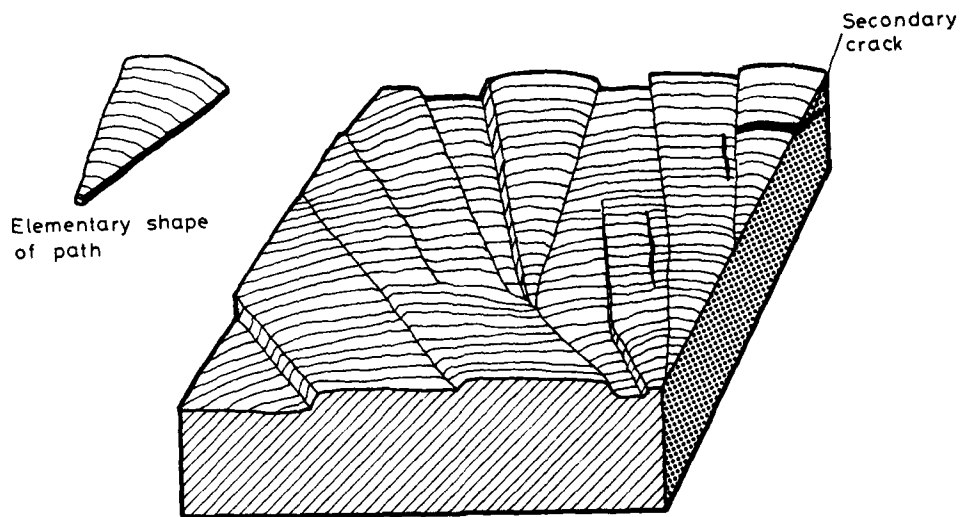


Fig. 17. Fatigue fracture with elementary shape of the fracture path.

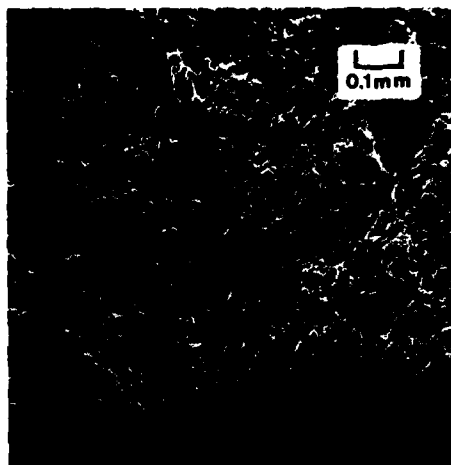


Fig. 13. Fatigue fracture in Ti-6Al-4V, forming a radial pattern.

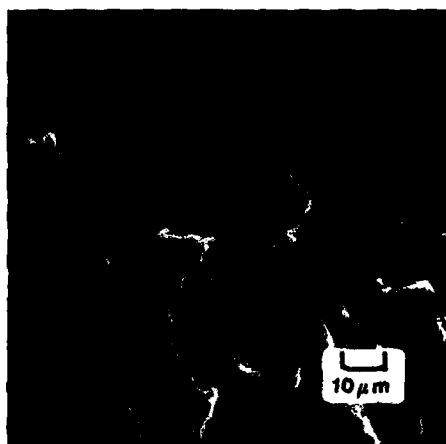


Fig. 14. Fatigue fracture origin at a pore. Ti-alloy IMI 685.

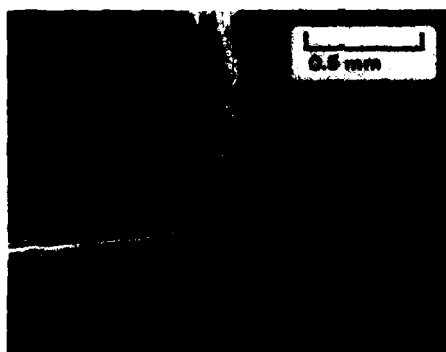


Fig. 15. Plastic deformation and overload cracks (left side) near the end of fatigue fracture (lower part, right side) in ferritic steel.



Fig. 11. Stage I of fatigue fracture in Inconel 713 C. The flat fracture surface shows intersecting slip steps (2).

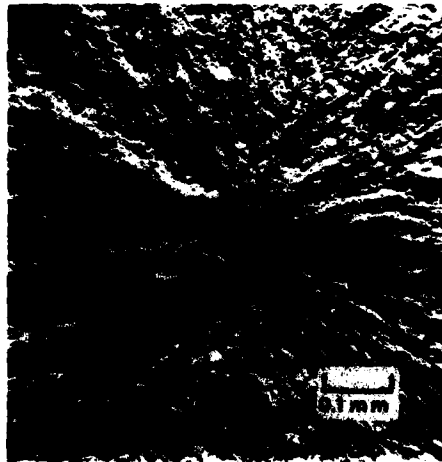


Fig. 12. Fatigue fracture, originating in the middle of the cross section of a laboratory specimen at a big inclusion. Powder metallurgically produced Nickel-base alloy.

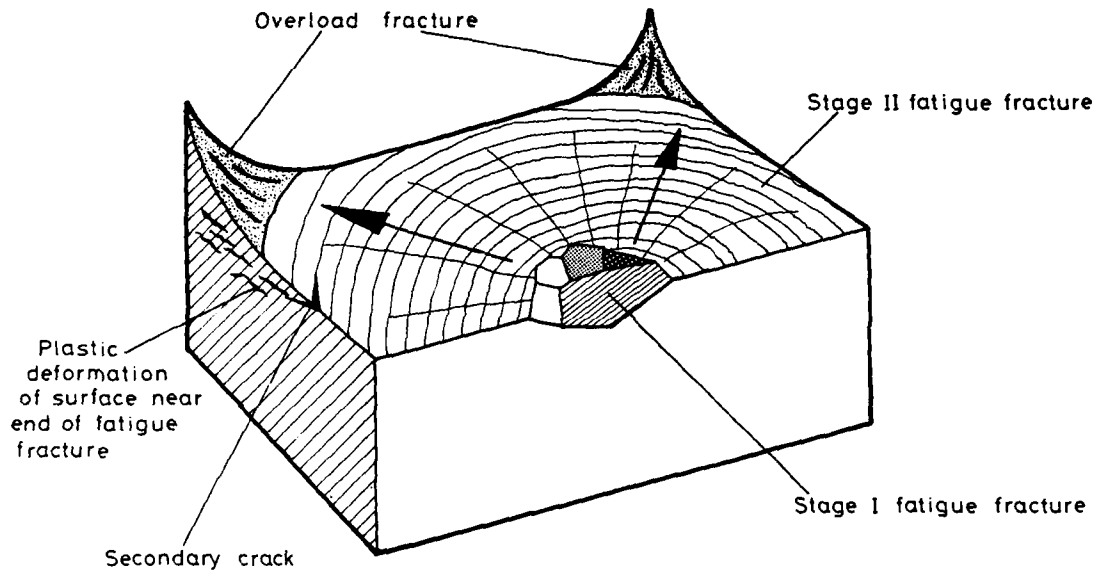


Fig. 9. Stage I origin of fatigue fracture. No striations for quantitative evaluation in this area.

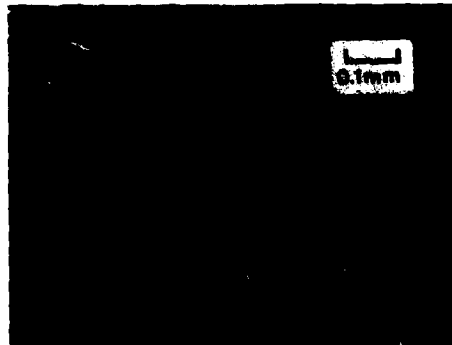


Fig. 10. Stage I of fatigue fracture in a nickel-based alloy turbine blade (Nimonic 105). The initiation region shows the cleavage-like facets which typically form in nickel-based alloys (2).



Fig. 6. Fatigue fracture in Nitrile-butadien rubber (NBR).

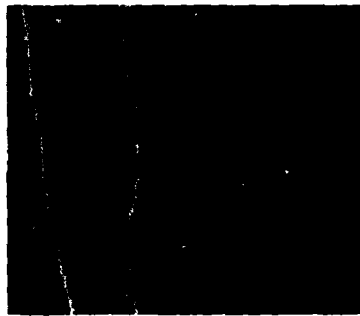


Fig. 7. The characteristic features of fatigue fracture in press moulded SAN are as follows: sharp-edged paths and striations with flat, low-deformation profiles (1).

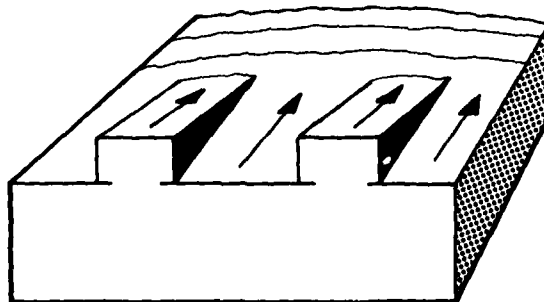


Fig. 8. Formation of steps or battlements at the origin of fatigue fracture.

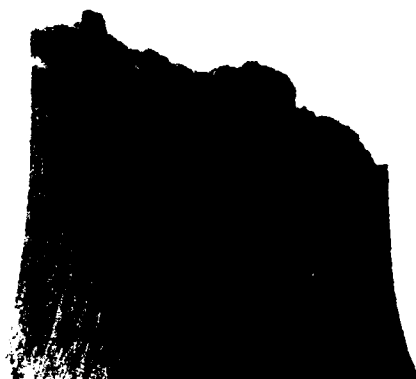


Fig. 3. Fatigue fracture caused by reversed bending in the wood of a beech tree.

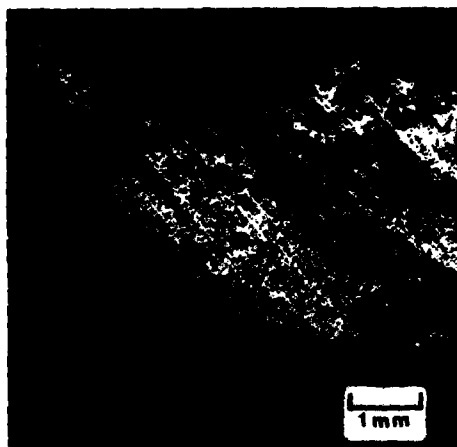


Fig. 4. Fatigue fracture caused by reversed bending in the wood of a beech tree.



Fig. 5. Fatigue fracture in human bone.



Fig. 34. Fatigue crack-growth bands in the aluminum alloy 2024-T3. Five load levels of a spectrum are clearly resolvable. In the middle of the photograph separate paths without common striations. In the upper part of the photograph connected paths with common striations in steps and adjacent paths (5).

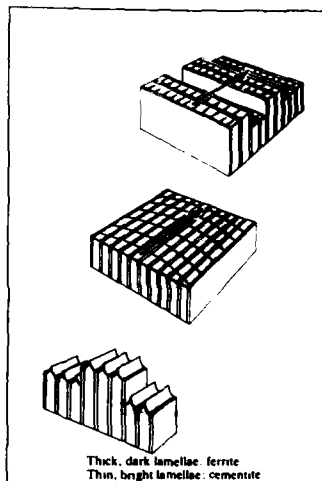


Fig. 35. Brittle fatigue fracture (top and middle) and ductile rupture (bottom) in pearlite (2).



Fig. 36. A fatigue fracture in pearlite cast iron. The dominant feature of the fracture surface is the presence of steps and facets resulting from the brittle fracture of the lamellar ferrite constituent of the pearlite. Fracture propagation direction from top left to bottom right (2).

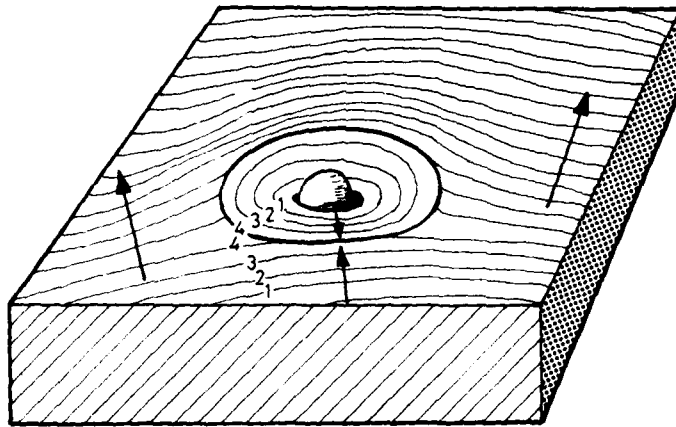


Fig. 37. Fatigue-overload transition region. The elliptically shaped striations around an inclusion were formed in front of the crack tip before main fatigue front reached this area. Not appropriate for quantitative evaluation.



Fig. 38. Fatigue-overload transition region in Ni, 12Cr-TaC (fatigue region comprising bottom two thirds of the photograph). Propagation direction from bottom to top (6).



Fig. 39. Transition area from fatigue fracture to overload fracture in Ti-6Al-4V.

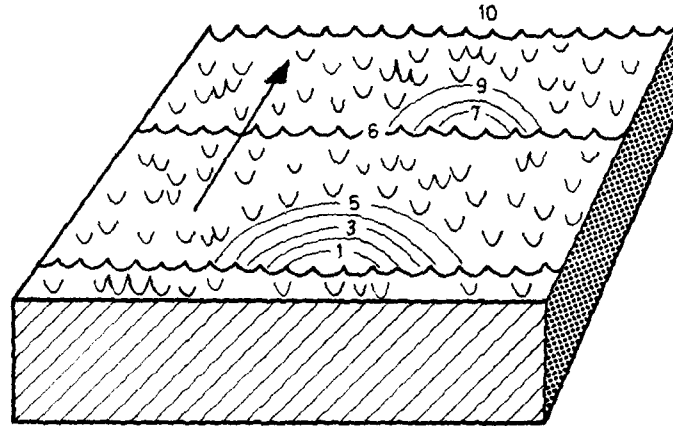


Fig. 40. Fatigue-overload transition region. Isles of striations and regions of dimple fracture have to be evaluated as indicated by numbers.



Fig. 41. Isle with striations in the overload fracture of Inconel 718.

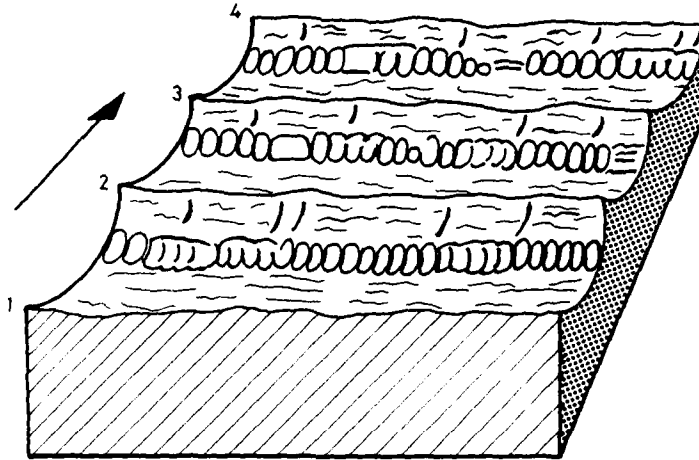


Fig. 42. Overload fracture in steps forming bonds of dimples and serpentine glide patterns.

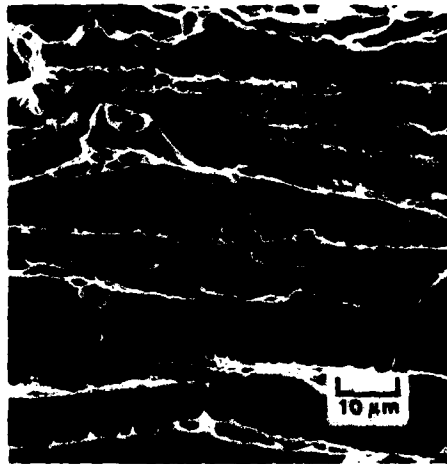


Fig. 43. Steps of ductile fracture in a sheet of austenitic Chromium-Nickel-Steel.



Fig. 44. Fatigue fracture and subsequent ductile overload fracture in steps in a ferritic screw of a connecting rod.



Fig. 45. Serpentine glide in Cu overload fracture (2).

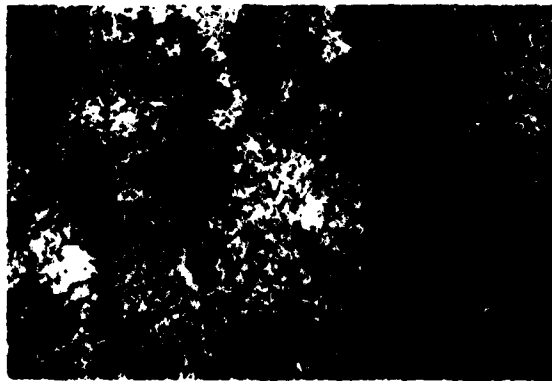


Fig. 46. Fracture line Rhine-trench, probably a fatigue fracture.



Fig. 47. Mid-Atlantic Ridge fracture (center), probably a fatigue fracture.



Fig. 48. Mid-Atlantic Ridge fracture (Iceland area)

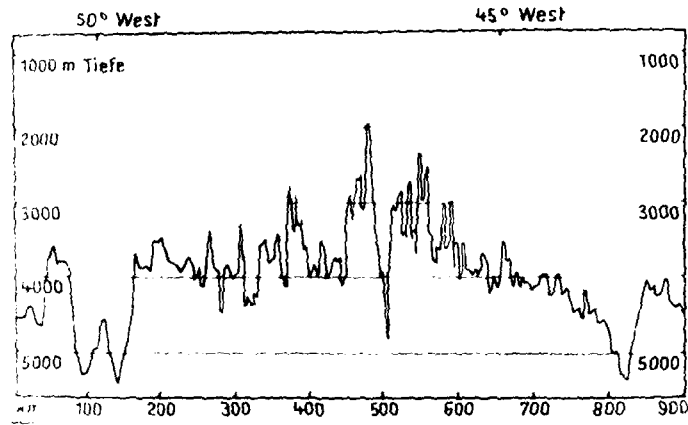


Fig. 49. Cross section through the Mid-Atlantic-Ridge (9). Fatigue fracture in the middle of the ridge.

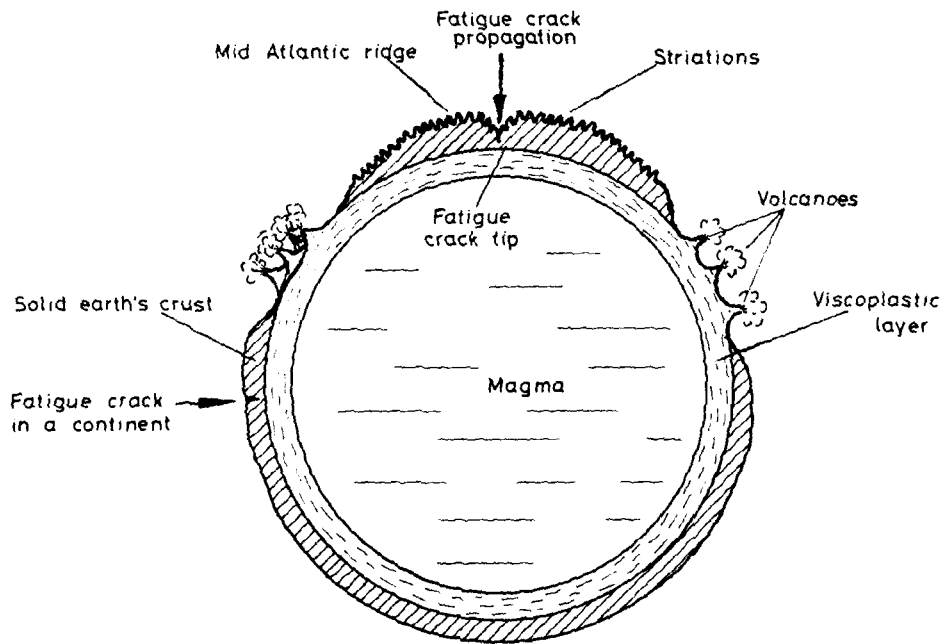


Fig. 50. Cross section through the earth featuring the Mid-Atlantic-Ridge.

## FATIGUE FRACTURE TOPOGRAPHY

by

P J E Forsyth  
 Materials and Structures Department  
 Royal Aircraft Establishment  
 FARNBOROUGH, Hants GU12 4NT  
 England

## SUMMARY

The texture of a fatigue fracture can vary between the extremes of a bright reflective surface (with facets that may approach planarity) to a rough highly irregular surface. Roughness is imparted by microstructural heterogeneity in its various forms and represents tortuous fragmented crack paths. The degree of roughness generally increases with increasing  $K_{max}$  and degree of triaxiality. The crack tip plastic zone is bound to increase with  $K_{max}$  and inasmuch as the larger zone will encompass more off-plane particles that initiate further microcracks, so the fracture becomes rougher.

On a finer scale of the fatigue striations, whether they relate to individual loads or to 'flight' loads ie (a ground-air-ground cycle), crack front deviation or tilting from and to the general fracture plane occurs in a periodic manner. This can be demonstrated for both metals and polymers and frequently this deviation is considerably greater than the crack tip opening displacement.

Abrupt changes in fracture reflectivity or abrupt changes in crack front tilt make very effective crack position markers, and the loading conditions to produce these can be optimized.

## 1. INTRODUCTION

A fatigue fracture gives a direct three dimensional display of the path that the crack took thereby greatly adding to the information that might eventually be gained from a microsection. Fractography and metallography are both necessary activities in microstructure/fracture studies, but this paper will be more concerned with considering those fracture features that give, firstly, an understanding of the mechanism of fatigue failure and indicate relationship with the applied stress and, secondly, a quantitative estimate of crack life by the procedure of counting identifiable fatigue striations.

The activity of fractography has been pursued increasingly over the last two decades both on service failures and fatigue fractures produced in the more controllable environment of the laboratory. The quantitative aspect of crack growth rate measurement and crack life estimation from fracture features had endeared the subject to engineers as well as Materials Scientists. In favourable circumstances the engineer can be wholly satisfied with the crack life estimates made, but difficulties may arise in identifying suitable striations on some fractures. Similarly for those people particularly interested in determining basic mechanisms of fracture there is yet a lot to be learnt.

Lack of understanding of mechanisms does not necessarily impede the day to day fracture analysis activities that take place but there are occasions where understanding and analysis impinges, one being provision of satisfactory markers for crack growth rate determinations in the difficult cases mentioned.

A study of the topography of fatigue fractures in various materials tested under a variety of conditions is also of considerable importance with regard to the degree of crack closure that will be experienced.

The aim of this paper will be to present recent observations that may help to advance our understanding of the fatigue cracking mechanism and this will also form a basis for considering the best arrangements of fatigue loadings to produce clearly defined fracture markers.

## 2. OBSERVATIONS

The contours or features of a fatigue fracture, as with a landscape, can be considered on various dimensional scales. For example, a fracture that might be classified as smooth when examined with a hand lens may yet appear rough when examined under the electron microscope. A smooth fracture might also be highly reflective depending on the dispersive power of the microscopic features present.

A hand lens may well be the best way to view macroscopic features such as shear lips and to determine crack growth direction from the coarser markings present. However, one aim of this paper is to emphasise the point that both the macro and the microscopic features must be considered together, and this must be particularly true in considerations of crack closure. This paper is also mainly concerned with Stage II fatigue crack growth although acknowledgement will be made to those circumstances where Stage I may play a part.

In general, fatigue fractures exhibit an increased roughness as one moves from origin to final failure position, i.e. moving progressively from slow to fast crack growth rates. The difference in texture or reflectivity arising from different fatigue crack growth rates is less evident on constant amplitude fatigue fractures than on a fracture where growth rate has changed abruptly with a sudden change of applied stress intensity factor such as occurs in block loaded programmes. An example of this is shown in Figure 1 where bright and dull bands are brought into juxtaposition.

Although it has been stated that the change in reflectivity with crack depth on a constant amplitude fatigue fracture is less perceptible, it can still be demonstrated by photometer measurement as shown in Figures 2 and 3. These measurements were made on aluminium alloy 7178 specimens that had been heat treated to the peakaged (T6) and the overaged (T73) conditions. It is of interest to note that there is an initial increase in reflectivity on the T6 specimen which is attributed to the joining up of many origins to form a more coherent crack which contains virtually planar facets at peak reflectivity. Further growth, with an attendant increase in stress intensity factor, begins to exploit particles in the microstructure which in turn reduce the general coherence of the fracture surface. It should be noted that the overaged condition shows less change with crack growth the difference being that the planar growth period is far less in evidence. However, it should be noted from the polar diagram in Figure 2 that facets, with only 15° tilt, even if highly reflecting, would contribute little to the photometric reading.

The topographical detail for these specimens has been summarised in schematic form in Figures 4 and 5.

Evidence for crack closure, which took the form of hammered and distorted surface layers, was only found in the 'flat facet' region of the fracture, although it is generally well accepted that steep faces such as shear lips on aluminium alloy fractures often exhibit black fretting product. This raises the immediate question as to the part played by lateral shift of the fracture faces in encouraging interference between mating features.

Aluminium alloys, as with other metals, show a tendency for fatigue fracture to progress with the sub-division of many small crack front segments or elements and within each element the crack seems to grow in a semi-independent manner because of some degree of mechanical isolation of that element from its neighbours. Polymers show far less tendency to do this; presumably because of their greater homogeneity<sup>(2)</sup>. The consequence is that metal fractures on a microscopic scale have a high proportion of steep sided facets or cliff edges where breakthrough has occurred between the different crack levels, and polymer fatigue fractures are relatively flat. Thus the coherence of the crack front of a fatigue crack in a metal changes more through its crack life than would be observed in a polymer.

There is also a tendency for those crack segments that advance at different levels to overlap somewhat in a manner illustrated in Figure 6. In a polymer such as polymethyl methacrylate (PMMA) where overlapping still occasionally occurs it releases slivers of the plastic which become hammered into other areas of the fracture. In all probability pieces of metal may be released in a similar manner, although their detection would be more difficult. Even if such fragments are not completely released their displacement will increase the interference between fracture faces. Many fatigue fractures also exhibit transverse microfissuring which also must increase the misfit. Having said this the major proportion of the area of most fatigue fractures shows little obvious damage from closure and very fine detail is preserved. The preservation of such detail would suggest extremely accurate mating and, in the main, a hill/valley configuration and is in itself no evidence against closure. As was mentioned earlier fracture topography can be considered at various scales of magnification and whereas no one would seriously deny that the long range hills and valleys illustrated in Figure 6 interlock, the question of the configuration of micro striations has been a cause of considerable argument, with protagonists for the hill to valley arrangement, and those that claim that hills meet with hills and valleys with valleys. The arrangement clearly depends on the model for crack extension that is adopted, particularly the degree of symmetrical plastic opening that is envisaged.

It should be considered, at this stage, that there are features on a larger scale than the microscopic individual striations and smaller than the long range hills and valleys where the hill to valley configuration has been confirmed, and these are the 'flight' striations that one observed when flight loads are imposed on a ground-air-ground loading condition. A study of the ground-air-ground loading with superimposed

cycles gives us an important new insight into crack front behaviour as well as enabling crack growth rate measurements to be made under very low growth rate conditions; a point that will be discussed later. Crack growth through the ground-air-ground condition follows a wavy path that develops interlocking corrugated fracture surfaces. The scale of this behaviour is such that it can be unequivocally demonstrated that this is so, both for metals and for polymers. The implication from this is that the rising mean stress biases the incremental crack growth from the individual loads in one direction and the diminishing mean biases them in another direction. The question now,  $\mu$ , if a rising mean does this to the incremental growth, would not an individual rising and falling load produce the same wavy action through its own associated crack extension distance? The answer is that it has been observed to do so in a number of cases and the effects of both a rising and falling mean load and the simple rising and falling individual load will now be described.

A simple R ratio switching programme will produce an undulating fracture surface<sup>(3)</sup>. Using a simple biharmonic load arrangement where the R ratio, ie the mean load is varied sinusoidally rather than as a square wave (Figure 7) produces very beautifully defined corrugations on both metal fractures and on polymers. Because, as has been previously stated, polymers show less crack front fragmentation than metals a material such as PMMA shows this feature to best advantage, Figure 8. Using interferometry it can be shown that for the biharmonic arrangement a long range corrugation is set up by the low frequency and a short range corrugation related to the higher frequency cycles is superimposed on the long range one. Thus as long as there is no displacement of the mating fracture surfaces in the x or z directions a virtually complete fit is obtained. In fact there is a fractional residual permanent opening (y direction) displacement related to both frequencies so that striation fitting is not quite perfect and points of crack closure occur.

Referring back to the more fragmented fractures observed in metals and alloys, it is observed that similar crack features are observed on considerably different scales. This phenomenon has been described elsewhere<sup>(2)</sup> and Figure 9 summarised this for the development of a corner crack such as might appear in a fastener hole in a plate. It introduces the idea of secondary focal points which relate in part to (1) the shape of the part and (2) the heterogeneity of metallic structural materials. A macroscopic heterogeneity such as is frequently observed in plate materials is the partial discontinuity or delamination as indicated at C' in Figure 9. Its presence has the effect of subdividing the crack front into two segments. On a microscopic scale grain boundaries and other macroscopic discontinuities may act in a similar manner, and the scalloped crack front indicated at DD' is observed. The subdivision of the metal into macro and microscopic crack elements has the effect of increasing the crack front length. Crack front length is increased on a smaller scale still by the involvement of particles as Figure 6 indicates. It will be noted in Figure 6 that the crack segments that develop at different levels overlap one another thus increasing the effective crack front length by deviations out of the fracture plane. These are additional to those resulting from crystallographic tilting although the curvatures that develop will also reduce the measured reflectivity by dispersion. Such curvatures are of considerable interest as they suggest a degree of non-crystallographic behaviour. This aspect has been studied in some depth and the conclusion can be stated as follows:

In a coarse microstructural sense relatively low  $\Delta K$  fatigue cracks may appear to follow crystallographic paths, ie to a first approximation they are planar. However, local perturbations from planarity commonly occur and it is clear that even small deviations of the local principal tensile stress direction can move the crack plane away from the crystal plane. One of the most obvious cases is that resulting from the presence of a particle or some imperfection that initiates a new crack segment (Figure 6) the two pairs of neighbouring crack tips now interact and turn towards one another. This non-crystallographic crack growth follows paths that would be predicted from the linear elastic fracture mechanics solutions for approaching pairs of cracks. The conclusion from these observations must be that fatigue cracks in metals, by producing an intensely disturbed plastic zone in their path lose their propensity for strictly crystallographic growth, although the crystal anisotropy still has some influence on a coarser scale. Polymers, on the other hand, have no equivalent grain anisotropy and thus show no facetting. Apart from the absence of faceted fractures in polymers the other details of fracture are remarkably similar to those in metals, because, as has been stated, the metal fatigue crack is always growing through its own disturbed crystal zone which is virtually amorphous.

Although metals and alloys may deviate from strict crystallographic crack growth the facetting which may be well developed at relatively low stress intensity factors is an indication that preferred planes of fracture exist. As mentioned earlier over-aged aluminium alloys develop very irregular fracture surfaces but even in this condition there are grains so oriented that smoother facets are observed. Figure 10 shows such growth through a grain which is embedded within others that show the typical roughness. In this instance with the crack growing along the long axis of the elongated grain any tendency for faster growth through this grain is largely suppressed because the associated crack front segment is small compared with that front growing in the more irregular manner. If we now compare Figure 10 with Figure 11 where the

crack is growing in the short axis direction of an elongated grain, thus having a long crack front segment, then more rapid growth is observed, as indicated by the positions of the programme markings.

The question of orientation of plate microstructure with respect to crack growth direction has been discussed elsewhere<sup>(2)</sup>, and the relevant crack forms are shown in Figure 12. The crack growth direction in Figure 10 is with the grain boundaries in the crack dividing mode and Figure 11 with them in the crack stopping mode.

### 3 LOADING PATTERNS AND MARKERS

The requirements for an effective marker on a fatigue fracture surface are that it must be resolvable in the optical sense, and unambiguously identifiable against the general pattern of striations.

Resolution, in this context, depends on:

- i The maximum vertical displacement of the feature.
- ii The width of the feature.
- iii The spacing between successive features.

The first relates to the stress intensity factor and the second and third indirectly via the growth rate. In the case of the ground-air-ground cycle all three aspects are bound up with the total shape of the flight cycle.

The first two factors, vertical displacement and width, together control the slope of the fracture surface and from the viewpoint of optical detection this is of particular importance because it is this that causes dispersion, the same comment applies to scanning electron microscopy and to shadowed replicas used in transmission electron microscopy.

The importance of spacing between the markers is self-evident and is a straightforward question of resolution, but as it is important that markers shall be detectable down to the smallest crack depths, one requires sufficient spacing at these relatively small stress intensity factors and slow growth rates. Again, with the ground-air-cycle the spacing is directly related to total cycle damage.

Markers can be divided into 3 categories:

- i Ground-air-ground loadings that produce their own natural undulation, where the width of the flight marking depends on the total crack damage per flight.
- ii Markers derived from one or a group of higher than average loadings applied at regular intervals during the fatigue test.
- iii Periods of low damage input applied at regular intervals that will produce more reflective bands as shown in Figure 1.

All of these three categories have been used in various fatigue testing programmes with some success. The first one, which is clearly an essential arrangement in itself, is the ideal because no question of abnormal damage or of retardation arises. The other two must be considered as abnormal arrangements with respect to the service load sequences and, perhaps, some question of abnormal damage conditions might arise. However, such effects could be judged in a very direct manner i.e. by examination of the fracture itself. Certainly groups of higher than average loading may produce some retardation and groups of low loads are followed by a few cycles of excessive crack growth<sup>(3)</sup> but these effects are quantifiable by fractography itself and need cause no problems. Finally, referring back to Figure 1, the low level loading block that had been applied was constant in amplitude and numbers and yet the width of the band it produced (smooth, reflective fracture) clearly does not expand with crack depth in a manner that would be expected while the high level loading band (rough fracture) does. The probable explanation for the constant band width would seem to be that only a limited range of stress intensity factors cause the 'bright' fracture; below a certain level, perhaps  $K_{th}$ , no growth will occur, and above a certain level the crack changes from a crystallographic Stage II to a non-crystallographic Stage II mode. The programme used consisted of ascending load level blocks so it can be imagined that low level loads can start to contribute as the crack grows to a depth where the  $K$  produced lies within the critical range. Similarly, load levels producing  $K$  values at the top end of the range will move out of the range and become non-crystallographic crack producers as the crack grows. Thus one might expect to see a constant band width as is, in fact, observed.

### 4 CONCLUSIONS

The general conclusions related to the mechanism of fatigue crack growth can be stated as follows:

i Fatigue cracks in metals and alloys extend with crack fronts that may become fragmented, and the degree of fragmentation generally increases with stress intensity factor.

ii There is tendency for fatigue cracks to follow crystallographic paths, but considerable deviations from the planar growth form are observed.

iii Such deviations are the result of heterogeneity of microstructure, and the main feature that results from this is the displaced crack segment whereby new, interacting crack fronts may be produced.

iv Such deviations from the crystal plane are in accordance with predicted changes in the local direction of the principal tensile stresses as indicated by stress analysis.

v Conclusion (iv) leads to the suggestion that fatigue cracks progress through their own highly disturbed plastic zone within which the tendency for crystallographic growth is diminished or even completely suppressed.

vi The fatigue fracture of polymers such as PMMA is similar in many respects to that of metals and alloys where this suppression of crystallographic cracking has occurred.

vii Observations on both metals and alloys emphasise the important role of brittle crack extension during the fatigue cycle. Where it dominates fatigue striations are the product of crack tip deviation rather than opening displacement.

#### REFERENCES

- 1 P. J. E. Forsyth      The relationship between fatigue crack behaviour and micro-  
A. W. Bower            structure in 7178 aluminium alloy.  
Int. J. Fatigue January 1981 p. 17-25
- 2 P. J. E. Forsyth      A unified description of micro and macroscopic fatigue crack  
                              behaviour.  
Int. J. Fatigue January 1983 p. 3-14
- 3 P. J. E. Forsyth      Fatigue crack growth rates for very short cracks developing  
P. M. Powell            at fastener holes in 7075 and 7010 aluminium alloys.  
Journal of Materials Science 18 (1983) p. 1852-1862

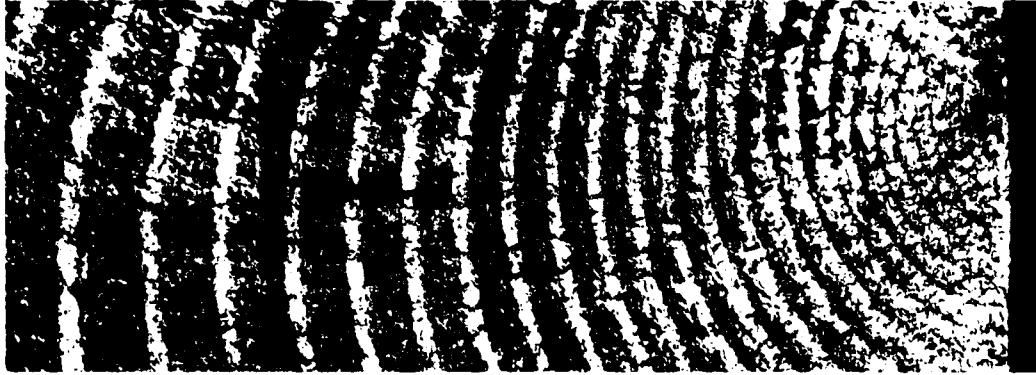


Figure 1 'Programme' markings produced on an Al-Zn-Mg-Cu alloy fatigue fracture surface.

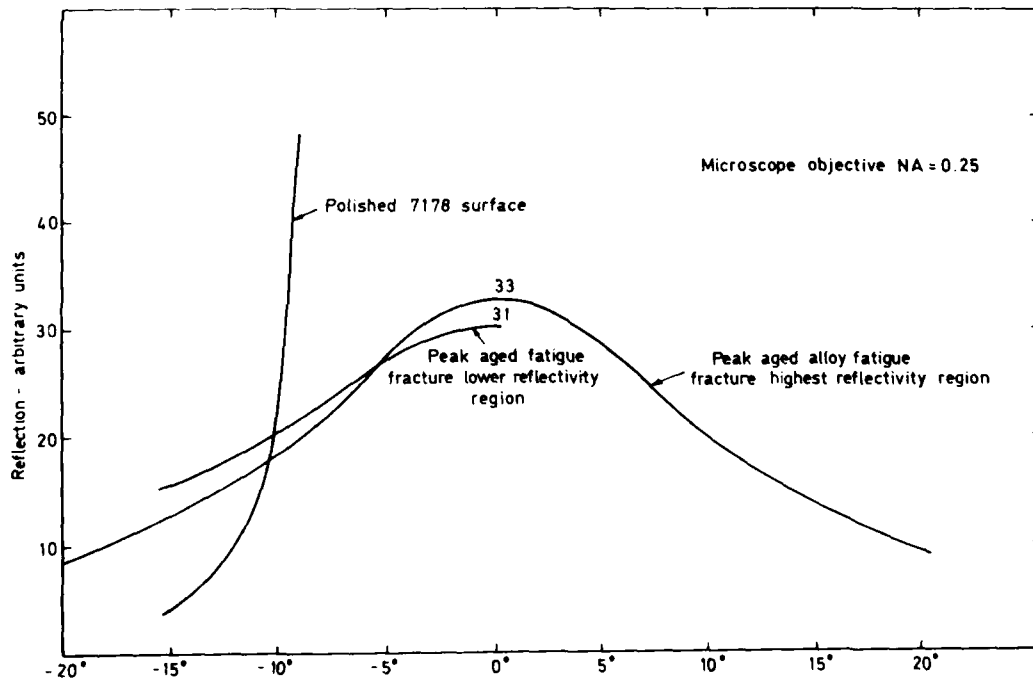


Figure 2 Polar diagram of reflection versus specimen tilt

#### 7.4. Mixed Mode fatigue Crack Growth in 7091-T7E69

An overview and detailed fractographs of mixed mode fatigue crack growth in 7091-T7E69 specimens tested under constant amplitude loading are given in figure 25. The fracture path consisted of roughly horizontal and vertical ledges with numerous secondary cracks. The roughly vertical ledges had a dimpled appearance, as is illustrated in figure 25c, with microvoids mostly  $< 0.5 \mu\text{m}$  or less.

### 8. MICROSTRUCTURAL ANALYSIS

#### 8.1. Transmission Electron Microscopy (TEM)

Thin foils were prepared from 3 mm diameter discs spark machined from the fatigue crack propagation specimens at locations just below the fracture surfaces. Microstructural analysis results are summarised in table 6 and examples are shown in figures 26 and 27: there was no evidence of planar slip in either alloy.

Apart from the finer grain size in 7091-T7E69, the most striking differences between the two alloys were the presence of  $\text{Co}_2\text{Al}_9$  particles and an abundance of elongated clusters of oxides in the PM alloy. The spacing between oxide clusters varied from about  $0.2 - 1 \mu\text{m}$ .

#### 8.2. Textures

(111) and (220) pole figures for both alloys are shown in figure 28. 7050-T736 had a fairly sharp (111) texture, but the texture of 7091-T7E69 was virtually random.

### 9. CONCLUDING DISCUSSION

The fractographic and microstructural results are consistent with the hypothesis proposed earlier and elaborated using Thomason's theory of tensile fracture. Specifically:

- (1) The wide range of  $K_{\text{max}}/K_Q$  values for which tensile crack jumping occurred in 7091-T7E69 can be explained by microvoid nucleation beginning at large or small particles depending on the amount of crack tip blunting, i.e. microvoid nucleation probably begins at large particles during a fracture toughness test, which exhibits more crack tip blunting, but at small particles during fatigue crack propagation testing. The small particles are most probably oxides: the importance of oxides is indicated both by the sheets of small microvoids and by the "layered" fractures, which probably derive from the oxides being present in elongated clusters in the microstructure.
- (2) For 7050-T736 the occurrence of tensile crack jumping at  $K_{\text{max}}/K_Q < 1$  is most probably due to crack tip geometry effects only, i.e. significantly sharper crack tips during fatigue crack propagation testing.
- (3) For 7178-T6 (reference 8) and 7075-T651 and 7075-T7 (reference 9) the occurrence of tensile crack jumping at  $K_{\text{max}}/K_{\text{IC}} \approx 1.0$  is most probably due to crack tip blunting always being limited owing to the presence of many large particles.
- (4) Through-thickness irregularity and microscopic branching and kinking of the fatigue crack fronts may well have affected the  $K_{\text{max}}$  and  $K_Q$  values for tensile crack extension. However, since the fatigue crack fronts in 7091-T7E69 were, if anything, more irregular and branched than those in 7050-T736 (e.g. compare figures 18 and 19) these geometric effects would have tended to reduce the differences in tensile crack jumping behaviour between the two alloys.

The fractographic and microstructural results also provide some insight into the mixed mode fatigue crack growth in 7091-T7E69 tested under constant amplitude loading at  $R=0.1$ . Neither planar slip nor texture, which was virtually random, could have played a role. On the other hand, the crack growth that appeared to take place by modes I and II was actually a combination of fatigue crack growth on roughly horizontal ledges and sheets of microvoids on nearly vertical ledges. These sheets of microvoids probably corresponded to elongated clusters of oxides in the microstructure.

Noting in addition the macroscopically brittle behaviour of 7091-T7E69 in a fracture toughness test, as discussed earlier, we conclude that the presence of a relatively high volume fraction of small oxide particles had a profound effect on the fatigue crack propagation and fracture properties of this alloy. In particular, the fatigue crack propagation resistance under spectrum loading was greatly inferior to that of several IM alloys, represented by 7050-T736 in the present work.

The poor fatigue crack propagation behaviour of 7091-T7E69 constitutes a major limitation to its use in engineering structures. A potential remedy might be to prepare the powder in inert environments rather than in air. However, this may lead to unacceptable losses in strength. Further research should consider these aspects, both for 7091 and other PM alloys.

### 10. ACKNOWLEDGEMENTS

This investigation was performed with the sponsorship of the Netherlands Agency for Aerospace Programs (NIVR). The assistance of Drs. A.W. Bowen and C.J. Peel in obtaining pole figures is greatly appreciated. H.N. Huisman and K.A. van der Sijde assisted with the fractographic and microstructural work.

almost immediately away from perpendicular to the loading direction. Crack propagation appeared to take place macroscopically at first by modes I + II and later by modes I + III. The reason for this behaviour is unknown. A similar phenomenon has been found for an aluminium-lithium alloy and has been correlated with a tendency for deformation by planar slip, reference 26. Material texture may also play a role. In any event, the present results indicate that the combination of crack propagation modes increased the resistance to tensile crack jumping.

#### 6.5. Suggestions for Fractographic and Metallographic Investigations

In view of the preceding discussions in chapter 6 the following fractographic and metallographic features are of primary importance:

- (1) Stretch zones between fatigue crack fronts and tensile crack extension. Stretch zones can provide evidence of the amount of crack tip blunting.
- (2) Microvoid sizes and distributions ahead of the fatigue crack fronts.
- (3) The particles responsible for small microvoids.
- (4) Microstructural analysis, especially particle sizes and compositions of small particles.
- (5) Mixed mode (I+II, I+III) fatigue crack growth in 7091-T7E69, notably fractography and any evidence of planar slip in the microstructure.
- (6) Material textures at the locations of fatigue crack growth.

In addition, other features of interest are fatigue crack front branching, kinking, through-thickness irregularity and the general characteristics of fatigue fracture.

### 7. FRACTOGRAPHY

#### 7.1 Macroscopic Appearances

Representative fracture surfaces for the IM 7050-T736 and PM 7091-T7E69 fracture toughness specimens are given in figure 13. There were two major differences:

- (1) For 7091-T7E69 the fracture surfaces of the fatigue precracks and tensile crack extensions were more regular. This is most probably the result of the very fine grain size, reference 5.
- (2) In the LS specimen orientation the tensile crack extension deviated out of the LS crack plane, especially for 7050-T736, as figure 13 illustrates.

Comparisons of representative fracture surfaces for the fatigue crack propagation specimens are given in figures 14-17. These figures show only the first part of crack propagation, up to half crack lengths ~ 22-23 mm. For 7050-T736 these fracture surfaces were due entirely to fatigue crack growth. However, for 7091-T7E69 it can be seen that except for constant amplitude loading with  $R = 0.1$  (figure 14) the fracture surfaces were a mixture of fatigue crack growth and tensile crack jumps. This difference is especially brought out by spectrum loading (figures 16,17) for which complete failure of 7091-T7E69 specimens occurred after only a few millimetres of fatigue crack growth and tensile crack jumps.

#### 7.2. Stretch Zones

Fatigue crack propagation specimens of 7050-T736 and 7091-T7E69 and LS orientation fracture toughness specimens of 7050-T736, 7091-T7E69 and 7075-T73 were examined by scanning electron fractography. (7075-T73 was included in order to check whether the presence of many more large particles resulted in a narrower stretch zone and hence less crack tip blunting before tensile crack extension as compared to 7050-T736.)

The maximum and minimum widths of stretch zones at the start of tensile crack extension were measured from fractographs and are given in table 5. Examples are shown in figures 18-22.

Insofar as stretch zone widths are a measure of crack tip blunting, the results indicate the following trends:

- (1) Crack tip blunting before tensile crack extension was less in 7091-T7E69 and 7075-T73 than in 7050-T736.
- (2) Crack tip blunting before tensile crack extension was less during fatigue crack propagation testing than during fracture toughness testing.

#### 7.3. Microvoids Ahead of Fatigue Crack Fronts

Representative views of microvoids ahead of the fatigue crack fronts and stretch zones in 7050-T736 and 7091-T7E69 are given in figures 23 and 24. For 7050-T736 the tensile fracture surfaces consisted mainly of large microvoids ~ 6  $\mu\text{m}$  in diameter with occasional sheets of small voids ~ 0.5  $\mu\text{m}$  in diameter. Energy dispersive analysis of X-rays showed that particles responsible for large voids contained Al, Fe and Cu, i.e. they were probably  $\text{Al}_7\text{Cu}_2\text{Fe}$  inclusions (reference 27).

For 7091-T7E69 the tensile fracture surfaces exhibited a "layered" appearance caused by sheets of small microvoids at high angles to the macroscopic plane of fracture. Most voids were less than 0.5  $\mu\text{m}$  in diameter, but larger voids were also present.

Figure 12 shows how these hypothetical conditions can be related to fracture toughness testing and tensile crack jumping during fatigue testing. During fracture toughness testing significant fatigue pre-crack blunting usually occurs. This results in shallower normal stress and strain gradients and a region of triaxiality that extends for a considerable distance ahead of the crack. In this case the onset of tensile fracture is most probably determined by microvoid nucleation at large particles.

On the other hand, if the fatigue crack tip remains fairly sharp prior to a tensile crack jump, the onset of tensile fracture may or may not be determined by microvoid nucleation at small particles. Consider the first possibility: this requires the presence of a relatively high volume fraction of small particles such that the spacing between them,  $d_s$ , is so small that they are on average much closer to the crack tip than large particles. Consequently, the small particles are much more likely to be found in the region of highest triaxiality, which is close to the crack tip because of its sharpness. The combination of a fairly sharp crack tip and microvoid nucleation at small particles close to it may result in the nominal  $K_{max}$  for tensile crack jumping being well below  $K_{IC}$  or  $K_Q$ . However, if there are insufficient numbers of small particles (the second possibility) the onset of tensile fracture will still be determined by microvoid nucleation at large particles, and nominal  $K_{max}$  values below  $K_{IC}$  or  $K_Q$  must be attributable to crack tip geometry effects only.

This hypothesis provides a potential answer to question (1) listed at the beginning of chapter 6. With some additional information, as will be discussed, it is also possible to give potential answers to questions (2), (3), (4) and (6) as well.

An important feature of the PM alloy 7091 is the presence of many small oxide particles (0.01 - 0.05  $\mu$ m) in the microstructure owing to air atomization of the powder. These particles most probably lower the fracture toughness, reference 22, but it is also possible that they facilitate tensile crack jumping during fatigue. This is primarily because of their abundance (1 - 2 volume %, reference 23) which signifies a very small  $d_s$  value. However,  $\epsilon_f$  may also be relatively low compared to that of other small particles, since the oxide particles are brittle and likely to have weak interfaces with the matrix.

The presence of oxide particles therefore provides a potential explanation of the especially low  $K_{max}/K_Q$  values at which tensile crack jumping occurred in 7091-T7E69. Also, it means that the spectrum loading fatigue crack propagation resistance should be improved by powder atomization in inert environments.

Another aspect that can be ascribed to the presence of oxides in 7091-T7E69 is the macroscopically brittle behaviour as evidenced by the load-displacement records for fracture toughness testing. It has been shown theoretically (reference 24) that a dense population of small microvoids (e.g. nucleating at oxide particles in 7091-T7E69) can greatly reduce the macroscopic ductility. Thus although microvoid nucleation may occur first at large particles (upper diagram in figure 12) the resulting local strain concentration soon causes microvoid nucleation at the nearest small particles, and so on. In other words, once microvoid nucleation occurs only a slight increase, if any, in macroscopic strain is sufficient for the nucleation, growth and coalescence of many microvoids to cause tensile fracture. Note that this explanation requires the possibility of macroscopic straining being necessary after microvoid nucleation has occurred. This is a complication which limits the predictive capability of Thomason's theory but does not necessarily invalidate it, especially if the crack tip is sharp (reference 25).

Considering now the tensile crack jumping results for 7178 and 7075 alloys, i.e.  $K_{max}/K_{IC}$  consistently  $\approx 1.0$ , it is known that these materials contain many more large particles than the newer alloys like 7050 and 7091. This means that the spacing between large particles,  $d_l$ , is much less for 7178 and 7075. Consequently large particles in these alloys are on average closer to the fatigue crack tip and so is the knee in the fracture strain curve. Thus it is probable that the onset of tensile fracture is always determined by microvoid nucleation at large particles, and also that the amount of crack tip blunting is always limited such that tensile crack extension takes place at a fairly constant  $K_{max} \approx K_{IC}$  (or  $K_Q$ ).

In enabling potential answers to be given to questions (1) - (4) and (6) listed at the beginning of chapter 6, the foregoing hypothesis raises a new question. Namely, why should a fatigue crack sometimes blunt much more during fracture toughness testing than during a load cycle that causes tensile crack jumping?

The most likely explanation involves cyclic strain hardening. High strength aluminium alloys cyclically strain harden, and the material ahead of a fatigue crack tip will be "conditioned" such that as long as  $K_{max}$  in the next load cycle is not much higher than in previous cycles the crack tip remains fairly sharp. However, if  $K_{max}$  in the next load cycle greatly exceeds previous  $K_{max}$  values, the material ahead of the fatigue crack tip will strain monotonically over a large part of the load cycle and the crack tip will blunt.

The experimental results from the present investigation support this explanation. For fatigue the  $K_{max}$  values during load cycles causing tensile crack jumping could not have exceeded average  $K_{max}$  values in previous load cycles by factors more than about 1.5 (MINITWIST) and 1.4 (FALSTAFF). These factors are based on the total shape of each spectrum, see e.g. reference 4, and since peak loads occur in severe flights the factors are probably too high. On the other hand, the records for fracture toughness testing showed that  $K_Q$  exceeded the fatigue precrack  $K_{max}$  by factors of 4.2 (7050-T736) and 2.2 - 3.0 (7091-T7E69).

Finally, question (5) at the beginning of chapter 6 remains to be answered. As mentioned in section 5.3, for the 7091-T7E69 alloy tested under constant amplitude loading at  $R=0.1$  the fracture path deviated

which link up to the crack and each other via sheets of small voids nucleated at dispersoids. From this qualitative description two factors are evident:

- (1) Crack tip blunting is important. Blunting will be beneficial to fracture toughness since it lowers the maximum normal stress and strain ahead of the crack. Therefore void nucleation, growth and coalescence will require higher remote stresses.
- (2) The sizes and spacings of particles will greatly affect fracture toughness. Larger particles and higher volume fractions of particles and dispersoids (i.e. decreased spacings between particles and dispersoids) will be detrimental.

These factors are interrelated. Crack tip blunting depends not only on the matrix ductility but also on the ease with which voids nucleate, grow and coalesce with the crack tip: at that instant blunting ceases.

Grain size and fibering also have an influence on the resistance to static crack extension in aluminum alloys. A larger grain size lowers the fracture toughness in overaged 7000 series alloys, reference 18. This effect correlates with an increase in the amount of intergranular microvoid coalescence, which in turn is due to the presence of coarser and more numerous grain boundary precipitates, reference 17. Fibering results in alignment of grains, particles and dispersoids in the plane normal to the short transverse (S) direction. The fracture toughness in this plane (specimen orientations SL and ST) is therefore usually much less than that in other orientations.

### 6.3. The Probability of Microvoid Coalescence as a Function of K

A simple statistical analysis (references 19,20) has shown that the probability of tensile crack extension by microvoid coalescence depends strongly on whether overall crack growth can take place by one or more mechanisms.

For example, if crack growth can take place only by a particular process of microvoid nucleation and coalescence, then there is a sudden increase in the probability of tensile crack extension at a critical nominal value of K. (The qualification "nominal" is added in view of possible crack tip geometry effects, see section 6.1.)

On the other hand, if there is more than one mechanism available for crack growth, e.g. fatigue striation formation and microvoid coalescence, then it is possible for tensile crack extension to occur over a wide range of nominal K values.

### 6.4. An Hypothesis for "Premature" Tensile Crack Jumping

The transition from fatigue crack propagation to tensile crack jumping at nominal  $K_{max}$  values significantly less than  $K_Q$  is distinct, i.e. the jumps do not take place by a mixture of fatigue and tensile fracture mechanisms, references 8 and 9. Therefore the occurrence of crack jumping over a wide range of nominal  $K_{max}$  values must be due to two (or more) processes of tensile fracture and/or any variation in actual K values owing to crack tip geometry effects.

In fact, it is most probable that both factors, i.e. different fracture processes and crack tip geometry effects, were responsible in the case of 7091-T7E69. This is because:

- (1) It is very unlikely that crack tip geometry effects could be the sole cause of the wide ranges of nominal  $K_{max}/K_Q$  values for which tensile crack extension occurred (0.34 - 1.0).
- (2) There is no reason why different tensile fracture processes should initiate from geometrically similar crack fronts.

The following hypothesis is proposed: There are at least two processes by which tensile fracture can occur, and the choice of fracture process depends to some extent on the fatigue crack tip geometry immediately before tensile fracture. To be more specific it is necessary to consider the achievement of critical strains for microvoid nucleation, growth and coalescence to give tensile crack extension ahead of the fatigue crack tip.

Thomason (reference 21) has developed a theory for which tensile fracture begins ahead of the crack tip at a point where triaxiality reduces the strain after tensile instability to zero. (Tensile instability is here defined as the commencement of the process of microvoid growth and coalescence.) The conditions leading to incipient tensile fracture ahead of the crack tip are illustrated in figure 10:  $\epsilon_1$  is the strain at tensile instability and  $\epsilon_f$  is the total strain to fracture. Increasing triaxiality away from the crack tip causes  $\epsilon_f$  to decrease steeply such that there is a "knee" in the fracture strain curve. Incipient tensile fracture occurs when  $\epsilon_y$  becomes equal to  $\epsilon_1$  at the knee. The position of the knee depends on the triaxiality distribution ahead of the crack (and hence on crack tip blunting), the volume fraction of nucleated microvoids and the value of  $\epsilon_1$ .

Thomason's theory, which has been fairly successful in predicting experimental trends for ductile fracture and fracture toughness, is nevertheless a simplification. The theory assumes the microvoids to be of one size and uniformly spaced. Also, no distinction is made as to the sites at which microvoids nucleate. It is these aspects, together with crack tip geometry, that may be crucial to explaining the present results for the differences between  $K_{max}$  for tensile crack jumping and  $K_Q$ .

Figure 11 extrapolates from Thomason's theory to show hypothetical conditions for tensile crack extension that begins by microvoid nucleation at large or small particles, depending on the amount of prior crack tip blunting. These hypothetical conditions are entirely reasonable if the volume fraction of small particles (and hence small microvoids) is relatively high.

ile crack jumping could immediately be determined. However, for spectrum loading it was necessary first to use the crack propagation records to check which severe flight (and hence peak stress) corresponded most closely to the start of crack jumping.

The calculated  $K_{max}$  values at the start of tensile crack jumping are given in table 4: note that there is ambiguity in two cases. A comparison with table 3 shows that tensile crack jumping in 7091-T7E69 alloy began at  $K_{max}/K_Q$  values as low as 0.34. For 7050-T736 the minimum value of  $K_{max}/K_Q$  is 0.64.

Studies of tensile crack jumping (references 8,9) have assumed that it begins when  $K_{max} \sim K_{IC}$ . The present work shows (assuming that  $K_Q$  can be substituted for  $K_{IC}$ ) that this is not always so.

## 6. POSSIBLE REASONS FOR THE "PREMATURE" OCCURRENCE OF TENSILE CRACK JUMPING

In this section an attempt will be made to indicate the most likely cause of tensile crack jumping commencing in the present tests at  $K_{max}$  values well below  $K_Q$ . The discussion leads to a working hypothesis which served as a background to the detailed fractographic and metallographic investigations that are described in sections 7 and 8.

There are several questions that arise from the results so far:

- (1) Why was  $K_{max}$  for the commencement of tensile crack jumping significantly less than  $K_Q$  for 7050-T736 and 7091-T7E69 in the present tests?
- (2) Why was  $K_{max}/K_Q$  for the commencement of tensile crack jumping especially low for 7091-T7E69 ?
- (3) In view of the present results, why was  $K_{max} \sim K_{IC}$  for 7178-T6 (reference 8) and 7075-T651 and 7075-T7 (reference 9)?
- (4) Why, as evidenced by the load-displacement records for fracture toughness testing, was the behaviour of 7091-T7E69 macroscopically much more brittle than that of 7050-T736 and other IM alloy specimens?
- (5) Why did tensile crack jumping not occur in 7091-T7E69 during constant amplitude fatigue crack propagation tests with  $R=0.1$  ?
- (6) Is there any way in which the spectrum loading fatigue crack propagation resistance of 7091-T7E69 can be improved?

The  $K$  value at the onset of tensile crack extension is influenced by crack tip geometry and microstructural effects. The geometric effects are crack tip blunting, branching and kinking, through-thickness irregularity, and a change of mode (e.g. mode I + modes I + III). Microstructural effects arise through the choice of fracture path (transgranular and/or intergranular), the presence of inclusions, particles and precipitates, the grain size, and fibering and texturing owing to mechanical working.

### 6.1. The Effects of Crack Tip Geometry

Crack tip blunting always occurs and most cracks exhibit at least small amounts of branching, kinking and through-thickness irregularity.

Crack tip blunting may be very limited or extensive. Blunting has a minor effect on the size and shape of the plastic zone (reference 10). However, for plane strain conditions the distributions of stress and intense strain ahead of the crack tip may be greatly altered. This is schematically illustrated in figure 7. Increased blunting decreases the maximum stress and moves its location away from the crack tip towards the elastic-plastic boundary. Also, the strain gradient within the plastic zone is much less steep and the region of intense plastic strain extends much further from the crack tip.

Microscopic crack branching, kinking and through-thickness irregularity commonly occur. Their significance in fracture mechanics terms is often overlooked. Any of these features will lower the mode I stress intensity factors at crack tips. This is illustrated for branched and kinked cracks in figure 8.

A high degree of through-thickness irregularity has been reported to raise  $K_{IC}$  by as much as 50 % for a titanium alloy, reference 14, but more typical increases for aluminium alloys would appear to be 5 - 15 %, reference 15.

Finally, a change in crack plane orientation from mode I to modes I + III (often called the flat-to-slant transition) has been shown to considerably enhance the resistance to tensile crack jumping, reference 16. Usually this is the consequence of increased fracture toughness owing to a change from predominantly plane strain to predominantly plane stress conditions. However, if the flat-to-slant transition occurs under plane strain conditions this explanation cannot apply.

### 6.2. The Effects of Microstructure

Tensile crack extension in aluminium alloys typically occurs by transgranular microvoid coalescence, although limited amounts of intergranular microvoid coalescence can occur, especially in overaged (T7X) 7000 series alloys. The microvoids nucleate at various sites, the most important of which are large particles and dispersoids, reference 17.

A schematic of tensile crack extension by coalescence of microvoids nucleated at particles and dispersoids is given in figure 9. Large particles provide weak spots for the nucleation of large voids,

#### 4. FRACTURE TOUGHNESS

A survey of the fracture toughness test results is given in table 3. Only two of the tests met all the ASTM validity criteria. Most of the invalidations were minor and due to the fatigue precrack front being excessively curved. However, the high  $K_{Ic}$  for LS specimens of 7050-T736 indicates a substantial violation of the specimen thickness criterion: the specimen thickness would have to have been  $\sim 30$  mm for a valid  $K_{Ic}$ .

Table 3 shows that 7050-T736 had a significantly higher fracture toughness than 7091-T7E69, especially in the LS orientation. As in the tensile tests, the 7091-T7E69 alloy was more isotropic.

As mentioned in the introduction to this paper, the load-displacement records for fracture toughness testing showed that 7091-T7E69 specimens failed macroscopically in a much more brittle manner than IM alloy specimens. An example of this difference, notably for the LS orientation specimens of 7050-T736 and 7091-T7E69 is presented in figure 4.

#### 5. FATIGUE CRACK PROPAGATION

##### 5.1 Types of Loading

Three types of fatigue loading were used to determine the fatigue crack propagation behaviour:

- (1) Constant amplitude loading with stress ratios ( $R = \sigma_{\min}/\sigma_{\max}$ ) of 0.1 and 0.5.
- (2) Gust spectrum loading (MINITWIST).
- (3) Manoeuvre spectrum loading (FALSTAFF).

Descriptions of the two types of spectrum loading have been given in previous reports (references 5-7) and will be omitted here.

##### 5.2 Test Conditions

All tests were carried out at room temperature in laboratory air (40-60 % relative humidity). Three specimens from each alloy were subjected to each type of loading. The constant amplitude tests were done using a 200 kN AMSLER electrohydraulic machine at a cycle frequency of 16 Hz. The spectrum loading tests were done using a 250 kN MTS electrohydraulic machine at a nominal cycle frequency of 15 Hz. Buckling of the specimens during compression loading was prevented by felt-lined aluminium alloy antibuckling guides which had cutouts for visual observation of the cracks.

The maximum remote stress levels were as follows:

- (1) Constant amplitude,  $R = 0.1$  :  $\sigma_{\max} = 50$  MPa.
- (2) Constant amplitude,  $R = 0.5$  :  $\sigma_{\max} = 65$  MPa.
- (3) MINITWIST truncated to level III:  $\sigma_{\max} = 126.5$  MPa.
- (4) FALSTAFF:  $\sigma_{\max} = 171.3$  MPa.

##### 5.3 Constant Amplitude Loading Results

Constant amplitude fatigue crack propagation data are presented in figure 5. The IM alloy 7050-T736 behaved normally: crack growth occurred in a regular manner, and the macroscopic plane of cracking was perpendicular to the loading direction.

The PM alloy 7091-T7E69 behaved very differently. For  $R=0.1$  the fracture path deviated almost immediately away from perpendicular to the loading direction: the data in figures 5a and 5c refer to "equivalent" crack lengths obtained by projecting the actual crack front onto the plane perpendicular to the loading direction. For  $R=0.5$  the macroscopic plane of cracking started to deviate away from perpendicular to the loading direction, but for two out of three specimens tensile crack jumping commenced after only a few millimetres of fatigue crack propagation.

Figures 5c and 5d show that the crack growth rates in 7091-T7E69 became consistently higher than those in 7050-T736 at a constant  $K_{\max}$  of  $12 \text{ MPa}\sqrt{\text{m}}$ .

##### 5.4 Spectrum Loading Results

Spectrum loading fatigue crack propagation data are presented in figure 6. As before, the 7050-T736 alloy exhibited regular crack growth. However, at longer crack lengths small amounts of tensile crack jumping were associated with peak stresses.

The 7091-T7E69 alloy specimens failed by tensile crack jumping and instability after only a few millimetres of fatigue crack growth. The contrast with 7050-T736 is even more dramatic than for constant amplitude loading at  $R=0.5$  (cf. figure 6 and figure 5b).

##### 5.5 Relation of Tensile Crack Jumping to Fracture Toughness

In several cases it was possible to determine accurately the crack lengths at which tensile crack jumping commenced. This was done by measuring the side surface crack lengths corresponding to tensile crack extension on the fracture surfaces. For constant amplitude loading ( $R=0.5$ ) the  $K_{\max}$  at commencement of tensile

FATIGUE CRACK PROPAGATION AND FRACTURE IN  
7050 AND 7091 ALUMINIUM ALLOY FORGINGS

by  
R.J.H. Wanhill, H.J. Kolkman and L. Schra  
National Aerospace Laboratory NLR  
Emmeloord, The Netherlands

SUMMARY

The fatigue crack propagation and fracture behaviour of 7050-T736 and 7091-T7E69 aluminium alloy die forgings was investigated. Under spectrum loading the fatigue crack propagation resistance of 7091-T7E69 was greatly inferior owing to early commencement of tensile crack jumping, which also occurred under constant amplitude loading with  $R=0.5$ . Early crack jumping could be explained by application of Thomason's theory of tensile fracture. Fractographic and microstructural analysis provided support to this explanation and indicated that the oxides due to air atomization of the powder have a profound effect on the fatigue and fracture properties of 7091-T7E69. It is concluded that the poor fatigue crack propagation behaviour of 7091-T7E69, which is a major limitation to its use in engineering structures, might be remedied by preparing the powder in inert environments. However, this may lead to unacceptable losses in strength.

1. INTRODUCTION

Over the last 15 years the NLR has conducted an extensive programme to characterize the engineering properties of high strength aluminium alloy forgings, e.g. references 1-5. This programme has followed three main developments in high strength aluminium alloy technology, namely:

- (1) Development of alloys with good resistance to stress corrosion and good fracture toughness at strengths equivalent to the T6 condition of older alloys. An example is 7175-T736, which is a specially processed and modified 7075.
- (2) Development of alloys with high strength through thick sections and a good combination of other properties. Examples are 7050 and 7010.
- (3) Development of powder metallurgy (PM) alloys with properties beyond those of ingot metallurgy (IM) alloys. Examples are 7090 and 7091.

The IM alloys so far included in the programme are 7079 (T6 and T7X), DTD 5024 (T6 and T7X), AZ 74.61 (T7X), 7075-T73, 7175-T736, 7050-T736 and 7010-T736. The properties that have been determined include strength, fracture toughness, stress corrosion crack initiation and propagation resistance, and fatigue crack growth resistance under constant amplitude and spectrum loading. Broadly speaking, the latter four alloys were very similar in terms of a balance of properties, although 7050-T736 was superior in resistance to fatigue crack propagation and fracture toughness.

The only PM alloy in the programme has been 7091-T7E69. The behaviour of this alloy differed from that of the IM alloys in several respects. First, the PM alloy exhibited better combinations of strength and resistance to stress corrosion. Second, the load-displacement records for fracture toughness testing indicated that the PM alloy specimens failed macroscopically in a much more brittle manner, although this was not reflected in a much lower fracture toughness. Third, and most important, for spectrum loading the fatigue crack propagation resistance of the PM alloy was greatly inferior.

It was decided to investigate the poor fatigue crack growth behaviour of the PM alloy in more detail, since it is potentially a major limitation to practical use. This paper presents results of the detailed investigation, in which the fatigue crack growth and fracture behaviour of 7091-T7E69 is compared with that of the best representative IM alloy, 7050-T736.

2. MATERIALS AND SPECIMENS

The IM alloy 7050-T736 and PM alloy 7091-T7E69 were supplied in the form of die forgings by ALCOA Cleveland, U.S.A. The chemical compositions were determined by atomic absorption spectrophotometry and are given in table 1 together with the specifications. The Zr and Si contents of 7050 appeared to be too high.

The shape of the forgings and the positions of the fatigue crack propagation and fracture toughness specimens are illustrated in figure 1. The fatigue crack propagation specimens were centre cracked tension (CCT) panels with dimensions and starter notch configuration as shown in figure 2. The fracture toughness specimens were of compact tension (CT) type conforming to ASTM Standard E 399. The CT specimen configuration is shown in figure 3.

Tensile test specimens dimensioned according to ASTM Standard E 8-79 were also machined from the forgings. The tensile axes were L and T, see figure 1.

3. MECHANICAL PROPERTIES

Results of the tensile tests, which were carried out in accordance with ASTM E 8-79, are given in table 2. The 7091-T7E69 alloy was significantly stronger (by 7-17 %) and more isotropic than 7050-T736.

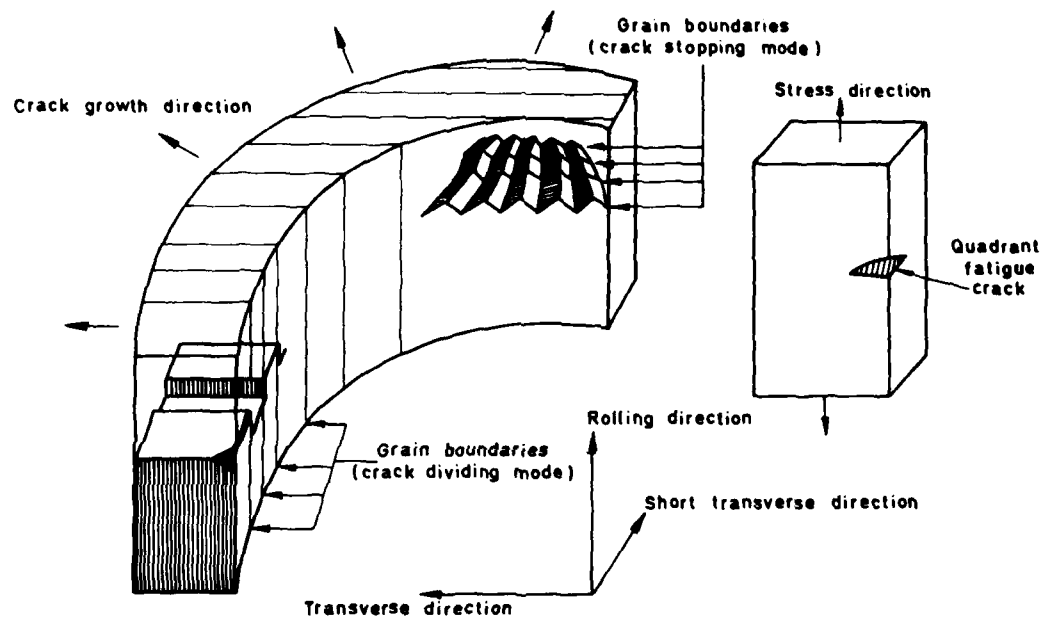


Figure 12 The form of the cracking elements around a quadrant fatigue crack in an aluminium alloy plate

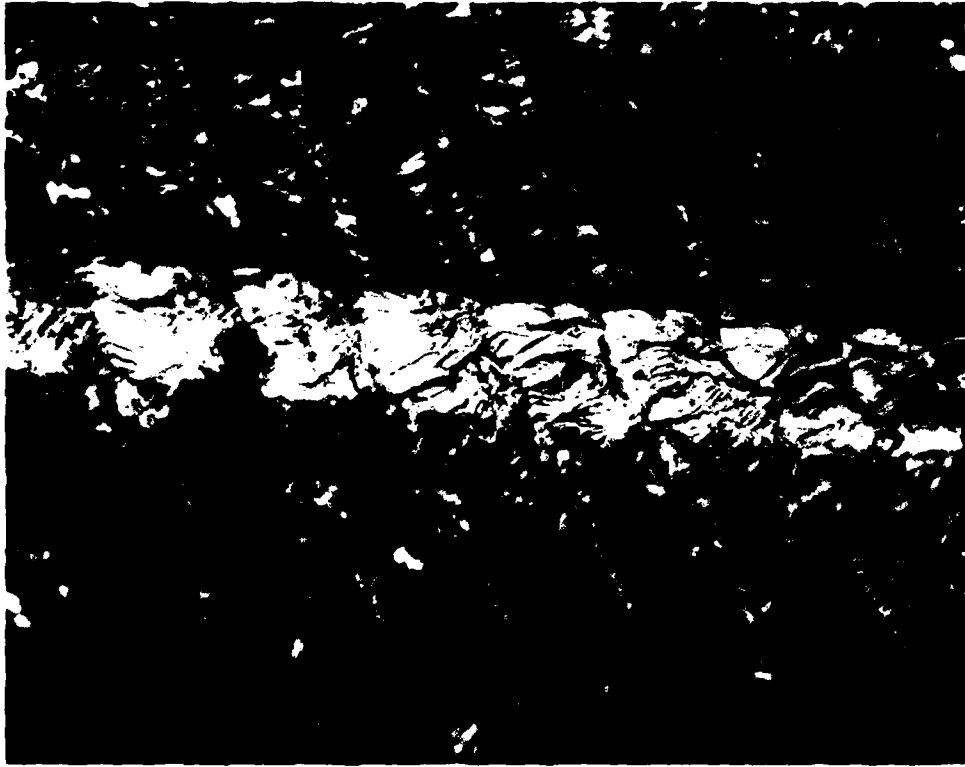


Figure 10) Fatigue fractures in 7010 aluminium alloy x 500 using the simple R ratio  
Figure 11) switching programme used in reference (3)

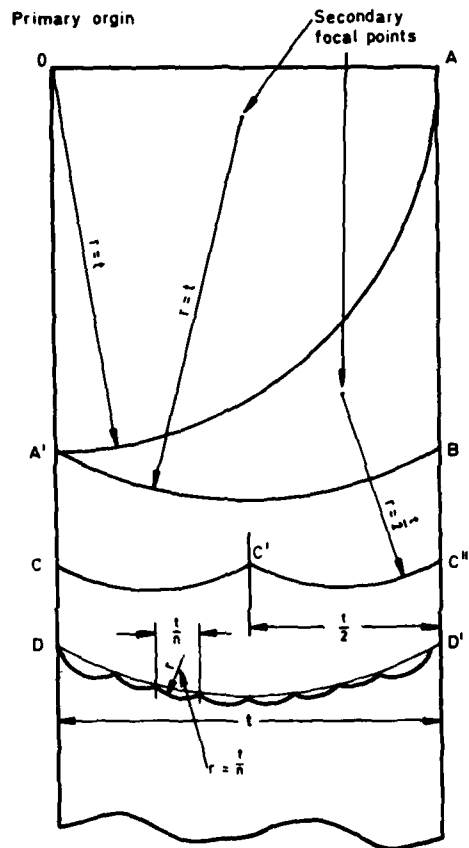


Figure 9 The development of various forms of fatigue crack front

Frequency ratio 16 : 1  
Amplitude ratio 7 : 1

R ratio change  
-0.75 to -1.33

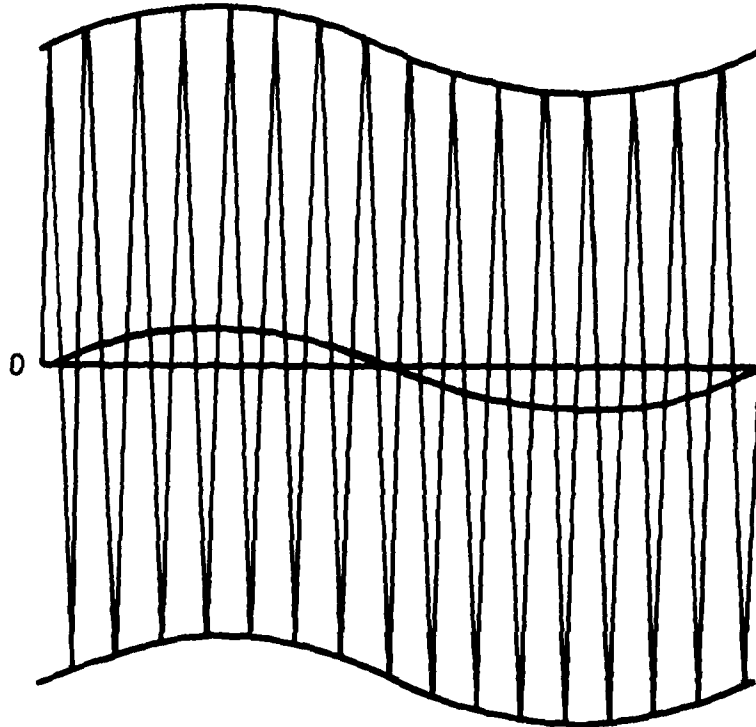


Figure 7 Biharmonic loading pattern

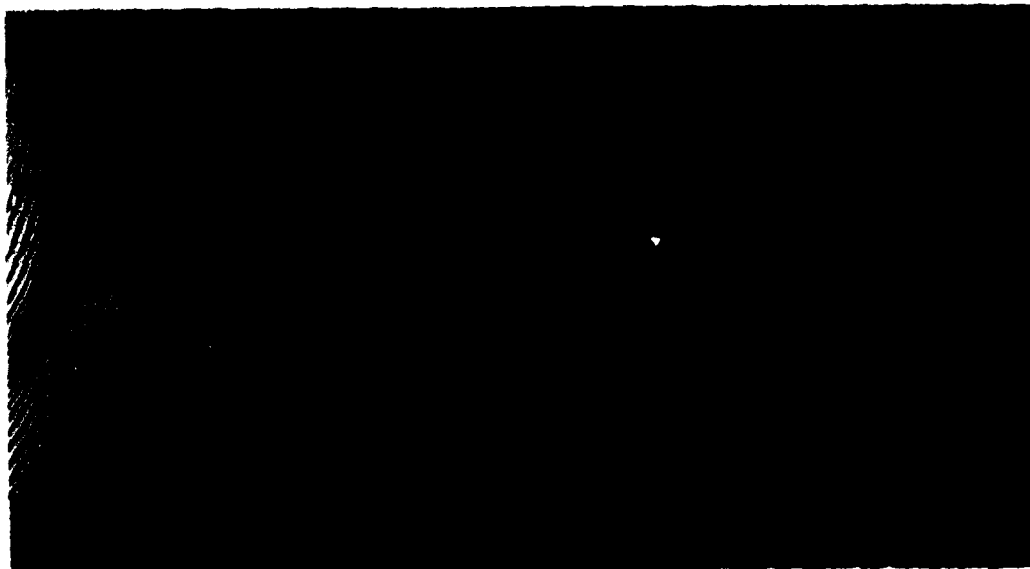


Figure 8 PMMA fracture under biharmonic loading

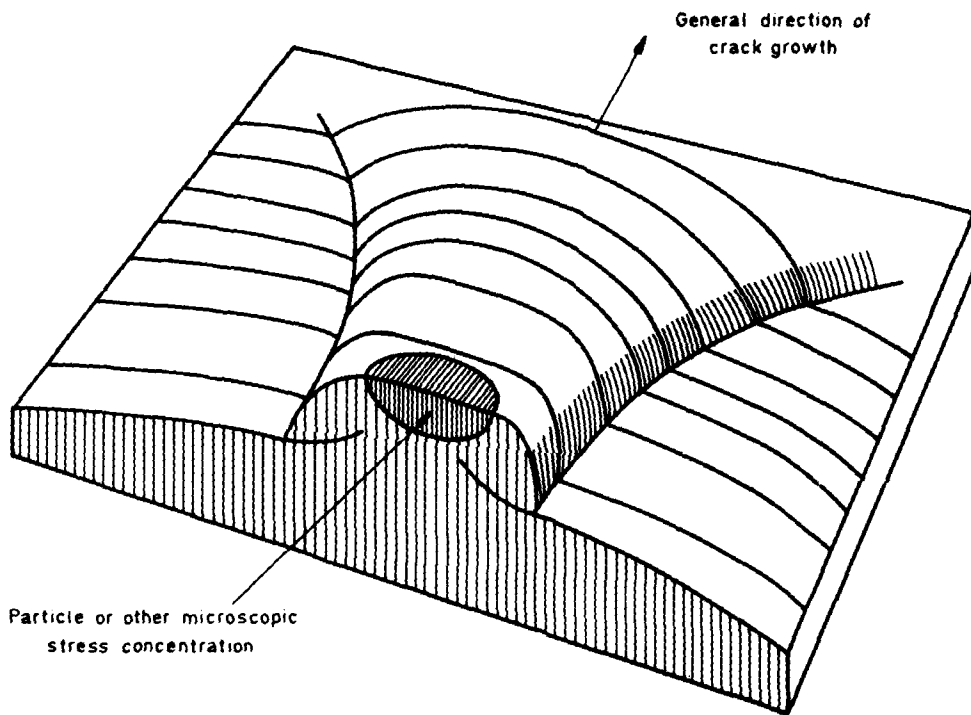
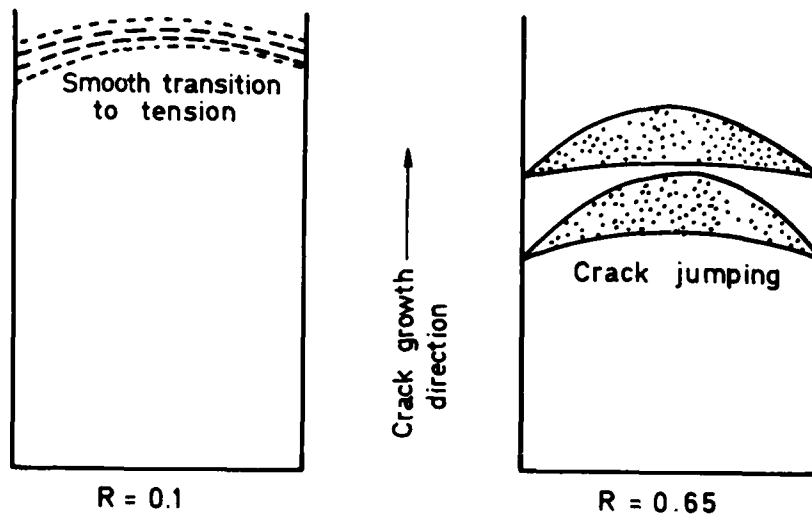


Figure 6 Offset crack originating at particle

## Peak aged 7178



## Over aged 7178

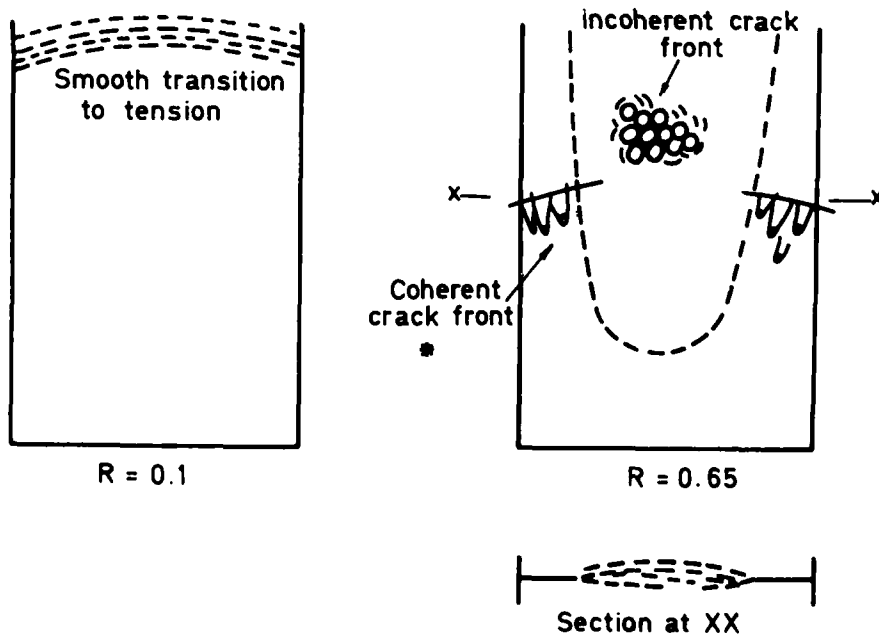


Figure 5 Schematic illustration of fracture features in peak and over-aged conditions

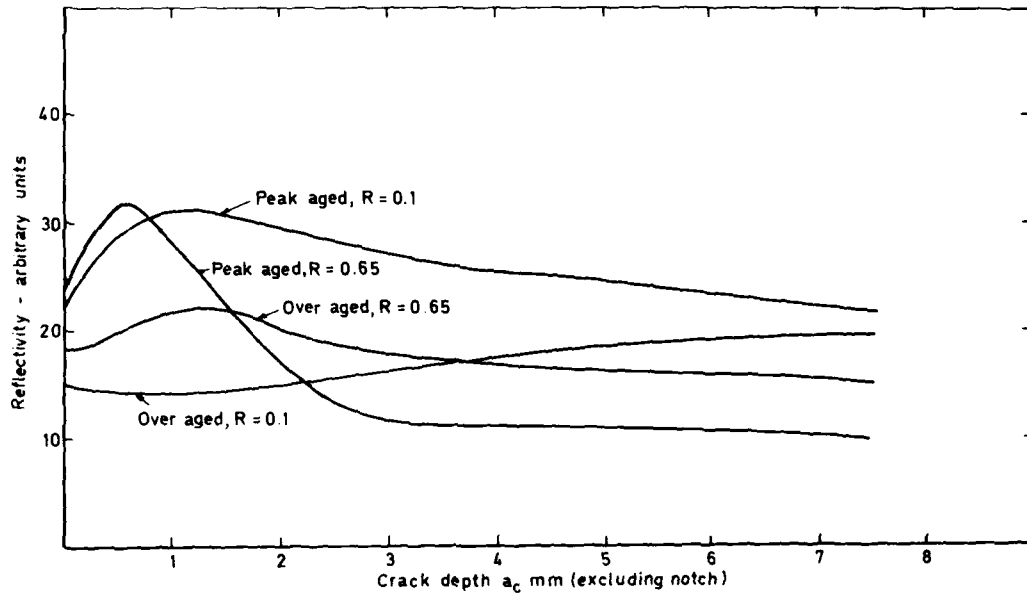


Figure 3 Reflectivity versus crack depth curves

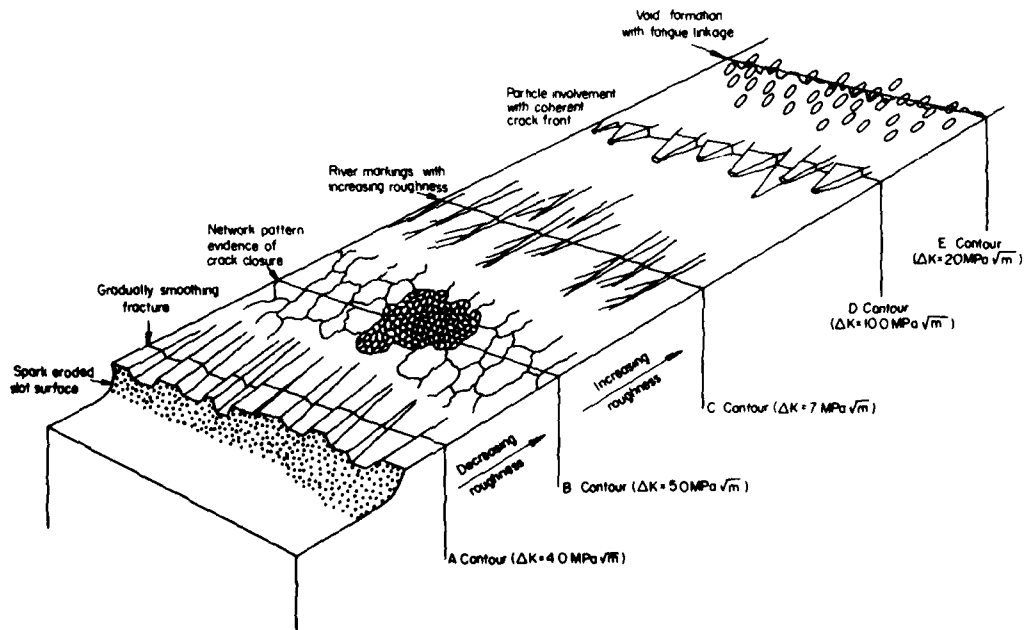


Figure 4 Schematic illustration of the cracking sequence in peak-aged 7178 aluminium alloy R = 0.1

## 11. REFERENCES

1. Van Leeuwen, H.P., Schra, L. and van der Vet, W.J., "The relationship between heat-treatment, micro-structure, and properties of Al-Zn-Mg alloy forgings of the 7079 type", *Journal of the Institute of Metals*, Vol. 100, pp. 86-96 (1972).
2. Van Leeuwen, H.P., Schra, L. and van der Vet, W.J., "Heat treatment studies of Al-Zn-Mg alloy forgings of the DTD 5024 type", NLR TR 72032 U, March 1972.
3. Wanhill, R.J.H., Schra, L. and Van Leeuwen, H.P., "Some engineering property comparisons for 7050 and AZ 74.61 die forgings", *Engineering Fracture Mechanics*, Vol. 11, pp. 507-524 (1979).
4. Schra, L., "Engineering property comparisons for four AlZnMgCu type forging alloys", NLR TR 79022 U, April 1979.
5. Schra, L. and 't Hart, W.G.J., "Engineering property comparisons of PM alloy X7091-17E69 and IM alloy forgings", NLR TR 82054 U, June 1982.
6. Lowak, H., De Jonge, J.B., Franz, J. and Schütz, D., "MINITWIST. A shortened version of TWIST", NLR MP 79018 U, May 1979.
7. "FALSTAFF, Description of a Fighter Aircraft Loading STandard For Fatigue evaluation", combined report of the NLR, LBF, IABG and F+W, March 1976.
8. Forsyth, P.J.E., "The causes of mixed fatigue/tensile crack growth and the significance of microscopic crack behaviour", RAE Technical Report 75143, February 1976.
9. Vlasveld, J.A. and Schijve, J., "Tongue-shaped crack extension during fatigue of high strength aluminium alloys", *Fatigue of Engineering Materials and Structures*, Vol. 3, pp. 129-145 (1980).
10. McGowan, J.J. and Smith, C.W., "A plane strain analysis of the blunted crack tip using small strain deformation plasticity theory", *Advances in Engineering Science*, NASA, Vol. 2, pp. 585-594 (1976): Hampton, Virginia.
11. Rice, J.R. and Johnson, M.A., "The role of large crack tip geometry changes in plane strain fracture", *Inelastic Behaviour of Solids*, McGraw-Hill Book Company, pp. 641-672 (1970): New York.
12. Rice, J.R., "Mechanics aspects of stress corrosion cracking and hydrogen embrittlement", *Stress Corrosion Cracking and Hydrogen Embrittlement of Iron Base Alloys*, National Association of Corrosion Engineers, pp. 11-15 (1977): Houston, Texas.
13. Gerberich, W.W. and Jatavallabhula, K., "Quantitative fractography and dislocation interpretations of the cyclic cleavage crack growth process", *Acta Metallurgica*, Vol. 31, pp. 241-255 (1983).
14. Stubbington, C.A. and Gunn, N.J.F., "Effects of fatigue crack front geometry and crystallography on the fracture toughness of Ti-6Al-4V alloy", RAE Technical Report 77158, October 1977.
15. De Jong, H.F., "Effects of cracklength and crackfront on  $K_{I0}$ -values of aluminium 7075 T651 CT-specimens", Delft University of Technology Report LR-294, February 1980.
16. Wanhill, R.J.H. and Schra, L., "Effects of crack plane orientation transitions on flight simulation fatigue crack propagation in a high strength aluminium alloy (7050)", *Aluminium*, Vol. 53, pp. 430-433 (1977).
17. Wanhill, R.J.H., "Microstructural influences on fatigue and fracture resistance in high strength structural materials", *Engineering Fracture Mechanics*, Vol. 10, pp. 337-357 (1978).
18. Rosenfield, A.R. and McEvily, A.J., "Some recent developments in fatigue and fracture", *Metallurgical Aspects of Fatigue and Fracture Toughness*, AGARD Report No. 610, pp. 23-54, December 1973.
19. Rhodes, D., Radon, J.C. and Culver, L.E., "Analysis of combined static and fatigue crack growth data", *Fatigue of Engineering Materials and Structures*, Vol. 4., pp. 49-63 (1981).
20. Rhodes, D., Nix, K.J. and Radon, J.C., "Void coalescence during fatigue crack growth", *Fracture and the Role of Microstructure*, Engineering Materials Advisory Services, Vol. II, pp. 443-448 (1982): Warley, West Midlands, U.K.
21. Thomason, P.F., "A theoretical relation between  $K_{IC}$  and basic material properties in ductile metals", *International Journal of Fracture Mechanics*, Vol. 7, pp. 409-419 (1971).
22. Lyle, J.P. and Cebulak, W.S., "Powder metallurgy approach for control of microstructure and properties in high strength aluminium alloys", *Metallurgical Transactions A*, Vol. 6A, pp. 685-699 (1975).
23. Zedalis, M. and Fine, M.E., "The effect of aluminium oxide particles and precipitate type on near-threshold fatigue crack propagation rate in P/M 7XXX aluminium alloys", *Scripta Metallurgica*, Vol. 16, pp. 1411-1414 (1982).
24. Melander, M. and Ståhlberg, U., "The effect of void size and distribution on ductile fracture", *International Journal of Fracture*, Vol. 16, pp. 431-440 (1980).
25. Thomason, P.F., *Personal Communication from the University of Salford*, August 1983.

26. Peel, C.J., Personal Communication from the RAE, July 1983.
27. Staley, J.T., "Microstructure and toughness of high-strength aluminium alloys", Properties Related to Fracture Toughness, ASTM STP 605, pp. 71-103 (1976): Philadelphia, Pennsylvania.

TABLE 1: CHEMICAL COMPOSITIONS OF THE FORGINGS IN WEIGHT %

ELEMENT	7050-T736		7091-T7E69	
	SPECIFICATION	MEASURED	SPECIFICATION	MEASURED
Zn	5.7 - 6.7	5.88	5.8 - 7.1	6.36
Mg	1.9 - 2.6	2.08	2.0 - 3.0	2.43
Cu	2.0 - 2.6	2.08	1.1 - 1.8	1.52
Mn	0.1 max	< 0.01	-	-
Cr	0.04 max	< 0.01	-	-
Zr	0.08-0.15	0.17, 0.16*	-	-
Co	-	-	0.2 - 0.6	0.40
Si	0.12 max	0.14, 0.14*	0.12 max	0.07
Fe	0.15 max	0.06	0.15 max	0.06
Ti	0.06 max	0.02	-	-

\* REPEAT MEASUREMENTS

TABLE 2: MECHANICAL PROPERTIES

7050-T736				7091-T7E69			
0.2 % PROOF STRESS (MPa)		UTS (MPa)		0.2 % PROOF STRESS (MPa)		UTS (MPa)	
L	T	L	T	L	T	L	T
486	446	543	505	529	513	570	560
478	446	536	504	523	505	566	555
475	432	528	493	528	512	572	562
460	430	516	493	528	516	573	564
475	439	531	499	527	512	570	560

TABLE 3: FRACTURE TOUGHNESS VALUES

MATERIAL	LT ORIENTATION		TL ORIENTATION		LS ORIENTATION	
	$K_{Ic}$ (MPa $\sqrt{m}$ )	CRITERIA NOT MET*	$K_{Ic}$ (MPa $\sqrt{m}$ )	CRITERIA NOT MET*	$K_{Ic}$ (MPa $\sqrt{m}$ )	CRITERIA NOT MET*
7050-T736	42.3	1	37.5	1	51.5	1,2,4
	40.8	1	36.7	4	50.2	1,2,3,4
	42.0	1	36.9		51.9	1,2
	42.2	1	36.6	3		
7091-T7E69	27.8	4	29.3	4	28.2	3,4
	27.4	4	30.5	4	30.6	
	32.6	4	33.9	4	30.3	3,4
	32.1	4	35.5	4		

\* ASTM CRITERIA FOR A VALID  $K_{Ic}$ 

- (1) Specimen thickness  $B > 2.5 (K_{Ic}/\sigma_{ys})^2$ .
- (2) Load ratio  $P_{max}/P_Q < 1.10$ .
- (3) Difference between any two of three crack length measurements shall not exceed 5 % of the average crack length.
- (4) Surface crack length shall be not less than 90 % of the average crack length.

TABLE 4:  $K_{max}$  AT THE START OF TENSILE CRACK JUMPING (LS ORIENTATION)

MATERIAL	CONSTANT AMPLITUDE, R=0.5	MINITWIST		FALSTAFF	
	$K_{max}$ (MPa $\sqrt{m}$ )	FLIGHT NUMBER	$K_{max}$ (MPa $\sqrt{m}$ )	FLIGHT NUMBER	$K_{max}$ (MPa $\sqrt{m}$ )
7050-T736	-	9656	36.7	2232	37.4
	-	9656	33.4	1832	36.6
	-	9656	33.4	1832	37.4
7091-T7E69	-	1653	13.0	160 or 173	18.3 or 19.9
	13.0	1099	13.3	200	17.7
	10.3	1653	13.5	26 or 32	17.6 or 19.2

TABLE 5: STRETCH ZONE WIDTHS AT THE START OF TENSILE CRACK EXTENSION (LS ORIENTATION)

TEST SPECIMENS AND CONDITIONS		APPROXIMATE RANGES OF STRETCH ZONE WIDTHS ( $\mu m$ )		
		7050-T736	7091-T7E69	7075-T73
FRACTURE TOUGHNESS		40-140	0-12	10-33
FATIGUE CRACK PROPAGATION	CONSTANT AMPLITUDE, R=0.5	-	0-5.5*	
	MINITWIST	8-20	0-6.5*	
	FALSTAFF	8-17.5	0-5.5	

\* ISOLATED EVIDENCE: STRETCH ZONES OFTEN NOT VISIBLE

TABLE 6: TEM MICROSTRUCTURAL ANALYSIS OF 7050-T736 AND 7091-T7E69

MICROSTRUCTURAL FEATURES	7050-T736	7091-T7E69
GRAIN SIZE	$\sim 20 \mu m$	$\sim 5 \mu m$
DISPERSOIDS	coherent spherical $Al_3Zr$ , 12 nm diameter	incoherent spherical $Co_2Al_9$ , 100-250 nm diameter
OXIDES	-	elongated clusters of particles 20-50 nm diameter
FINE MATRIX PRECIPITATES	coherent $n'$ ; incoherent $n$ platelets 10 x 50 nm max	coherent $n'$ ; incoherent $n$ platelets 6 x 25 nm max
COARSE MATRIX PRECIPITATES	low density of $n$ in various shapes with sizes $\sim 200$ nm	-
GRAIN BOUNDARY PFZ WIDTH	$\sim 55$ nm	$\sim 35$ nm
GRAIN BOUNDARY PRECIPITATES	$n$ platelets ( $\sim 100$ nm wide) and needles (length $> 100$ nm)	$n$ platelets ( $\sim 60$ nm wide) and needles (length 170 nm max)

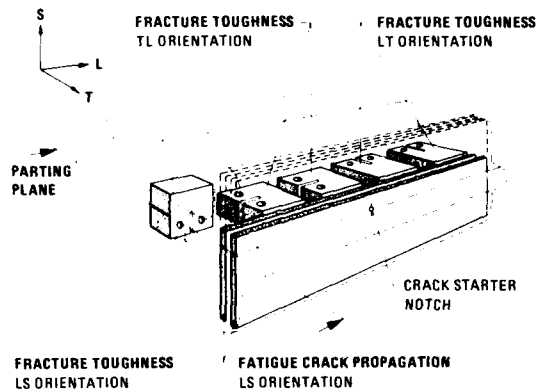


Fig. 1 The positions of the test specimens in the forgings

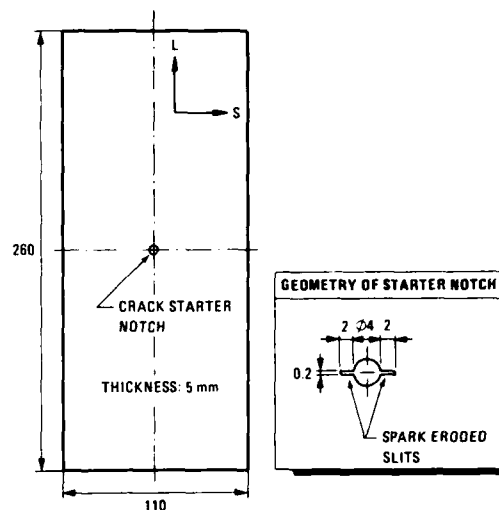


Fig. 2 Centre cracked tension (CCT) fatigue crack propagation specimen: dimensions in mm. Specimen orientation LS, see also figure 1

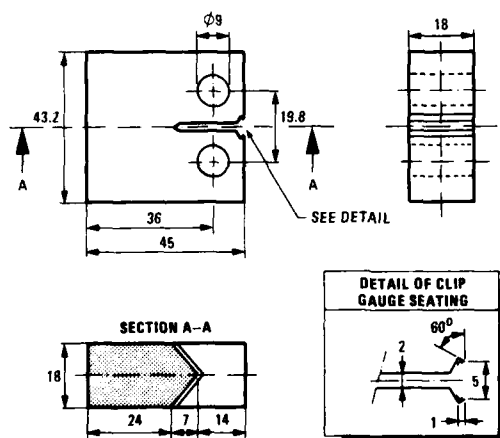


Fig. 3 Compact tension (CT) fracture toughness specimen: dimensions in mm. Specimen orientations LT, TL and LS, see figure 1

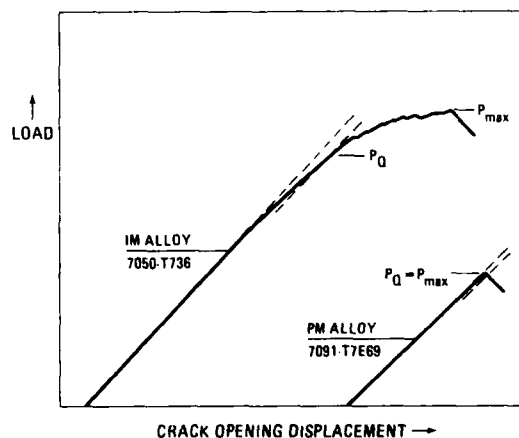
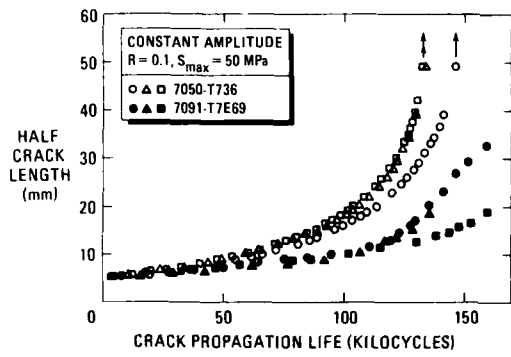
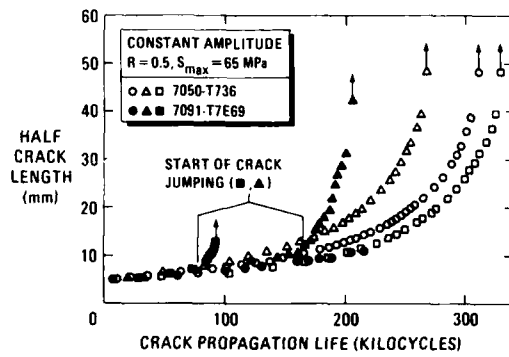


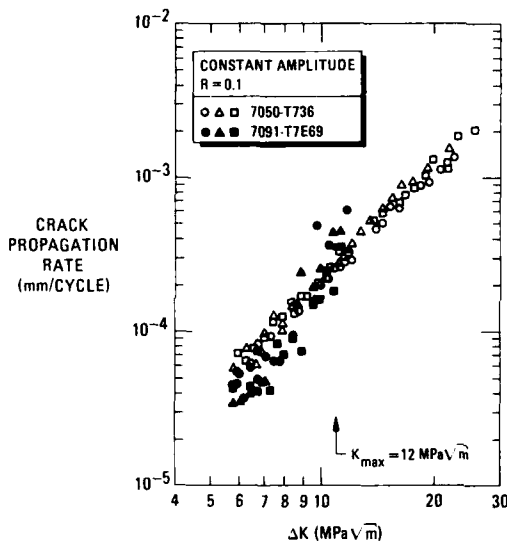
Fig. 4 Typical load-crack opening displacement records for fracture toughness testing: specimen orientation LS



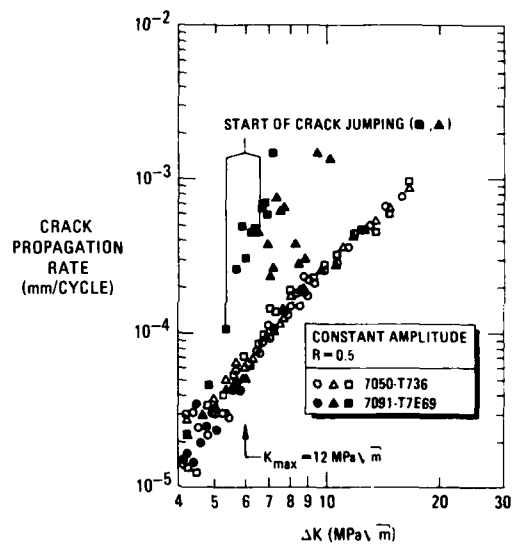
(a)



(b)

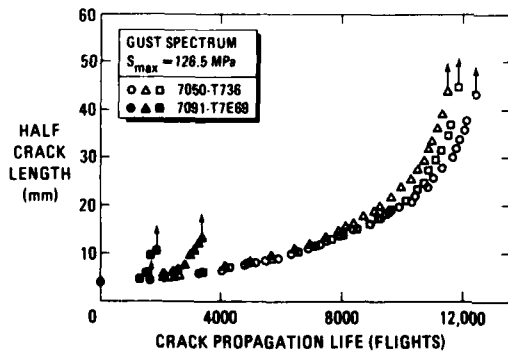


(c)

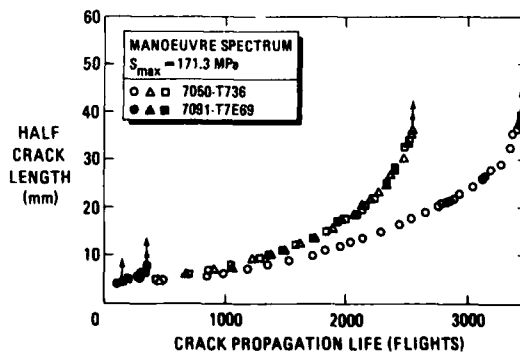


(d)

Fig. 5 Constant amplitude fatigue crack propagation results



(a)



(b)

Fig. 6 Spectrum loading fatigue crack propagation results

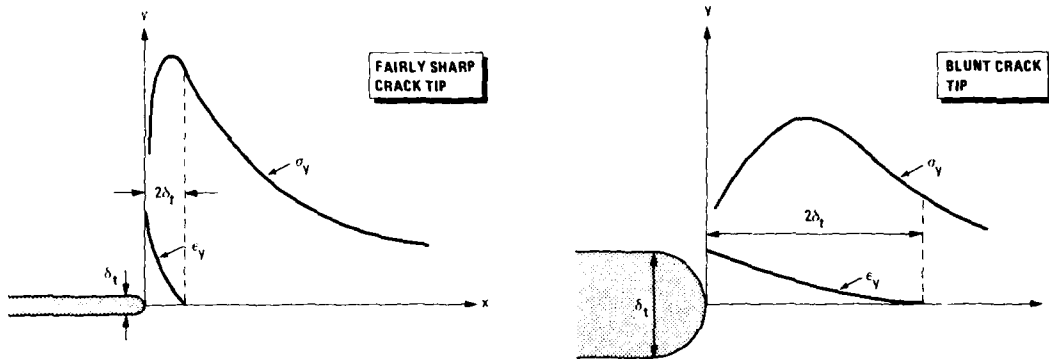


Fig. 7 Schematic normal stress-strain distributions ahead of fairly sharp and blunt cracks under plane strain and without significant strain hardening of the material. Freely adapted from refs. 11, 12

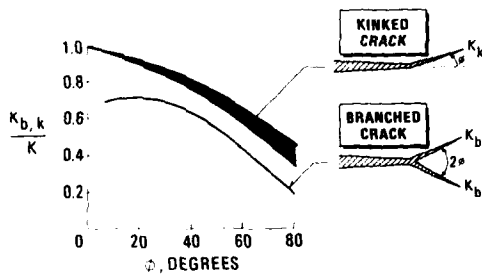


Fig. 8 Mode I stress intensity factors for branched and kinked cracks. After ref. 13

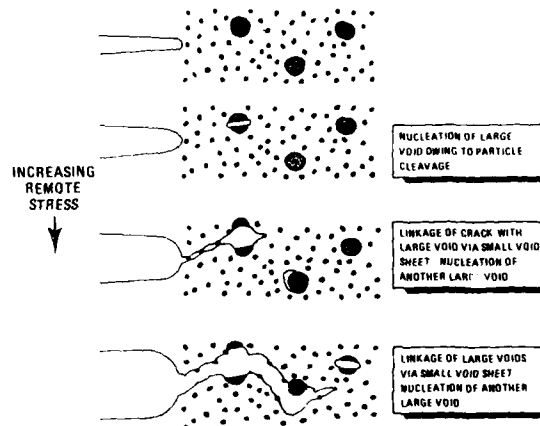


Fig. 9 Schematic of tensile crack extension by coalescence of microvoids nucleated at particles and dispersoids

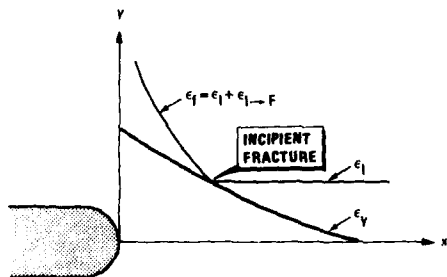


Fig. 10 Conditions leading to incipient tensile fracture ahead of a crack tip (ref. 21)

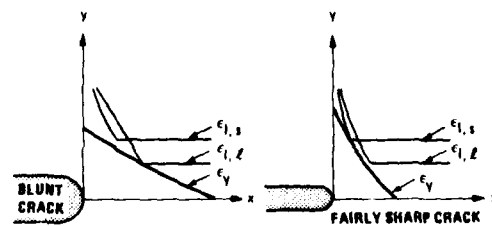


Fig. 11 Hypothetical conditions leading to incipient tensile fracture originating from large particles ( $\epsilon_{1,l}$ ; blunt crack) or small particles ( $\epsilon_{1,s}$ ; fairly sharp crack)

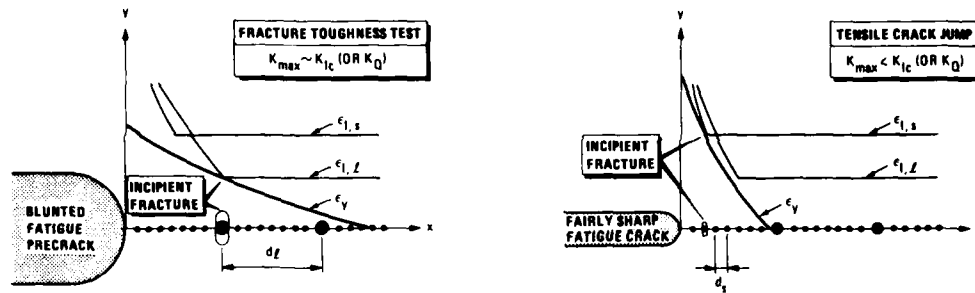


Fig. 12 Schematic of conditions leading to incipient tensile fracture originating from large particles (fracture toughness testing) or small particles (tensile crack jumps)

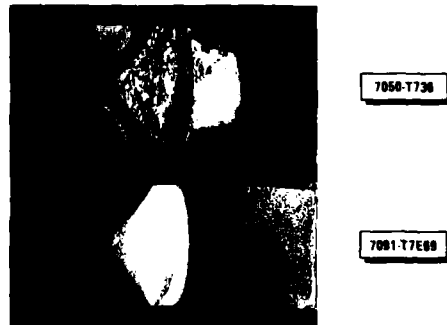


Fig. 13 Representative fracture surfaces of fracture toughness specimens. Specimen orientation LS, see figure 1

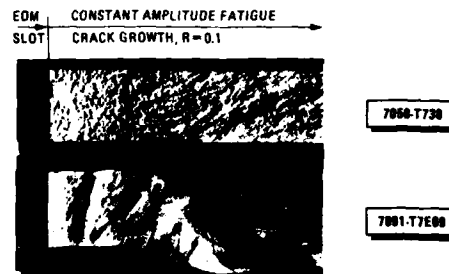


Fig. 14 Representative fracture surfaces for constant amplitude fatigue crack propagation with  $R = 0.1$ . Specimen orientation LS, see figure 1

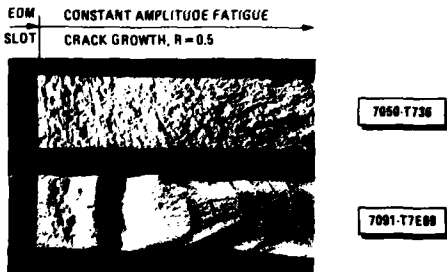


Fig. 15 Representative fracture surfaces for constant amplitude fatigue crack propagation with  $R = 0.5$ . Specimen orientation LS, see figure 1

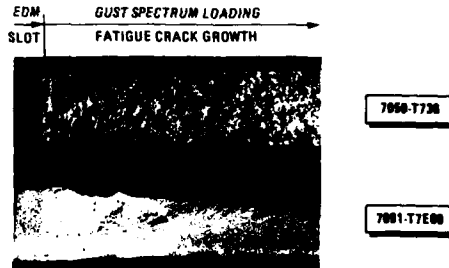


Fig. 16 Representative fracture surfaces for gust spectrum loading fatigue crack propagation. Specimen orientation LS, see figure 1

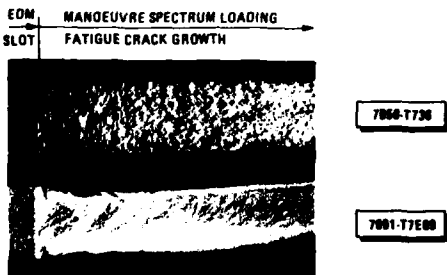


Fig. 17 Representative fracture surfaces for manoeuvre spectrum loading fatigue crack propagation. Specimen orientation LS, see figure 1

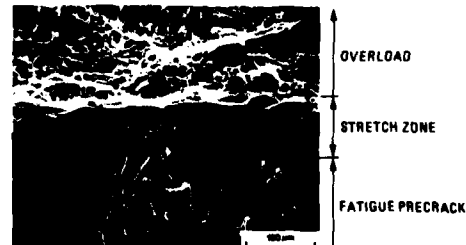


Fig. 18 Example of the stretch zones between fatigue precracks and overload failure in 7050-T736 fracture toughness specimens, LS orientation

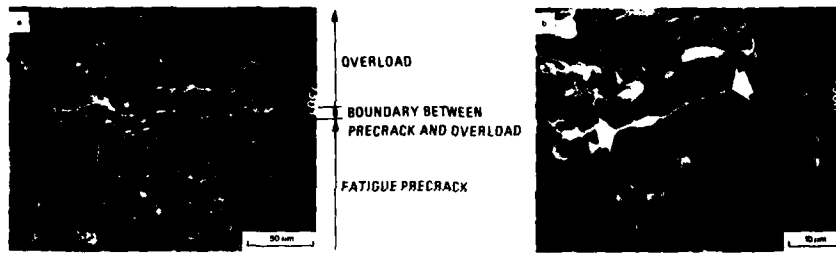


Fig. 19 Example (arrowed) of the stretch zones between fatigue precracks and overload failure in 7091-T7E69 fracture toughness specimens, LS orientation: (b) is the outlined area in (a)

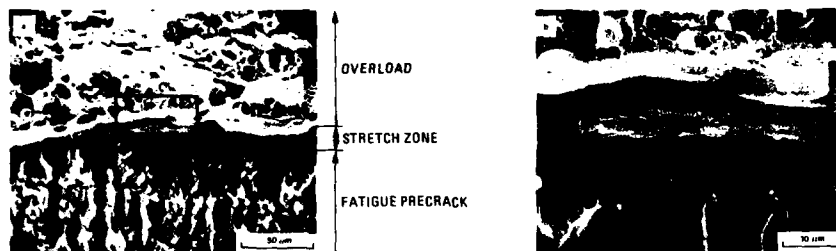


Fig. 20 Example of the stretch zones between fatigue precracks and overload failure in 7075-T73 fracture toughness specimens, LS orientation: (b) is the outlined area in (a)

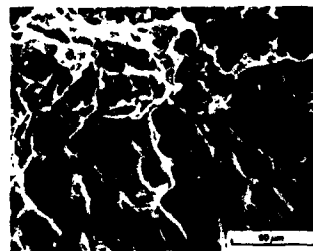


Fig. 21 Example (arrowed) of the stretch zones between gust spectrum fatigue crack propagation and tensile crack jumping for 7050-T736 specimens

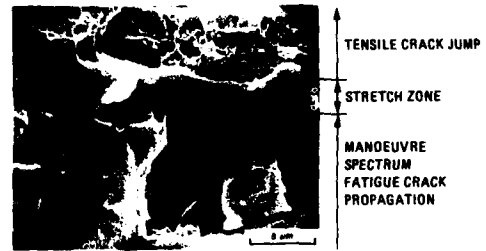


Fig. 22 Example of the stretch zones between manoeuvre spectrum fatigue crack propagation and tensile crack jumping for 7091-T7E69 specimens



Fig. 23 Microvoids ahead of a stretch zone in 7050-T736: (a) representative view, (b) identification of a particle (probably  $Al_7Cu_2Fe$ ) responsible for a large microvoid



Fig. 24 Representative views of microvoids ahead of a stretch zone in 7091-T7E69



Fig. 25 Mixed mode fatigue crack growth in 7091-T7E69 tested under constant amplitude loading. The arrow in (a) points to the location of (b) and (c), which is outlined in (b)

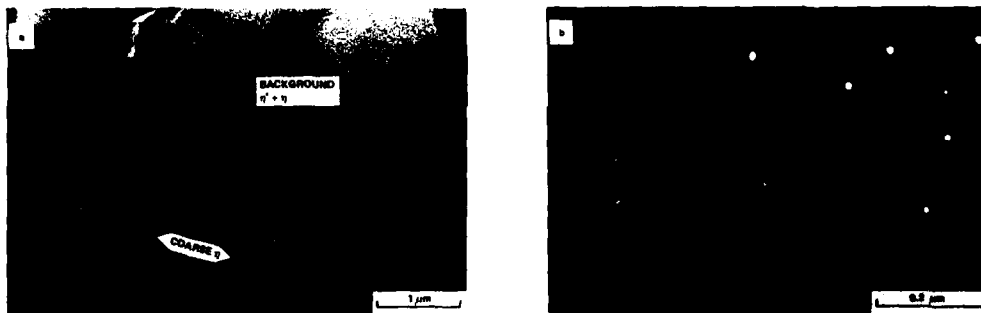
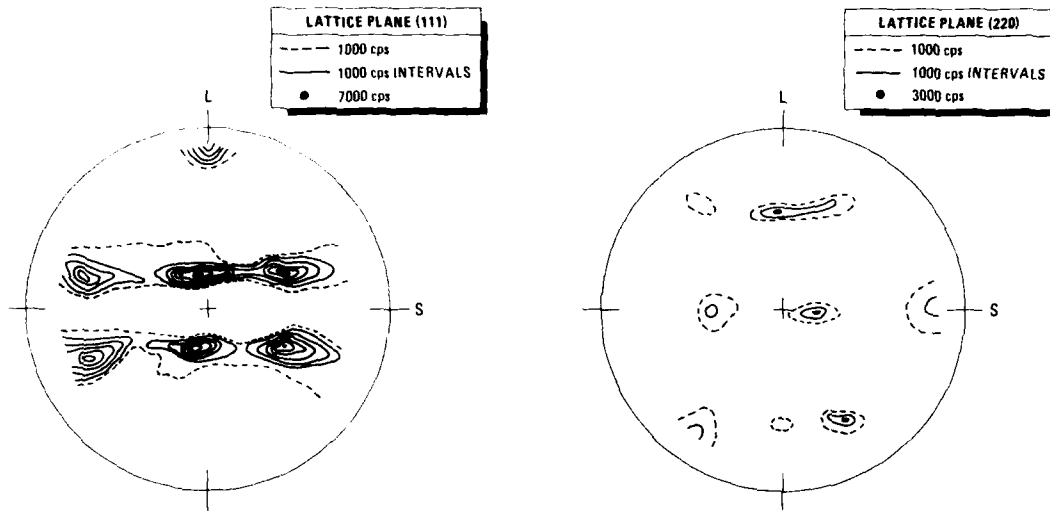


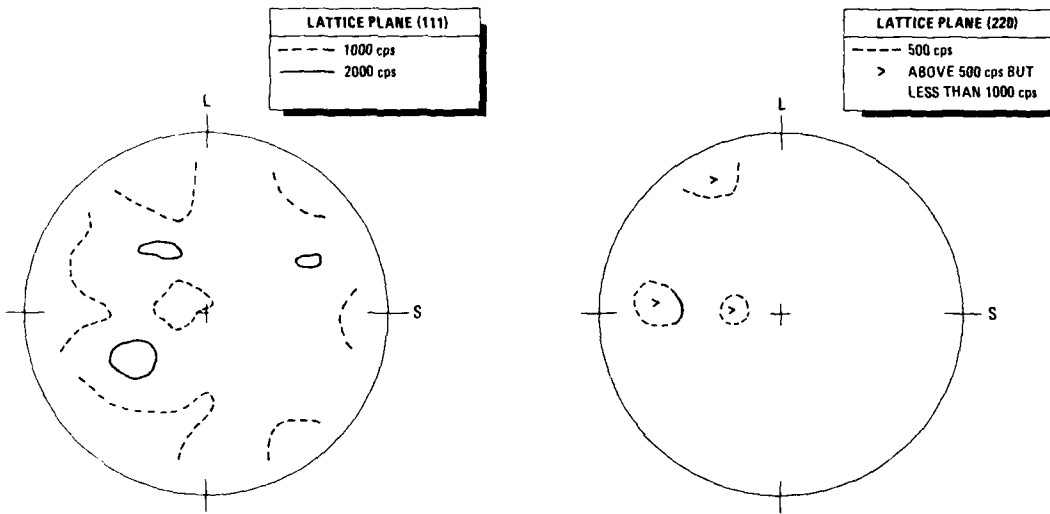
Fig. 26 Microstructural features in 7050-T736: (a) overall view, (b) dark field image of  $Al_3Zr$  dispersoids



Fig. 27 Microstructural features in 7091-T7E69: (a) overall view, (b) detail showing oxide clusters



(a) pole figures for 7050-T736



(b) pole figures for 7091-T7E69

Fig. 28 Texture measurements: courtesy Dr. A.W. Bowen, Materials and Structures Department, Royal Aircraft Establishment

TWO RECENT CASES OF MARKER LOAD APPLICATIONS  
ON CARGO/FIGHTER AIRCRAFT FATIGUE TESTS

by

DAVID R. ERSKINE  
JOHN L. HOPKINS

FRACTURE AND DURABILITY BRANCH  
DIRECTORATE OF FLIGHT SYSTEMS ENGINEERING  
AERONAUTICAL SYSTEMS DIVISION  
WRIGHT-PATTERSON AFB, OHIO  
USA

ABSTRACT

During the course of fatigue testing aircraft structures most cracks are discovered only after significant growth has occurred. With the advent of fracture mechanics a detailed fractographic analysis is imperative to determine the origin and to correlate the growth rate with the applied stress spectrum. Computer controlled fatigue tests have fostered the application of sophisticated, random sequence, flight-by-flight loading. A random sequence of load application results in nonidentifiable striations on the crack front which precludes after-the-fact crack growth rate determination. The insertion into the test spectrum of periodic, nonrandom cycles to mark the growth appears to be a solution.

This paper discusses two recent independent applications of marker cycles under distinctly different loading spectra. The first spectrum represents a cargo aircraft load environment, having a maximum load case of 60% limit. The other spectrum represents a fighter usage with the usually high frequency of near-limit load cycles. Examples are presented of the crack growth, the marking and the engineering approaches. The effects of the marker cycles on the natural growth are shown to be insignificant. Good fractographic correlation was found in both component and full scale tests.

1.) BACKGROUND

Over the past decade many changes have occurred in how we design, analyze and test aircraft structures. Our current procedures were developed as a result of several limitations; analysis techniques which did not address stress sequence effects; test equipment which could only apply a few load levels at a constant amplitude; test instrumentation, inspection, or failure interpretations which only addressed gross results. These limitations have been superseded.

In the era of classic fatigue analysis and block loading little attention was paid to striations on the fracture surface. A good example was the final failure in the early 1960s of the KC-135 tanker wing during full scale fatigue testing. The primary initiation site (see figure 1) shows the conchoidal nature of the crack front during stable growth.

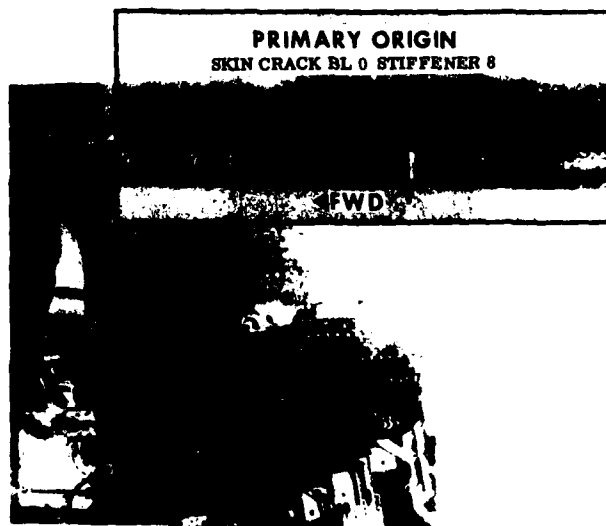


FIGURE 1 - KC-135 FULL SCALE WING TEST FAILURE

Figure 2 illustrates the test spectrum for another wing location. This spectrum contained a single flight which was simply repeated 10,800 times until final failure. Note the arbitrary full cycle of 90% limit load/stress (243 MPa (35.3 KSI)) to represent the occasional high load occurring in 1000 hours

(200 flights). Although intended to be ultraconservative in magnitude and frequency it was found, 10 years later, to unconservatively retard the rapid growth of the early failures which had serious fleet ramifications. The philosophy of this occasional high load was deemed necessary, for transport airframe tests, to enhance crack discovery. As it turned out the KC-135 test results did not correlate well with fleet experience. Subsequently another test was conducted.

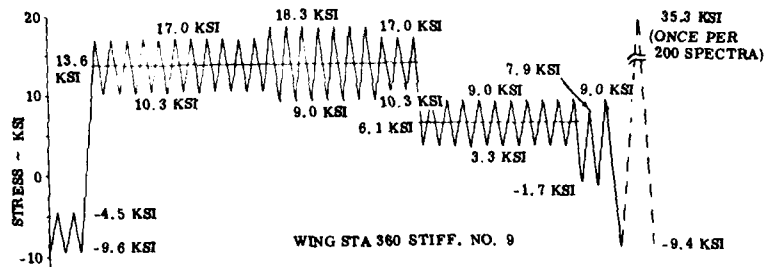


FIGURE 2 - KC-135 TEST SPECTRUM

Today fracture analysis can assess the interplay between load magnitude and sequence. Sophisticated test equipment allows an indefinite number of load levels as well as a random sequencing of loads. Strides have similarly been made in failure detection and interpretation. Two recent USAF test programs are discussed which successfully used marker loads to provide after-the-fact microscopic marking of the crack surface during full scale fatigue testing. The first case addresses the most recent test, the C-5 wing modification.

## 2.) C-5A WING MODIFICATION

The C-5A is the world's largest military heavy transport with "outsize" cargo capability. Figure 3 depicts the aircraft's general features.

**Maximum Take-Off Weight: 348,812 Kg (769,000 lb)**  
**Powerplant: Four General Electric TF 39's**

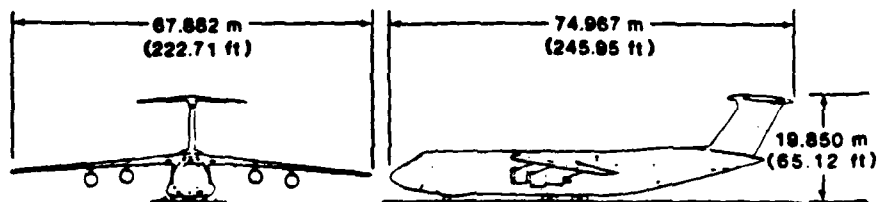


FIGURE 3 - C-5 AIRCRAFT

Because of severe wing structural problems on the original design, the Air Force and the Lockheed Georgia Company proceeded with a program to redesign and replace the primary structural wing box. It was identified as the C-5A Wing Mod Program. Figure 4 shows the extent of this redesign effort. As noted, the leading and trailing edge structure was salvaged from the old wings.

The various phases of the overall program are shown in Figure 5. Within the design phase was an effort to evaluate marker loads prior to introduction to full scale testing (Phase II). It is this marker evaluation program that this paper will review.

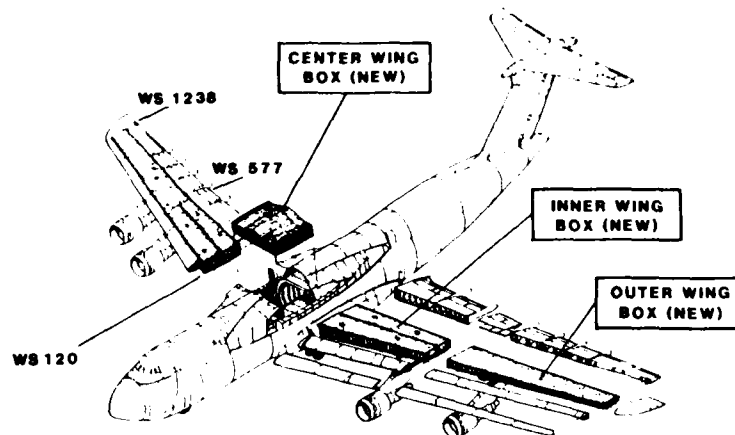


FIGURE 4 - WING MODIFICATION STRUCTURAL REPLACEMENTS

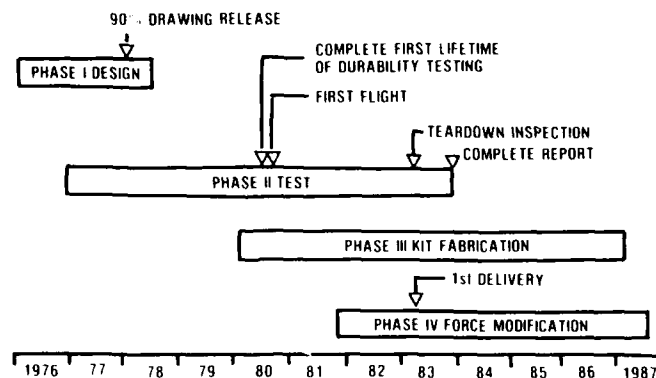


FIGURE 5 - PROGRAM SCHEDULE

To evaluate these marker loads a systematic approach was developed with the basic objectives:

- (1) To mark the majority of the wing structure rather than just a few discrete locations.
- (2) To not influence the full scale durability or damage tolerance test crack growth results.

The first objective was desired because the critical locations in the wing were unknown, and a significant portion of the lower surface had the same basic stress level and configuration. The second objective stands to reason that these marker loads should not affect the primary test purpose. Additionally, the contract exposed the contractor to repair and production costs for any failures within the first 45,000 test hours. If marker loads could mark the crack front, it would assist the failure interpretation. Thus, knowing when and how fast cracks grew were of contractual concern. These legal as well as technical concerns became meaningless because of the outstanding success of the full scale test.

#### COMPONENT TEST

A component test program was established. Various marker loads programs were applied on the original C-5A and the C-141 programs. The aspects of these programs will not be addressed. The experience gained from these contributed to the development of the C-5A Wing Mod marker criteria which would:

- (1) Not exceed the unmarked spectrum stress levels.
- (2) Minimize retardation, by applying the marker stress before a flight which contained a larger stress.
- (3) Be the same spectrum for component and full scale test.

(4) Be applied periodically throughout the component and the full scale test.

With these objectives a program was developed for three representative areas in the wing. Figure 6 shows these locations as control points 425, 535, and 629.

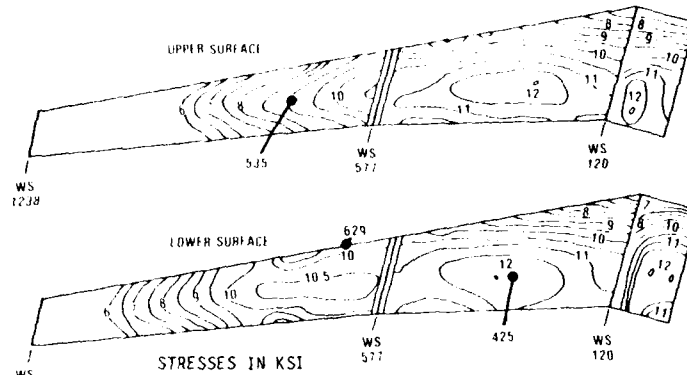


FIGURE 6 - WING ISO-STRESS PLOT FOR STEADY FLIGHT (1.0g)

Two points were necessary to encompass the lower surface because of stress spectrum differences. The spectrum for the inner point (425) was influenced by the normal gust and maneuvers while the outer wing location (629) was highly influenced by aerial refueling. The upper point (535) was always questionable because the upper surface was not critical. However, it was retained because of stress spectrum differences from the lower surface and to see if the upper surface could be marked. It is noted that the upper surface stresses had to be increased 15% to obtain sufficient crack growth in a reasonable time.

An axial stress spectrum was developed using six component loads, representing the final operational loads and 14 design mission profiles. All testing was randomized, flight-by-flight. The spectrum contained approximately 400,000 cycles, 6660 unique flights representing the 30,000 hour design lifetime (L.T.).

Figure 7 shows the magnitude and sequence of the marker loads. These markers were blocks of constant amplitude stresses applied between flights at approximately 1/3 lifetime or 2232 flights in the case of tension stresses on the lower surface. The compression stresses for the lower surface were applied at approximately 1/2 L.T. The upper surface was the reverse. The stress levels represents the load level occurring 100 times in 30,000 hours (1 L.T.).

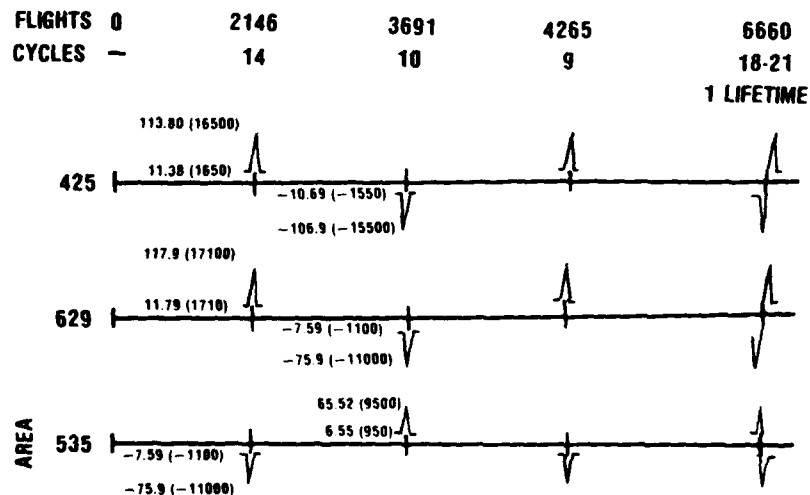


FIGURE 7 - MARKER LOAD SEQUENCE AND MAGNITUDE

The specimen configuration and geometry are shown in Figure 8. The test specimens (8) were removed from a single 7175-T73511 aluminum wing panel extrusion. The load transfer strap was attached with a 5/16 dia., 100° countersunk, steel Taper-lok (tapered fasteners), simulating the load transfer in a typical sparwise splice.

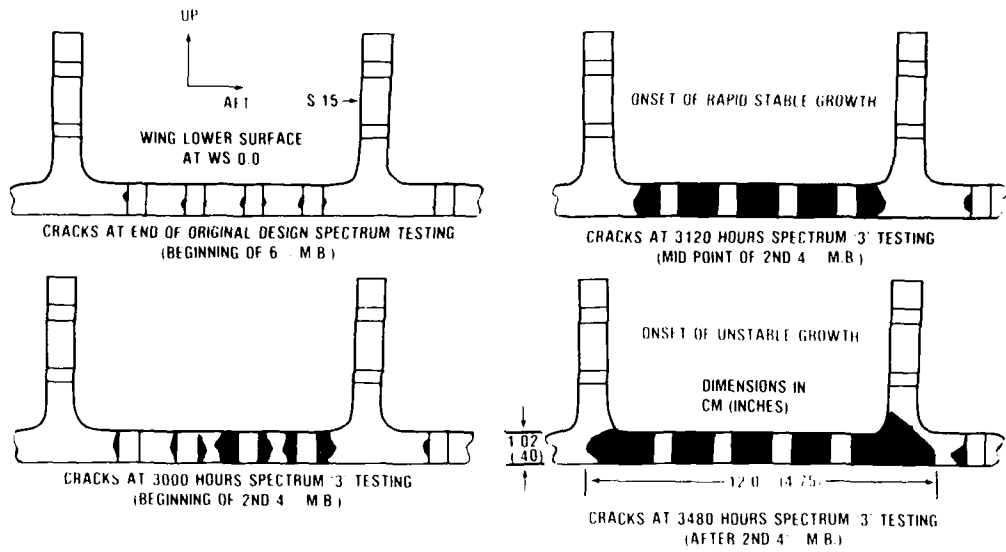


FIGURE 31 - WS 0.0 CRACK PROGRESSION

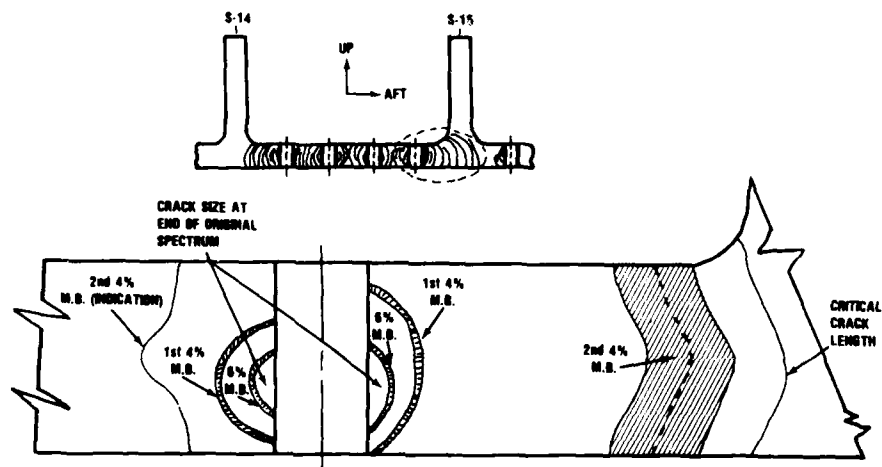


FIGURE 32 - CRACK PROGRESSION AT STIFFENER 15

Another method of verifying the small effect of marker banding on crack growth is shown in figure 28. Here the incremental growth is shown for every 4% marker band and for each of the two 4% normal spectrum bands which followed. Except for a few points, the crack growth attributed to the marker spectrum falls within the range of the normally sequenced 4% spectrum applications. This method of verification does not require a companion, non marker band test. Because the incremental growth is so small this method probably has significant measurement error.

It should be noted that the marker band coupon tests were a part of a larger test program. The primary purpose was to verify the analytical crack growth modeling, used in the A-10 program including retardation. Compounding this situation the program schedule required a restart of the full scale fatigue test as soon as possible. The subject coupon test program had to be completed in six weeks.

#### 6.) FULL SCALE TEST

All discussion pertaining to the A-10 so far has concerned itself with coupon tests and validating a marking scheme. The marker band revision F was selected for application on the full scale test. However it came to light that the highest loads in revision F banding were too numerous relative to the frequency of these maximum loads in the Spectrum 3 spectrum. Therefore the 4 occurrences of the maximum load applied every 1% of a lifetime were reduced to 2 occurrences. The full scale test experienced a major failure in the wing lower cover at the centerline of the fuselage producing an example of marking. This occurred after application of 3480 simulated hours of the revised Spectrum 3, for a total of 1.28 lifetimes; including three applications of marker band sequencing. This banding consisted of a 6% band applied at the beginning the spectrum '3'. Following the normal 20% of one lifetime random spectrum, a 4% marker band was applied. Figure 29 illustrates the total test history. Note that the failure occurred 240 hours after the last marker band application.

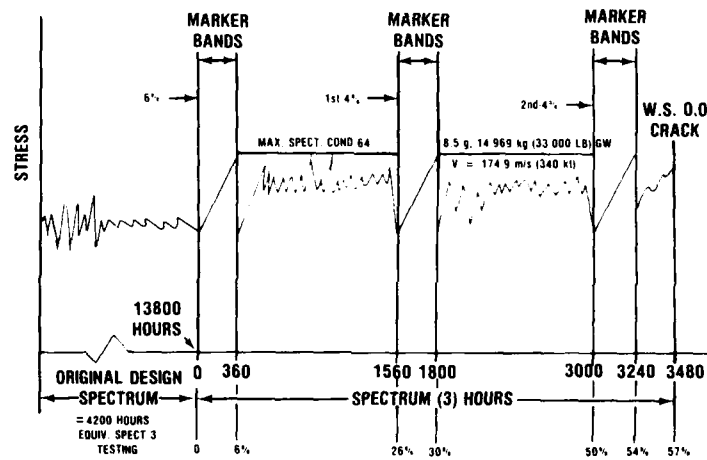


FIGURE 29 - FULL SCALE TEST HISTORY

Figures 30 through 33 show the crack growth with markings. All three marker bands were detectable. The point of spectrum change was detectable with the first 6% band.

This failure is seen as an excellent example of successful marking of crack growth of a relatively complex structural geometry under random spectrum loading.

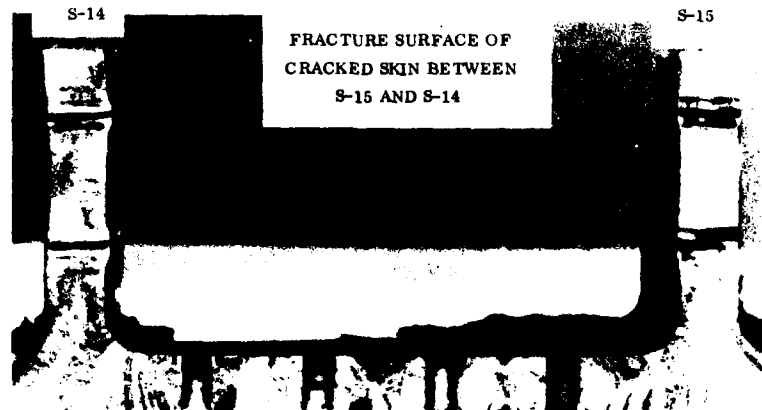
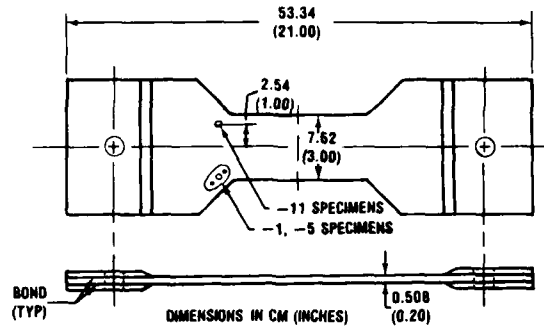


FIGURE 30 - W.S. O.O FRACTURE SURFACE



MATERIAL: 2024-T351 ALUMINUM PLATE

FIGURE 26 - W.S. 30 MARKER COUPON

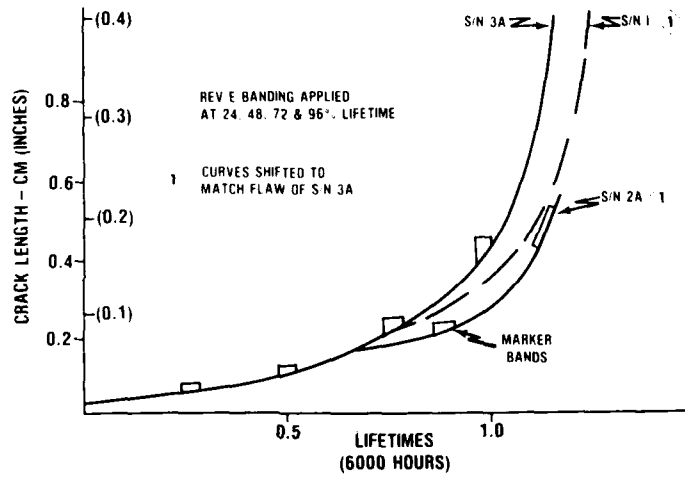


FIGURE 27 - W.S. 30 COUPON CRACK GROWTH

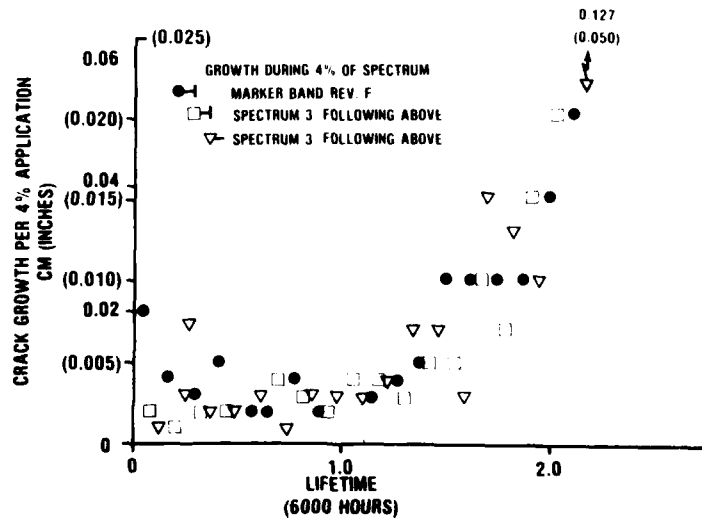


FIGURE 28 - COUPON INCREMENTAL CRACK GROWTH

Figure 24 shows the results of one set of coupon tests, with and without a marking scheme. Figure 25 shows the fracture surface with the marker bands for one specimen in this series of tests. For this set of tests the original design spectrum was applied for 8% of 6000 simulated hours. A 4% marker band spectrum was then applied. The new Spectrum 3 spectrum with marker loads at 12% intervals was subsequently applied until complete failure occurred at 95% of 6000 hours. Counting from the point of unstable growth to the initiation site, 6 of the 8 applied marker bands could be discerned.

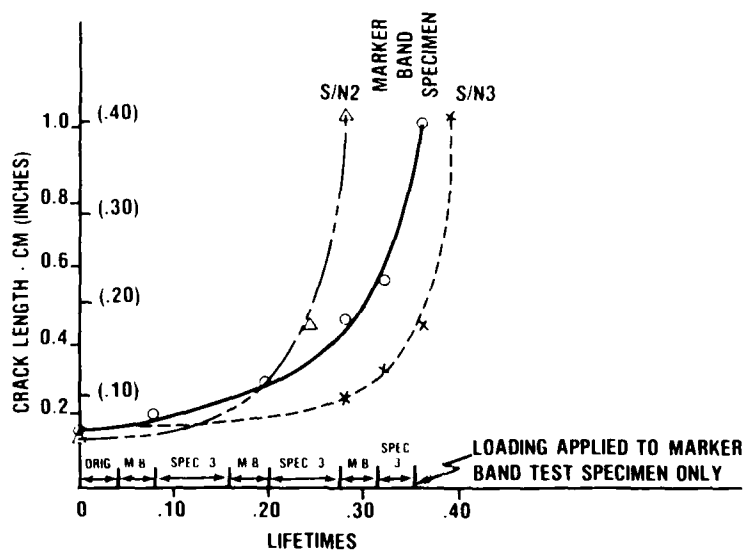


FIGURE 24 - MARKER COUPON CRACK GROWTH

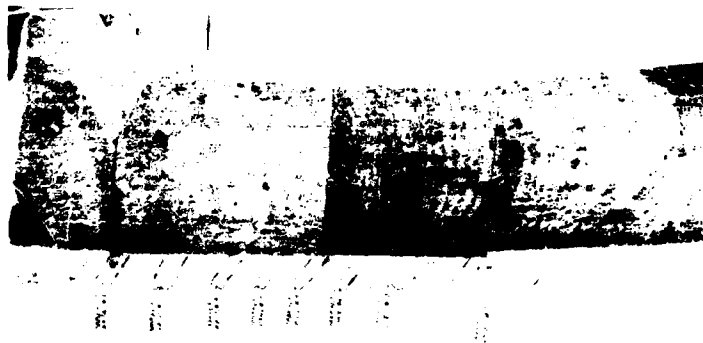


FIGURE 25 - MARKER COUPON FRACTURE SURFACE

Another set of data was obtained using a slightly more complex specimen, see figure 26, having a nutplate with associated rivet holes placed over the preflawed hole to more closely duplicate the loading condition and configuration of a lower surface area. This location at W.S 30 experienced cracking during design development testing. Additionally a slightly different marker banding, revision E, was applied. The differences between revision E and revision F marker banding was in the number of load levels. The exceedences of peak stress were similar as seen in figure 20. Figure 27 shows the minor effect of this marker banding on the crack growth.

The results of these coupon tests point out an interesting problem in comparison crack growth testing - the large variation in initial flaw sizes which can only be discovered after test completion. Although effort was made to make all initial flaw sizes the same, fracture surface examination in this case indicated that they were not. To normalize the results the data from the specimens with larger initial flaw sizes was shifted to a point common to all three curves. What is most desirable, of course, is to have the time and resources to run extra tests to essentially eliminate this common problem.

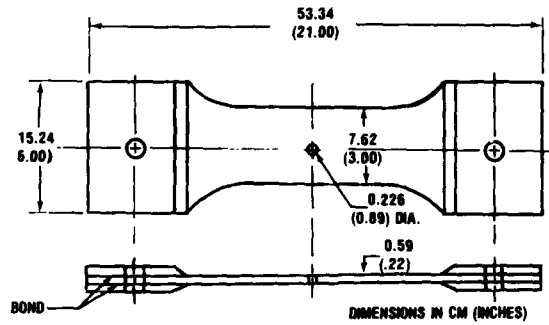


FIGURE 22 - MARKER TEST COUPON

Figure 23 presents these schemes pictorially and Table II gives the amplitudes, number of cycles and sequence of the ordered loading for Revision F.

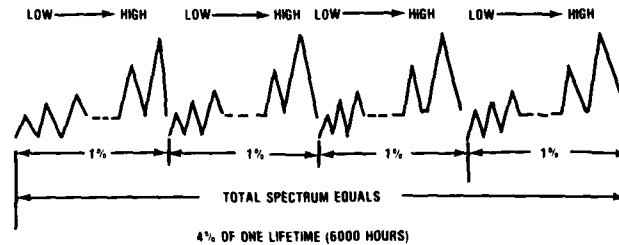


FIGURE 23 - MARKER BAND SPECTRUM SEQUENCE

SEQUENCE	STRESS - MPa		CYCLES
	MAXIMUM	MINIMUM	
1	66.19	26.61	75
2	80.81	32.48	415
3	92.53	26.61	34
4	96.94	32.48	353
5	105.70	26.61	13
6	111.49	32.06	243
7	119.21	26.96	7
8	129.28	32.82	175
9	145.55	32.82	69
10	145.55	26.96	37
11	145.55	32.82	69
12	161.68	32.82	17
13	171.89	26.96	45
14	177.75	32.82	11
15	185.27	27.10	2
16	191.41	32.54	34
17	194.03	32.96	7
18	207.26	32.54	22
19	210.16	32.96	7
20	223.19	32.54	16
21	226.29	32.96	4
22	237.95	27.10	11
23	251.12	27.10	1
24	254.98	32.54	8
25	254.98	32.54	4

TABLE II - REVISION 'F' MARKER BAND SPECTRUM AT W.S.- 23

The application frequency of the marker segments was varied. The most frequent application was every 8% of the 6000 hour lifetime. The most infrequent was every 24%. The total number of cycles and stress amplitudes were not significantly changed.

This new usage spectrum, identified as Spectrum '3', was incorporated into the loading spectrum of the full scale fatigue test after 13,800 simulated hours. It was desirable to 'mark' the subsequent crack growth to ascertain the point in any existing crack of the spectrum change.

#### 5.) COUPON TESTS

Following the recommendation of an Independent Review Team the contractor initiated an exploratory program to develop a marking scheme. First attempts of inserting cycles of a constant amplitude stress (figure 21) were marginally successful and the project almost abandoned (ref 6). However a previous fighter fatigue test program, the F-5, had successfully used constant amplitude cycles on coupon tests and recommended constant amplitude banding on the full scale test (ref. 7). For the A-10 program it was suggested that, rather than constant amplitude marker cycles, some of the randomly applied cycles would be regrouped in an ordered sequence.

TEST	SPECIMEN MATERIAL	MARKER BAND CYCLES	REPEAT INTERVAL (% OF 6000 HR)	RESULT
1	2024-T3511	12.4 ksi 4.0 7 CYCLES	4%	NON DETECTABLE
2	2024 T3511	20.7 4.0 5.23 CYCLES		
3	2024 T3511	12.4 4.0 7 CYCLES		
4	7075 T6	35.2 -2.2 3.9 CYCLES		
5	7075 T6	24.8 4.0 2 CYCLES	8%	DETECTABLE
6	2024 T3511	12.4 4.0 100 150 CYCLES		
7	2024 T3511	12.4 4.0 500 CYCLES	8%	NON DETECTABLE
		35.2 -2.2 1 CYCLE		
		12.4 4.0 5 CYCLES EVERY OTHER REPEAT		

FIGURE 21 - INITIAL (CONSTANT AMPLITUDE) MARKER TESTS

Several schemes were considered, analyzed, and tested. The sequences referred to as Revisions E and F were successful and will be addressed in this section of the paper. Figure 20 shows the relationship of both of these marker band spectra to the total spectrum (cumulative occurrences per 240 hours).

In retrospect this 'blocked' marker loading sequence would seem obvious since block loading generally results in distinctive marking of the crack growth. However it could unrealistically influence retardation of the crack growth. This would be especially true under the A-10 spectrum with its profusion of high stress cycles. Therefore it was necessary to derive a block loading sequence which would successfully mark but have minimal influence on retardation.

This follow-on evaluation program relied heavily on coupon tests and some details of these tests are warranted. The coupon specimens were made from both alloys of concern, 2024-T351 and 7075-T6. The coupon configuration is shown in figure 22.

Twelve specimens were tested, with seven banding schemes. The procedure was to 'precrack' the specimens by applying constant amplitude cyclic loading to producing a corner crack at the edge of the hole. When the desired crack surface length was reached, random spectrum cycling was started.

The successful marker banding schemes E and F consisted of extracting a group of randomly applied loads representing 1% of 6000 hours. After range-pair-range counting the group it was rearranged in order of ascending amplitude. The 1% block was applied 4 times in succession in place of 4% of the normal spectrum. This multipass application of ordered loading would then be periodically reapplied throughout the test. As was mentioned earlier the full scale test spectrum was changed after 13,800 hours. The marker banding, if applied, would start after this spectrum change.

The design limit load factor is 7.33g at the original basic design weight of 13,472 Kg (29,700 lbs). The design service life is 6000 hours. Military Specification MIL-A-8866 maneuver spectrum was used for the fatigue design spectrum. The damage tolerance design preceded the implementation of the damage tolerance criteria of Military Specification MIL-A-83444.

The basic wing box structure (figure 18) consists of three spars and covers with stringers. The inboard wing covers have integral stringers with the exception of the lower aft plate cover which is mechanically attached to the auxiliary spar cap. The covers are divided into two panels, from front to mid-spar and mid-spar to rear spar. The top cover is 7075-T76511 aluminum alloy extrusion and the bottom cover is 2024-T3511 extrusion and 2024-T351 plate. The outer wing consists of three spars and stringers attached to one piece covers which extend from the front to rear spar. The top covers and stringers are of 7075-T6 alloy and the bottom covers and stringers are 2024-T3 alloy.

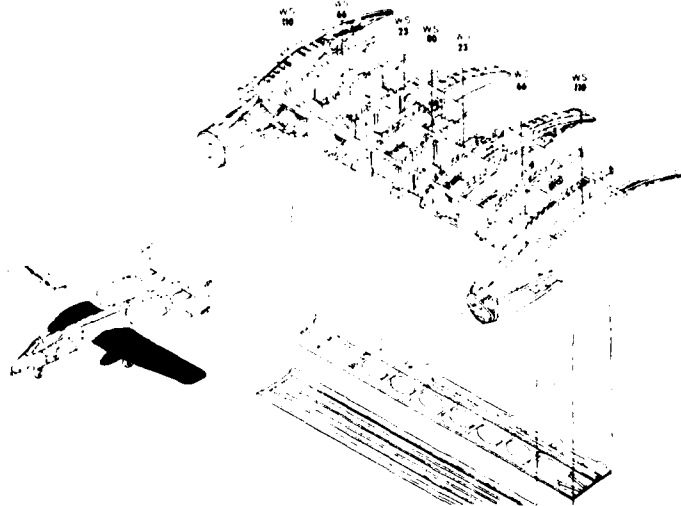


FIGURE 18 - INBOARD WING-STRUCTURAL ARRANGEMENT

After the A-10 was in service it became obvious from recorded data that the operational usage was much more severe than the design. Figure 19 shows a comparison of these spectra.

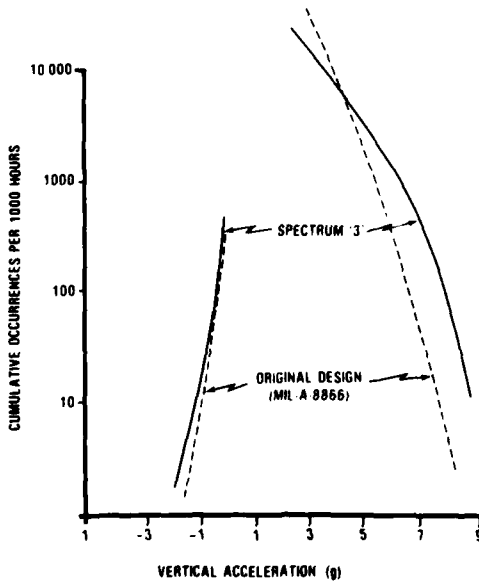


FIGURE 19 - DESIGN SPECTRUM COMPARISON

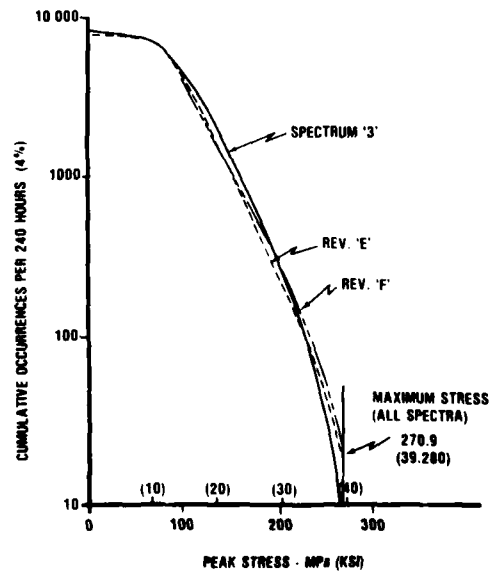


FIGURE 20 - MARKER SPECTRA COMPARISON

Figure 15 shows a summary plot of the wing lower surface where marker loads produced identifiable bands. As desired the full scale article was marked throughout the inner and a significant portion of the outer wing surfaces. Note that the points numbers 425 and 629 were the same locations evaluated in the component test program. The upper surface was not marked.

Another primary benefit of the marker loads is seen in figure 15 which shows a comparison of the analytical crack growth prediction to the fractographic measurements for the induced flaw at point 425. This figure is typical of the induced flaws. The earliest natural flaw marking was seen at 30,000 hours. Such fractographic capability allowed validation of the analysis.

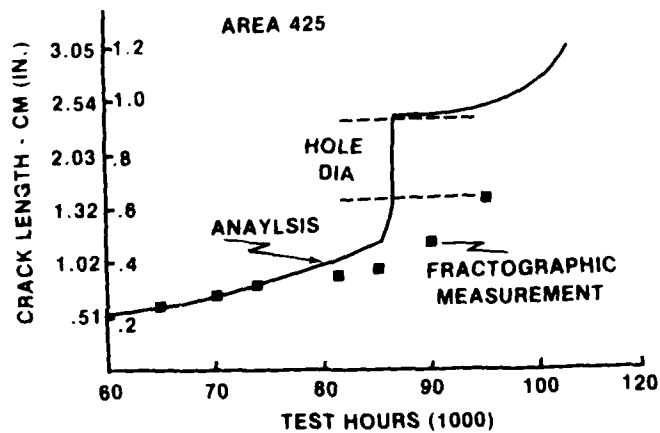


FIGURE 16 - CRACK GROWTH ANALYSIS VERIFICATION

It is concluded that the marker objectives were successfully achieved. Markings were not limited to isolated locations. Most importantly, these marker loads did not significantly affect the test results and validated the crack growth analysis.

#### 4.) A-10 FIGHTER AIRCRAFT PROGRAM

The A-10 (figure 17) was designed as a highly maneuverable, close support fighter capable of operating from semi-prepared forward airstrips. It has a wide spectrum of close air support missions due to its low altitude, range, and loiter capabilities; airspeed variability and aerial agility.

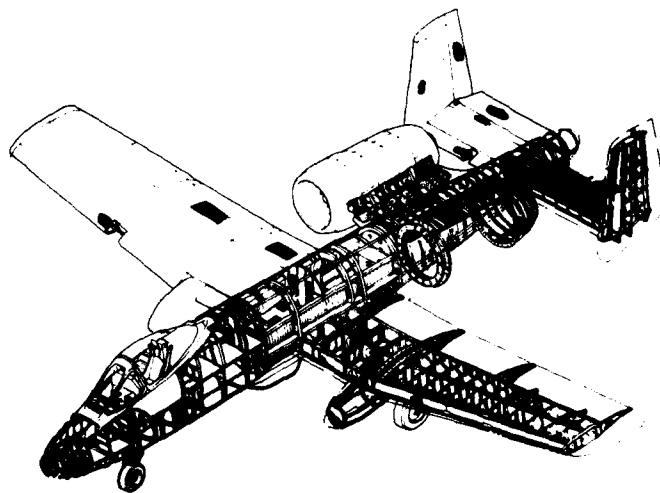


FIGURE 17 - A-10 STRUCTURAL ARRANGEMENT



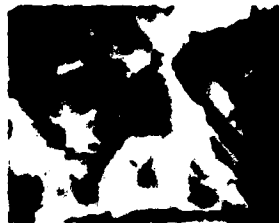
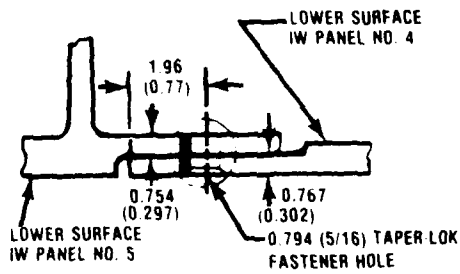
73,964 CTH



80,856 CTH



85,000 CTH



90,000 CTH



95,000 CTH

FIGURE 14 - CONTROL POINT 629 FRACTOGRAPHIC CORRELATION

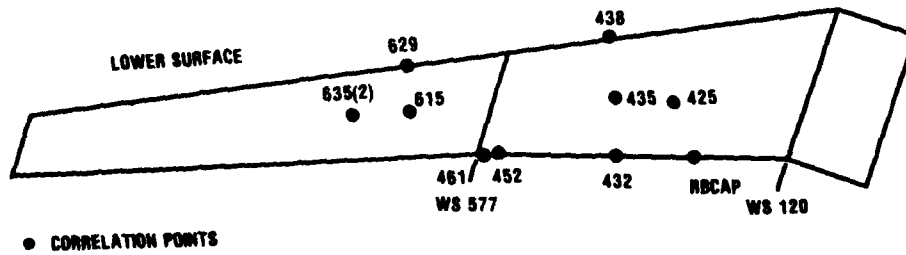


FIGURE 15 - FRACTOGRAPHIC CORRELATION SUMMARY

Detailed fractographic SEM examinations showed the typical markings seen in Figures 13 and 14. The distinct cycles were correlated with the values on figure 12. Average growth due to marker loads were measured in the range of .000508 - .000127 cm (.00002 - .00005 inches) per cycle. Such growth did not influence the final crack growth. Overall these cracks grew slower than predicted analytically.

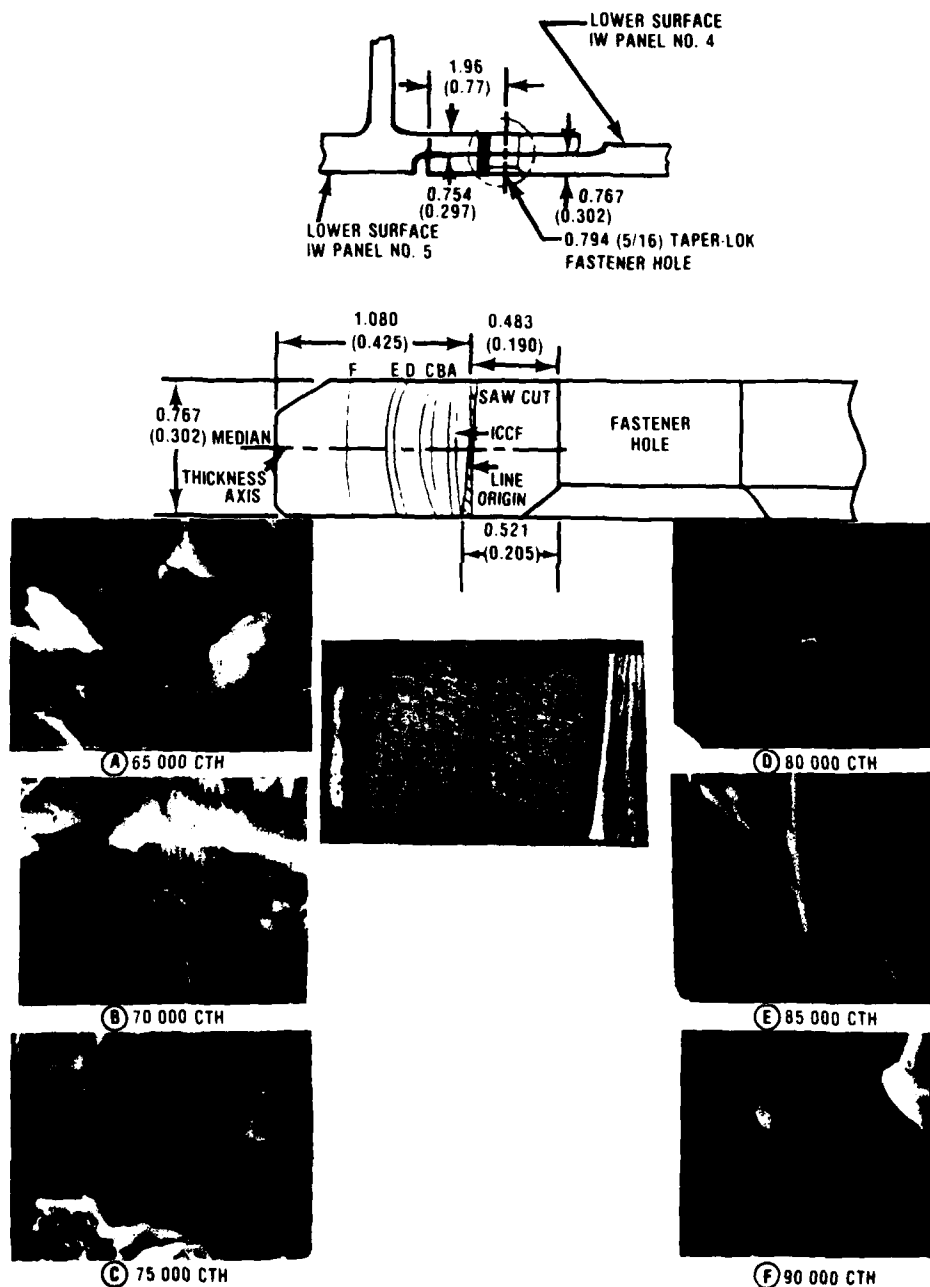


FIGURE 13 - CONTROL POINT 425 FRACTOGRAPHIC CORRELATION

3.) FULL SCALE TEST

Figure 11 is an overall view of the full scale test article. The test article consisted of the basic wing box. Other structure (i.e., pylon/engines, loading and trailing edges) were necessary to obtain proper load introduction to the wing primary structure. The wing was installed in a previous static test fuselage. Again the test spectrum was completely random, flight-by-flight, with the same test variables as the component tests.

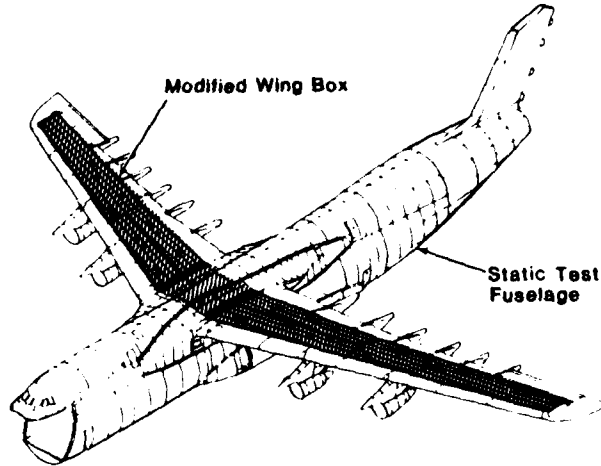


FIGURE 11 - FULL SCALE FATIGUE TEST SPECIMEN X 991

The structure proved to be extremely durable in that no natural fatigue cracks developed during the first two lifetimes or 60,000 hours (2 L.T.). In order to measure and verify the analytical crack growth analysis 59 man-made flaws were introduced on only the left wing at various locations at 60,000 hours. Similar to the component tests, these flaws were made with a jeweler's saw, X-ACTO knife, and diamond paste. Unlike the component tests, constant amplitude cycling was required to initiate a fatigue crack from the saw cut. Additional flaws were inserted at 75,000, 85,000 and 90,000 hours. At 85,000 hours the test spectrum was altered to reflect wartime operation. When compared to the original this spectrum was twice as damaging on the lower surface. The test continued to 105,000 test hours or 125,000 hours of the original spectrum. Following the final routine inspection at 105,000 hours the article was successfully subjected to a comprehensive damage tolerance test. At conclusion a detailed NDI and teardown inspection was performed.

Figure 12 shows the marker loads throughout the test program. The numbers in parentheses provide the number of unique marker stress cycles. The marker loads were developed for only the lower surface and produced stress levels equal to the component test values (ref fig 7).

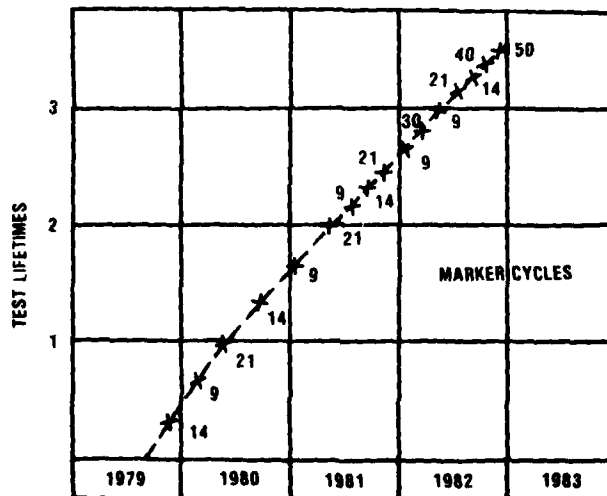


FIGURE 12 - TEST SCHEDULE WITH MARKER APPLICATIONS

Table I below provides a summary for each specimen.

TEST ENVIRONMENT - LABORATORY AIR Average Test Cycle Rate - 5 Hz				
Specimen No.	Loading Spectrum	Wing Location	Duration Of Test	Metallurgical Findings
1	A A 629 (With Marker Loads)	Outer Wing Lower Front Beam OWBRS 272	3 Lifetimes	Characterized size and growth pattern of test crack.
3	A A 629 (Without Marker Loads)	Outer Wing Lower Front Beam OWBRS 272	3 Lifetimes Plus 5100 Flights	Characterized size and growth pattern of test crack.
2	A A 425 (With Marker Loads)	Inner Wing Lower Mid Beam IWBR 263	4 Lifetimes	Characterized size and growth of test crack. Characterized size and growth pattern of natural crack in non-test hole. Fractographically correlated growth of natural crack with test history.
4	A A 425 (Without Marker Loads)	Inner Wing Lower Mid Beam IWBR 263	4 Lifetimes Plus 2146 Flights	Characterized size and growth pattern of test crack.
7	A A 425 (Marker Loads Alternated - odd lifetime)	Inner Wing Lower Mid Beam IWBR 263	3 Lifetimes	Characterized size and growth pattern of test crack. Fractographically correlated crack growth with test history for 1st lifetime.
8	A A 425 (Marker Loads Alternated - even lifetime)	Inner Wing Lower Mid Beam IWBR 263	3 Lifetimes	Characterized size and growth pattern of test crack. Fractographically examined fracture for natural markers.
5	A A 629 (With Marker Loads)	Outer Wing Lower Front Beam OWBRS 272	3 Lifetimes Plus 3337 Flights	Characterized size and growth pattern of test crack. Fractographically correlated growth of test crack with test history.
6	A A 535 (With Marker Loads)	Outer Wing Upper Crown OWBRS 327	4 Lifetimes Plus 1665 Flights	Characterized size and growth pattern of test crack. Attempted fractographic correlation unsuccessful, no marker loads detectable.

NOTE: One lifetime equalled 6660 flights or 30,000 hours.

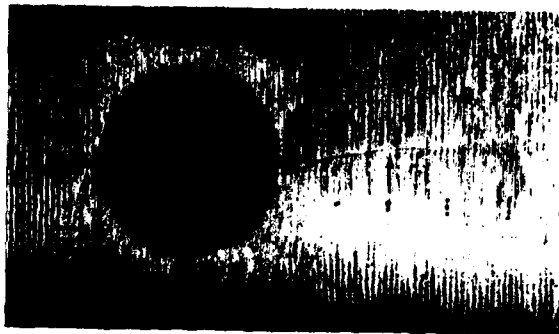
TABLE I - COMPONENT TEST SUMMARY

From these test results it was concluded that:

- The lower surface specimens were successfully marked.
- The upper surface specimen was not marked.
- Crack growth rates were not significantly affected by marker loads.
- There was good agreement between analyses and test results.

Having verified the technical objectives, marker loads could now be applied to the full scale test with reasonable confidence of achieving the desired results.

Figure 10 shows a typical fracture face. The surface scribe marks can be seen. Figure A, B and C show the correlation on the fracture face. This picture is of a natural flaw which developed on the opposite side of the test hole. However, the man-made flaws had similar markings and correlation. Note the crack could only be correlated to the twenty-one cycles applied at the first life-time.



(B) 9-CYCLE MARKER



(A) 14-CYCLE MARKER



(C) 21-CYCLE MARKER

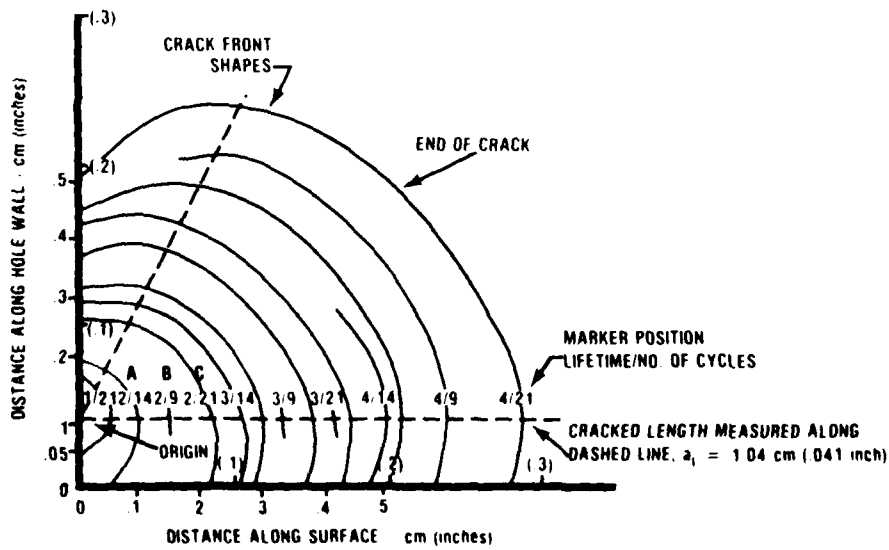


FIGURE 10 - TYPICAL LOWER SURFACE FRACTOGRAPHIC CORRELATION

Each specimen was preflawed with a notch, approximately 0102-.0127 cm (.004-.005 inch) using a sharpened X-ACTO (surgical) knife and six micron diamond paste. The flaw was then cycled to produce a natural crack with a final length of approximately .114 cm (.045 inch) after final hole reaming. The fastener in the test hole was installed with a neat fit installation to be compatible with the analysis capability. Also a neat fit was desirable since small cracks are slow to develop in a good Taper-Lok hole. The fastener at

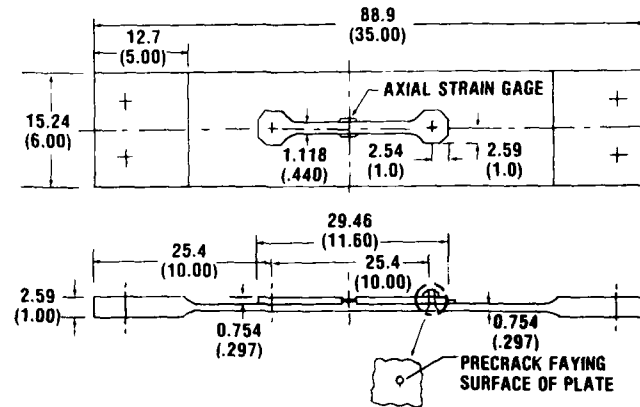


FIGURE 8 - COMPONENT TEST SPECIMEN CONFIGURATION

the other end of the load transfer strap was installed with low interference fit .0005-.0074 cm (.0002-.0029 inch)).

Loading was applied at a rate of approximately 5 HZ. Periodic surface crack measurements were obtained with the aid of an inscribed grid pattern approximately .025 cm (.010 inch) apart, ref fig. 10. At completion each of the eight specimens were removed for macro and micro metallurgical examination. Scanning electron microscope (SEM) correlation analysis was performed on specimens 2, 6, and 7.

Figure 9 shows typical crack growth with and without marker loads for specimens 2 and 4. The crack growth was recorded by surface measurements at 1/4 L.T. or, in the case of a detailed fractographic analyses, at each marker band. The predicted curve is valid for either marker configuration. When the initial crack size was equated, the incremental crack growth shows even better agreement.

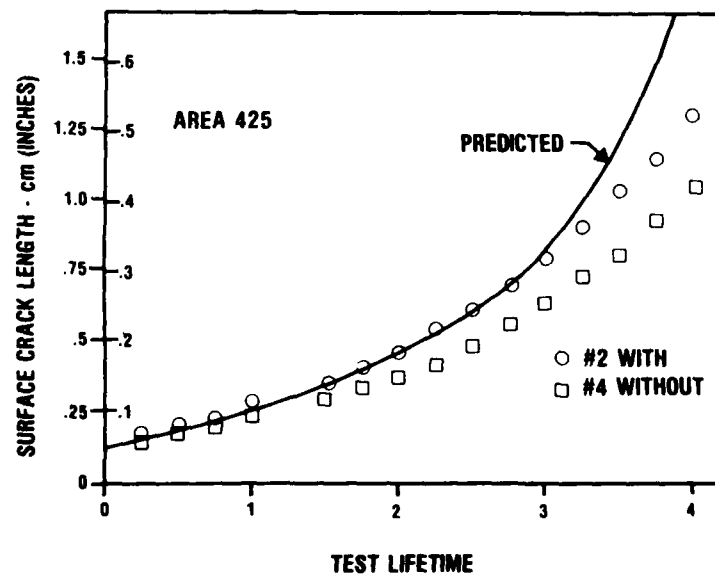


FIGURE 9 - ANALYSIS vs MEASURED CRACK GROWTH WITH/WITHOUT MARKERS



FIGURE 33 - FRACTURE SURFACE AT STIFFENER 15

### 7.) CONCLUSIONS

For the C-5 and A-10, it has been demonstrated that fatigue fracture surfaces from full scale durability testing were marked. This marking was achieved without significantly altering the growth of cracks under the random flight-by-flight load sequence. Further, it has been shown that a marking technique can be economically developed through the use of simple coupon tests. The use of markers to interpret unexpected failures and to verify the crack growth for damage tolerance analyses justifies its inclusion in the full scale test. Because of the complex spectrum interaction effects that are spectrum dependent, it is doubtful that any one marking technique would be suitable for all aircraft. This lack of a standardized approach has been noted before (see Reference 10). However, this is not a serious problem since low cost coupon test and analysis programs can be used to validate the marking schemes.

### 8.) REFERENCES

1. Boeing Company Report, "C/KC-135 Aircraft Structural Integrity," 1976, D3-9049-13
2. Lockheed-Georgia Company Report, "C-5A Wing Modification Program Verification of Fractographic Marker Loads for Modified Wing Cyclic Test Article, X991," 1979, L678ERO269
3. Lockheed-Georgia Company Report, "C-5A Wing Modification X991 Final Test Results," 1983, L683ER0092
4. Lockheed-Georgia Company Report, "C-5A Wing Modified Wing Structural Test Evaluation - Final Report," 1983, L683ER0089
5. Fairchild Republic Company, "A-10 Aircraft Structural Integrity Program Master Plan," 1981, SA160R9401
6. Fairchild Republic Company, "A-10 Damage Tolerance Reassessment Review," 1978
7. AGARD, "Fracture Mechanics Design Methodology" Conference Proceedings #221, 1976, pages 4-11, 4-31, 4-32
8. Fairchild Republic Company, "Marker Band Evaluation Specimen Preparation Phase," 1979, GT160R0181
9. Fairchild Republic Company, "A-10 Marker Band Evaluation - Analysis and Results," 1979, SA160R9416
10. R.L. Hewitt, National Research Council Canada, "A Numerical Investigation of the Effects of Marker Blocks on Crack Propagation Rates for the Snowbird Spectrum," 1982, LTR-ST-1409, pages 7 and 8.

### 9.) ACKNOWLEDGEMENTS

Any documentation of an engineering effort is never a singular effort. Many contributed who are too numerous to cite individually. We wish to particularly thank the following individuals: Messrs. C. Maidens, E. Kelley, and E. Ferko, Lockheed-Georgia Company; Mr. R. Wylam, USAF, A-10 System Project Office; Mr. M. Siegel, Fairchild Republic Company; and, Mr. J. Goodman, USAF, Systems Engineering. Their particular efforts and associated organizational efforts, documentation and professionalism contributed greatly to the writing of this paper and more importantly to the success of the C-5 Wing Mod and A-10 programs.

EFFECT OF FLIGHT SEQUENCES  
IN COMPLEX LOAD HISTORIES  
ON CRACK FRONT MARKING

by

A. LIBERGE and C. BLEUZEN

Centre d'Essais Aéronautique de Toulouse  
23, Avenue H. Guillaumet-31056-TOULOUSE CEDEX  
FRANCE

SUMMARY.

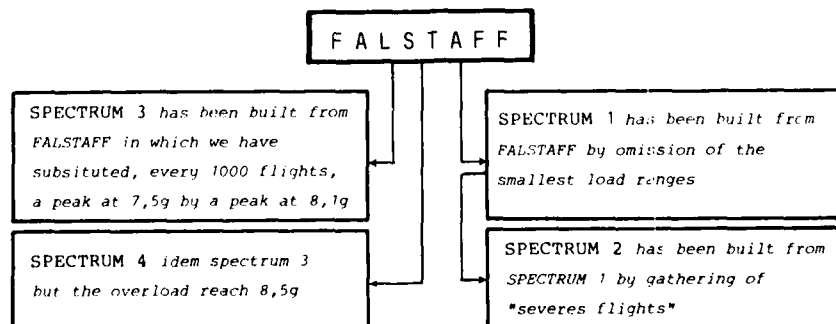
Some modifications of FALSTAFF have been studied :

- Spectrum 1 : omission of the smallest load ranges of FALSTAFF
- Spectrum 2 : gathering of severes flights of spectrum 1
- Spectrum 3 : FALSTAFF with an overload to 8,1g
- Spectrum 4 : FALSTAFF with an overload to 8,5g
- For aluminium alloys 2024 T351, 2214 T651 and 7475 T7351, C.E.A.T. has carried out :
  - . 1) - Fatigue test on - open hole specimens ( $Kt_{net} = 2,4$ )
    - joint specimens - no load transfer specimens
    - single shear specimen, high load transfer and secondary bending
  - . 2) - Crack growth test on ASTM CT specimens
- Spectrum (1) gives approximatively the same fatigue tests results that FALSTAFF but its crack surface is not readable in fractography
- Spectrum (2), (3) and (4) look traceable in the range of crack rates from  $3.10^{-5}$  to  $10^{-2}$  mm per flight, but they have increased fatigue lifes comparatively to FALSTAFF.

1 - INTRODUCTION.

Some modifications of FALSTAFF have been studied in order to promote the use of this loading spectrum in the case of structural or large specimens testing, for wich it is critical to assess a good fractographic traceability of the crack surface.

The different modifications which we have studied are summarized below :



## 2 - DEFINITION OF SPECTRA.

## 2.1. SPECTRUM 1

This spectrum has been built from FALSTAFF by omission in the flight loading sequence of all the load ranges equal to 3 FALSTAFF intervals whatever the values of peak or valley considered ; the ground loads remain unchanged (see fig 1).

The number of extrema is reduced from 35966 (FALSTAFF) to about 18012 (SPECTRUM 1). Fig. 2 and 3 show comparatively the level distributions for FALSTAFF and SPECTRUM 1.

## 2.2. SPECTRUM 2.

In this spectrum the location of "severes flights" inside spectrum 1 block has been changed. Most of flights including loads equal or greater than level 28 are gathered in the middle of block. The new order of flights in the block is described fig. 4. Fig 5 shows comparatively to FALSTAFF the succession of the maxima of each flight for one block

## 2.3. SPECTRUM 3.

In this case, every 1000 flights (5 blocks), the peak number 397 (level 32  $\rightarrow$  7,5g) of the flight number 32 is increased to a level of 34 (8,1g) - (See fig. 6).

## 2.4. SPECTRUM 4.

Idem spectrum (3), but every 1000 flights, the peak number 397 (flight 32) is increased to a level of 35,3 (8,5g) - (See fig. 6).

## 3 - TEST PROGRAMME.

## 3.1. TEST SPECIMENS.

## 3.1.1. METALLURGIC SPECIMENS.

- TYPE A SPECIMEN (see fig. 7)

It's an open hole specimen

Reference section = Net section =  $(60 - 20) \times 6 = 240\text{mm}^2$

$K_{t_{net}} = 2,4$  (stress concentration factor)

- ASTM-CT20 SPECIMEN for crack growth tests (see fig. 8)

Stress intensity factor (K) solution for this specimen are :

$$K = \frac{P}{B\sqrt{W}} f(\alpha)$$

with :  $\alpha = \frac{a}{W}$

$$f(\alpha) = 2 + \alpha (1 - \alpha)^{-3/2} (0,886 + 4,64\alpha - 13,32\alpha^2 + 14,72\alpha^3 - 5,6\alpha^4)$$

P = applied load

W = 40mm (specimen width)

B = 10mm (specimen thickness)

a = crack length

The test results have been analyzed using the propagation law

$$\frac{da}{dN} = c \left( \frac{K}{ng} \right)^m$$

with : K = stress intensity factor

ng = load factor

Crack growth rates  $\left( \frac{da}{dN} \right)$  have been calculated using the "secant method" with 5 points.

## 3.12. JOINT SPECIMENS

- TYPE B SPECIMEN (see fig. 9)

It's a no load transfer specimen

## FASTENER SYSTEM

- Broached hole
- TA6V Ø 6mm Rivet
- Interference  $\sim 25 \mu\text{m}$
- Surface treatment : chromic anodizing
- application of epoxy primer
- sealant PR 1431-S

Reference section = brut section =  $40 \times 5 = 200\text{mm}^2$

- TYPE C SPECIMEN (see fig. 10)

It's a high load transfer single shear joint with secondary bending

## FASTENER SYSTEM

- Idem type B specimen

Reference section = brut section =  $72 \times 5 = 360\text{mm}^2$

## 3.2. STUDIED ALLOYS

MECHANICAL PROPERTIES - LONG TRANSVERSE -				
	R (MPa)	R <sub>0,2</sub> (MPa)	A %	
2024 T351 Sheet 10mm	468	317	17	Types A and ASTM CT20 specimens
2024 T351 Sheet 50mm	482	358	14,3	Types B and C specimens
2214 T651 Sheet 10mm	497	427	13,2	Types A and ASTM CT20 specimens
2214 T651 Sheet 50mm	510	461	10	Types B and C specimens
7475 T7351 Sheet 55mm	509	443	11,3	Types B and C specimens
7475 T7351 Sheet 60mm	482	406	11,4	Types A and ASTM CT20 specimens

All the specimens were taken in long transverse direction.

## 3.3. TEST CASES.

The different studied test cases are indicated in table below

	ALLOY	TYPE A	ASTM CT20	TYPE B	TYPE C
FALSTAFF	2024	X	X	X	X
	2214	X	X	X	X
	7475	X	X	X	X
SPECTRUM (1)	2024	X	X		X
	2214	X	X		X
	7475				X
SPECTRUM (2)	2024				
	2214	X	X		
	7475				
SPECTRUM (3)	2024		X		
	2214	X	X	X	X
	7475		X	X	X
SPECTRUM (4)	2024				
	2214	X	X		
	7475				

## 3.4. TEST PARAMETERS.

- Room temperature ~ 20°C
- Relative humidity ~ 40-80 per cent
- frequencies - ~ 6 hz for ASTM CT20 Specimens
  - ~12 hz for types A, B and C specimens

## 4 - TEST RESULTS.

## 4.1. ALLOY 2214 T651

## 4.11. TYPE A SPECIMENS.

	LOADING RATE	DETAILED RESULTS (Flights to failure)	LOGARITHMIC MEAN	STANDARD DEVIATION
FALSTAFF	35 MPa/g	8773-10232-9997-10432-10600-9573	9900	0,030
	25 MPa/g	37032-31930-32081-32773-25560-47432-41797	34900	0,088
SPECTRUM (1)	35 MPa/g	11232-9773-11432-10197-9281-8881	10100	0,044
	25 MPa/g	34081-31773-30400-32773-36232-51025-41281-37597-34632	36100	0,070
SPECTRUM (2)	35 MPa/g	12704-16497-11689-10710	12730	0,080
	25 MPa/g	43830-59295-44694-56694	50660	0,070
SPECTRUM (3)	35 MPa/g	12373-14173-10597-14222	12750	0,061
	25 MPa/g	46225-31893-43597-39081	39810	0,070
SPECTRUM (4)	35 MPa/g	19373-15031-15730-14344-14240	15640	0,055

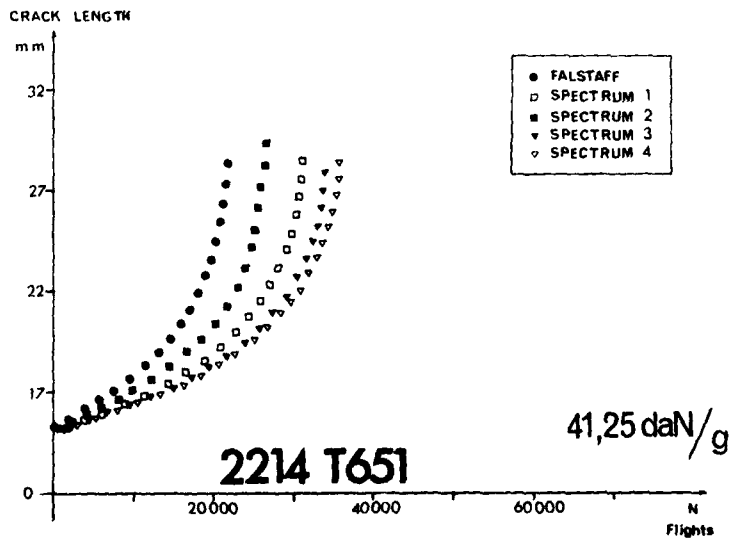
These test results are summarized on figure 11

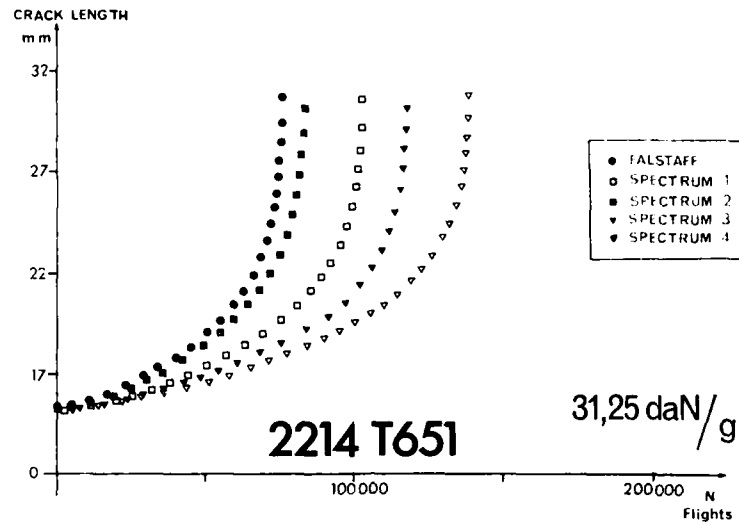
## 4.12. ASTM CT20 810 SPECIMENS.

Tests were conducted on two specimens :

- The first with a loading rate of 41,25 daN for n = 1g
- The second with a loading rate of 31,25 daN for n = 1g

The comparison of fatigue crack growth behavior for the different spectra is shown below (curves  $a = f(N)$ ) and fig 12 (propagation law :  $\frac{da}{dN} = c' \left(\frac{K}{ng}\right)^{m'}$ )





## 4.13. TYPE B SPECIMENS

	LOADING RATE	DETAILED RESULTS (Flights to failure)	LOGARITHMIC MEAN	STANDARD DEVIATION
FALSTAFF	26,7 MPa/g	60032-69632-133840 (No failure)	82400	0,185
	34,7 MPa/g	23232-24173-24081	23800	0,009
	46,7 MPa/g	8225-7373-7373	7650	0,027
SPECTRUM (3)	34,7 MPa/g	30360-41773-38832	36650	0,072

These test results are summarized on figure 13

## 4.14. TYPE C SPECIMENS.

	LOADING RATE	DETAILED RESULTS (Flights to failure)	LOGARITHMIC MEAN	STANDARD DEVIATION
FALSTAFF	15 MPa/g	56522-64944-41825	53500	0,097
	20 MPa/g	20973-19822-16232	18900	0,058
	26,7 MPa/g	4832-2925-3432	3650	0,111
SPECTRUM (1)	20 MPa/g	15173-19173-24373	19200	0,103
SPECTRUM (3)	20 MPa/g	35681-23632-18852	25100	0,140

These test results are summarized on figure 14

## 4.2. ALLOY 2024 T351.

## 4.21. TYPE A SPECIMENS.

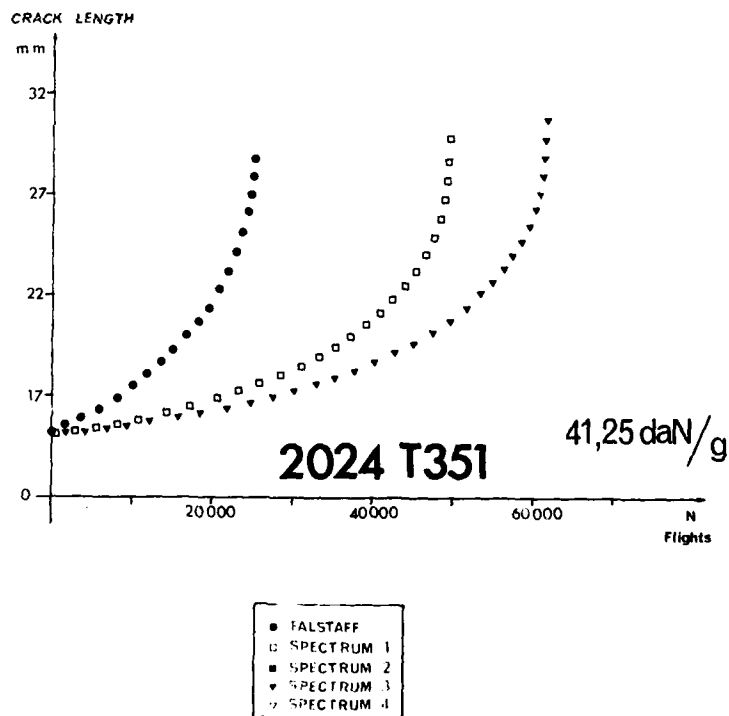
	LOADING RATE	DETAILED RESULTS (Flights to failure)	LOGARITHMIC MEAN	STANDARD DEVIATION
FALSTAFF	35 MPa/g	9597-7590-7434-6573-8197-8400	7900	0,06
	25 MPa/g	59597-62481-54973-44197-64327	56600	0,065
SPECTRUM (1)	35 MPa/g	7895-8630-10480-10432-9573-10266	9500	0,05
	25 MPa/g	55825-78330-47232-59960 48026-44755	54650	0,09

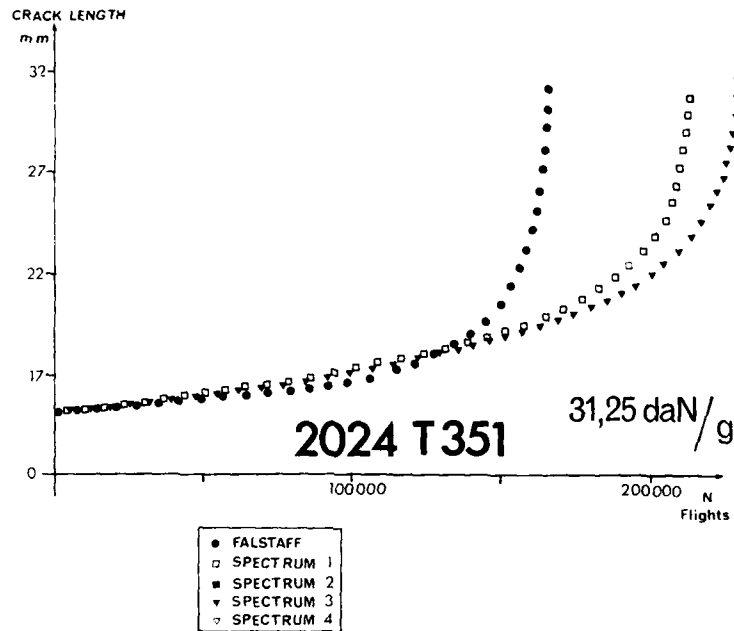
These test results are summarized on figure 15.

## 4.22. ASTM CT20 B10 SPECIMENS.

See below for  $a = f(N)$  curves and fig. 16 for propagation law

$$\frac{da}{dN} = c' \left( \frac{K}{ng} \right)^{m'}$$





## 4.23. TYPE B SPECIMENS

	LOADING RATE	DETAILED RESULTS (Flights to failure)	LOGARITHMIC MEAN	STANDARD DEVIATION
FALSTAFF	26,7 MPa/g	82973-78139-30960	58550	0,240
	34,7 MPa/g	24925-29150-27173	27000	0,034
	40 MPa/g	2032-2000	2015	0,04
	46,7 MPa/g	173-173-81	134	0,190

These test results are summarized on figure 17

## 4.24. TYPE C SPECIMENS

	LOADING RATE	DETAILED RESULTS (Flights to failure)	LOGARITHMIC MEAN	STANDARD DEVIATION
FALSTAFF	15 MPa/g	71596-63436-53634	62450	0,062
	20 MPa/g	14832-15432-10606	13400	0,089
	26,7 MPa/g	1130-1432-1431	1320	0,039
SPECTRUM (1)	20 MPa/g	22075-16973-17197	18600	0,064

These test results are summarized on figure 18

4.3. ALLOY 7475 T7351

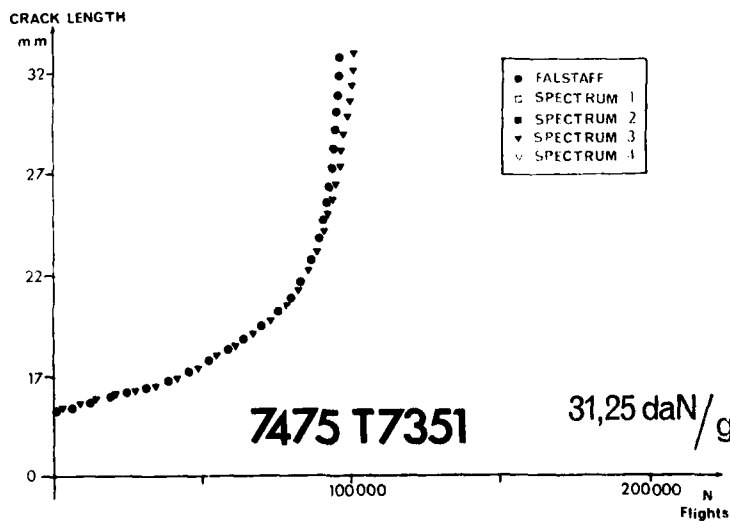
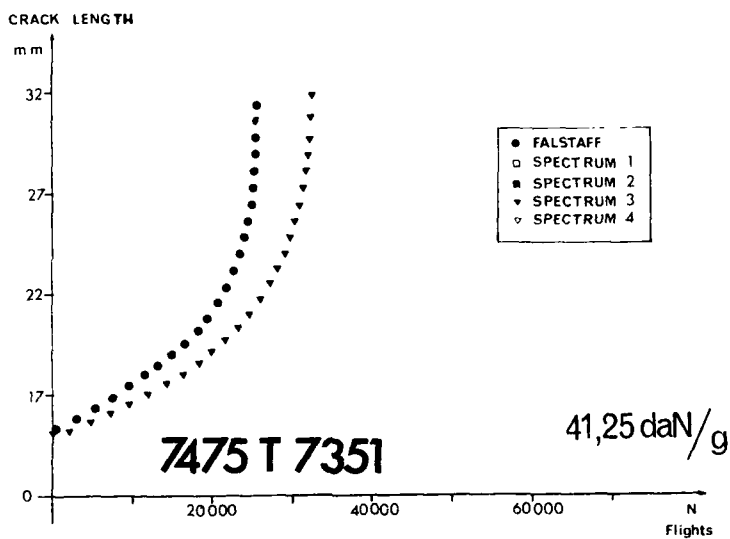
4.31. TYPE A SPECIMENS

	LOADING RATE	DETAILED RESULTS (Flights to failure)	LOGARITHMIC MEAN	STANDARD DEVIATION
FALSTAFF	35 MPa/g	7760-9825-11612-8130-9612	9300	0,070
	25 MPa/g	87973-41744-47825-99773-65426	64850	0,160

These test results are summarized on figure 19

4.32. TYPE ASTM CT 20 B10 SPECIMENS

See below for  $a = f(N)$  curves and fig 20 for propagation law  $\frac{da}{dN} = c' \left(\frac{K}{ng}\right)^{m'}$



## 4.33. TYPE B SPECIMENS.

	LOADING RATE	DETAILED RESULTS (Flights to failure)	LOGARITHMIC MEAN	STANDARD DEVIATION
FALSTAFF	26,7 MPa/g	43344-35160-68234	47000	0,147
	34,7 MPa/g	13432-14726-12760	13600	0,031
	46,7 MPa/g	373-432-573	450	0,094
SPECTRUM (3)	34,7 MPa/g	21573-19373-19725-15789-16632	18500	0,055

These test results are summarized on figure 21.

## 4.34. TYPE C SPECIMENS.

	LOADING RATE	DETAILED RESULTS (Flights to failure)	LOGARITHMIC MEAN	STANDARD DEVIATION
FALSTAFF	15 MPa/g	41625-26712-36206	34300	0,098
	20 MPa/g	13185-12330-8330	11000	0,107
	26,7 MPa/g	1112-1573-1681	1430	0,096
SPECTRUM (1)	20 MPa/g	13344-15573-10699	13000	0,082
SPECTRUM (3)	20 MPa/g	7432-13025	9850	0,172

## 5 - FRACTOGRAPHY.

Whatever the specimen type and the alloy, SPECTRA (2), (3) and (4) look traceable in the range of crack growth rates from  $3 \cdot 10^{-5}$  to  $10^{-2}$  mm per flight.

Figures 22, 23 and 24 show an example of the crack surfaces marking for 2214 1651 alloy on type A specimen.

## 6 - CONCLUSIONS.

Comparatively to FALSTAFF sequence, test results show that :

## - FOR SPECTRUM 1

- With 2024 and 2214 alloys, fatigue lifes on type A specimens remain unchanged, but it seems that crack growth decreases on ASTM CT20 specimens
- On type C specimens (2024 and 7475 alloys) spectrum 1 increases slightly fatigue lifes. The omission of the smallest amplitude cycles decreases fretting inter-sheet which is the principal reason, with secondary bending, of type C specimen failure.

## - FOR SPECTRUM 2.

- With 2214 alloy this spectrum increases fatigue lifes on type A specimen and decreases crack growth on ASTM CT20 specimens

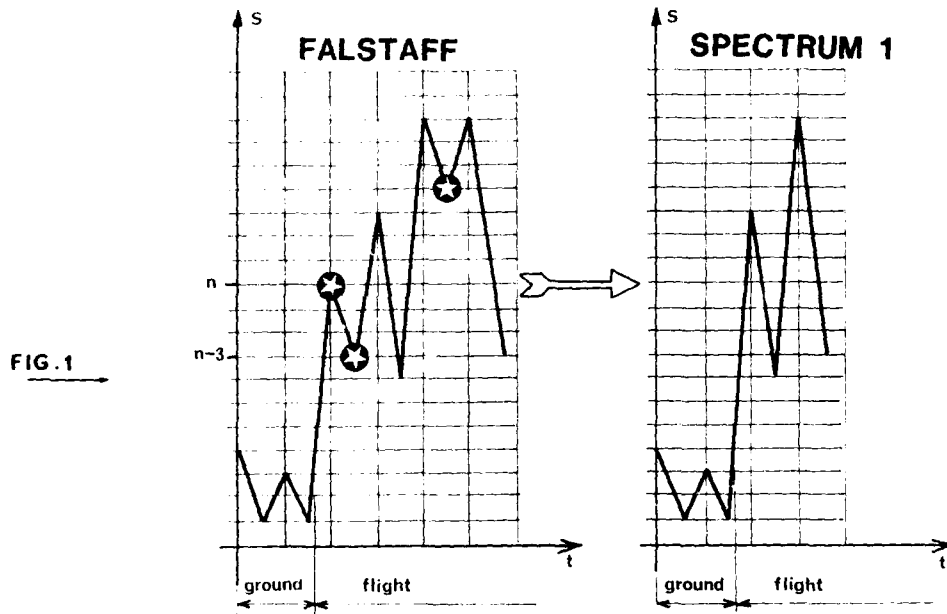
- FOR SPECTRA (3) AND (4).

- With type A specimens (2214 alloy) and for the loading rate of 35 MPa/g, the local plastic strains due to overloads (8.1g for spectrum 3 and 8.5g for spectrum 4) decrease the local mean stress and consequently fatigue lifes increase. With the loading rate of 25 MPa/g local plastic strains are very smaller and there is no effect on fatigue lifes.

With types B and C joint specimens, with the studied loading rates, spectrum (3) increases fatigue lifes comparatively to FALSTAFF.

- With ASTM specimens, tensile overloads of spectrum 3 and 4 cause crack retardation phenomenon and this effect is more sensitive for 2214 and 2024 alloys than for 7475 alloy.

REFERENCE ; CEAT Report M7 681900



LEVELS DISTRIBUTION									
FALSTAFF					SPECTRUM (1)				
LEVEL	PEAKS		VALLEYS		LEVEL	PEAKS		VALLEYS	
	N	Nc	N	Nc		N	Nc	N	Nc
1	0	17983	2	2	1	0	9006	2	2
2	0	17983	2	4	2	0	9006	2	4
3	0	17983	1	5	3	0	9006	1	5
4	0	17983	6	11	4	0	9006	6	11
5	0	17983	327	338	5	0	9006	327	338
6	0	17983	508	846	6	0	9006	508	846
7	155	17983	36	882	7	155	9006	36	882
8	445	17828	543	1425	8	445	8051	500	1382
9	0	17383	1941	3366	9	0	8406	1457	2839
10	0	17383	6711	10077	10	0	8406	2871	5710
11	43	7383	4387	14464	11	0	8406	1640	7350
12	493	17340	1445	15909	12	9	8406	750	8100
13	4058	16847	716	16625	13	218	8397	377	8477
14	4145	12789	511	17136	14	1398	8179	228	8705
15	1999	8644	321	17463	15	1304	6781	143	8848
16	1282	6645	234	17697	16	943	5477	35	8933
17	1151	5363	135	17832	17	868	4534	35	8968
18	987	4212	69	17901	18	803	3666	20	8988
19	954	3225	37	17938	19	805	2863	10	8998
20	640	2271	23	17961	20	540	2058	3	9001
21	533	1631	12	17973	21	484	1518	2	9003
22	404	1098	4	17977	22	377	1034	1	9004
23	233	694	3	17980	23	213	657	1	9005
24	193	461	2	17982	24	153	444	1	9006
25	104	268	1	17983	25	101	261	0	9006
26	76	164	0	17983	26	74	160	0	9006
27	45	88	0	17983	27	44	86	0	9006
28	24	43	0	17983	28	23	42	0	9006
29	10	19	0	17983	29	10	19	0	9006
30	7	9	0	17983	30	7	9	0	9006
31	0	2	0	17983	31	0	2	0	9006
32	2	2	0	17983	32	2	2	0	9006

N → Number of peaks or valleys per block of 200 flights

Nc → Cumulative number of peaks or valleys per block of 200 flights

FIG. 2

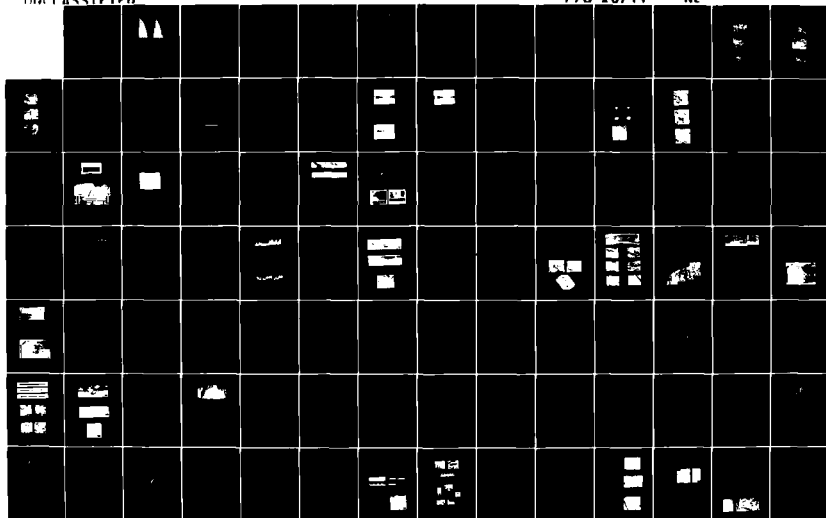
AD A152 368

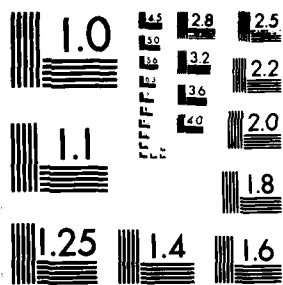
FATIGUE CRACK TOPOGRAPHY(U) ADVISORY GROUP FOR  
AEROSPACE RESEARCH AND DEVELOPMENT NEUILLY-SUR-SEINE  
(FRANCE) 1984 AGARD-CP-376

2/3

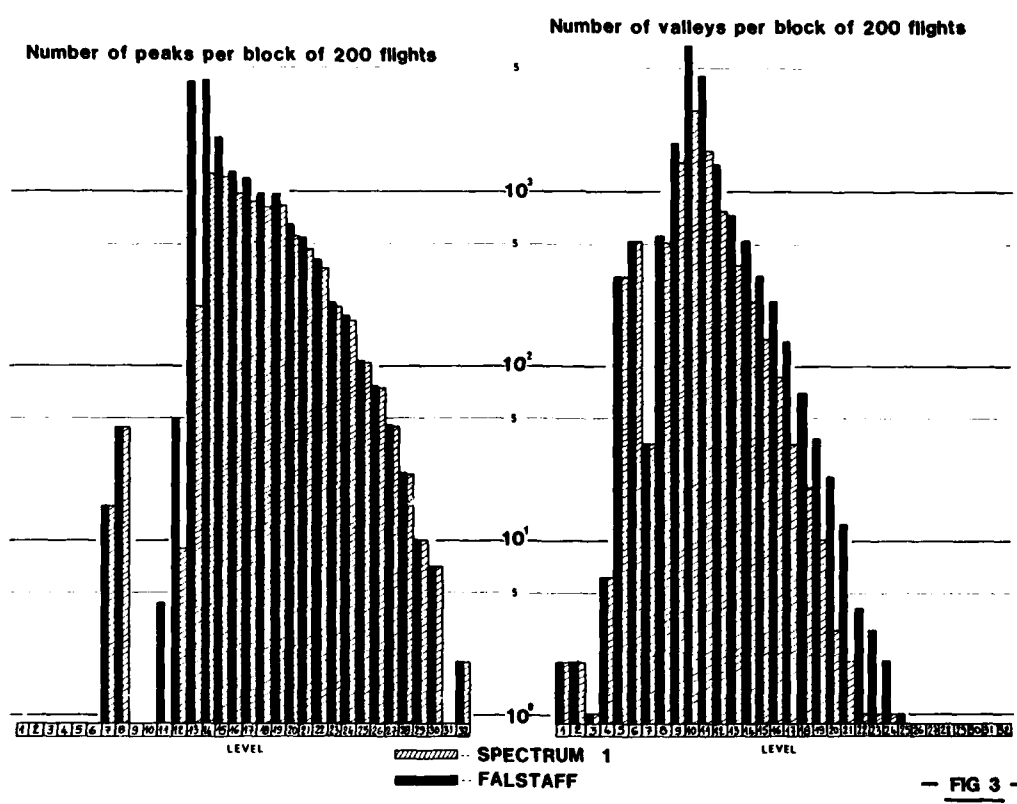
UNCLASSIFIED

F/G 20/11 NL





MICROCOPY RESOLUTION TEST CHART  
NATIONAL BUREAU OF STANDARDS-1963 A

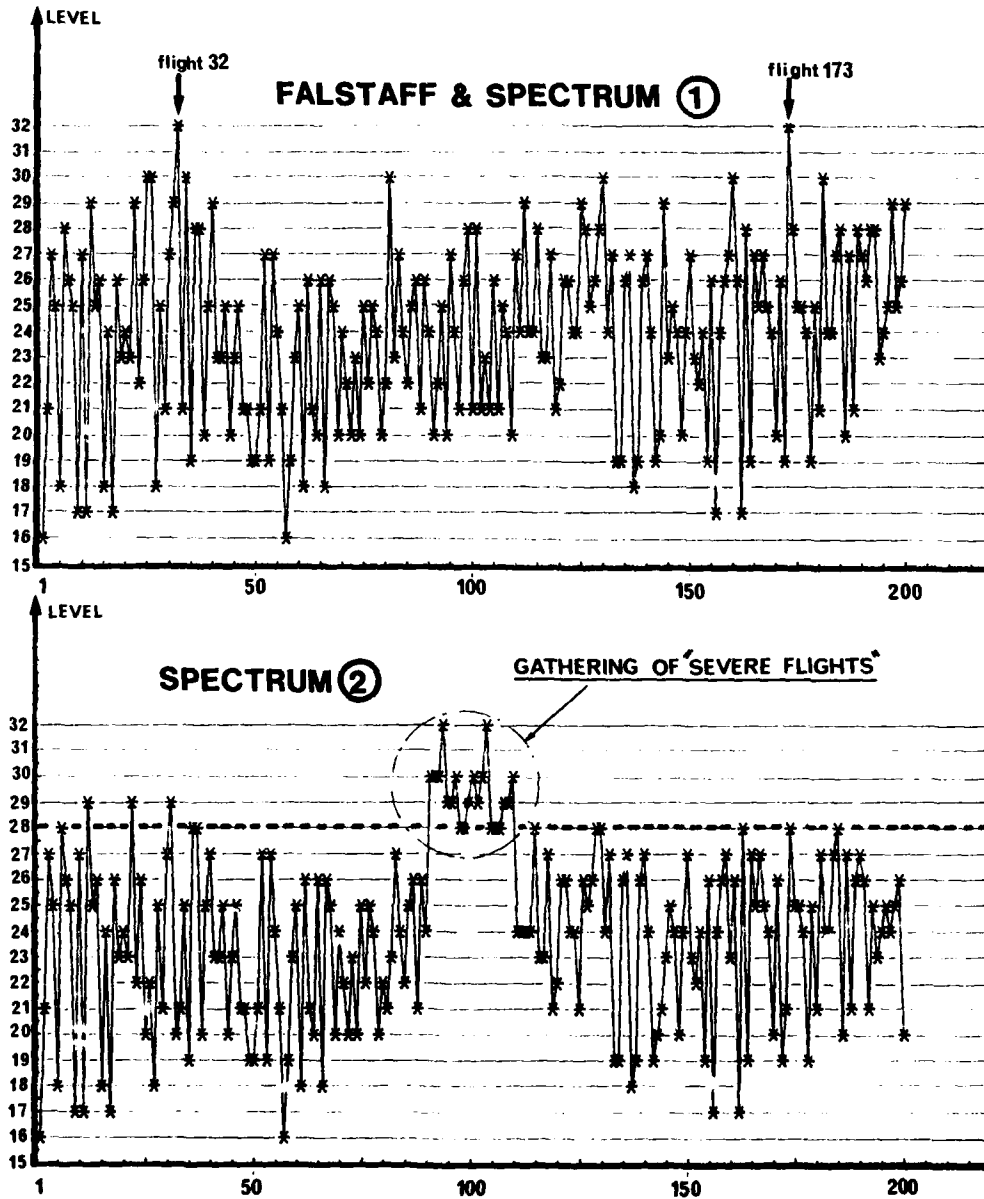


SPECTRUM (2)  
ORGANIZATION OF THE FLIGHTS IN THE BLOCK OF 200 FLIGHTS

	1				5					10					15					20					25				
	1	2	3	4	5	6	7	8	9	10	11	12	13	14	15	16	17	18	19	20	21	22	23	24	25				
26	92	27	28	29	30	31	32	33	34	35	36	37	38	39	40	41	42	43	44	45	46	47	48	49	50				
51	51	52	53	54	55	56	57	58	59	60	61	62	63	64	65	66	67	68	69	70	71	72	73	74	75				
76	76	77	78	79	80	81	82	83	84	85	86	87	88	89	90	25	26	27	28	29	30	31	32	33	34				
101	130	144	160	173	189	192	193	197	200	181	111	96	113	114	115	116	117	118	119	120	121	122	123	124	125				
126	98	127	128	99	101	131	132	133	134	135	136	137	138	139	140	141	142	143	102	145	146	147	148	149	150				
151	151	152	153	154	155	156	157	158	159	103	161	162	163	164	165	166	167	168	169	170	171	172	104	174	175				
176	176	177	178	179	180	110	182	183	184	185	186	187	188	105	190	191	106	107	194	195	196	108	198	199	109				

---Flights including a peak equal or greater than level 28  
 ---Gathering of "severe flights"

FIG. 4



↑ FIG 5 - Sequences of the maxima levels of each flight

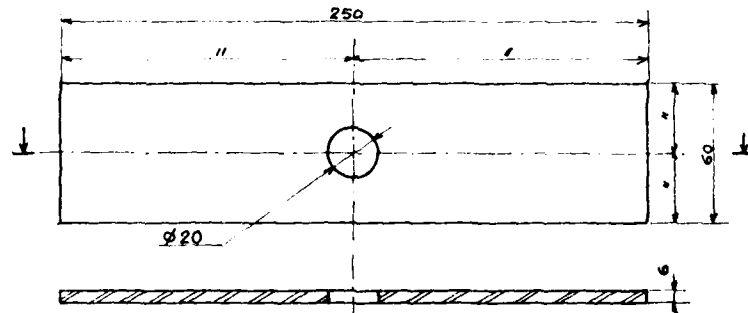
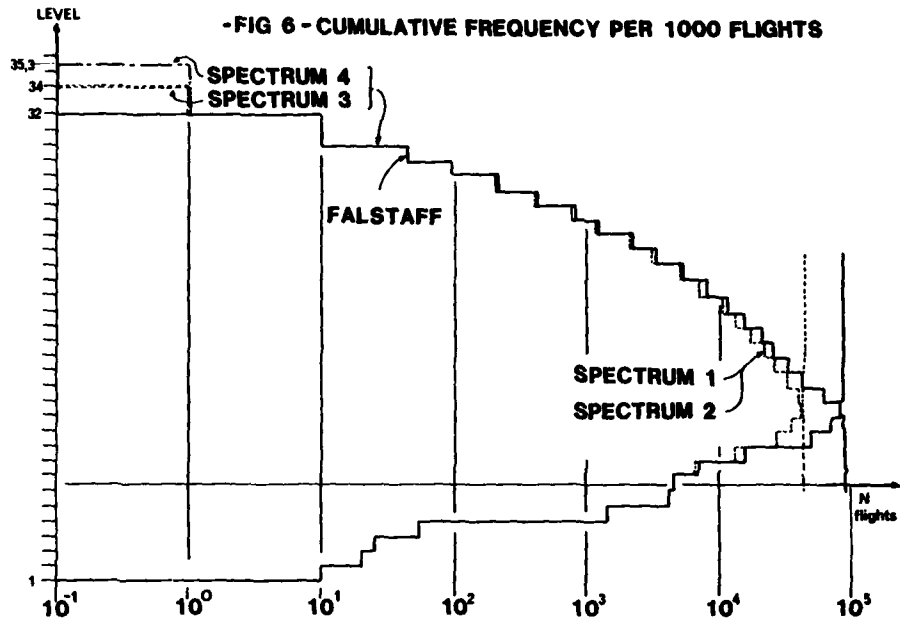


FIG-7 TYPE A SPECIMEN

$S_{net} = 240 \text{ mm}^2$      $K_t = 2.4$

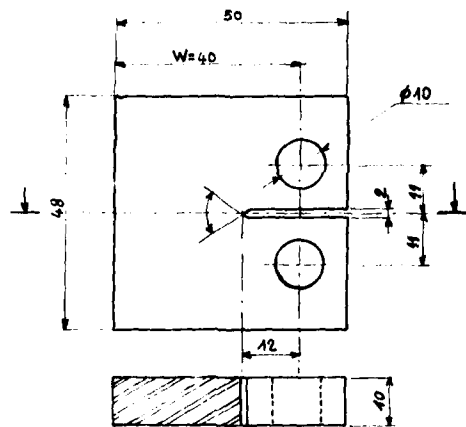


FIG-8 ASTM CT20-B10 SPECIMEN

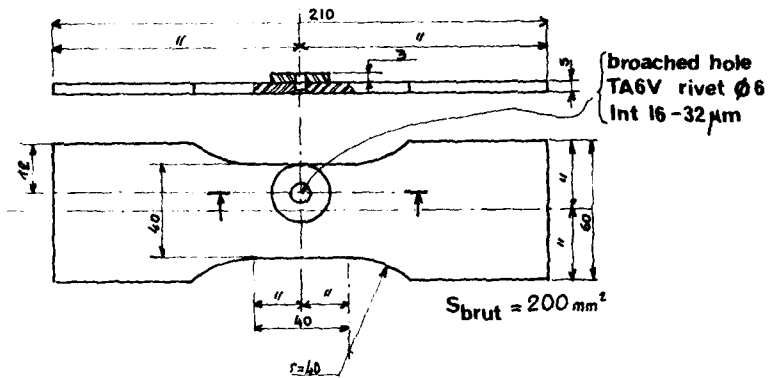


FIG-9 TYPE B SPECIMEN

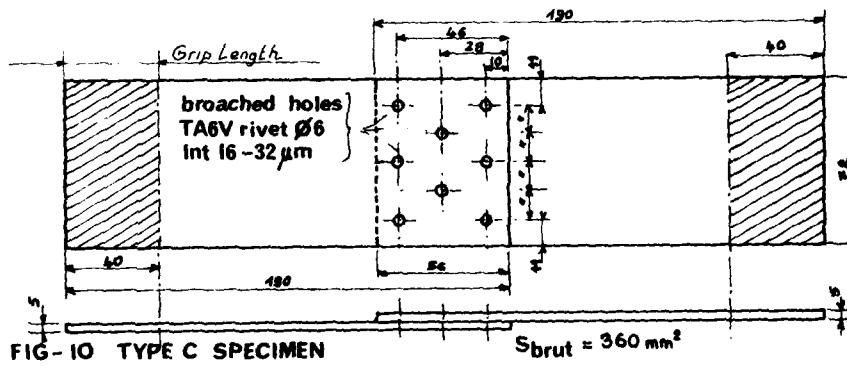
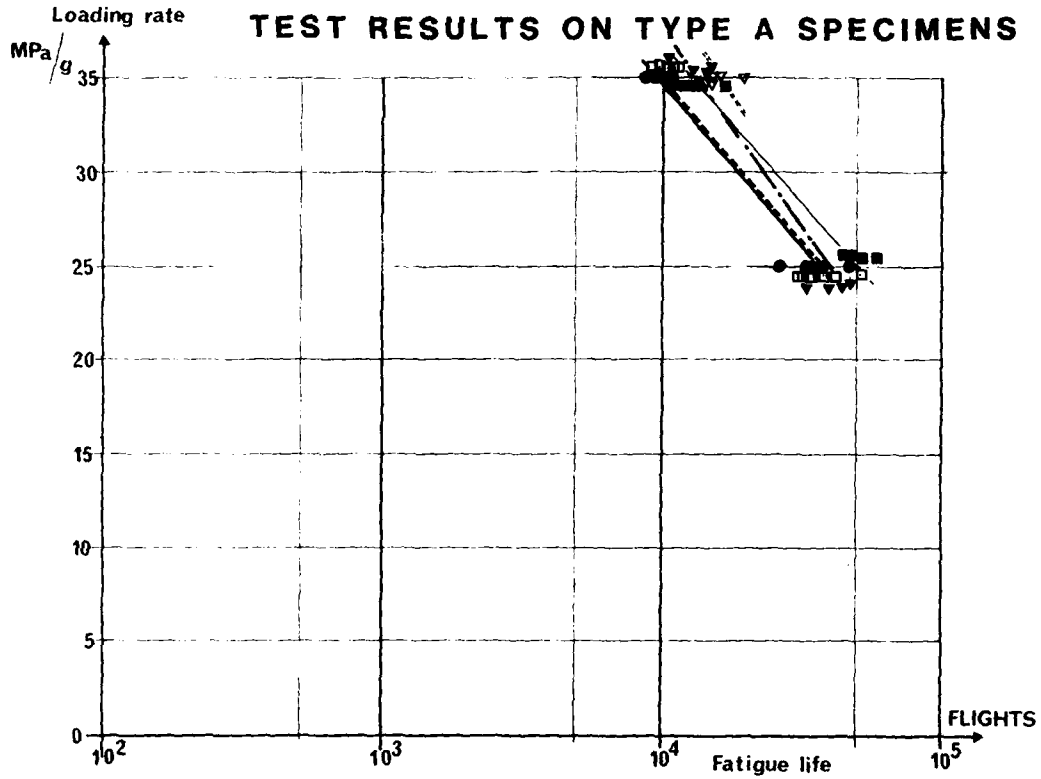


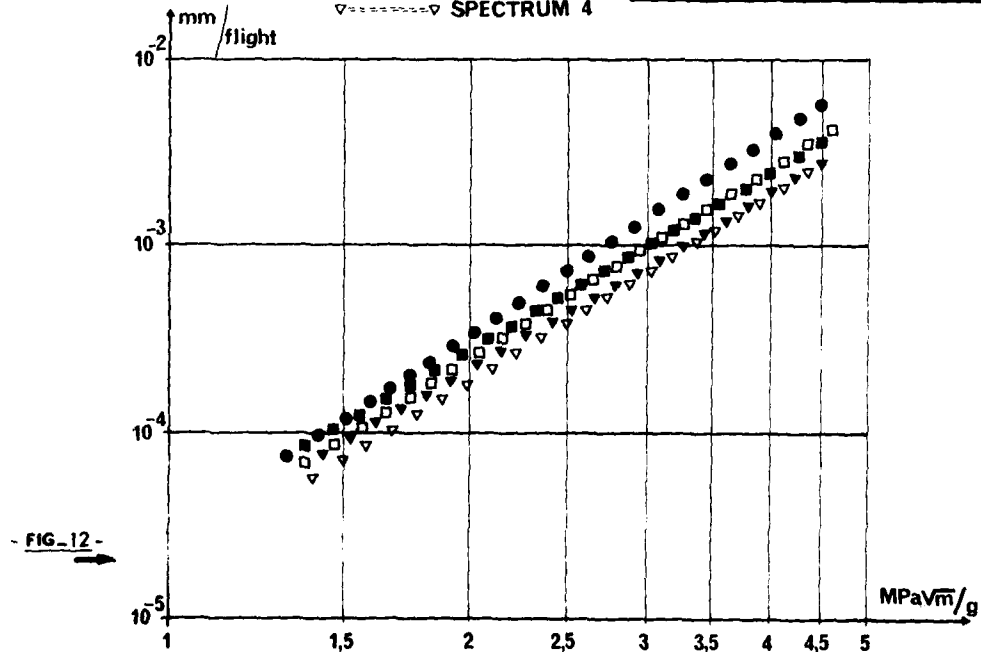
FIG-10 TYPE C SPECIMEN



- FIG-11 -

- FALSTAFF
- SPECTRUM 1
- SPECTRUM 2
- ▼ SPECTRUM 3
- ▽ SPECTRUM 4

**alloy 2214 T651**



- FIG-12 -

**TEST RESULTS ON ASTM CT SPECIMENS**

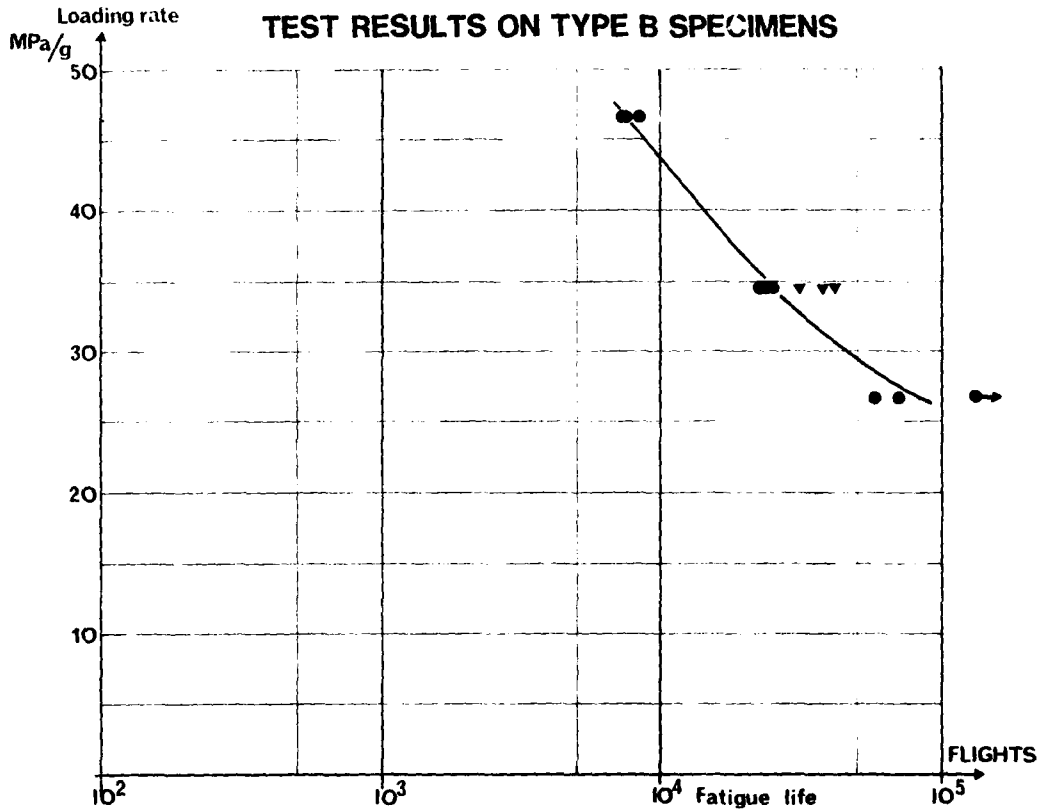
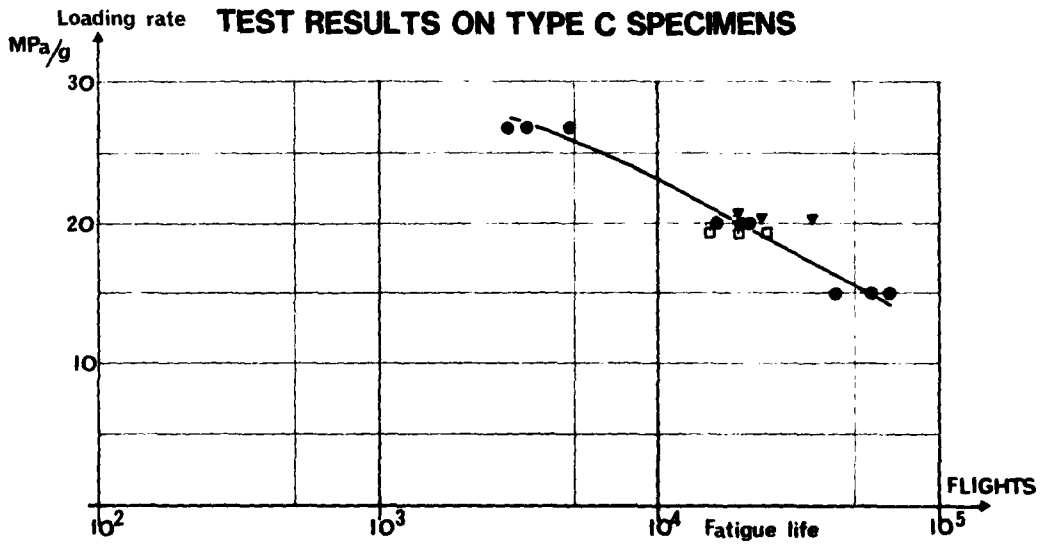


FIG-13 ↑

FIG-14 ↓

- FALSTAFF
- - - □ SPECTRE 1
- SPECTRE 2
- ▼——▼ SPECTRE 3
- ▽- - - ▽ SPECTRE 4

**alloy 2214 T651**



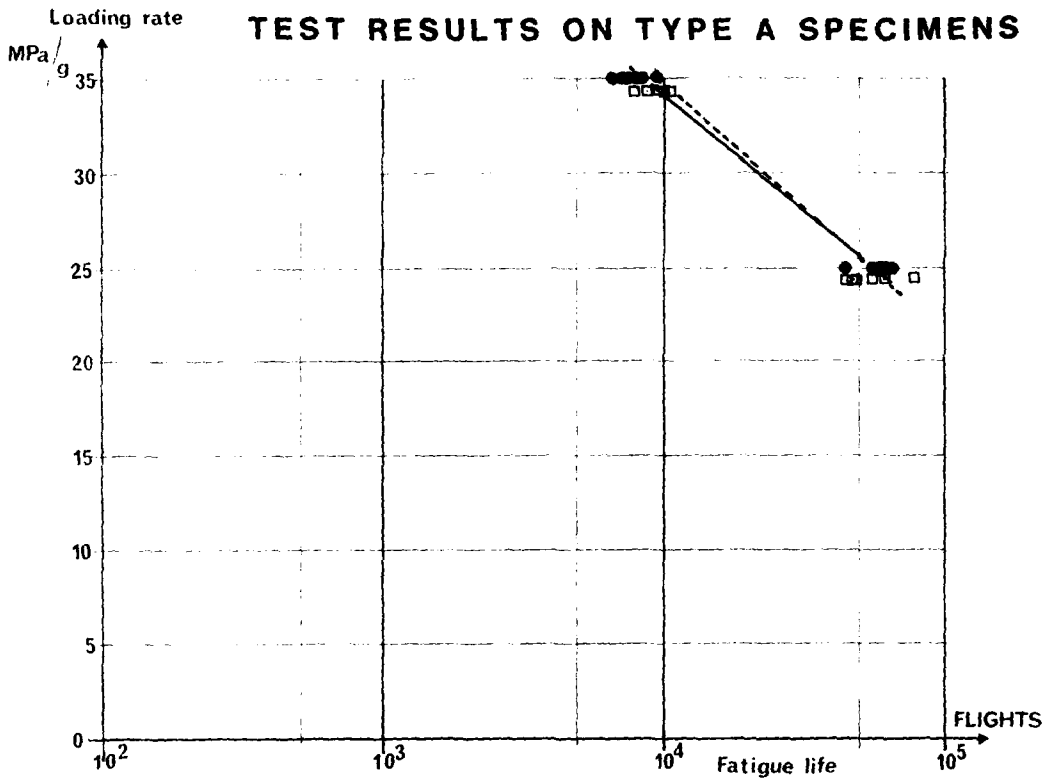
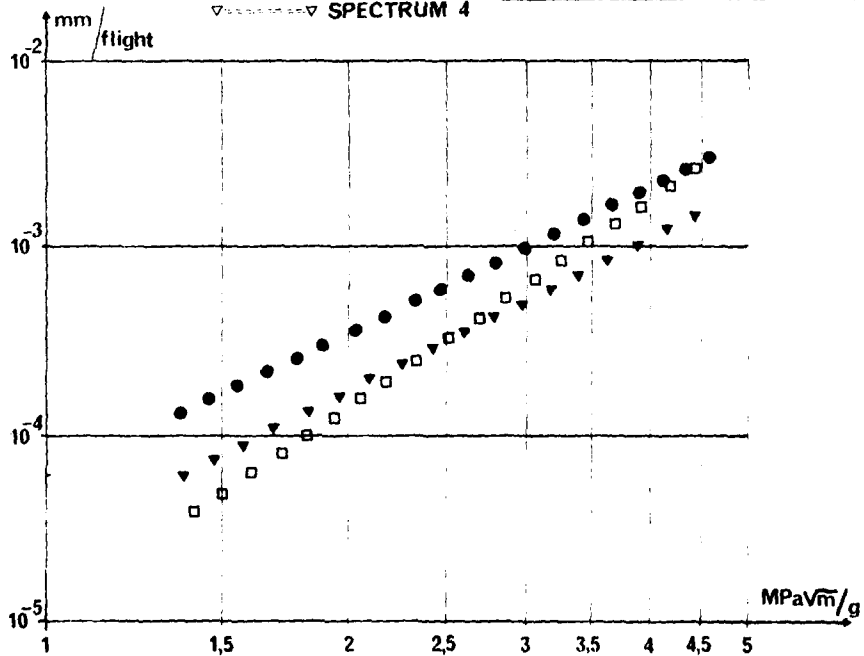


FIG-15 ↑

FIG-16 ↓

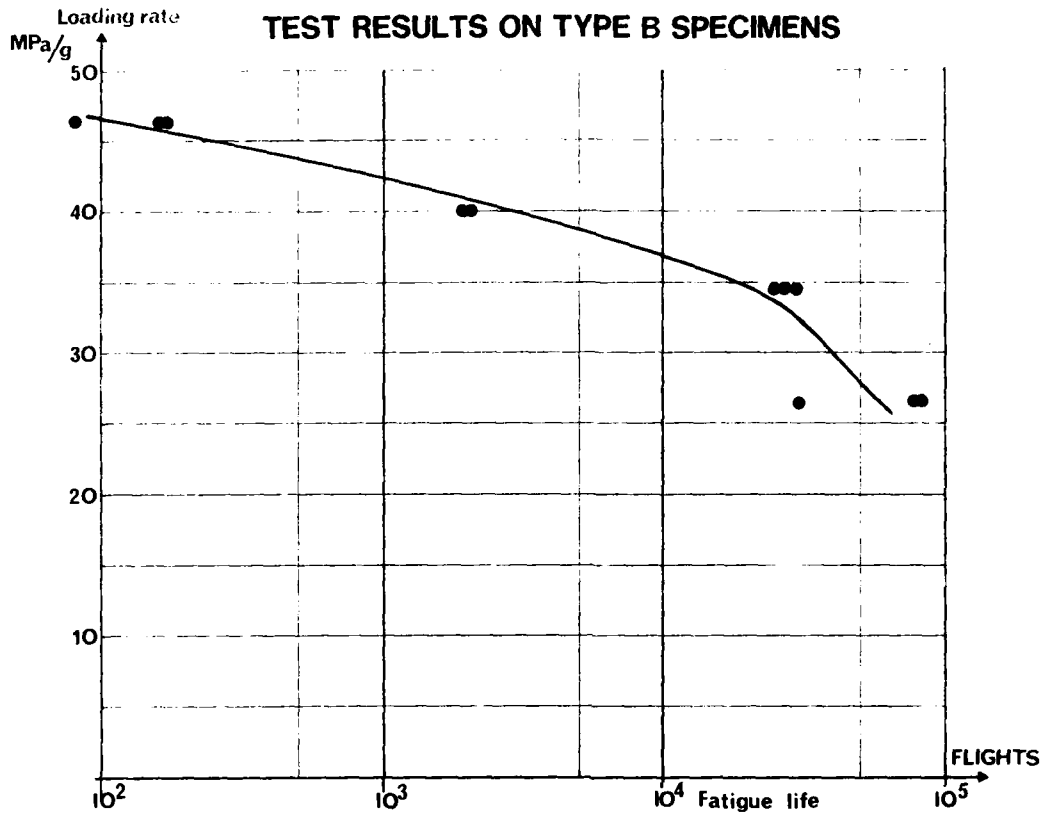
- FALSTAFF
- SPECTRUM 1
- SPECTRUM 2
- ▼ SPECTRUM 3
- ▽ SPECTRUM 4

**alloy 2024 T351**



TEST RESULTS ON ASTM CT SPECIMENS

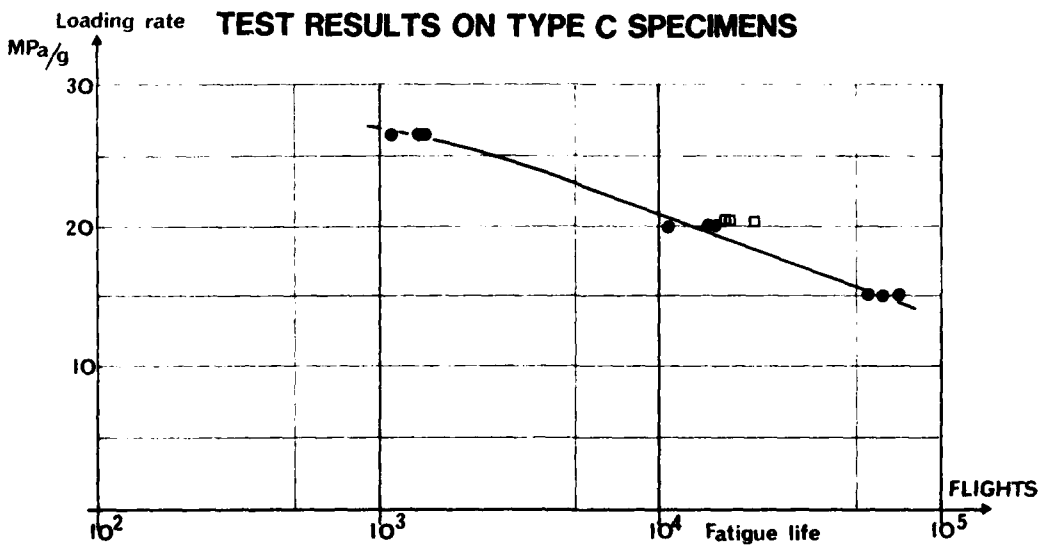
Stress intensity factor / Load factor

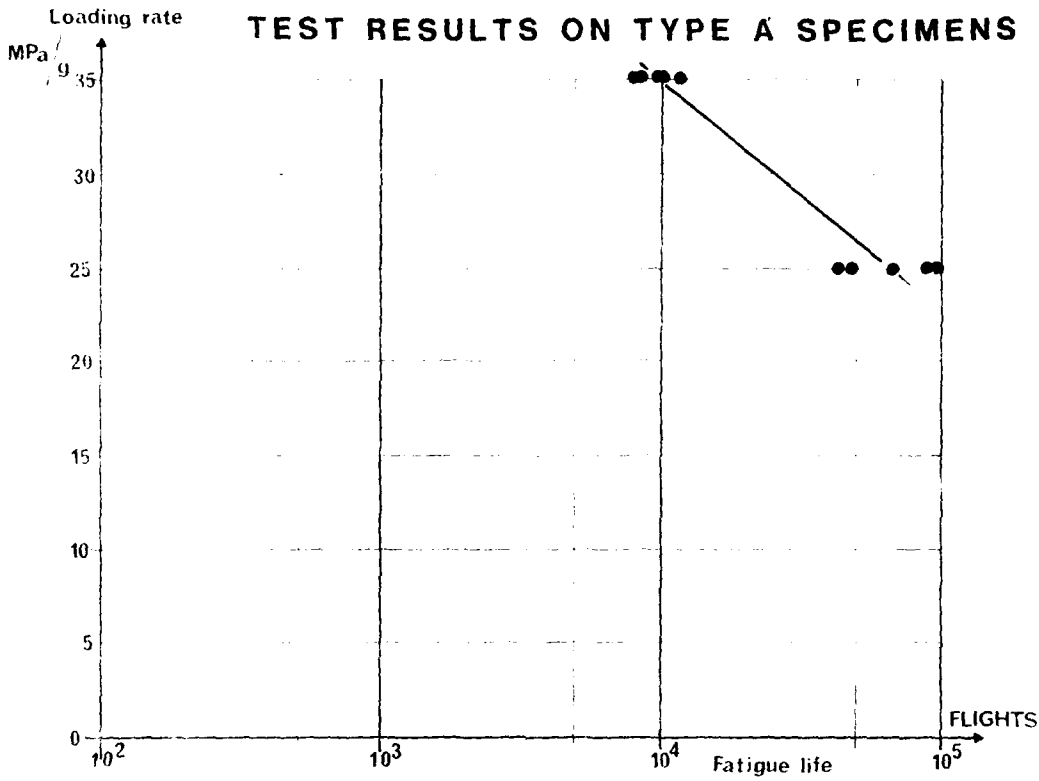


- FIG-17- ↑  
- FIG-18- ↓

- FALSTAFF
- SPECTRE 1
- SPECTRE 2
- ▼ SPECTRE 3
- ▽ SPECTRE 4

**alloy 2024 T351**



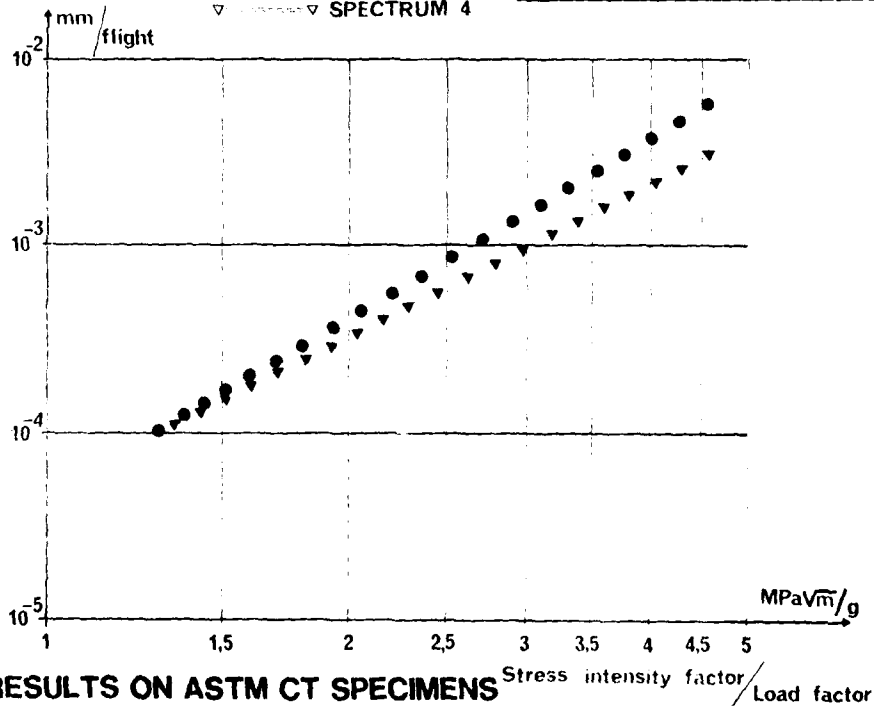


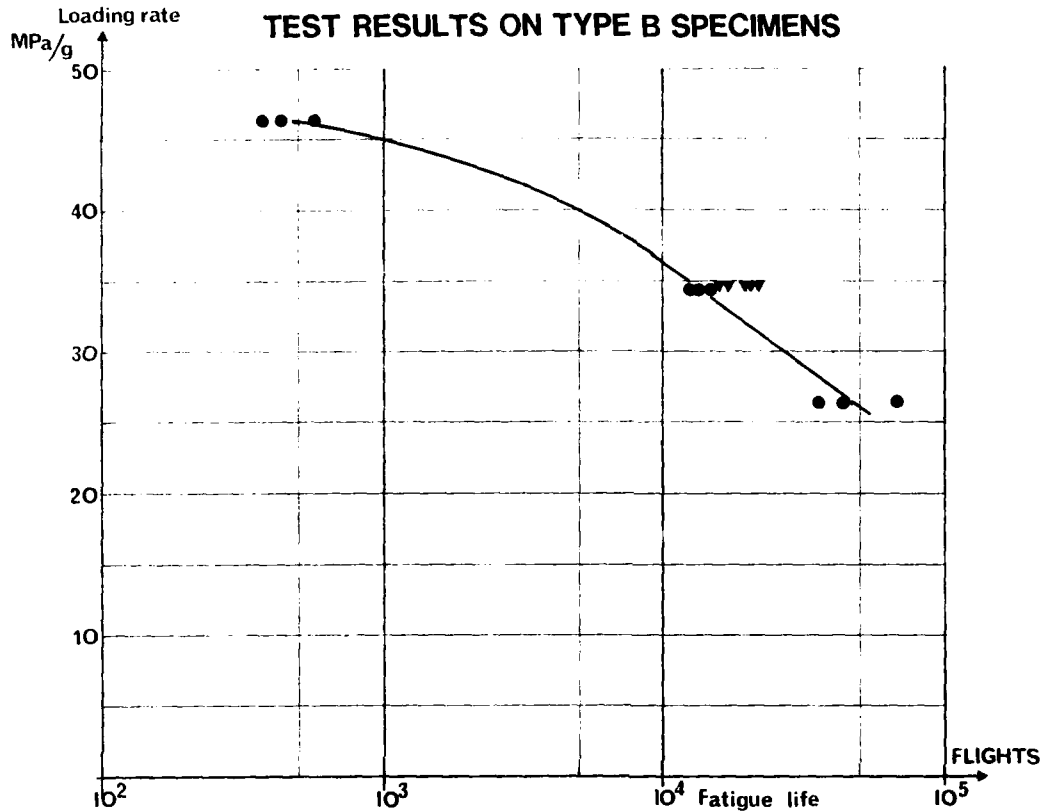
- FIG-19 - ↑

- FIG-20 - ↓

- — ● FALSTAFF
- - - - □ SPECTRUM 1
- - - - ■ SPECTRUM 2
- ▼ - - - ▼ SPECTRUM 3
- ▽ - - - ▽ SPECTRUM 4

**alloy 7475 T7351**



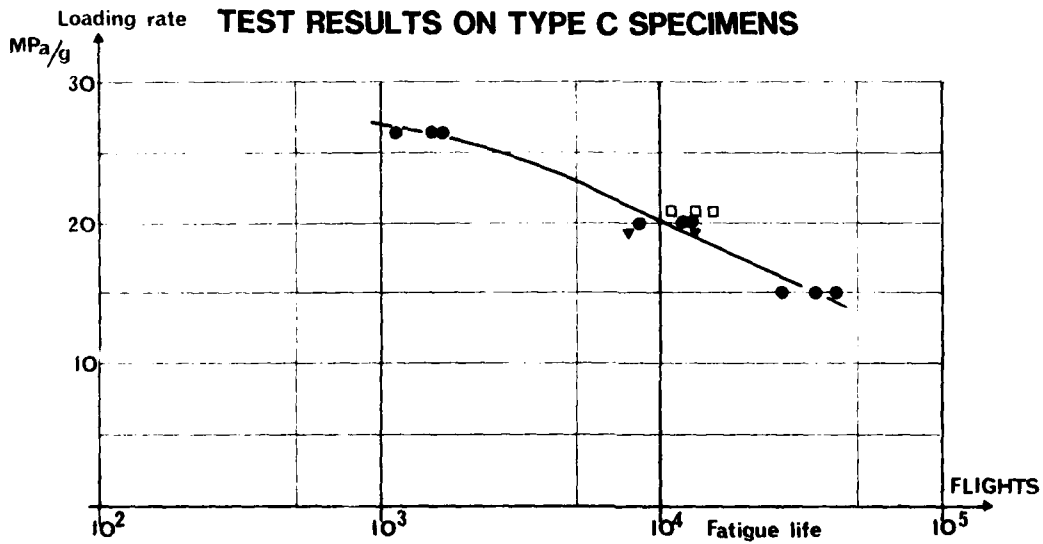


- FIG -21- ↑

- FIG -22- ↓

- — ● FALSTAFF
- — □ SPECTRE 1
- — ■ SPECTRE 2
- ▼ — ▼ SPECTRE 3
- ▽ — ▽ SPECTRE 4

**alloy 7475 T7351**



SPECTRUM (2)

GATHERING OF SEVERE FLIGHTS

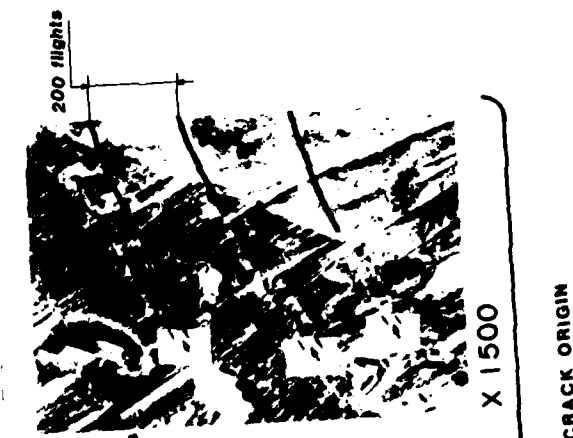
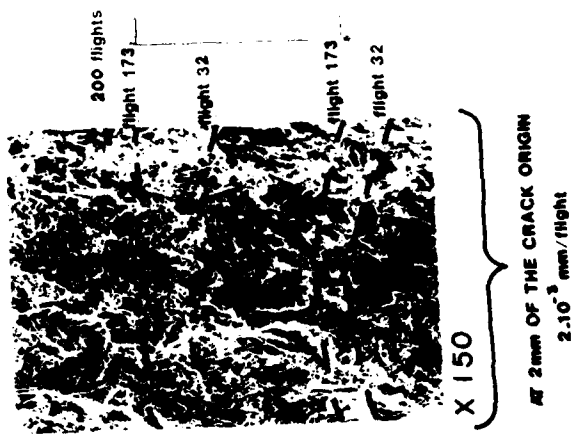


FIG-23

SPECTRUM (3)

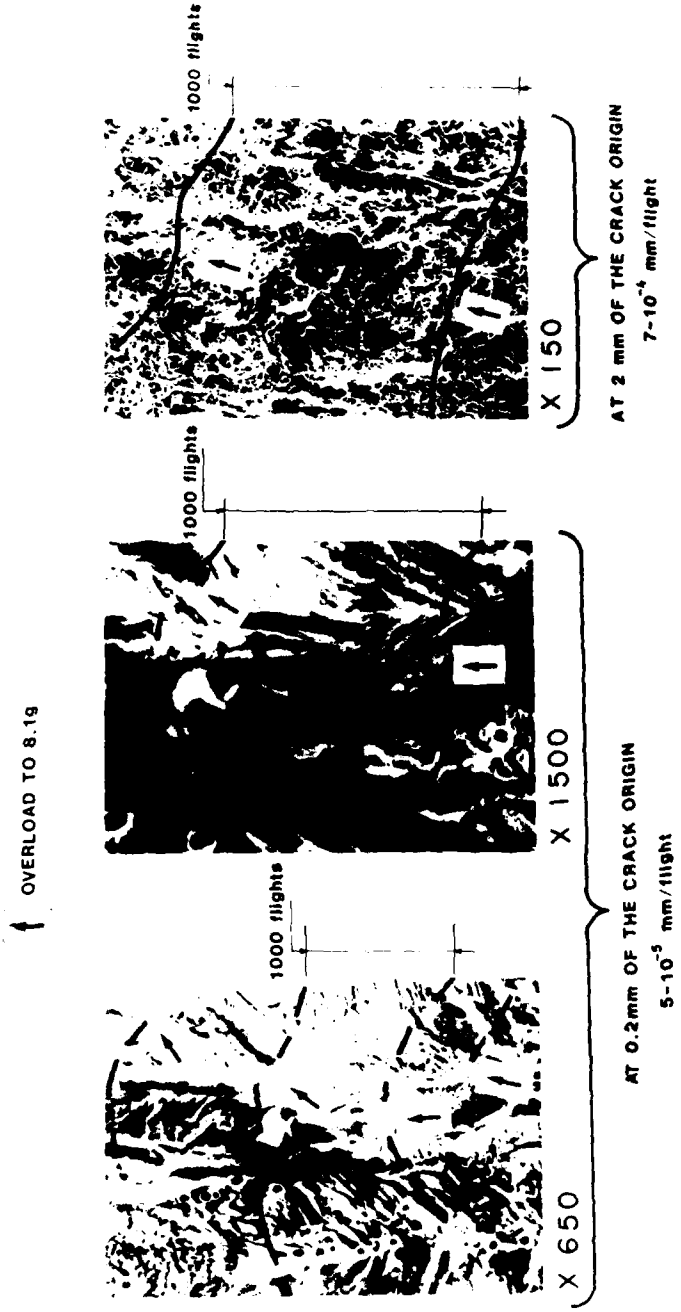


FIG. 24

PERIODIC LOADING SEQUENCES FOR THE SYSTEMATIC MARKING  
OF FATIGUE CRACK FRACTURE SURFACES

by  
J. C. Ekvall, L. Bakow and T. R. Brussat  
Lockheed-California Company  
Burbank, California 91520  
USA

INTRODUCTION

Periodic loading sequences which leave characteristic markings on the fracture surface are useful for evaluating the results of crack growth tests. These markings aid in the evaluation of crack growth rates and prediction formulations, and define the shape of cracks at specific times during the test.

To illustrate how loading sequences can be used to produce regularly spaced fracture surface markings in crack growth tests, three examples are presented. These include a fighter spectrum, a transport spectrum, and constant amplitude loading sequences. The composition of each of the loading sequences is discussed, and photographs of some of their resultant fracture surfaces are shown. The fracture surface markings produced by the three loading sequences are visible to the naked eye and can be directly photographed without magnification.

FIGHTER SPECTRUM LOADING SEQUENCE

Reference [1] presents some crack growth test results of simulated structure made from 7075-T6 aluminum plate and extrusions containing small initial corner cracks at fastener holes. Some of the specimens were tested using an 80-flight loading sequence representative of the training syllabus for the F-4 aircraft. The spectrum consists of an 80-flight sequence of load occurrences representative of 115 hours of flying. The different types of flights were separated into two broad classifications of usage, severe maneuver flights (simulated attack and combat) and typical maneuver flights (other). The flight sequence is random and consists of 40 typical flights and 40 severe flights. Each typical flight contains seven randomly sequenced maneuver loading cycles drawn from a "typical usage" fatigue loading spectrum. Similarly, each severe flight contains 20 randomly sequenced maneuver loading cycles, drawn at random from a "severe usage" fatigue loading spectrum. Before and after each flight the taxi load is simulated by a load magnitude of nearly zero, representing the ground loading of the ground-air-ground cycle. Figure 1 shows a computer plot of the loading tape that resulted from this procedure, and Table 1 is a summary of the rainflow count of the cycles.

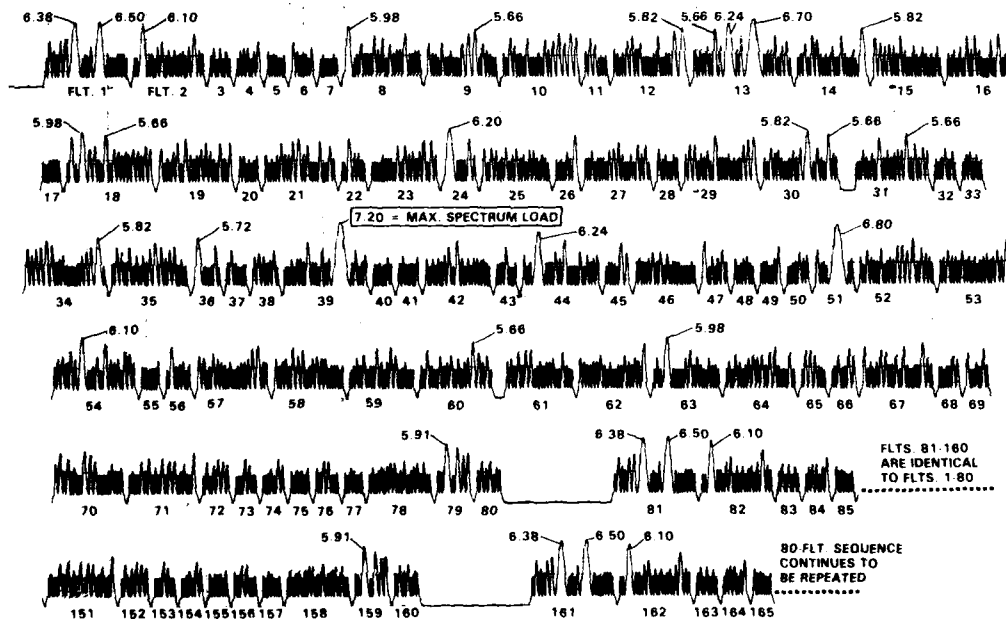
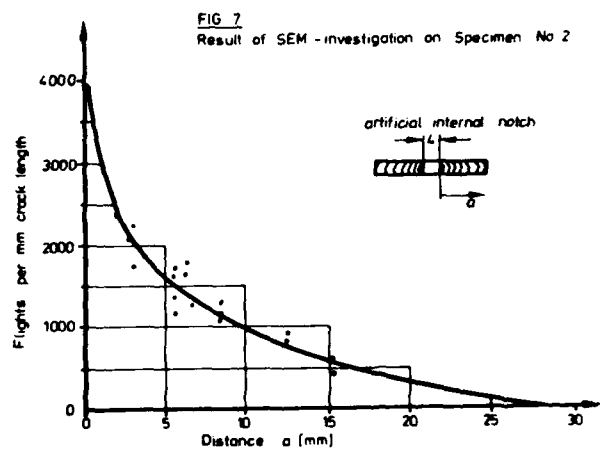
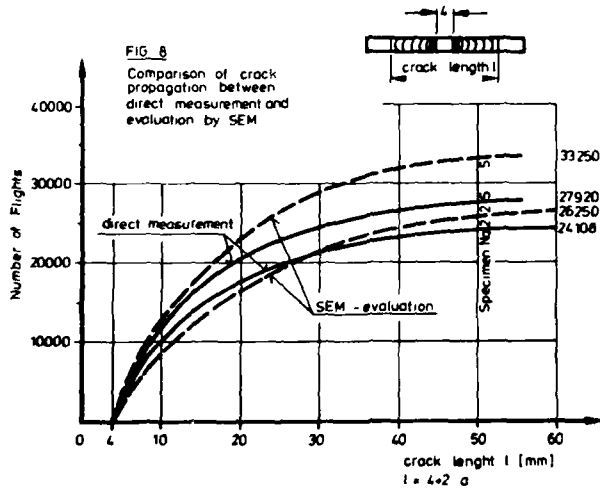
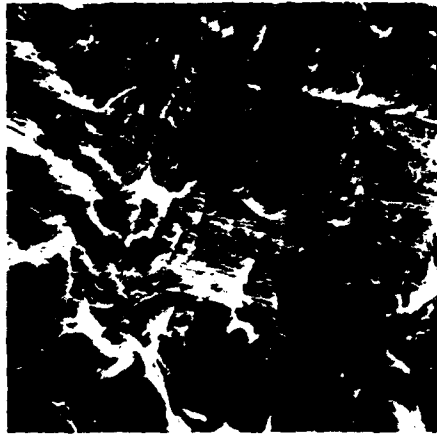


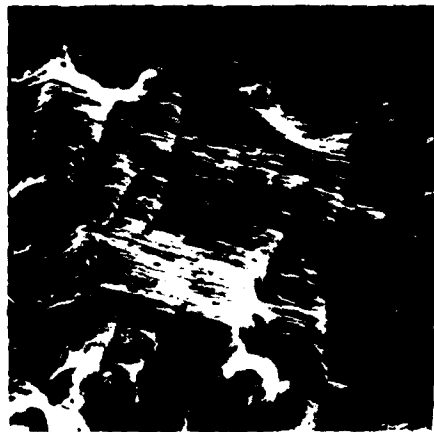
Figure 1. The 80-Flight Test Loading Sequence





↑  
CRACK PROPAGATION

FIG. 4 MAGNIFICATION OF FIG. 3  
(CENTRAL REGION)



←  
TRANSITION OF  
LC WITH HIGH  
AMPLITUDE  
TO LOW  
AMPLITUDE

←  
TRANSITION OF  
LC WITH LOW  
AMPLITUDE  
TO HIGH  
AMPLITUDE

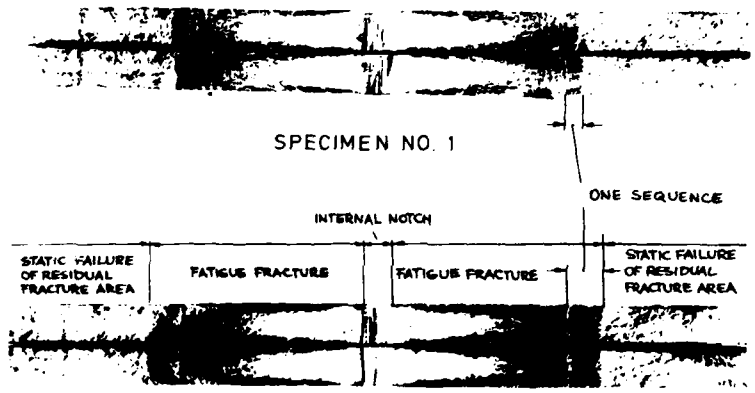
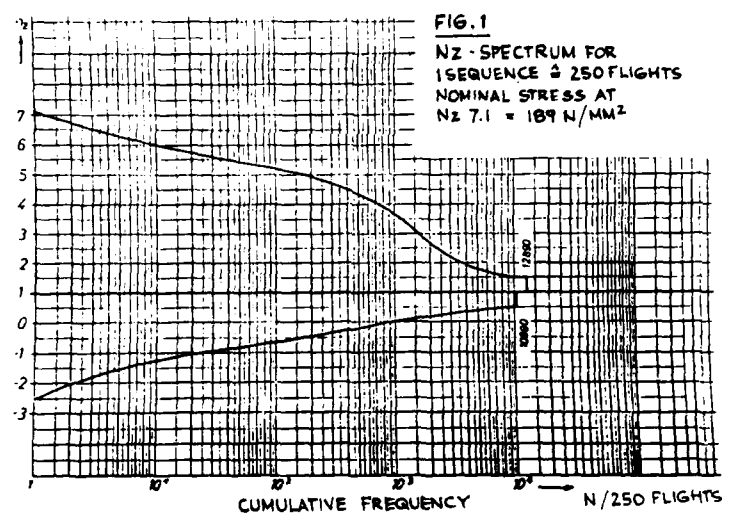
FIG. 5 MAGNIFICATION OF FIG. 3  
(45 LOAD CYCLES WITH HIGH AMPLITUDES)



←  
1 LOAD CYCLE  
WITH HIGH  
AMPLITUDE

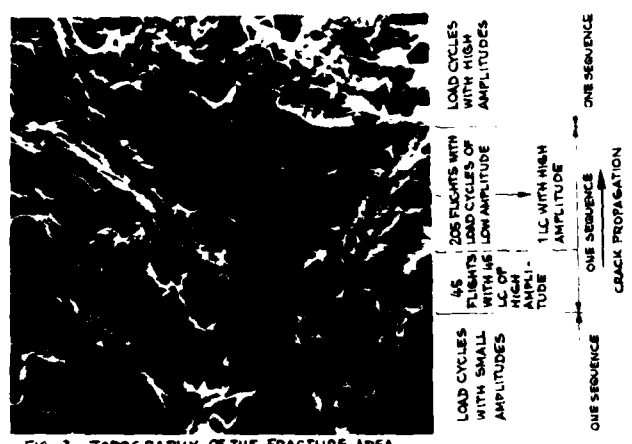
←  
TRANSITION OF  
LC WITH HIGH -  
TO LOW  
AMPLITUDE

FIG. 6 MAGNIFICATION OF FIG. 3  
(TRANSITION OF LOAD CYCLES WITH HIGH  
AMPLITUDE TO LC WITH LOW AMPLITUDE)



**SPECIMEN NO. 2**

**FIG. 2** TOPOGRAPHY OF FRACTURE AREA OF THE MARKER LINE - SPECIMENS



**FIG. 3** TOPOGRAPHY OF THE FRACTURE AREA AT A DISTANCE OF 1.05 MM FROM THE INTERNAL NOTCH (SPECIMEN NO. 2)

to 250 contained only load cycles with  $n_z = 5.5$ . The third highest load cycle with  $n_z = 6.65$  was placed into flight No. 130. This was done to determine if this single high load cycle would also show up on the fatigue fracture surface. The distribution of the negative load cycles below  $n_z = 1$  took place purely at random over all 250 flights. In total, the flight length scattered between 30 and 90 load cycles. Each flight contained a ground-air-ground load cycle.

Program 2 was a purely random type program. All load cycles were distributed randomly over the 250 flights without any special pattern. The number of load cycles per flight were of the same magnitude as for program 1.

The marker line specimens No. 1, 2 and 5 were tested with program 1, and the specimens No. 3 and 4 with program 2 for the purpose of comparison. The maximum tension loading in both programs amounted to 9466 daN, i.e. at  $n_z = 7.1$ . The nominal stress in the test specimen was 189 N/mm<sup>2</sup> based on the gross area of  $100 \times 5 = 500$  mm<sup>2</sup>. During the tests the crack propagation was measured.

With the specimens No. 5 to 9, fatigue tests were conducted. Specimen No. 6 and 7 were tested according to program 1 and specimens No. 8 and 9 to program 2.

The maximum tension loadings at  $n_z = 7.1$  were 3028 daN for the specimens No. 6 and 8 and 4000 daN for the specimens No. 7 and 9. The maximum nominal tension stress based on the net area of  $32 \times 5 = 160$  mm<sup>2</sup> amounted to 189 and 250 N/mm<sup>2</sup> respectively.

The test results obtained, indicated that both loading programs were leading to the same results with respect to crack propagation and endured fatigue life.

Due to the small number of tests performed, no statically founded, quantitative statement could be made. However, because of the small scope of a partial sequence consisting of 250 flights only, no significant influences from the loading sequence were expected. The achieved results confirmed this supposition.

There was satisfactory agreement between crack propagation curves obtained from the marker line tests with both loading programs. The fatigue life obtained differed by about 20 % maximum. The results obtained from the plain fatigue tests showed also satisfactory agreement. Significant deviations between the results obtained with both of the loading programs could not be identified.

The fracture surfaces (see FIG 2 for example) of the specimens tested with program 1 (modified random) were investigated for the existence of marker lines by means of scanning electron microscopy (SEM). Thereby, no very distinct fracture lines, crossing the total crack width, could be identified; however, the fracture surfaces contained numerous very small areas from which the sequence of the loading program could be traced (see FIG 3 to FIG 6). The crack propagation caused by a partial sequence of 250 flights could be measured at various distances from the artificially introduced internal notch. In FIG 7, the inverted values of these measurements are plotted, exemplified on specimen No. 2. FIG 8 illustrates the crack progress derived by integration of the curve in FIG 7.

Also for the purpose of comparison, the crack length measured directly during the fatigue test is plotted versus the number of flights. Furthermore, FIG 8 contains the measured and the post-evaluated crack propagation from the fracture surface of specimen No. 5. The crack propagation rate obtained by post-evaluation of the fatigue fracture areas were in both cases somewhat slower than in reality. The total deviations of the endured fatigue life between crack initiation and static failure of the residual fracture area amounted to about 9 % for specimen No. 2 and about 19 % for specimen No. 5.

Post-evaluation of crack propagation was not possible in case of the specimens which were tested with program 2 (Purely random), since no correlation between loading sequences and accompanying crack propagation could be derived.

Since the specimen tests, run with the modified loading sequence (program 1), proved the possibility of post-evaluating crack initiation time and crack propagation, program 1 was used for performing the major fatigue test with the aircraft structure. In investigating the fracture surfaces of the occurring fatigue damages in this major test, the loading sequence could be recognized even in the case of multiaxial loading, hence allowing a post-evaluation for the time of crack initiation.

In conclusion it should be mentioned, that E. Gassner has referred to the possibility of an evaluation of the marker line intervals in 1954 /1/ and, that this method is already being applied for fatigue tests on transport aircraft structures.

#### REFERENCES

- /1/ E. Gassner  
Betriebsfestigkeit, eine Bewertungsgrundlage für Konstruktionsteile mit statistisch wechselnden Betriebsbeanspruchungen.  
Konstruktion, 6. Jahrg. (1954) Heft 3, Seite 97 bis 104.

GENERATION OF MARKER LINES ON FATIGUE  
FRACTURE SURFACES

by

Dipl.-Ing Manfred Kalweit

INDUSTRIEANLAGEN-BETRIEBSGESELLSCHAFT MBH  
Einsteinstraße, 8012 Ottobrunn, Germany

The present standard for proof of sufficient durability of aircraft structures calls for the performance of major fatigue tests on total aircraft structures or at least on complete structural components such as fuselage sections, wings, stabilizers etc. Thereby, the test structure will be subjected to loads, which occur or will be expected to occur in service, in the form of a flight-by-flight program; that means, magnitude, frequency and sequence of loads will be simulated as exactly as possible as encountered during service usage. The purpose of this type of fatigue test, however, is not only the experimental evaluation of the fatigue life till total failure of a structural component but also, at the same time, to reveal all weak points, to detect possible early fatigue cracks as well as to analyse crack propagation in order to be able to derive appropriate inspection schedules and intervals for aircraft in service.

Modern aircraft structures consist of many highly loaded structural components which are, partly due to their location in the interior of the wing or fuselage, in practice not accessible to inspection after assembly. In the course of a fatigue test, fatigue failures occurring in these components may stay unnoticed till total failure occurs. For these failures, a statement concerning the actual time of crack initiation and/or crack propagation can only be made if the fracture surface contains indications from which important information can be drawn for the evaluation of the fatigue damage.

It is common knowledge, that the appearance of the fracture surface of fatigue cracks can be influenced by the sequence of the loading program. Individual load cycles with high stress amplitude generate characteristic fracture lines - so called marker lines - in a fatigue fracture surface. These lines can be recognized by scanning electron microscopy. These lines can also be seen occasionally in the area of the crack origin.

If the loading spectrum contains relatively few high load cycles which distinctly differentiate themselves from the majority of the fatigue load cycles, and if these high load cycles are arranged within the flight-by-flight spectrum in periodically reoccurring intervals, than the crack propagation and the fatigue life between crack initiation and static failure of the residual fracture area can be derived relatively exactly by evaluating the marker line intervals. This procedure is already common practice in fatigue tests for civil aircraft which are essentially subjected to gust load cycles.

In connection with establishing a flight-by-flight loading program for a predominantly manoeuvre loaded military aircraft structure it was proposed, with respect to the generation of marker lines, to alter the more or less arbitrary arrangement of the loading sequence which is representative for normal service operation. The 45 most severe load cycles in each partial sequence comprising of 250 flights were interspersed into the first 45 flights of each of the partial sequences.

First of all, fatigue tests with simple test specimens had to be run in order to investigate if, with the proposed loading arrangement, easily visible, clearly identifiable marker lines could be generated. Secondly, it had to be investigated if and to what extent the concentration of the high load cycles in the first flights of a partial load sequence would create any misleading test results with respect to crack propagation and fatigue life. Within the scope of this test program, flight-by-flight fatigue tests with a total of nine notched AL-specimens (3.1354 T 351), loaded uniaxially in tension and compression, were performed. From these nine specimens, five (specimen No. 1 to No. 5) were used to generate marker lines and the remaining four (specimen No. 6 to No. 9) to determine fatigue life. The tests were conducted with two loading programs differing only in the selected sequence of load cycles. The basis for all tests was the spectrum given in FIG 1.

Program 1 represented a modified random type program. It was specially developed for the generation of marker lines in the fracture surfaces. The first 45 flights, therefore, contained the highest positive load cycles in the g-level range between  $n_z = 7.1$  and  $5.5$ , whereby flight No. 1 contained the highest load cycle with  $n_z = 7.1$  and flight No. 45 the second highest with  $n_z = 6.8$ .

Flights No. 2 to 44 each contained one high load cycle in the range between  $n_z = 5.5$  and  $6.5$  in random sequence and arrangement. All remaining load cycles of flights No. 1 to 45 were in the range below  $n_z = 5.5$ . Flights No. 46 to 129 and No. 131.

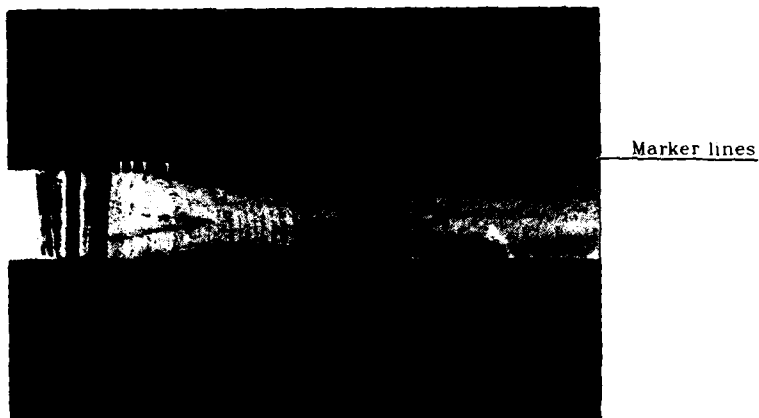


Fig. 7 Fatigue-fracture surface with marker loads Type II

Summary

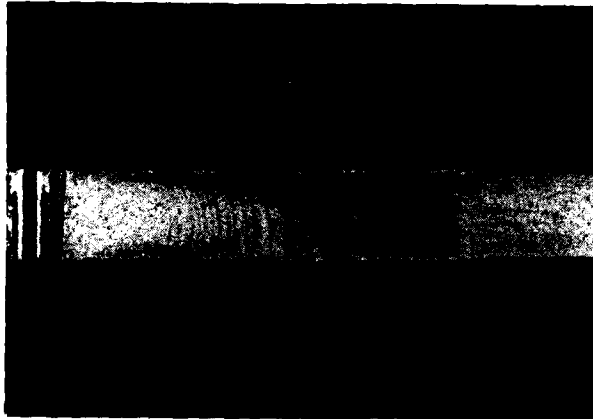
The crack propagation tests recently run on flat specimens showed that it is possible to generate marker lines on the fatigue fracture surface. It was also found that the marker lines are clearly visible. A comparison of results obtained from crack propagation tests showed the constant-amplitude loads interspersed in the FALSTAFF flight-by-flight loads to be damage-equivalent to the flights not simulated in the flight-by-flight sequence.

Since these tests were only run on a random basis, it is necessary to demonstrate the validity of these procedures by further tests.

It is also necessary to investigate whether or not the results from the crack propagation tests are applicable to fatigue strength properties.

There is a possibility that this method may lead to substantial differences in the crack-free endurance limit.

For satisfactory results, additional tests and evaluations should be performed in the future



$$\text{FALSTAFF } \bar{\sigma}_0 = 220 \text{ N/mm}^2$$

Fig. 5 Fatigue-fracture surface without marker loads

Fig. 5 shows the fracture surface without the marking loads interspersed. Fig. 6 and 7 illustrate the fracture surfaces of the specimens subjected to type I loading (800 FALSTAFF flights plus 800 cycles) and type II loading (800 FALSTAFF flights plus 900 cycles).



Marker lines

Fig. 6 Fatigue-fracture surface with marker loads Type I

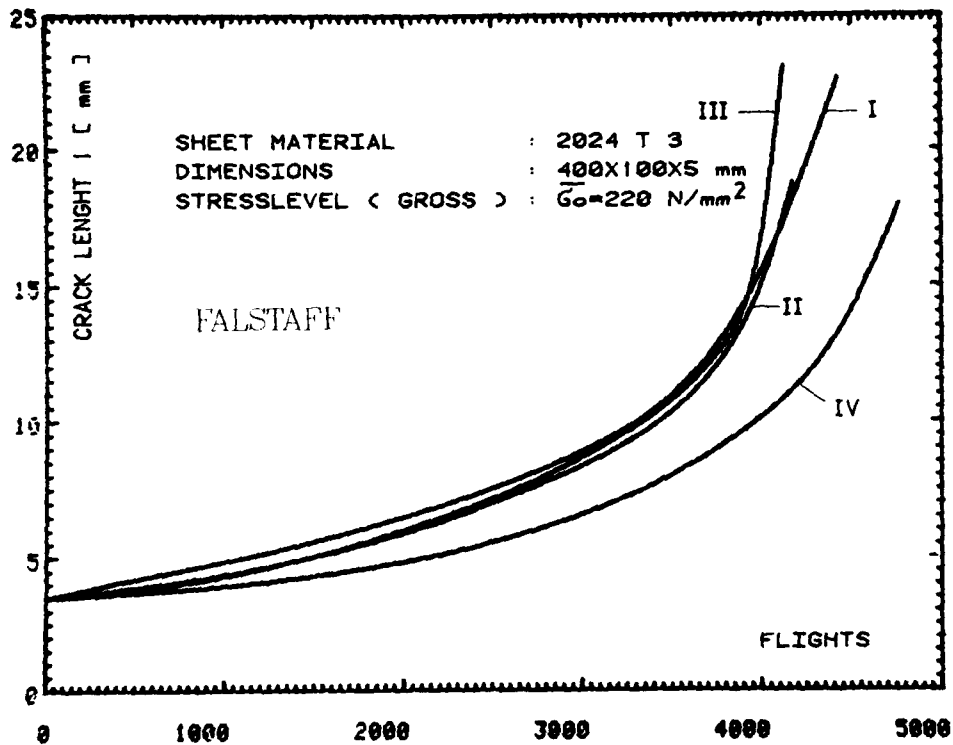


Fig. 4 Crack propagation with marker load and without them

- I. Each time 800 FALSTAFF flights ( $\bar{\sigma}_0 = 220 \text{ N/mm}^2$ ) plus 800 cycles  
 $\sigma_0 = 220 \text{ N/mm}^2$  ( $R = 0,67$ )
- II. Each time 800 FALSTAFF flights ( $\bar{\sigma}_0 = 220 \text{ N/mm}^2$ ) plus 900 cycles  
 $\sigma_0 = 184 \text{ N/mm}^2$  ( $R = 0,5$ )
- III. FALSTAFF ( $\bar{\sigma}_0 = 220 \text{ N/mm}^2$ ) No constant amplitude cycles
- IV. FALSTAFF ( $\bar{\sigma}_0 = 220 \text{ N/mm}^2$ ) No constant amplitude cycles.

A check of the fracture surfaces of the specimens tested revealed that the interspersed constant-amplitude load cycles produced visible marker lines. These marker lines are clearly distinguishable from the marker lines produced by FALSTAFF loading.

Fig. 2 illustrates the FALSTAFF load cycle without constant-amplitude loading, as well as FALSTAFF plus constant-amplitude loads interspersed.

Selecting damage equivalent constant-amplitude loads required evaluation and comparison of numerous crack propagation tests performed earlier with constant-amplitude and flight-by-flight-loading.

During the crack propagation tests, the crack lengths were measured by means of a measuring amplifier with a magnification factor of 40.

#### Test results

The results of these crack-propagation tests have been plotted in the form of crack-propagation graphs. Fig. 3 shows the crack propagation behavior of the specimens for FALSTAFF flight-by-flight loading without interspersions of constant-amplitude loads.

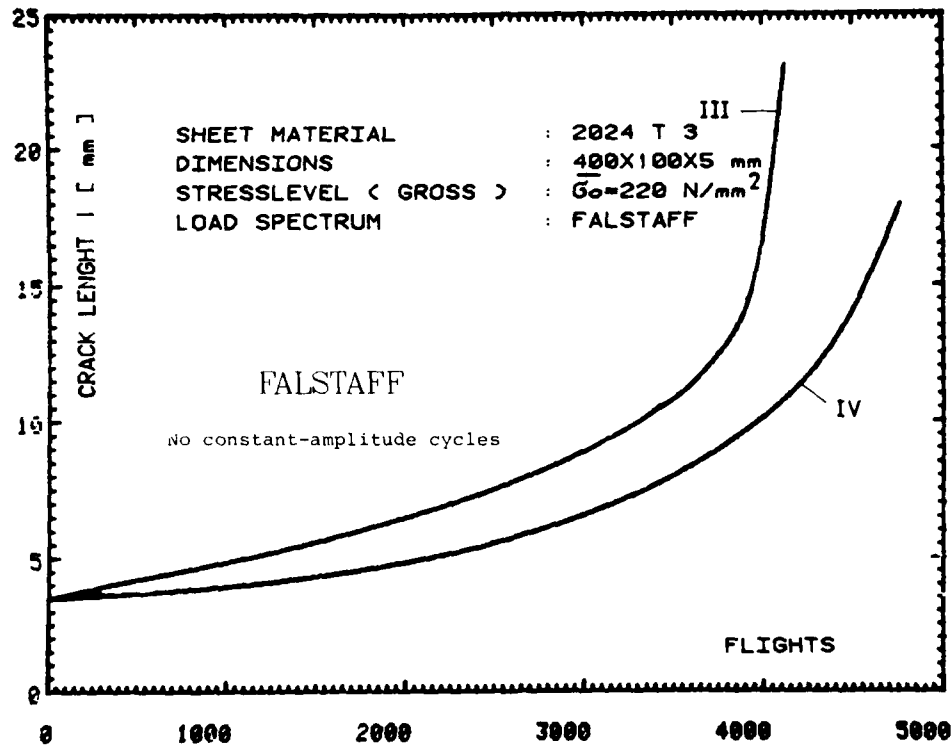


Fig. 3 Crack propagation in FALSTAFF flight-by-flight loading

Scatter of similar magnitude was also found in other test series.

Fig. 4 shows the crack-propagation behavior of specimens with constant-amplitude loads interspersed and without them.

### Test Set-up

A computer-controlled servohydraulic 100 KN-Test-System was used. The specimens were held by semi-cardanic clamping devices, which largely eliminated on-edge bending loads. During the tests, the specimens had been provided with a support against buckling, to avoid buckling during the compression loads that occur in the FALSTAFF-Spectrum.

### Test performance

Crack propagation was tested on 4 specimens under the following conditions:

2 specimens were subjected to FALSTAFF flight-by-flight loads with a stress horizon of  $\bar{\sigma}_0 = 220 \text{ N/mm}^2$  without interspersions of constant-amplitude loads.

1 specimen was subjected to mixed loading by FALSTAFF flight-by-flight loads and constant-amplitude loads. This test periodically simulated 800 FALSTAFF flights ( $\bar{\sigma}_0 = 220 \text{ N/mm}^2$ ) followed by 800 constant-amplitude cycles ( $\sigma_0 = 220 \text{ N/mm}^2$ ,  $R = +0,67$ ) (type I marker loads).

Subsequently, again FALSTAFF flights were simulated, which began with flight No. 1000.

Instead of the 200 FALSTAFF flights, 800 constant-amplitude loads were thus applied.

1 specimen was subjected to a different type of mixed loading that periodically simulated 800 FALSTAFF flights ( $\bar{\sigma}_0 = 220 \text{ N/mm}^2$ ) followed by 900 constant-amplitude cycles ( $\sigma_0 = 184 \text{ N/mm}^2$ ,  $R = 0,5$ ) (type II marker loads).

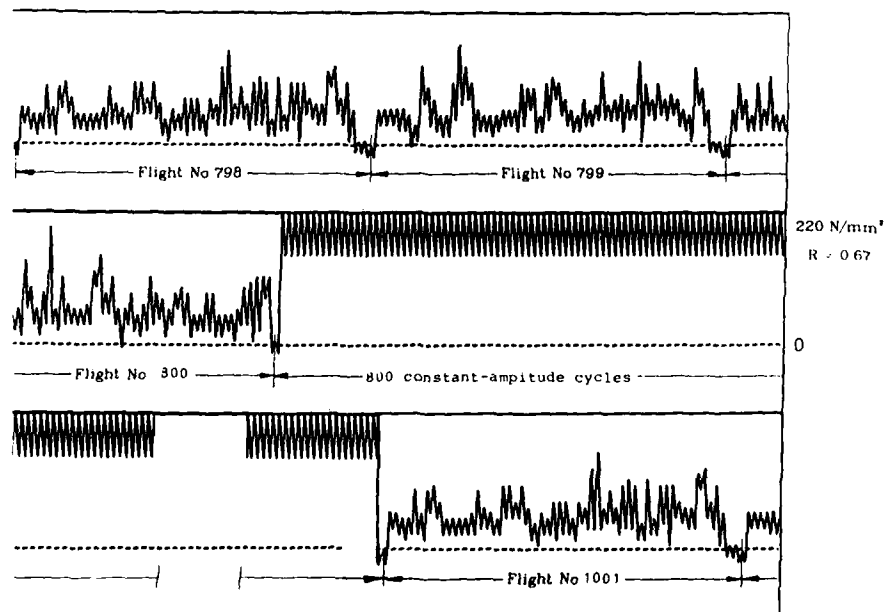


Fig. 2 Loading sequence with marker loads

It was the purpose of the random-type tests run by MBB to meet above requirements. Another requirement associated with the generation of marker lines was to minimize alteration of the test results.

Interspersion of excessive constant-amplitude loads may produce work hardening in critical areas, which will adulterate the results of tests performed on real structures.

#### Test Specimens

Flat specimens, as shown in Fig. 1, from 2024T3 (3.1364T3) sized 400x100x5 mm (15.7"x3.94"x0.2") were used. The specimens were produced from sheet metal. The grain direction of the specimens was longitudinal.

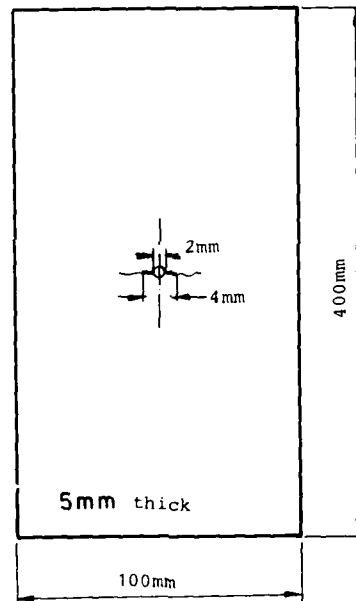


Fig. 1 Crack propagation test specimen

The specimens were provided with an artificial crack consisting of a 2 mm dia. hole and saw cuts.

GENERATION OF MARKER LINES BY MEANS OF MARKER LOADS

K. Hoffer  
R. Hillbrecht  
MBB/VFW Bremen

Investigation and evaluation of numerous fatigue damages revealed that it is extremely difficult to pursue the crack formation whenever the tests simulate flight-by-flight loads. Consequently, various methods to generate marker lines have already been proposed in the past.

Fatigue tests (FALSTAFF flight-by-flight loads) were performed by MBB i.e. constant-amplitude tests interspersed in their crack propagation phase at regular intervals. At the same time, the number of simulated flight-by-flight cycles is being reduced. These procedures aim at achieving damage equivalence. Consequently, the following requirements have to be met:

- o The crack propagation rates produced by interspersed constant-amplitude loads must be equal to the rates that would have been produced by the load sequences not simulated in the flight-by-flight-program.
  
- o The marker lines caused by the interspersed constant-amplitude loads must be visible on the fatigue fracture surface.

SPECTRUM (4)

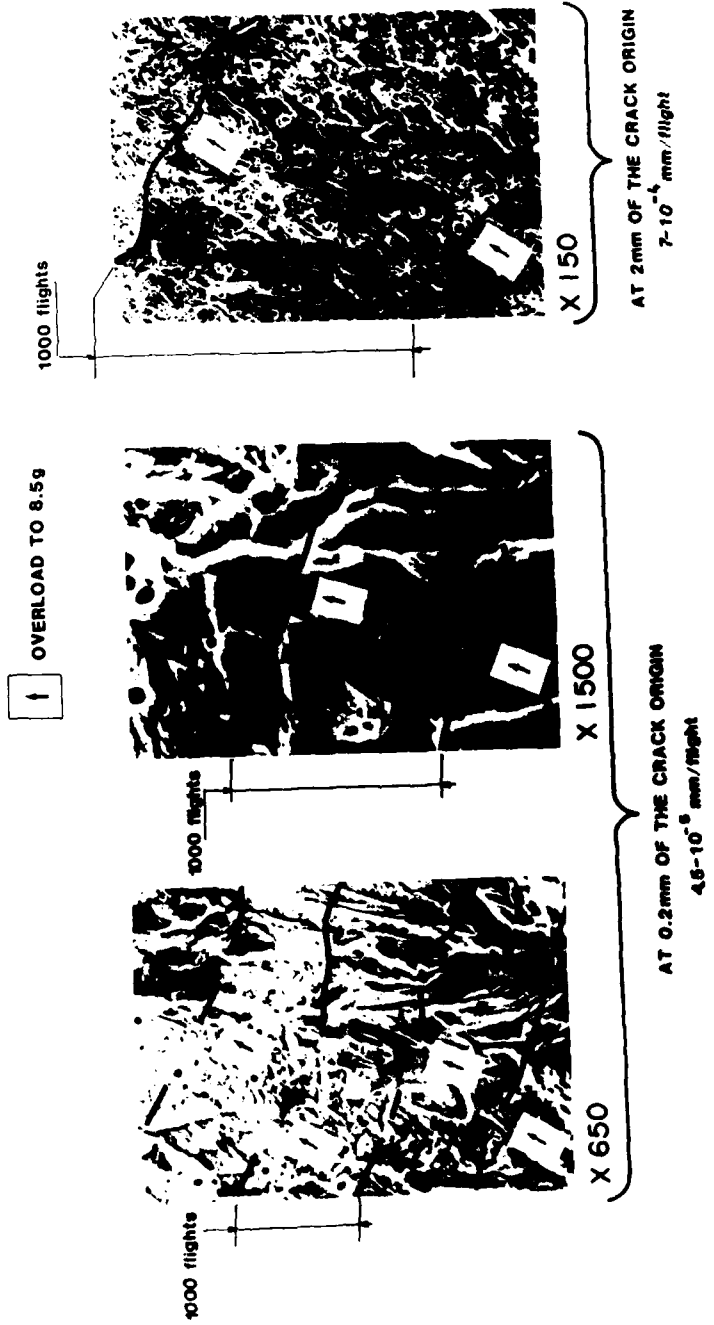


FIG-25

TABLE 1. SUMMARY OF RAINFLOW COUNT OF CYCLES FOR 80-FLIGHT MANEUVER SPECTRUM

Loading Spectrum: 80 Flight Fighter Spectrum Repeatable Number of Flights: 80				
Level	Max. Load Factor	Min. Load Factor	Cycles/Block	Comments
1	7.20	0.1	1	
2	6.70	0.1	1	
3	6.50	0.1	1	
4	6.24	0.1	1	
5	6.10	0.1	2	
6	5.98	0.1	3	40
7	5.82	0.1	4	Severe
8	5.66	0.1	3	GAG
9	5.50	0.1	5	Cycles
10	5.30	0.1	8	
11	5.10	0.1	6	
12	4.85	0.1	2	
13	4.33	0.1	3	
14	6.80	0.1	1	
15	6.20	0.1	1	
16	5.91	0.1	1	
17	5.72	0.1	1	
18	5.52	0.1	1	
19	5.35	0.1	2	40
20	5.20	0.1	2	Mild
21	5.00	0.1	2	GAG
22	4.78	0.1	4	Cycles
23	4.52	0.1	7	
24	4.25	0.1	6	
25	3.92	0.1	6	
26	3.63	0.1	4	
27	3.37	0.1	2	
28	6.38	1.0	1	
29	6.24	1.0	1	
30	5.66	1.0	3	
31	5.50	1.0	5	
32	5.30	1.0	8	760
33	5.10	1.0	19	Severe
34	4.85	1.0	28	Maneuver
35	4.60	1.0	40	Cycles
36	4.33	1.0	55	
37	4.08	1.0	80	
38	3.73	1.0	120	
39	3.38	1.0	170	
40	3.00	1.0	230	
41	5.52	1.0	1	
42	5.20	1.0	1	
43	5.00	1.0	2	
44	4.78	1.0	2	240
45	4.52	1.0	3	Mild
46	4.25	1.0	10	Maneuver
47	3.92	1.0	19	Cycles
48	3.63	1.0	26	
49	3.37	1.0	38	
50	3.15	1.0	58	
51	2.92	1.0	80	

Figure 2 shows the fracture surface markings on a hole notched specimen made from 3/16-inch thick 7075-T6 aluminum and fatigue tested using the 80-flight random cycle flight-by-flight sequence. The cracks initiated by fatigue at the edge of the hole and propagated to the edge of the specimen. The small light colored bands are made by the large number of small maneuver loading cycles. The darker areas between the bands are made by a single high maneuver loading cycle. For this specimen no attempt was made to relate these markings to specific applied loadings in the spectrum.

Figure 3 shows the fracture surface of a tee-reinforced specimen, made from two nine-inch wide sheets of 7075-T6 aluminum spliced together longitudinally by a 7075-T6511 tee extrusion. This precracked structural specimen was spectrum fatigue tested using the 80-flight loading sequence. Initial flaws were made at the corner of the fastener hole in both the left-hand sheet and the tee extrusion. Shortly before specimen failure a fatigue crack developed at the countersunk fastener hole in the right-hand sheet. Throughout most of the crack growth history the largest tensile loading in the 80-simulated flight periodic sequence, a load factor of 7.2 which occurs in the 39th flight, caused the crack front to jump, especially at mid-thickness. The dark gray areas or bands on the fracture surface show the length of the jump. The thin silvery bands indicate fatigue crack growth during the other (smaller) 1079 cycles that recur each 80 simulated flights.

Except near the end of the test, only that largest tensile loading (the one occurring in the 39th flight) caused visible jumps in crack growth. Therefore, the crack growth rates, and in fact the entire crack growth history, can be identified by counting or

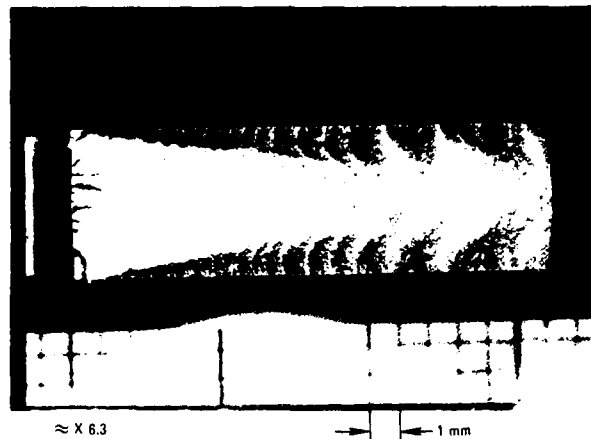


Figure 2. Markings on Fracture Surface of 7075-T6 Aluminum Specimen Fatigue Tested Using an 80-Flight Random Cycle Flight-by-Flight Fighter Spectrum



Figure 3. Close-Up of Fracture Surface Markings on Reinforced Spliced Panel

measuring the spacing of these fracture surface markings. Furthermore, final specimen failure occurred upon application of the largest tensile loading.

Figure 3 provides detailed data for both the growth rate and flaw shape. The integer numbers in Figure 3 provide a countdown of the number of 80-flight sequences remaining until failure of the specimen. The number 1 near the countersunk hole in the right-hand sheet defines the size of the crack one 80 flight sequence prior to specimen failure. At that time the tee extrusion was completely failed. The number 8 in the tee extrusion identifies the crack front in the tee-extrusion eight 80-flight sequences (8 x 80 flights) prior to specimen failure. At about 3000 (37.5 x 80) flights prior to failure, the crack reached the fillet radius of the tee extrusion where the base and protruding leg intersect. Markings were not carried back beyond 4400 (55 x 80) flights prior to failure although additional marks are clearly evident in Figure 3. The spacing between markings can be used to calculate average crack growth rates per flight for various crack sizes.

For this particular flight sequence, jumps only occurred during the application of the highest load level. The growth due to the other 1079 loadings was sufficiently small so that growth rates were always controlled by highest loading in the spectrum. This would not be the case if more growth occurred between peak loads so that the crack would grow beyond the plastic zone size effect of the largest loading before it occurred again.

The marking cycles were very clear in this test because the spectrum did not contain compression loadings. Large compression loadings cause fracture surfaces to rub together and will usually obliterate the markings on the fracture surface. To evaluate the effect of compression loadings, a test was conducted using the 80-flight sequence with compression loadings added after each flight to simulate taxi loadings. A compression peak equal to 35 percent of the maximum tension load, considered typical of peak taxi loadings of fighter/attack aircraft, was used. As seen in Figure 4, visible markings were achieved despite the compression loadings, and are nearly as clear as those obtained for tension only.

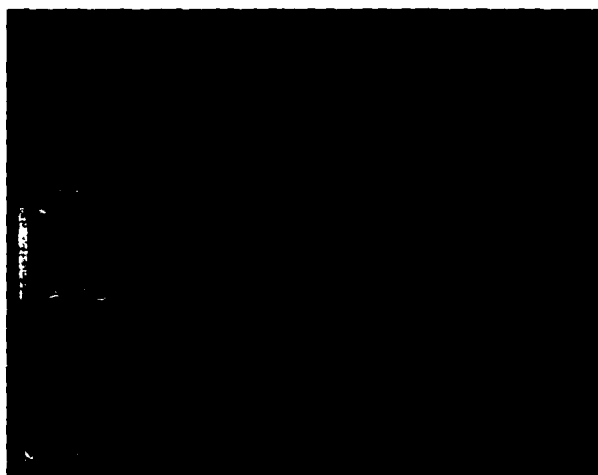


Figure 4. Fracture Surface Markings for 80-Flight Fighter Spectrum with Twice-Per-Flight Compression Loading ( $P_{\min} = -.35P_{\max}$ )

#### MODIFIED MINITWIST TRANSPORT WING SPECTRUM

The 'Minitwist' fatigue loading spectrum [2], applicable for the wing lower surface of transport aircraft, has been used extensively for evaluating the fatigue and crack growth properties of materials and mechanically fastened joint specimens. Fracture surfaces obtained from tests using this spectrum do not contain readily identifiable characteristic markings because the fatigue loadings are applied in a random half-cycle sequence. To aid in the fractographic evaluation of test specimens, the sequence was modified by resequencing the fourteen most severe flights. (This modification was called Modification "A"). Groups of two or three of the fourteen most severe flights were spaced at 800 flight intervals within the basic 4000 flight spectrum as shown in Table 2. Each group of severe flights was arranged in a low-high sequence. Also, the flight groupings with A, B, and C flights were arranged in a low-high sequence after the first application of the A flight. By these adjustments to the sequence, characteristic markings were obtained every 800 flights.

To evaluate the effect of this sequence modification on crack growth, tests were conducted on six-inch wide center notched specimens taken from one 0.16-inch thick 7075-T6 bare sheet. The crack propagation curves for these specimens are plotted in Figure 5. The number of flights plotted in Figure 5 includes the flights prior to initiation of cracking (dwell flights) from an elox notch which was approximately 0.010 inches wide and 0.24 inches long. These data show that the crack growth for the Minitwist (Modification "A") sequence falls within the scatterband for the basic Minitwist sequence. For the large crack lengths in Figure 5, the discontinuities in the crack growth curves occur when the loadings for the A, B, and C flights are applied.

Minitwist (Mod. "A") flight-by-flight spectrum fatigue tests were also conducted on six-inch wide center notched ( $K_t = 3.9$ ) panels made from 0.40 inch thick 7091-T7E69 (powder metallurgy) plate machined to 0.16-inch thickness and 0.16-inch thick 7075-T6 bare (ingot metallurgy) sheet. The notch consisted of two 0.25-inch diameter holes 0.48 inches apart connected by a 0.135  $\pm$  0.010 inch wide slot.

The results for the tests conducted at two gross area 1-g stress levels of Minitwist (Mod. "A") spectrum are shown in Figures 6 and 7. The number of flights plotted in Figure 6 includes the time to crack detection (fatigue). The number of flights plotted in Figure 7 includes only the crack growth data, while the time to crack detection is given in tabular form for each specimen.

TABLE 2. LOCATION OF 14 MOST SEVERE FLIGHTS FOR MINITWIST (MODIFICATION "A") SPECTRA

TYPE OF FLIGHT	FLIGHT NUMBER IN SPECTRUM SEQUENCE	
	MINITWIST	MINITWIST (MODIFICATION "A")
A	1656	2800
B	2856	2001
C	501, 2926, 3841	401, 1201, 3601
D	106, 412, 689, 1099, 1653, 2682, 3360, 3538, 3894	399, 400, 1199, 1200, 1999, 2000, 2799, 3599, 3600

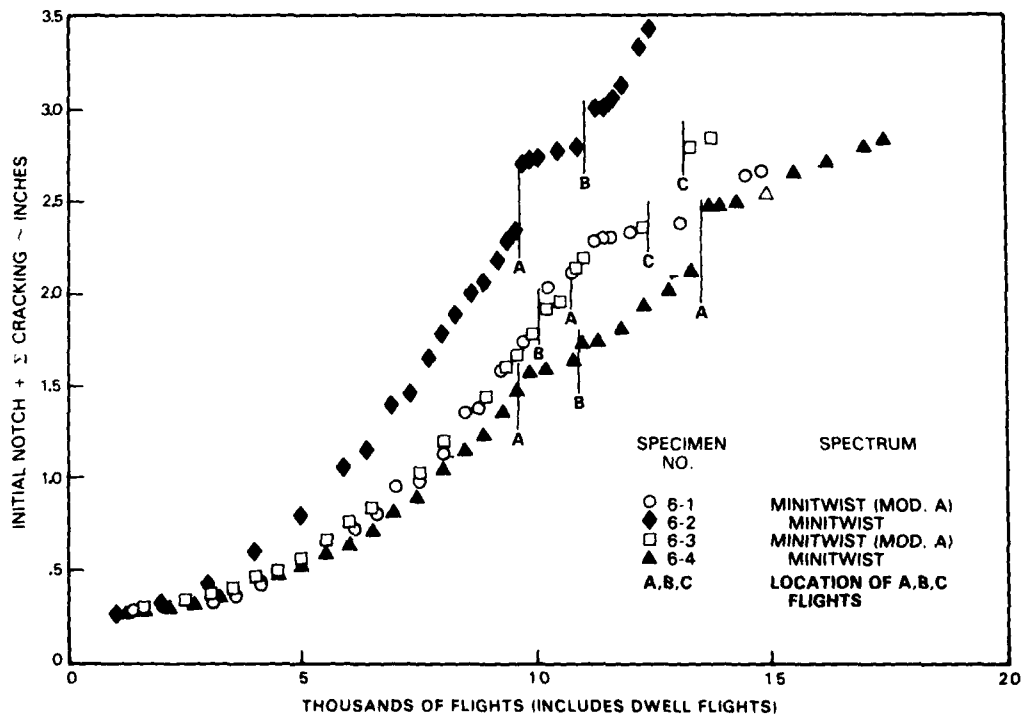


Figure 5. Comparison of Crack Growth Data for Minitwist and Minitwist (Mod A) on Crack Growth for Center Cracked Panels of 7075-T6 Sheet

No cracks were detected in Specimen B2-1 (Figure 7) up to 132,800 flights; at which time, razor cuts were made at each end of the notch to accelerate fatigue cracking. The data indicate that both the spectrum fatigue and crack growth properties of 7075-T6 I/M material are slightly better than 7091-T6E69 P/M material.

The sudden increases in crack growth and subsequent retardation for the 7075-T6 material in Figures 6 and 7 occur at the intervals (multiples of 800 flights) where the A, B, and C flights are applied. This can be clearly seen in the photomicrographs of the fracture surface of a specimen for each material in Figure 8. These data show that the Minitwist (Mod. "A") sequence makes characteristic markings on the fracture surfaces of both ingot metallurgy and powder metallurgy aluminum alloys. Therefore, this version of the Minitwist spectrum would be useful for tests conducted on structural specimens where visual crack growth measurements cannot be obtained during testing.

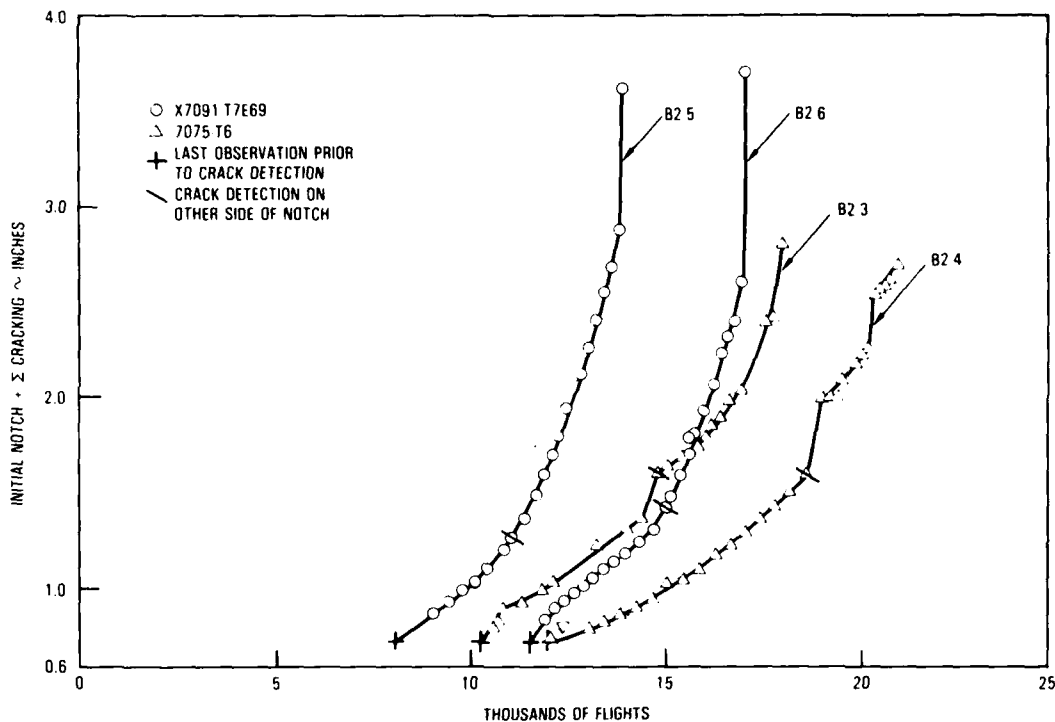


Figure 6. Minitwist (Mod. "A") Spectrum Fatigue Crack Growth of 0.16 inch 7091-T7E69 Plate and 7075-T6 Sheet with Flights to Crack Initiation Tested at a 1-g Gross Area Stress of 11.0 ksi

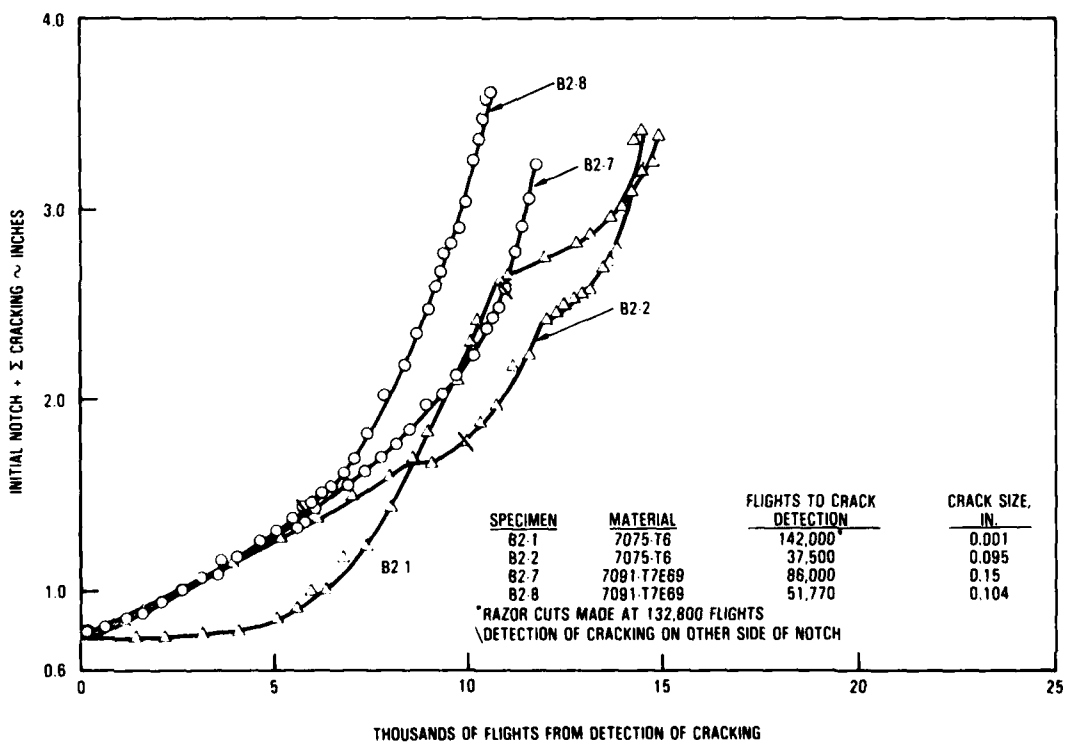


Figure 7. Minitwist (Mod. "A") Spectrum Fatigue Crack Growth of 0.16 inch 7091-T7E69 Plate and 7075-T6 Sheet Tested at a 1-g Gross Area Stress of 9.0 ksi

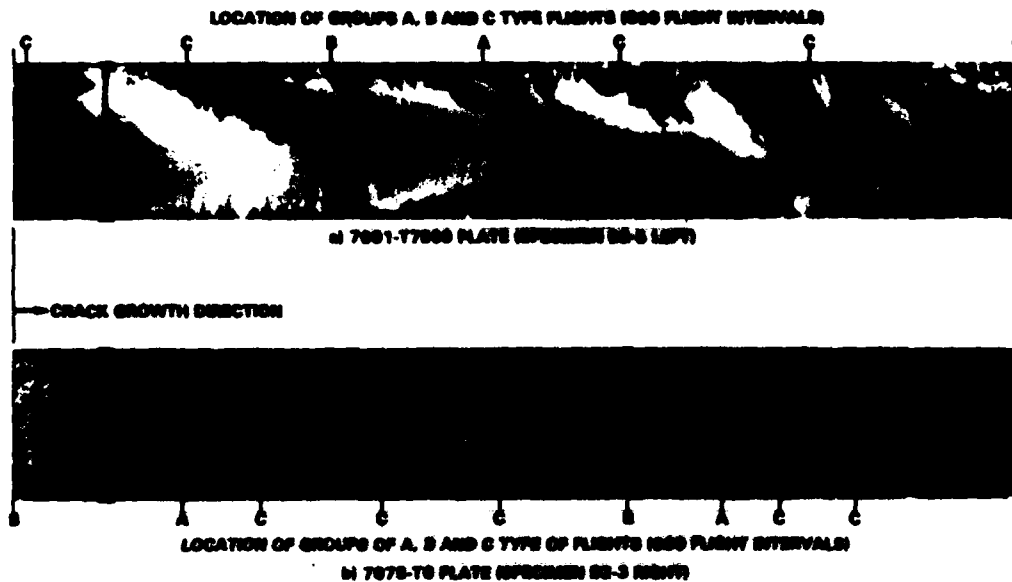


Figure 8. Comparison of Fracture Surface Markings for Two Materials Subjected to Minitwist Mod A Spectrum Loadings

#### CONSTANT AMPLITUDE LOADING SEQUENCE

Fracture surfaces from constant amplitude fatigue tests typically do not leave easily identifiable characteristic markings on the fracture surface. For these types of tests, groups of constant amplitude loading cycles for a different stress ratio are added periodically during the test for marking purposes. The stress ratio has to be significantly different so that the added cycles leave a different marking on the fracture surface than the basic constant amplitude loading cycle. Also a sufficient number of loading cycles have to be added so that the band width will stand out on fractographic examination.

In Reference [3] some constant amplitude fatigue tests are reported on aluminum and steel lug specimens. In these tests, it was desired to add marking bands with another loading cycle such that the crack growth rates would be approximately the same as the basic constant amplitude fatigue loading cycle. This can be done approximately by adding some mild overload cycles such that the effect of retardation due to the overloads is balanced by the increased crack growth rates for the added cycles.

The loading sequence selected consisted of a periodic sequence of 1900 operating cycles followed by 100 cycles of 30 percent overloads where the minimum load was held constant. The loading sequence and crack growth test results for both constant amplitude loading and the marking cycle sequence are shown in Figure 9. These data show there is very little difference in the crack growth rates for the two loading histories. From these data, the marker band width will vary from approximately 0.001 inch for  $\Delta K = 10 \text{ ksi} \sqrt{\text{inch}}$  to 0.010 inches for  $\Delta K = 25 \text{ ksi} \sqrt{\text{inch}}$ . For these same stress intensities, the marker band widths for the 1900 cycles would be approximately 0.0086 inches and 0.076 inches. Marker band widths less than 0.001 inches would be difficult to see without some magnification.

The fracture surfaces obtained from two 7075-T6 aluminum specimens are shown in Figure 10. An initial flaw was introduced at one corner of the lug hole in both specimens. The marker bands are clearly visible down to very small crack sizes. The shape of the crack is also clearly evident. Crack growth rates are readily determined for various crack sizes. Using the crack growth rate curves in Figure 10 one can correlate measured stress intensities with predicted stress intensities.

#### CONCLUDING REMARKS

Fracture surface markings which are regularly-spaced and clearly visible without magnification provide reliable, inexpensive data on crack growth rate, growth sequence, and crack front shapes in hidden areas of structural fatigue tests. Three examples of producing such markings in aluminum structure have been presented, each using periodic high tensile loadings. The three examples are a fighter wing spectrum sequence, a transport wing spectrum sequence, and a constant amplitude sequence. In each case the high tensile loadings produce the markings without nullifying the validity of the test: They are either an intrinsic part of the loading spectrum or, in the constant amplitude case, the amount of crack retardation they produce is small and is cancelled by the additional growth they induce.

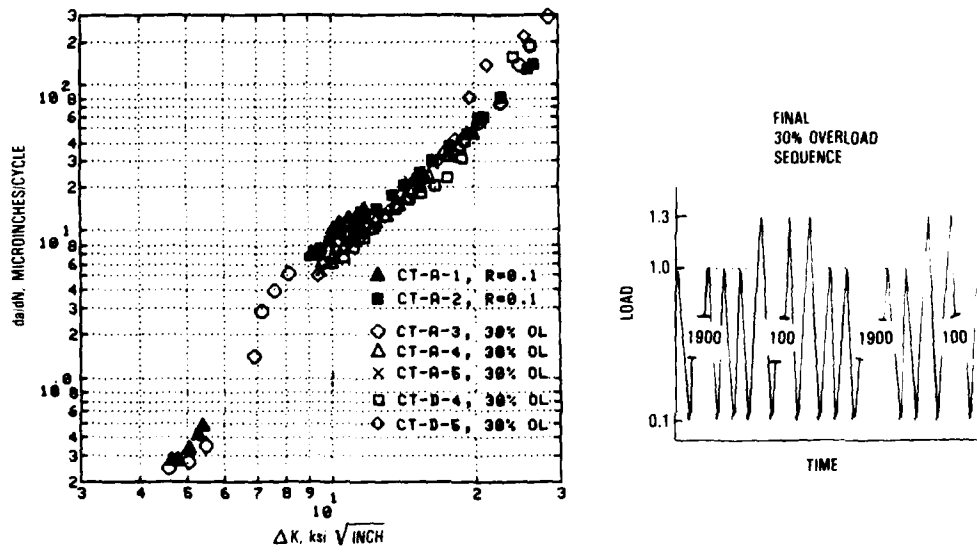


Figure 9. Effect of Overload Marking Cycles on  $da/dN$

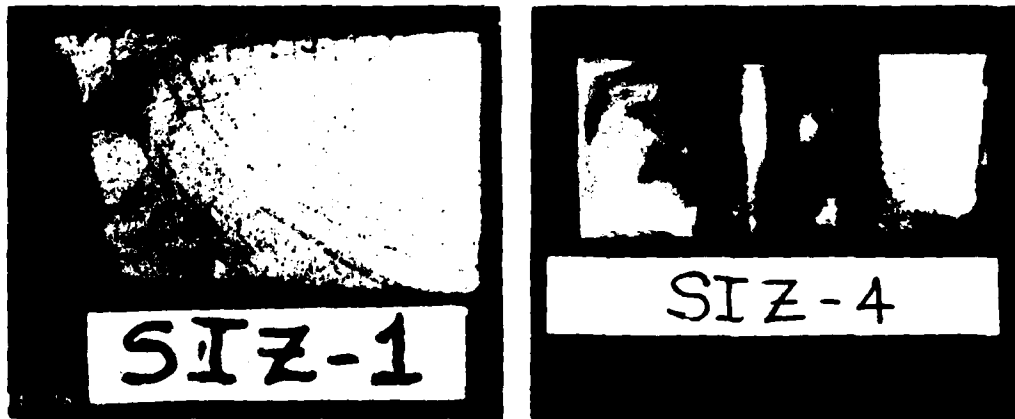


Figure 10. Fracture Surfaces of Two Lug Specimens Tested Using 30% Overload Loading Sequence

## REFERENCES

- [1.] Brussat, T. R. and Chiu, S. T., "Flaw Growth in Complex Structure Final Report, Volume I Technical Discussion," AFDDL-TR-77-79, Vol I, December, 1977.
- [2.] NLR MP 79018 U, "MINITWIST, Shortened Version of TWIST," by Lowak, H., de Jonge, J. B., Franz, J. and Schutz, D., National Aerospace Laboratory (NLR), Amsterdam, The Netherlands, 1, May, 1979.
- [3.] Kathiresan, K. and Brussat, T. R., "Advanced Life Analysis Methods, Volume III - Experimental Evaluation of Crack Growth Analysis Methods for Attachment Lugs," AFWAL Technical Report, Air Force Wright Aeronautical Laboratories, Wright-Patterson AFB, OH, to be published.

MODIFICATIONS OF FLIGHT-BY-FLIGHT LOAD SEQUENCES TO  
PROVIDE FOR GOOD FRACTURE SURFACE READABILITY

by

H.H. van der Linden  
National Aerospace Laboratory NLR  
Anthony Fokkerweg 2, 1059 CM Amsterdam  
The Netherlands

ABSTRACT

In order to establish an inspection schedule for fatigue critical fastener holes in the wing lower skin of a fighter aircraft crack growth data under realistic loading was required. Experimental determination of these data was a logical choice since a representative specimen was available. However, the spectrum and load sequence, representative for the Dutch usage of the aircraft, do not mark the fracture surface well enough.

Methods to identify markers were evaluated: scanning electron microscopy gives the best results. Goals, means of accomplishment and detailed results are described of a pilot programme in which modifications of the load sequence were investigated.

Simple centre notched and complex representative specimens were used. A marker version of the original sequence was validated.

The paper ends with a summary of lessons learned.

1. INTRODUCTION

Analysis, full scale fatigue test and service incidents led to the identification of a highly fatigue critical area in the root structure, near the rear spar, of the wing lower skin of a small twin-engine fighter aircraft, which is in service in the Royal Netherlands Air Force. This critical area consist of a relatively sharp radius with nearby located fastener holes.

In order to guarantee enduring safe operation of the aircraft an inspection schedule, based on the Damage Tolerance approach, was required. The experimental determination of crack growth data was selected over an analytical one since a representative specimen was available (Ref. 1). Crack growth data for the radius could be obtained by visual observation of crack growth. Since the critical crack length is relatively short this approach could not be followed for the fastener holes. Therefore, fracture surfaces should be analyzed to establish the fastener holes crack growth curves. Since the spectrum, representative for the Dutch usage, does not mark the fracture surface well enough the load sequence should be modified.

Therefore, a pilot programme has been carried out with the primary objective to develop a version of the load sequence which marks the fracture surface sufficiently well.

The basic requirements for the modified sequence were:

- a traceable pattern of sharp markers
- no or minor change in crack growth rate and crack growth life.

The load sequence modifications evaluated are described in chapter 3.

Chapter 4 describes the fatigue test details and chapter 5 the test results and fractographic analysis. Further, a fracture surface from a specimen tested under a modification of FALSTAFF was used to evaluate different macro- and microscopical techniques to identify markers; this evaluation is reported in the next chapter. On the basis of this evaluation it was decided to use only scanning electron microscopy for crack growth measurements in the further programme.

2. EVALUATION OF METHODS TO IDENTIFY MARKERS

A test has been carried out on a modified version of FALSTAFF, the fighter aircraft loading standard (Ref. 2), with the objective to get a legible fracture surface.

This chapter presents the results of a macro- and microscopic investigation on one of the fracture surfaces (Ref. 3).

A simple centre notched specimen (width 80 mm, thickness 5 mm) was made from 7050-T76 material; the notch was a 6.35 mm diameter straight hole provided with two corner flaws (dimension 0.1 x 0.1 mm<sup>2</sup>). Each FALSTAFF block was followed by two thousand constant amplitude cycles (maximum stress is 157.5 MPa and minimum stress is 109.7 MPa); the FALSTAFF maximum stress was 234 MPa.

The micro- and microscopical techniques used in the fractographic analysis are given in table 1; this table also presents the crack length measurements and a qualification of each method.

The working hours spent are given in table 2; it should be kept in mind that the tasks were carried out by experienced microscopists, who did not have much experience in tracing marker load bands resulting from FALSTAFF type loading. A major conclusion from this investigation is that scanning electron microscopy gives the best results for the recognition of the marker loads, the reading of the fracture surface and the fracture surface crack growth measurements. The latter is difficult, and less accurate, when using the transmission electron microscope. Therefore, scanning electron microscopy was used in the pilot programme.

3. DESCRIPTION OF THE PILOT PROGRAMME

To evaluate the different fracture surface marking techniques and to select an appropriate one a step-by-step approach was followed:

- synopsis and selection of means to simplify the topography of the flight-by-flight load sequence.
- fatigue tests on simple open hole specimens under selected modified sequences, followed by a fractographic investigation which should lead to one or two suitable modifications.
- further evaluation of these options using specimens with open or filled countersunk and preflawed holes.

. Tests on the complex representative specimens with the unmodified sequence and the final marking version.  
After a short description of the basic spectrum each of these steps will be briefly discussed.

### 3.1 BASIC load spectrum

The BASIC spectrum and load sequence are derived from counting accelerometer data and strain gage data measured in the wing centre section (Ref. 1). The load sequence, representative for the critical area of the wing lower skin, is a flight-by-flight one; details are given in table 3, figures 1 and 2. It may be noted that the load figures are given in linearly scaled arbitrary levels, which correspond with test machine load levels. The load sequence does not include a pronounced ground-air-ground (GAG) cycle and the ground stress level remains positive.

### 3.2 Means to simplify the topography and selection

A first option is to change the sequence of flights. Ordering all flights of the block in decreasing or increasing severity will affect the loading sequence representativeness very much. A less drastic approach is to cluster a relatively small number of severe flights. References 4 and 5 show good marking if the twenty most severe flights of short-FALSTAFF are put in a cluster positioned in the middle of the short-FALSTAFF block. However, crack growth behaviour is changed considerably.

Stressing the good marking characteristics of this approach two clustered versions were selected:

- . a cluster of the twenty most severe flights
- . a cluster of the seven most severe flights

The severe flights were selected on the basis of their highest peak load value and were sequenced in decreasing magnitude of highest peak loads. The clusters were positioned in the middle of the BASIC sequence by exchanging, on one-to-one basis, the original flights by the severe flights.

The second option is the insertion of a constant amplitude marker block, which either can be added to or extracted from the BASIC sequence. Table 3 presents the added constant amplitude marker blocks that were investigated.

*Dainty* (Ref. 6) extracted constant amplitude cycles from the spectrum to establish the well marking Snowbird test spectrum. In the present investigation the BASIC sequence was searched for cycles with specific range sizes. In order not to disturb the original sequence too much and to limit the number of extracted constant amplitude cycles additional criteria were defined (Fig. 3). In total 427 cycles were extracted from the basic sequence.

The mean stress and stress range of these marker cycles were taken equal to the average mean and the average range of the extracted cycles. The marker block was positioned after a relatively large number of moderate flights and before a severe flight (nr. 51). This sequence has been denoted as Snowbird I.

In order to increase the number of marker block cycles the selection criteria were changed (Fig. 3); this resulted in 1177 accepted cycles; again the average mean and average range defined the marker loads of Snowbird II.

Next all ranges with specific range size were accepted (Fig. 3); 2204 constant amplitude cycles were defined in Snowbird III.

In an other test programme, carried out much later in time, the marker block as defined in Snowbird III was added to the BASIC sequence on a once per block and a once every second block basis (Tab. 3).

A third option is to modify loads within one or more flights.

Two possibilities are mentioned here:

- . to remove the ground-air-ground cycles
- . to increase significantly the highest peak load.

This option is not evaluated here because the modifications will affect strongly the crack growth characteristics (Refs 7, 8).

## 4. FATIGUE TEST DETAILS

### 4.1 Test specimen

Three specimen designs were used (Figs. 4, 5 and 6). Material of specimen types 2 and 3 is from one batch. Manufacturing details of specimen type 3 are given in table 4; fastener hole manufacturing and fastener type (if applicable) were identical in specimen type 2.

Different initial flaw configuration were selected (Tab. 5) to obtain information on different crack starting points in relation with the crack shape development. Initial flaws of specimen types 2 and 3 were circle segments with a radius of intentionally 1 mm. The flaws were made by electrical discharge machining.

### 4.2 Test procedures and loads

Clamping of the specimens was done using 160 mm wide wedge type clamping heads. Anti-buckling guides were only needed for specimen type 3. A 900 kN servo-hydraulic Wolpert Amsler testing machine was used to test the specimen under load control. The test frequency was 15 Hz for the small load changes. For the larger ones the frequency was reduced. The required specimen loads were calculated starting from the BASIC spectrum maximum stress, which is 236.5 MPa, and the gross section area. The specimens were tested until final failure.

## 5. FATIGUE TEST RESULTS AND FRACTOGRAPHIC ANALYSIS

The test schedule is given in table 5. The results of the fatigue tests in combination with the fractographic analysis will be presented for the sequences evaluated.

### 5.1 Evaluation of seven marker versions using specimen type 1

#### 5.1.1 Clustering of flights

The Scanning Electron Microscope (SEM) photograph (Fig. 7) clearly shows the onset of the marker no. 3 up to 6 incl. of the twenty severe flights cluster. At larger magnification marker no. 2 also can be found; marker 7 and on can be seen by the naked eye. All markers could be found also on the one specimen type 2 tested with this sequence. The fracture surface of the "seven cluster" sequence resembles the "twenty cluster" one. However, experience learned that the "seven cluster" version is somewhat more difficult to read in the SEM.

#### 5.1.2 Constant amplitude cycles added to the sequence

The markers of the 1000 cycles high level constant amplitude block, located after the highest peak, could not be found. The second version, using a large amplitude, unfortunately gave very wide marker bands.

Application of a low level marker after the highest peak did only result in a marker "visible" at isolated spots at very large magnification factors. Locating the same low level marker after a relatively large number of moderate flights and directly before a severe flight (nr. 51) revealed macroscopically visible markers, except at small crack lengths. For these crack lengths the SEM proved to be successful, see figures 8 and 9.

#### 5.1.3 Constant amplitude cycles extracted from the sequence: Snowbird

Both the Snowbird I and II sequences produced very good markers. However, the markings at relatively short crack lengths were not that good.

#### 5.1.4 Analysis of specimen type 1 results

Figure 10 presents the crack growth per flight versus the crack length and figure 11 the crack growth curves, both resulting from the surface crack growth measurements.

From a fractographic (SEM) point of view the following versions are suitable:

- . 20 flights cluster version
- . low level marker loads before severe flight
- . Snowbird versions.

From these the best crack growth characteristics are from the Snowbird I. Therefore, further research in the pilot programme, using specimen type 2, focused on application of the Snowbird concept.

### 5.2 Specimen type 2: evaluation of the three Snowbird sequences

Initial flaw sizes, fatigue life figures and crack growth curves are given in table 6 and figures 12 and 13.

The Snowbird I sequence is evaluated on four specimens (Tab. 5). The SEM fractographical analysis showed that:

- . For the 6 mm open hole specimen all markers could be found, while for the 12.5 mm thick specimen the first two and the last marker could not be detected.
- . The introduction of Jo-bolts resulted in an increase in fatigue life (Tab. 6). The first two and the last four markers could not be found (specimen 2-11). Further, tracing back on the fracture surface was a very difficult job on the SEM: at shorter crack length only isolated parts of the marker bands could be found at large magnifications (Fig. 14).

The specimen tested under Snowbird II (nr. 2-13), having an installed Jo-bolt, showed no markers close to the flaw (< 1 mm). Further, some markers were missed completely.

Therefore, Snowbird III, with about twice as much extracted marker cycles, was developed. Very fine markers (Fig. 15) were obtained in specimen 2-14, which had a Jo-bolt. Only the last marker band, nr. 41, could not be found. Figure 16 demonstrates the crack shape development. Figure 17 up to and incl. 22 give details of a number of marker bands. Figure 23 presents the crack growth measurements made in the SEM. Down to the first marker could be detected (Fig. 24) on specimen 2-15, 12.5 mm thick and with installed Jo-bolt.

#### 5.3 Final check of Snowbird III using specimen type 3

The fracture surface of specimen 3-3, tested under Snowbird III, has been evaluated in detail in the SEM: all 60 marker bands could be identified. The general lay-out of the fracture surface is given in figure 25. Figure 26 presents the crack growth curve; it is noted that the curve is a very smooth one. Figure 27 shows the different crack growth behaviour of the BASIC and Snowbird III sequences as observed on the complex specimen during testing.

#### 5.4 Subsequent evaluation on specimen type 2

The 12.5 mm thick version of specimen type 2, provided with a Jo-bolt, has been used in an evaluation of different non-destructive inspection techniques. Since the Snowbird III version leads to a relatively long life as compared to the BASIC spectrum and since the marking characteristics were good it was decided to add an identical marker block to the BASIC sequence. This was done on basis of once per block and on once every second block; the constant amplitude block was inserted as in the Snowbird versions, i.e. in between flight 50 and 51. Upon fractographic analysis in the SEM the once every second block version appeared to result in easier and better readability of the marker bands on the fracture surface. Therefore, this version was used for further testing in the NDI-evaluation programme. Though not further evaluated and compared also the results from other initial flaw locations are presented.

Only at the free surfaces there is some uncertainty in the crack front because of occurring shear lips, which result from the plane stress situation. It is noted that in test specimen 2-24 the fatigue crack started from multiple origins in the mid-bore section of the hole, instead of starting from the initial flaw. Only in the last phase of crack growth a secondary fatigue crack was initiated from the initial flaw. Since marker no. 20 is the first detectable one it is clear that the crack started late in life.

It is remarked that for one other specimen a secondary fatigue crack did initiate. Figure 28 shows that the primary fatigue crack started from the initial flaw in the faying surface section of the bore, and that a secondary fatigue crack initiated from the countersink section. This is probably a consequence from the fact that the countersink location generally has the highest stress-concentration in the hole. Initial flaw sizes and flights to failure are given in table 7.

Marker block identification was carried out for the specimen 2-17 up to 2-25. For some test specimens all present marker bands could be identified in the SEM; see figures 29 and 30. For the other specimens identification of the first marker bands was not possible because of pollution of the fracture surface (probably caused by not completely cured primer). The data of the marker band patterns of test specimens 2-18 up to 2-25 are summarized in table 8; results are plotted in figure 31. Table 9 shows, as an example, a comparison of visual and marker band surface crack readings: a good correlation was found.

## 6. SUMMARY AND DISCUSSION

The fractographic investigations on the specimen tested under a modified FALSTAFF version showed that scanning electron microscopy is the best overall technique:

- . to recognize the marker bands
- . to read the fracture surface
- . to measure crack growth from the fracture surface.

Further, the time spent per fracture surface decreased considerably when experience was gained in reading marked fracture surfaces.

Since the BASIC flight-by-flight sequence does not give a legible fracture surface a modified version was developed.

Numerous modified versions were investigated.

The pilot programme showed that a constant amplitude block could mark the fracture surface well if:

- . the block is of a low level type, i.e. the maximum load of the block is considerably less than the spectrum maximum load and the minimum load is a positive one.
- . the block is positioned after a relatively large number of moderate flights and before a severe one.

Analysis of the Snowbird versions showed that a sufficiently large number of marker cycles should be applied to detect all markers.

Using scanning electron microscopy the crack growth curve could be determined easily and accurately from the fracture surface of the specimens tested under Snowbird III. All markers could be identified.

The crack growth data will only be discussed in relation with the sequences evaluated, since the evaluation of crack growth data as such was beyond the scope of this paper. Further, no attempt has been made to correct the crack growth data for the marker width.

In the selection of means to simplify the topography seven marker versions were evaluated on open hole specimen, type 1 (Figs. 10, 11). The crack growth behaviour might deviate largely from the BASIC sequence.

Tests on the open hole type 2 specimens indicated that the difference in crack growth behaviour between the BASIC and the 20 flights cluster versions can be attributed largely to differences in initial flaw sizes. Further, the Snowbird sequences tend to cause somewhat larger lives. The latter observation leads to the conclusion that the extracted constant amplitude cycles if put in a marker block are less damaging than in the case that they are spread over the sequence. Apparently, the crack opening stress levels of these cycles was altered considerably. The discontinuities of some crack growth curves at a crack length of 5 mm to 6 mm might be due to increased plasticity corresponding with the shear lip formation and causing retarded crack growth. Shear lips increased towards final failure.

The effect of different initial flaw sizes, i.e. a large scatter in crack growth lives, was also observed in tests of specimen type 2 with Jo-bolts (Fig. 13). But also the fastener fit, which varies from light clearance to light interference (Tab. 10), influences early crack growth. Still, Snowbird III is less damaging than the BASIC sequence.

Laying more emphasis on the good marking characteristics than on the requirement that the crack growth behaviour should not or only slightly be changed, the Snowbird III sequence was applied on the complex specimen (type 3). From the fracture surfaces an accurate crack growth curve could be established.

However, the crack growth behaviour of the Snowbird III sequence differed more than expected from the BASIC sequence. The small load transfer might also play a role in this. At the time when these tests were completed neither funds nor capacity were available to continue this programme.

Fortunately, the research could be continued in an other test programme, carried out much later in time. Then the Snowbird III marker was added to - instead of extracted from - the BASIC sequence on a once per block and a once every second block basis. Application of the second marker type resulted in a crack growth behaviour relatively close to the one of the BASIC sequence. As far as SEM fractography is concerned no difference exists between the version in which cycles are added to and the version in which cycles are extracted from the BASIC sequence.

It should be noted that the selected modifications were not created off-hand before the test-programme started.

Several were defined after that results of fatigue tests and fractographic analysis showed that an option did not work well enough. In other words: the selection of a sequence modification was a trial and error procedure. This is inevitable because present analytical tools can not predict with certainty that a marker version of a sequence will not affect the crack growth behaviour of corner flaws under manoeuvre type flight-by-flight loading (Ref. 9).

Finally it is noted that not in every case the crack started from the electrical discharge machined initial flaw. In general a good correlation is found between visual crack growth measurements during testing and the marker band surface crack readings. However, the occurrence of shear lips results in inaccuracies in the latter reading since marker bands could not be identified on the shear lips. Probably the bands were rubbed away.

## 7. LESSONS LEARNED

Scanning electron microscopy proved to be the best overall technique to read the fracture surface. The pilot programme showed that of all marker versions evaluated the one with a low level constant amplitude block, positioned after a relatively large number of moderate flights and before a severe flight, gave the best legible fracture surface. In general all markers can be found; accurate fracture surface crack growth curves were determined. This is valid if transition fit is used. The topography of the marker is the same for the added constant amplitude block and the marker block extracted from the BASIC sequence; about 2200 constant amplitude cycles of a certain range were used. Extracting the marker block cycles results in a less damaging sequence: the crack opening stress of these cycles was altered considerably. Acceptable crack growth characteristics were obtained when the same marker block was added to the sequence.

In general a good correlation was found between visual and topographic crack growth observations. However, on shear lips no markers could be identified.

It will be clear that "adding or extracting" cycles to let a fracture surface mark is not a simple task. The best and quickest way would be to use a refined crack growth model, based on crack closure, to evaluate modified versions. This should be followed by an experimental verification to check the topography and crack growth behaviour. In doing this the initial flaw size and fastener fit are among the parameters which should be considered.

## 8. ACKNOWLEDGEMENT

The fatigue tests and fractographic analyses have been carried out under contract with the Royal Netherlands Air Force. The author wishes to express his appreciation to several colleagues from the NLR: Mr. A.A. ten Have for the generation of the modified sequences, Mr. D.T. du Pon and Mr. A. Nederveen for the specimen preparation and the fatigue tests, Mr. A.M. Otter for the SEM investigations. The discussions with these colleagues and others are gratefully acknowledged here.

## 9. REFERENCES

1. De Jonge, J.B., Re-assessment of service life by comparative specimen tests. NLR MP 79008 U. February 1979. Also published in the Proceedings of the 10th ICAF Symposium, 16-18 May 1979, Brussels, ICAF Document No. 1169.
2. Various authors, FALSTAFF, Description of a Fighter Aircraft Loading STandard For Fatigue, F+W, Switzerland, LBF, Germany, NLR, The Netherlands, IABG, Germany, March 1976.
3. Bongers, J.A.M., Evaluation of recognizability of marker loads on the fracture surface of specimens tested under a modified version of FALSTAFF, (in Dutch) NLR Memorandum SL-82-005, July 1982.
4. Herteman, J.P., Development of modification of FALSTAFF loading spectrum. CEAT. ICAF National Reviews, Minutes of the 17th Conference held in Noordwijkerhout, The Netherlands, 18 and 19 May 1981, ICAF Document No. 1215, pp. 7/12-7/14.
5. Private communications with J.P. Herteman, CEAT.
6. Dainty, R.V., The use of 'marker blocks' as an aid in quantitative fractography in full-scale aircraft fatigue testing - A case study. National Research Council Canada, National Aeronautical Establishment, LTR-ST-1374, May 1982.

7. De Jonge, J.B., Nederveen, A. and Tromp, P.J., Effect of flight load spectrum variations on fatigue life of riveted specimens and crack propagation in sheet made of alclad 7075-T6. NLR TR 78071, June 1978.
8. Nederveen, A., De Jonge, J.B. and Tromp, P.J., Effects of variations in gust spectrum and ground load level on fatigue life and crack propagation. NLR TR 80009, January 1980.
9. Hewitt, R.L., A numerical investigation of the effects of marker blocks on crack propagation rates for the Snowbird spectrum. National Research Council Canada, National Aeronautical Establishment, LTR-ST-1409, September 1982.

TABLE 1  
Evaluation of five marker band identification techniques

METHOD	MEASURED DURING FATIGUE TEST	MACROSCOPY	OPTICAL MICROSCOPY	OPTICAL MICROSCOPY	SCANNING ELECTRON MICROSCOPY	TRANSMISSION ELECTRON MICROSCOPY
MAGNIFICATION FACTOR	-	14	80	160	608-4750	2400-6750
DISTANCE BETWEEN MARKER BANDS (mm)	0.3 0.3 0.4 0.4 0.7 0.9 1.2 1.9 3.1 5.7 11.4	0.57 0.79 1.1 1.4 2.2 3.4 5.0	0.27 0.34 0.42 0.55 0.76 1.24 1.53 2.4	0.28 0.33 0.45 0.52 0.62 0.9	0.13 0.25 0.36 0.51 0.71 1.02 1.28/1.43 1.94/2.20 3.21/3.52 5.30/5.81 10.71/11.37	0.26 0.38 0.47 0.59 0.78 1.03 1.04 1.9/2.0 3.2/3.3 5.1/5.4
REMARKS		.MEASURED FROM POLAROID PICTURE	.USING DARK-FIELD TECHNIQUE	.CARBON EVAPORATED ON REPLICA  .BRIGHT FIELD TECHNIQUE .LARGER MAGNIFICATION DUE TO LESS REFLECTION	.GOLD SPUTTERED ON FRACTURE SURFACE  .TIME CONSUMING JOB DUE TO ROUGH SURFACE	.6 mm LONG REPLICA CUT INTO 1 mm x 1 mm PIECES .LAST MARKER NOT ON REPLICA
CONCLUSION		.REASONABLE AGREEMENT WITH TEST MEASUREMENTS  .MARKERS NOT IDENTIFIED WITH CERTAINTY			.FIRST 5 MARKERS ON 1 REPLICA: ACCURACY $\pm 15 \mu\text{m}$ .OTHER MARKERS: ACCURACY $\pm 120 \mu\text{m}$  .MARKERS IDENTIFIED WITH HIGH RELIABILITY	

Note: crack lengths were measured along the sheet surface

TABLE 2  
Working-hours spent for different marker band identification techniques

METHOD \ TASK	MACROSCOPY (14x)	MICROSCOPY (80x)	MICROSCOPY (160x)	SCANNING ELECTRON MICROSCOPY	TRANSMISSION ELECTRON MICROSCOPY
PREPARATION OF FRACTURE SURFACE, REPLICA ETC.	1	1	3	3	5
MICROSCOPIC WORK	-	1	1	6	6
PHOTOGRAPHS	1	1	2	-	-
INTERPRETATION	2	2	2	2	2
TOTAL	4	5	8	11	13

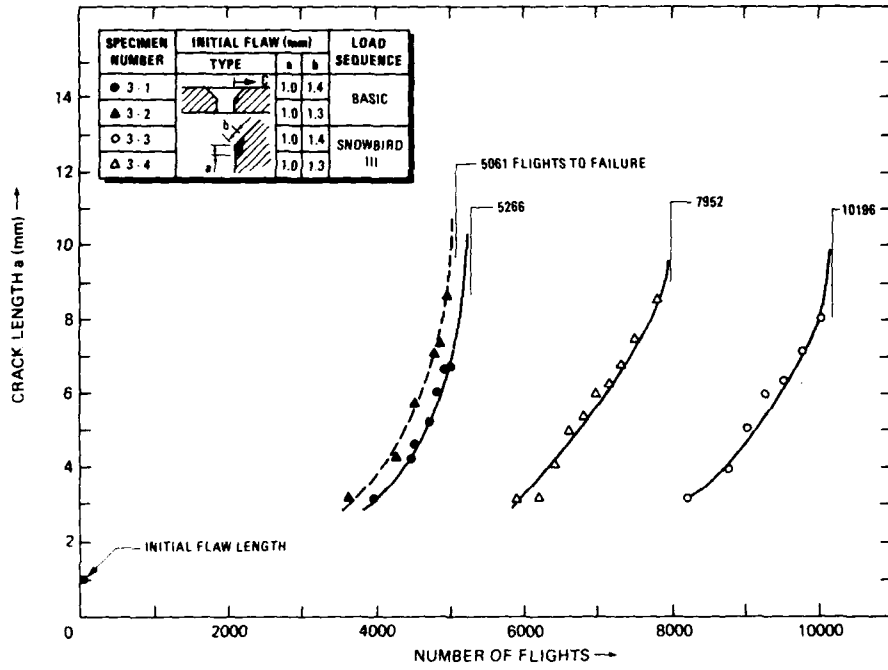


Fig. 27 Crack growth curves observed visually during test, specimen type 3

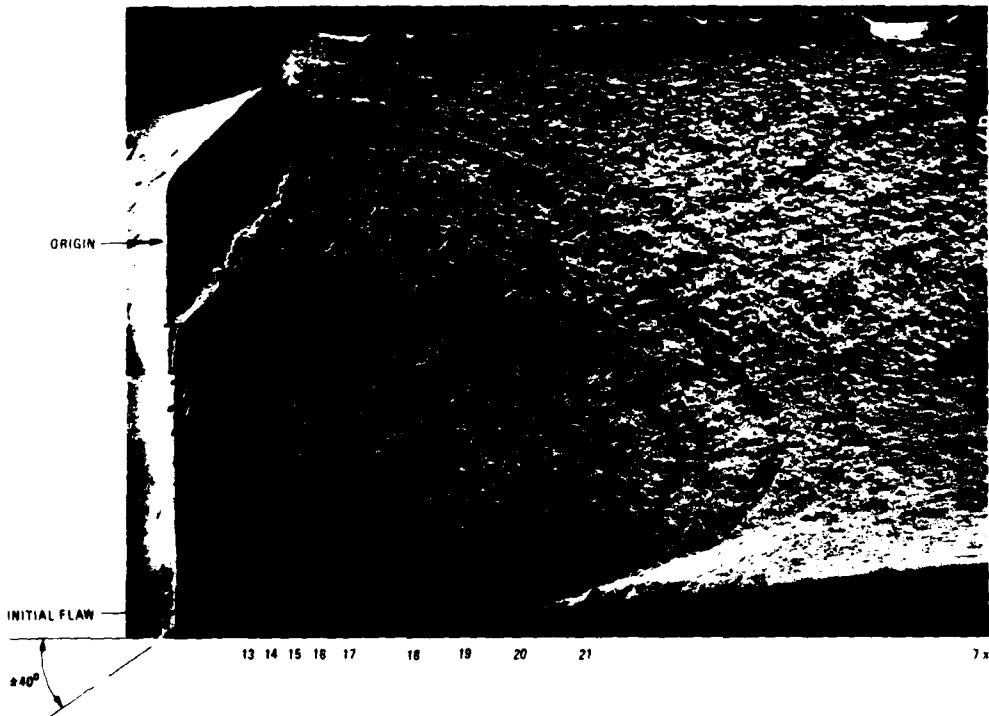


Fig. 28 Fracture surface and marker band notation of test specimen 2-22

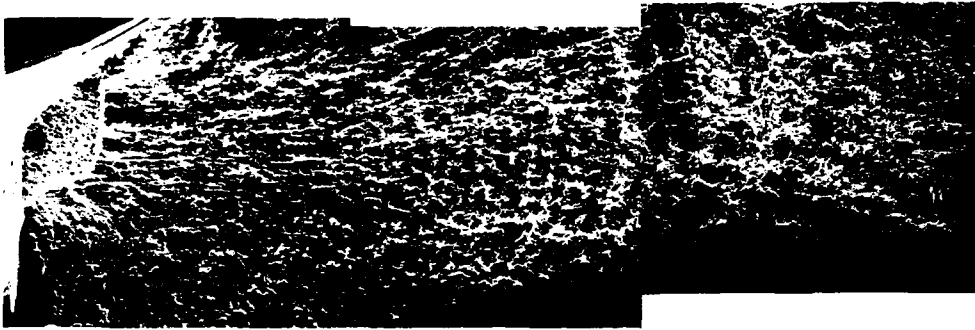


Fig. 25 Fracture surface of specimen 3-3 tested under Snowbird III

14x

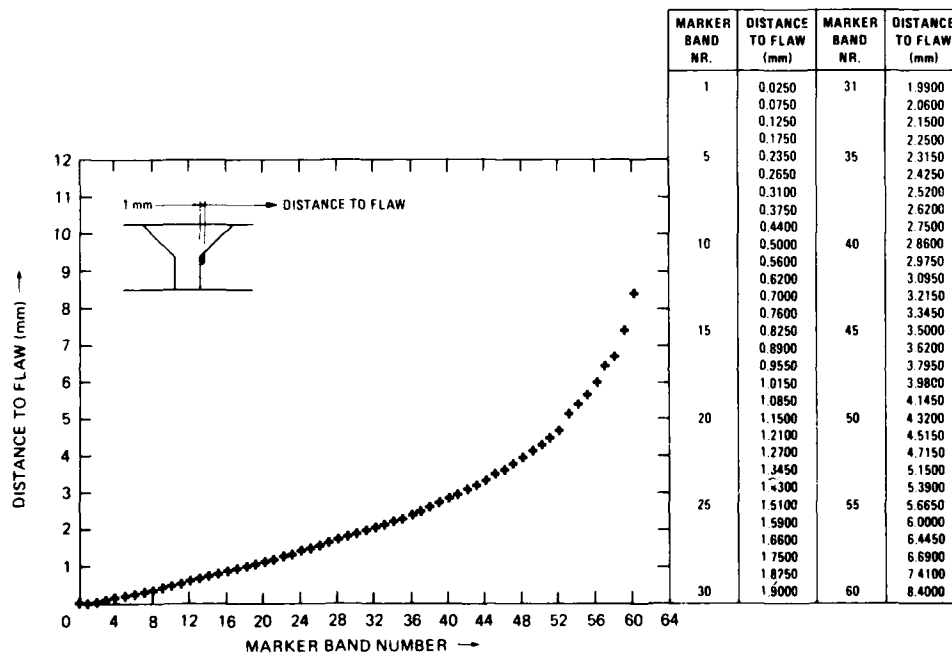


Fig. 26 Crack growth curve measured in the SEM, specimen 3-3 tested under Snowbird III

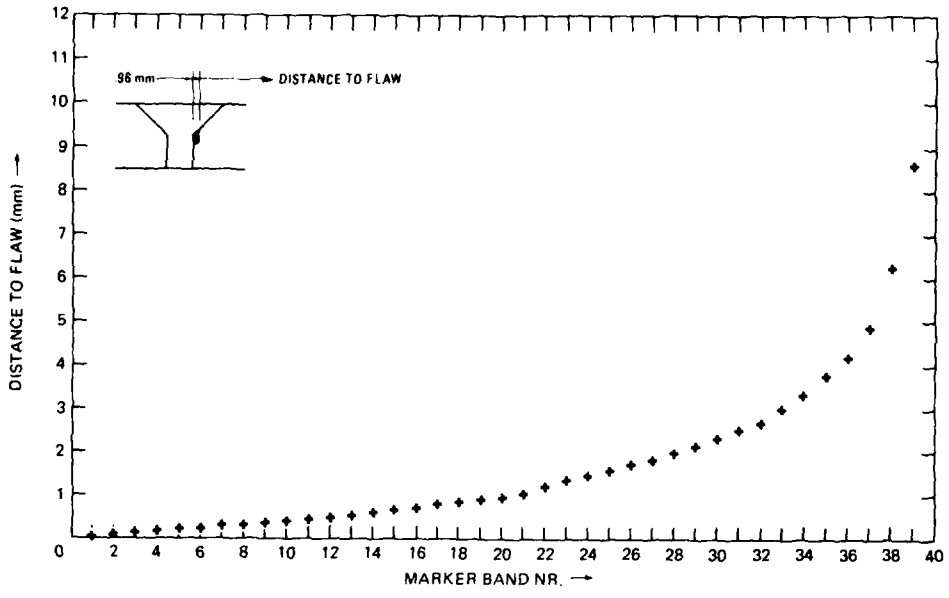


Fig. 23 Crack growth curve measured in the SEM, specimen 2-14 tested under Snowbird III

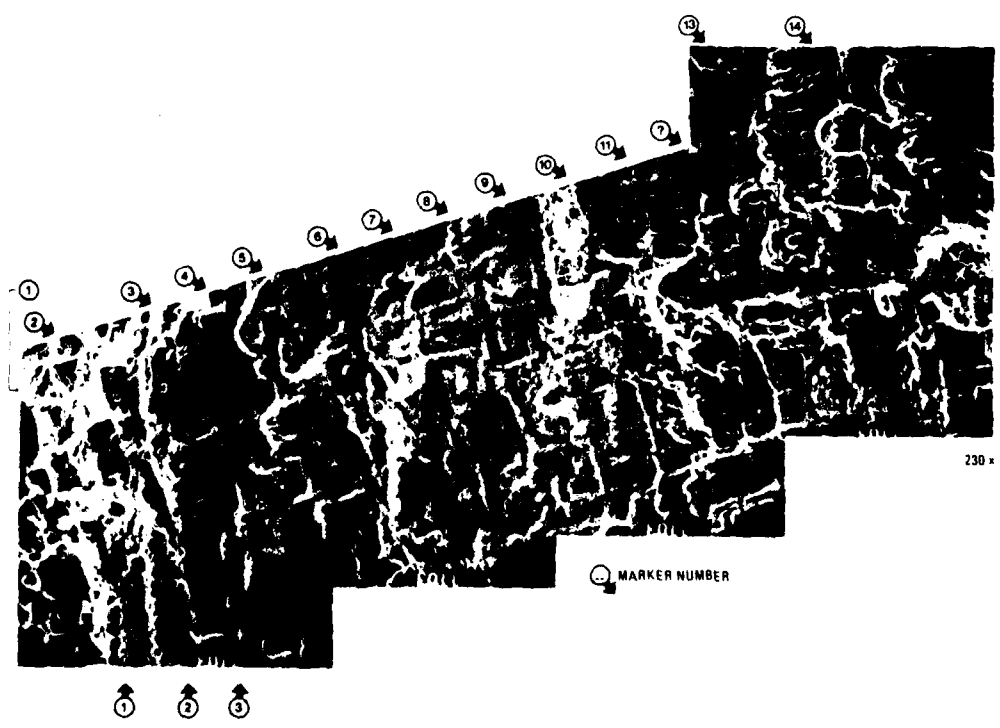


Fig. 24 Fracture surface of specimen 2-15, Snowbird III

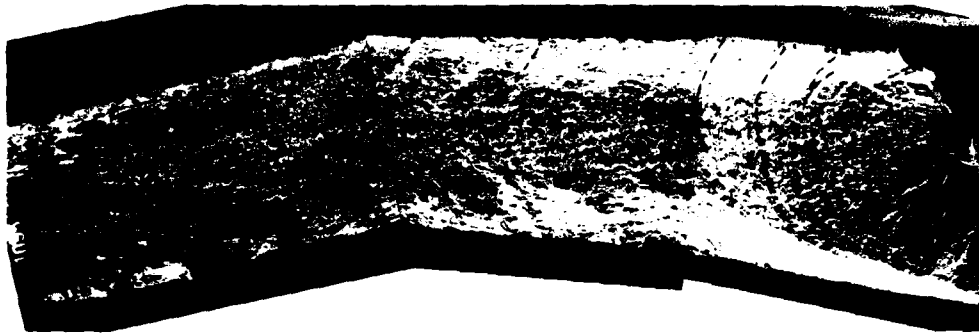
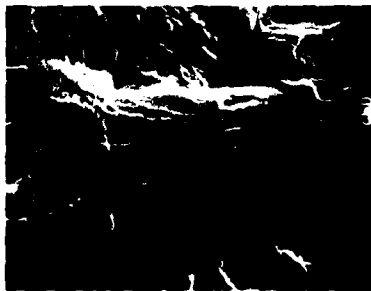


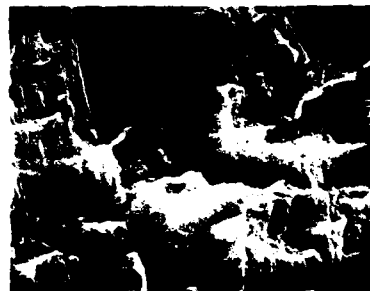
Fig. 16 Fracture surface (SEM) of specimen 2-14, tested under Snowbird III

7x



3330 x  
FLIGHT BY FLIGHT SEQUENCE MARKER

Fig. 17 First marker band of specimen 2-14, Snowbird III



3330 x  
MARKER

Fig. 18 Marker no. 10 of specimen 2-14, Snowbird III



1665 x  
MARKER

Fig. 19 Marker no. 20 of specimen 2-14, Snowbird III



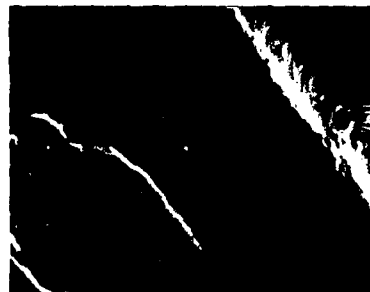
830 x  
MARKER

Fig. 20 Marker no. 30 of specimen 2-14, Snowbird III



205 x  
MARKER

Fig. 21 Marker no. 35 of specimen 2-14, Snowbird III



6500 x

Fig. 22 Marker no. 36 of specimen 2-14, Snowbird III

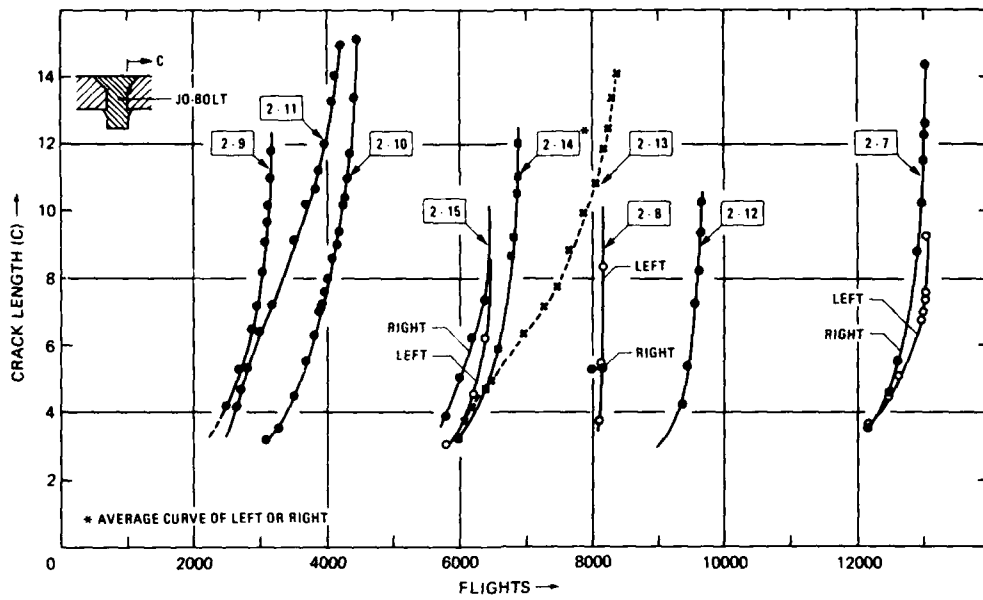


Fig. 13 Crack growth curves of specimen type 2 with filled holes, measured along the surface during test

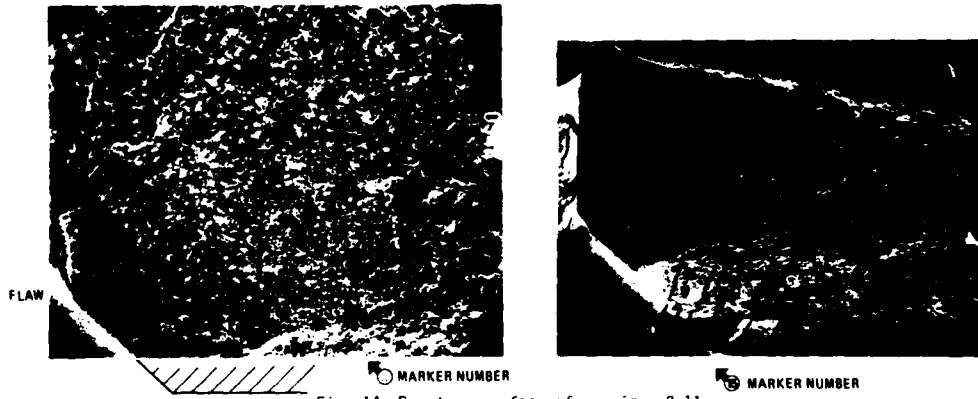


Fig. 14 Fracture surface of specimen 2-11

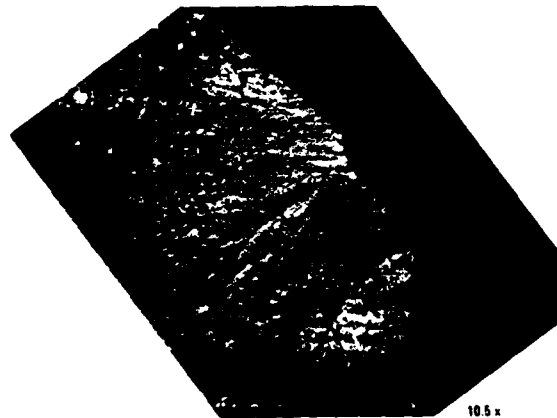


Fig. 15 Fracture surface of specimen 2-14, tested under the Snowbird III sequence (optical microscope)

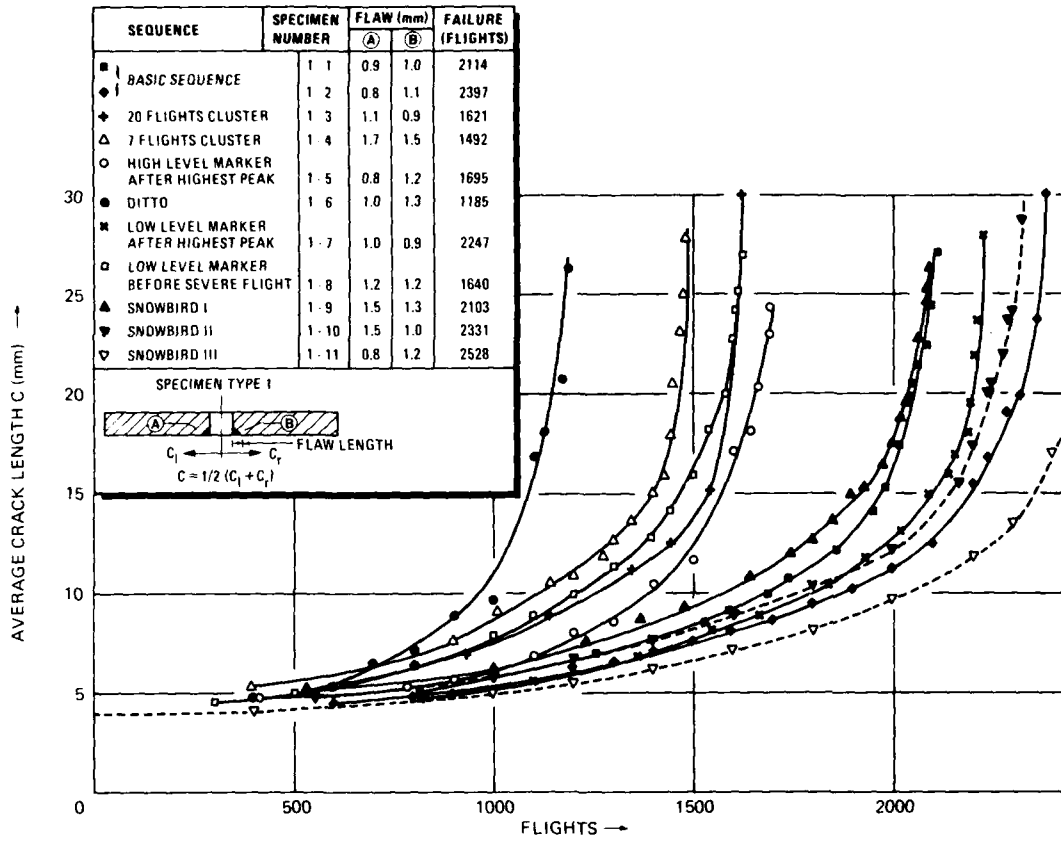


Fig. 11 Crack growth curves of tests of specimen type 1

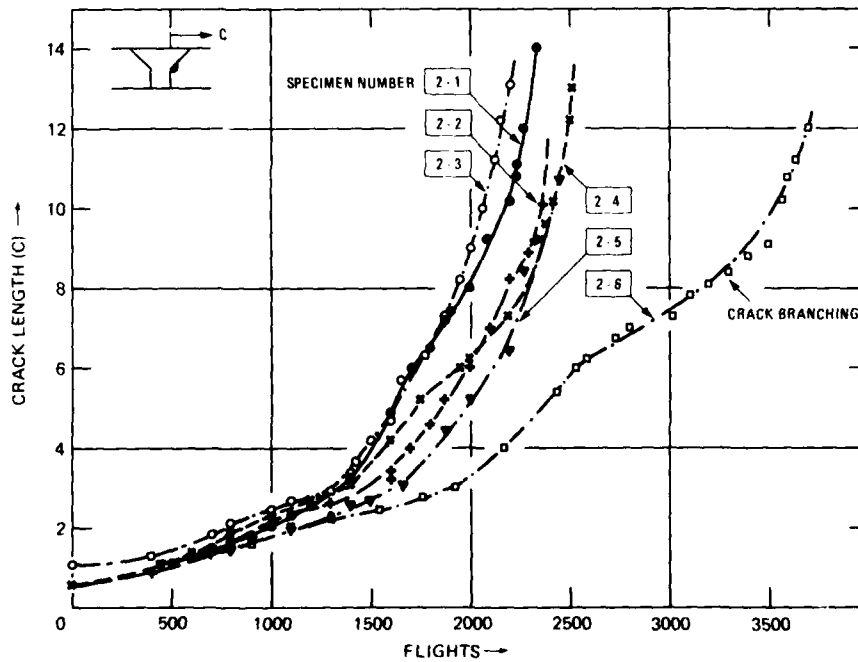


Fig. 12 Crack growth curves of specimen type 2 with open hole, measured along the surface during test

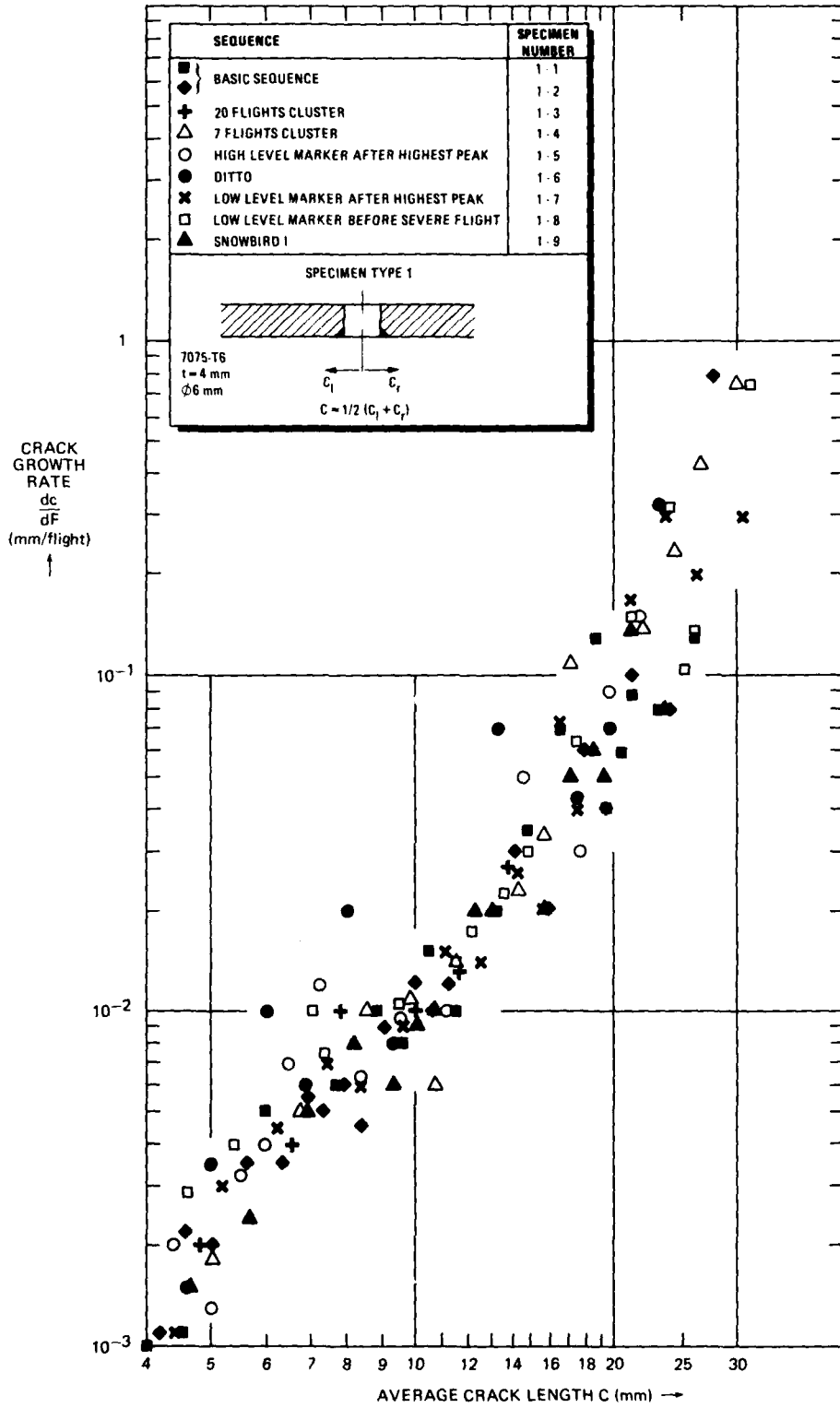


Fig. 10 Crack growth rate as a function of crack length

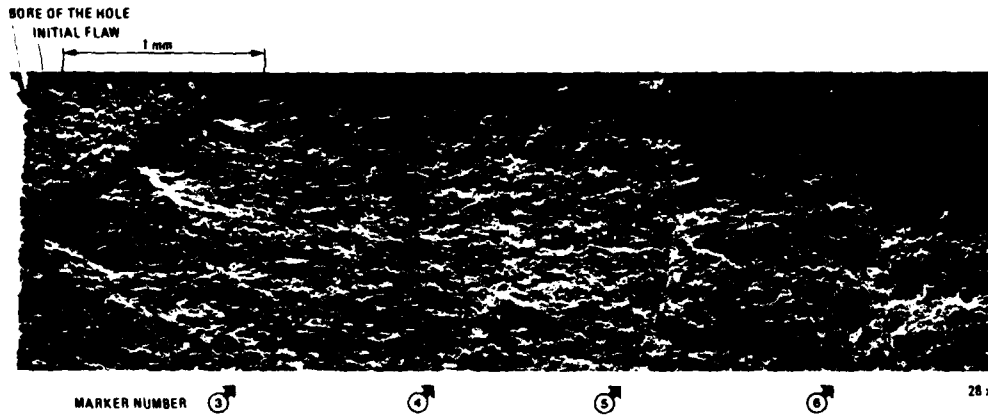


Fig. 7 Fracture surface of specimen 1-3: clustering of 20 severest flights



Fig. 8 Fracture surface of specimen 1-8: low level constant amplitude marker block before severe flight



Fig. 9 Detail of fracture surface of specimen 1-8: transition from low level constant amplitude marker to the flight-by-flight loading

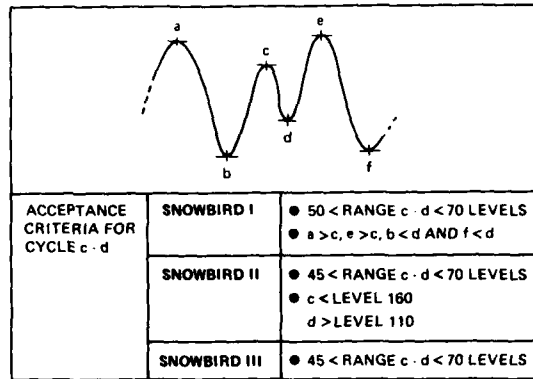


Fig. 3 Criteria used in the development of the Snowbird sequences

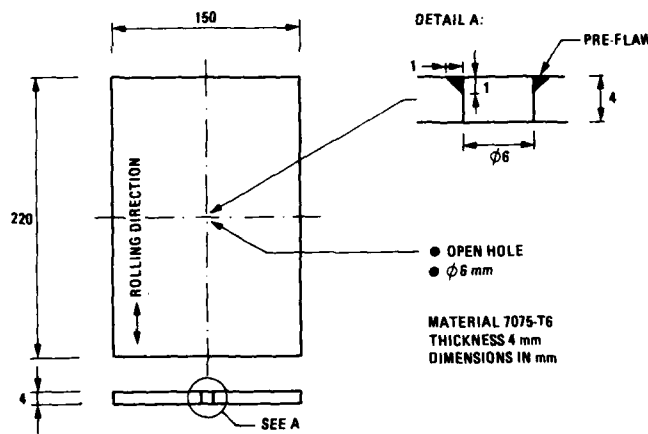


Fig. 4 Fatigue test specimen (nr. 1)

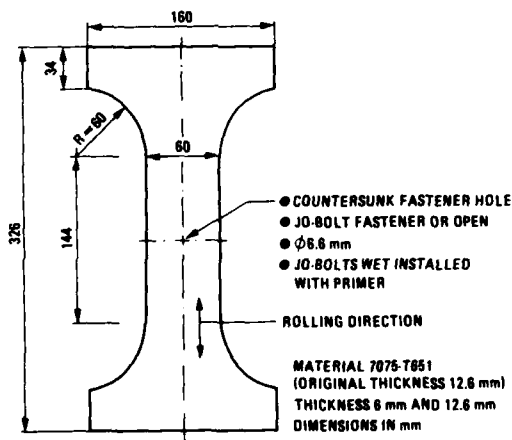


Fig. 5 Fatigue test specimen (nr. 2)

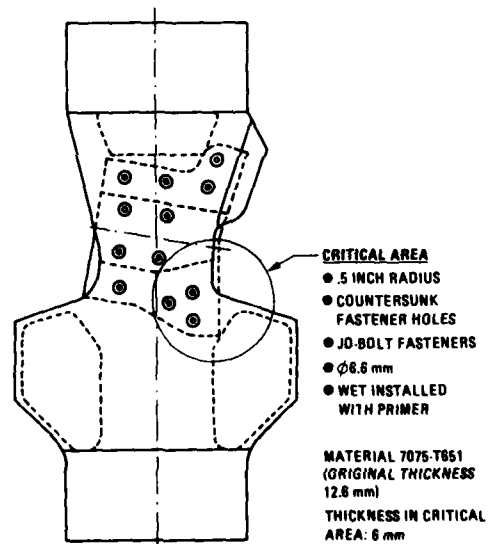


Fig. 6 Complex fatigue test specimen (nr. 3), representative of a wing lower skin critical area

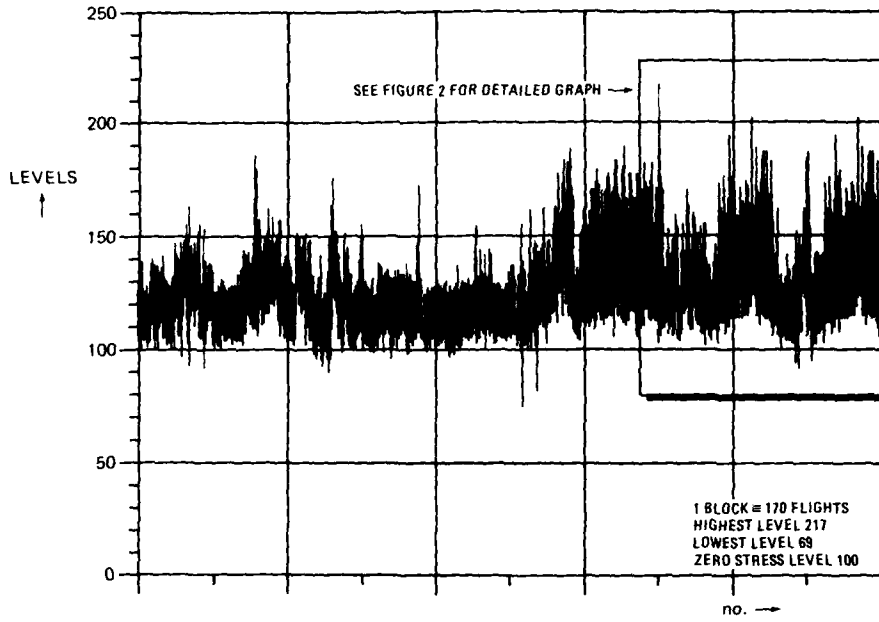


Fig. 1 Sample of the BASIC sequence

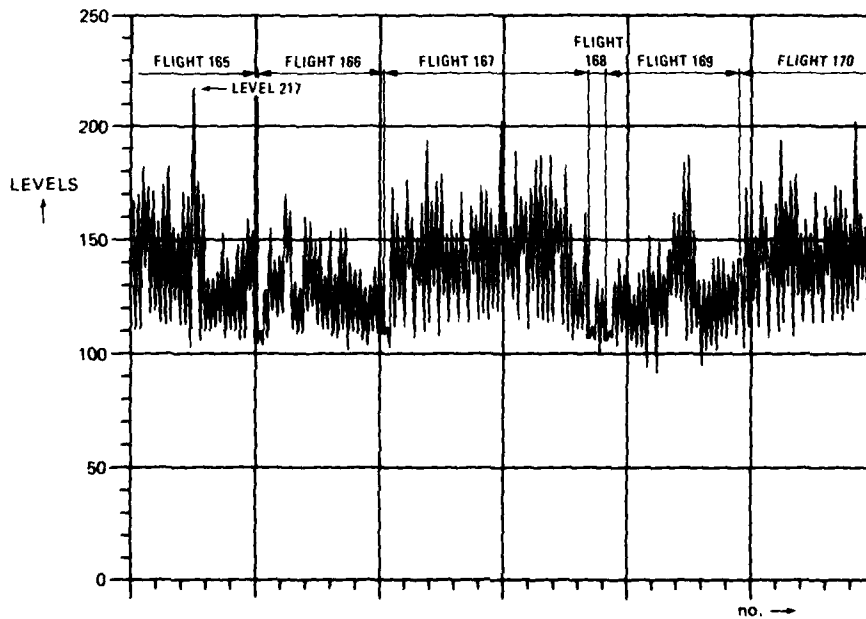


Fig. 2 Sample of BASIC flight sequence (Flight 165 contains highest level 217)

TABLE 9  
Comparison of visually observed- and marker load crack lengths

SPECIMEN NUMBER	FLIGHTS	SURFACE CRACK LENGTH (mm)													
		2-18		2-19		2-20				2-21				2-23	
		ML	V	ML	V	LEFT		RIGHT		LEFT		RIGHT		ML	V
8	2602	-	-	-	-	~3.2	3.7	~3.2	~3.2	4.3-5.0	4.3	4.4-5.0	4.9	-	-
9	2942	-	-	-	-	6.9	5.9	5.2	5.5					-	-
10	3282	-	-	-	-									-	-
11	3622	-	-	~3.2	-									-	-
12	3962	-	-	~5.4	-									-	-
13	4302	-	-	~7.0	6.1									-	-
14	4642	-	4.4	10.8	10.6									-	-
15	4982	5.7	6.1											~3.4	3.2
16	5322	7.9	7.8											~5.1	4.7
17	5662	10.7												~6.2	6.7
18	6002													~8.5	7.8
19	6342													~10.5	9.9



SURFACE CRACK LENGTH

ML - marker load surface crack length  
V - visually observed surface crack length

TABLE 10  
Measured fastener and hole diameters, together with the fit obtained

SPECIMEN Nr.	FASTENER DIAMETER (mm)		HOLE DIAMETER *) (mm)				FIT (μm) + clearance - interference
	TOP	BOTTOM	0°	45°	90°	135°	
2-9	6.585			6.585			0
2-13	6.58			6.59			+10
2-14	6.585			6.59			+5
2-15	6.57			6.595			+25
2-16	6.575	6.575	6.57	6.575	6.57	6.57	-4
2-17	6.575	6.575	6.57	6.57	6.57	6.57	-5
2-18	6.575	6.57	6.57	6.575	6.57	6.57	-1
2-19	6.575	6.575	6.57	6.58	6.58	6.58	+2
2-20	6.565	6.565	6.575	6.575	6.57	6.57	-7
2-21	6.58	6.58	6.59	6.59	6.59	6.59	+10
2-22	6.58	6.585	6.56	6.57	6.575	6.57	-14
2-23	6.57	6.575	6.56	6.56	6.55	6.57	-12
2-24	6.57	6.575	6.58	6.595	6.585	6.585	+14
2-25	6.58	6.58	6.58	6.59	6.59	6.575	+4
3-1	5.58		5.58	5.58	5.58	5.59	+2
3-2	6.57		6.59	6.58	6.59	6.58	+1
3-3	6.58		6.60	6.60	6.59	6.59	+15
3-4	6.59		6.60	6.60	6.60	6.60	+10

Notes: . \*) 0° corresponds with length axis of specimen  
. No systematic measurements have been carried out on specimen nr. 2-1 up to incl. 2-15.



TABLE 5  
Test schedule and initial flaw configuration

SPECIMEN TYPE	NR OF MARKERS	POSITION OF MARKER							COMPLEX SPECIMEN
			1	2	2	2	2	3	
BASIC LOAD SEQUENCE	-	-	1-1 1-2	2-1 (A)	2-2 (A)	2-7 (A)	2-8 2-9 2-10 (A)	3-1 3-2 (A)	
CLUSTERING OF SEVEREST FLIGHTS	20 FLIGHTS	IN THE MIDDLE OF THE BASIC BLOCK	1-3		2-3 (A)				
	7 FLIGHTS		1-4						
HIGH LEVEL MARKER BLOCK ADDED TO SEQUENCE	1000 CYCLES	AFTER HIGHEST PEAK	1-5 1) 1-6 2)						
		BEFORE SEVERE FLIGHT	-						
LOW LEVEL MARKER BLOCK ADDED TO SEQUENCE		AFTER HIGHEST PEAK	1-7						
		BEFORE SEVERE FLIGHT	1-8						
LOW LEVEL MARKER BLOCK CYCLES EXTRACTED FROM SEQUENCE	SNOWBIRD I	BEFORE SEVERE FLIGHT	1-9	2-4 (A+B)	2-5 (A+B)	2-11 (A)	2-12 (A)		
	II		1-10 1-11			2-13 (A)			
	III				2-6 (A)	2-14 (A+B)	2-15 (A+B)	3-3 3-4 (A)	
LOW LEVEL MARKER BLOCK ADDED TO SEQUENCE	2204 CYCLES					2-16 (A)			
	2204 CYCLES ONCE EVERY 2 BLOCK					2-17 (A) UPTO (A+B) 2-25 (C) (D)			

INITIAL FLAW POSITIONS

1-9  
└ sequence nr.  
└ specimen type

1) minimum load of marker block on level 192  
2) ditto level 180

TABLE 6  
Measured initial flaw dimensions of specimen type 2, specimen 2-1 up to 2-15

Specimen number	Hole configuration	Flaw dimensions (mm)			Load sequence	Flights to failure
		a	b	c		
2-1	open hole	1.0	1.4	0.6	BASIC	2341
2-2			0.8	0.6	BASIC	2488
2-3			1.4	1.1	Cluster 20	2286
2-4			0.92	0.55	Snowbird I	2528
2-5			0.66	0.33	Snowbird I	2476
2-6			0.9	1.4	Snowbird III	3718
2-7			0.6	0.20	BASIC	13068
2-8	transition fit Jo-bolt	1.0	0.5	0.15	BASIC	8211
2-9			1.5	1.69	BASIC	3225
2-10			1.4		BASIC	4494
2-11			0.36	0.32	Snowbird I	4245
2-12					Snowbird I	9685
2-13			1.0	1.25	Snowbird II	8596
2-14			0.8	left 1.07	Snowbird III	6921
			1.0	right 1.07		
	1.0	left 1.00				
2-15			1.1	right 1.53	Snowbird III	6455

TABLE 3  
Details of the load sequences used in the pilot programme

	NR OF MARKERS	POSITION OF MARKER	DETAILS OF LOAD SEQUENCES
BASIC LOAD SEQUENCE	-	-	.1 BLOCK CONTAINS 170 FLIGHTS .BLOCK IS REPEATED CONTINUALLY .ZERO STRESS IS ON LEVEL 100 .MAXIMUM STRESS IS ON LEVEL 217 .MINIMUM STRESS IS ON LEVEL 69 .AVERAGE FLIGHT LENGTH: 51 CYCLES .EXAMPLE IN FIGURE 2
CLUSTERING OF SEVERE FLIGHTS	20 FLIGHTS	IN THE MIDDLE OF THE BASIC BLOCK	.ALL FLIGHTS WITH PEAK(S) GREATER THAN OR EQUAL LEVEL 199 .CLUSTER IN DECREASING ORDER OF PEAK LOAD LEVEL .ONE-TO-ONE EXCHANGE OF FLIGHTS
	7 FLIGHTS		.ALL FLIGHTS WITH PEAK(S) GREATER THAN OR EQUAL LEVEL 208 .CLUSTER IN DECREASING ORDER OF PEAK LOAD LEVEL .ONE-TO-ONE EXCHANGE OF FLIGHTS
HIGH LEVEL MARKER BLOCK ADDED TO SEQUENCE	1000 CYCLES	AFTER HIGHEST PEAK	.CONSTANT AMPLITUDE BLOCK AFTER PEAK OF LEVEL 217, FLIGHT 165 .MAXIMUM ON LEVEL 217, MINIMUM ON LEVEL 192 AND .MAXIMUM ON LEVEL 217, MINIMUM ON LEVEL 180
		BEFORE SEVERE FLIGHT 51	.NOT EVALUATED
LOW LEVEL MARKER BLOCK ADDED TO SEQUENCE	1000 CYCLES	AFTER HIGHEST PEAK	.CONSTANT AMPLITUDE BLOCK AFTER PEAK OF LEVEL 217, FLIGHT 165 .MAXIMUM ON LEVEL 179, MINIMUM ON LEVEL 154
		BEFORE SEVERE FLIGHT 51	.CONSTANT AMPLITUDE BLOCK BEFORE FLIGHT 51, WHICH CONTAINS PEAK OF LEVEL 209 .MAXIMUM ON LEVEL 179, MINIMUM ON LEVEL 154
LOW LEVEL MARKER BLOCK EXTRACTED FROM SEQUENCE	SNOWBIRD I	427 CYCLES	.CONSTANT AMPLITUDE BLOCK .MAXIMUM ON LEVEL 168, MINIMUM ON LEVEL 112
	II	1177 CYCLES	.CONSTANT AMPLITUDE BLOCK .MAXIMUM ON LEVEL 164, MINIMUM ON LEVEL 112
	III		.CONSTANT AMPLITUDE BLOCK .MAXIMUM ON LEVEL 165, MINIMUM ON LEVEL 111
LOW LEVEL MARKER BLOCK ADDED TO SEQUENCE	2204 CYCLES	BEFORE SEVERE FLIGHT 51	
	2204 CYCLES EVERY 2ND BLOCK		

TABLE 4  
Manufacturing details of specimen type 3

<u>Material</u>	: aluminium alloy 7075-T651, starting thickness 0.5 inch.
<u>Surface roughness</u>	: as machined.
<u>Protective treatment</u>	: - sulphuric acid anodized. - sealed in hot water (96 °C - 100 °C). - coated with epoxy primer S15/76; primer properties according to NAI 1269.
<u>Fastener holes</u>	: - double margin drill, nominal diameter 6.6 mm. - hole diameter between .2585 and .2615 inch.
<u>Fasteners</u>	: - Jobolt, code PLT-110-8-.. - nominal diameter .2590 inches - transition fit installation, ranging from a clearance fit of 15 µm and an interference fit of 15 µm appr. - wet installed with epoxy primer S15/76.

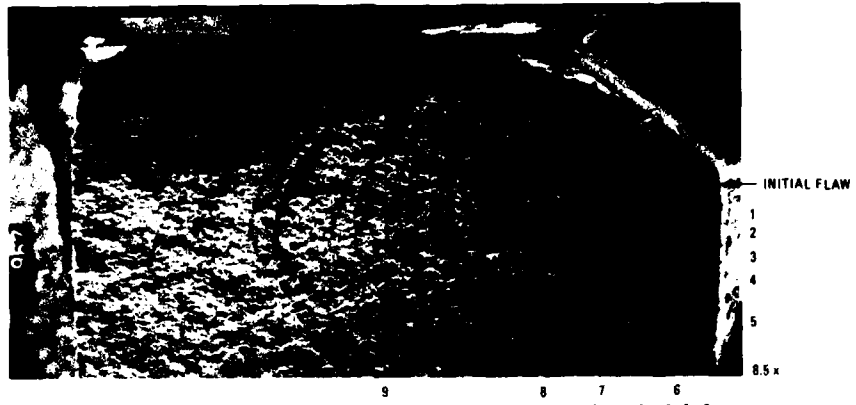


Fig. 29 Fracture surface and marker band notation of test specimen 2-20 left

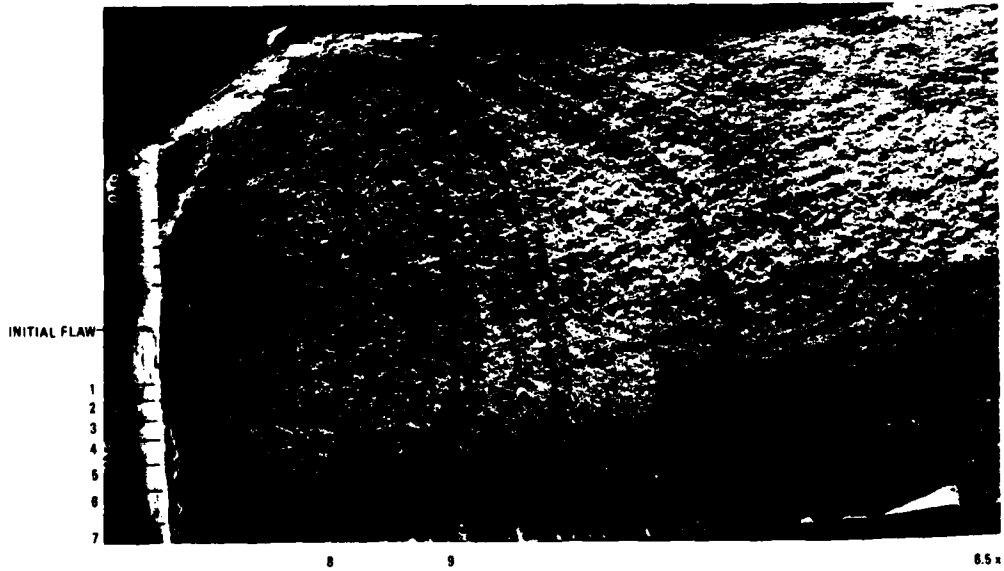


Fig. 30 Fracture surface and marker band notation of test specimen 2-25

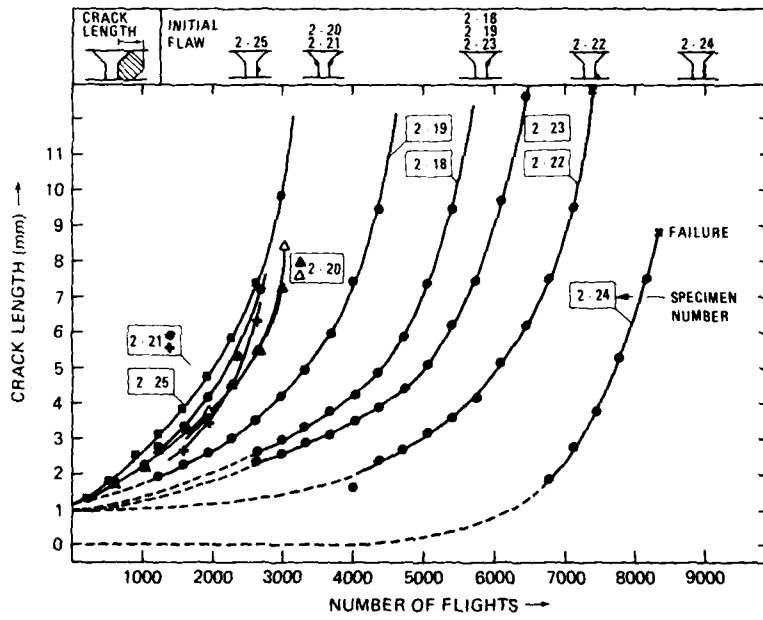


Fig. 31 Crack growth curves (crack length versus the number of flights) using marker band measurements (table 9)

ON THE USE OF MARKER LOADS AND REPLICAS FOR MEASURING  
GROWTH RATES FOR SMALL CRACKS

M. H. Swain\* and J. C. Newman, Jr.  
NASA Langley Research Center  
Hampton, Virginia 23665, U.S.A.

ABSTRACT

The initiation and growth of small cracks (5-500  $\mu\text{m}$ ) from edge notches in 2024-T3 aluminum alloy sheets were studied under constant-amplitude loading. Two methods were used to measure crack shape and size. In the first method, striation marker bands were periodically formed along the crack front by interrupting the constant-amplitude loading by either an elevated R-ratio load sequence, or by an overload sequence. In each case the marker loading was selected so as to have minimal influence on the growth rate under the primary loading. In the second method, the surface crack length was monitored by taking surface replicas at regular intervals. The marker band techniques did not provide reliable crack length and crack shape information for cracks smaller than 2 mm. The replica technique provided accurate information for surface crack length at all crack lengths, and fracture tests on specimens with small cracks provided crack-shape information.

Crack growth rates were plotted against the stress-intensity factor ranges. The results exhibited the small-crack effect, in that the small cracks grew faster than large cracks at the same stress-intensity factor range.

A crack-closure model was also used to analyze the growth of small cracks from small (inclusion) defects at the notch surface. Reasonable agreement was found between measured and predicted crack-growth rates and crack shapes.

NOMENCLATURE

a	one-half surface crack length, m
c	surface-crack depth or through crack length, m
$F_{Sn}$	boundary-correction factor on stress intensity
K	stress-intensity factor, $\text{MPa}\cdot\text{m}^{1/2}$
N	cycles
Q	shape factor for surface crack
R	stress ratio ( $S_{\min}/S_{\max}$ )
r	semi-circular notch radius, m
S	applied gross stress, MPa
$S_{\max}$	maximum applied stress, MPa
$S_{\min}$	minimum applied stress, MPa
$S_0$	crack-opening stress, MPa
t	one-half specimen thickness, m
$t_i$	location of initiation site from centerline of specimen, m
w	specimen width, m
$\lambda$	constraint factor
$\Delta K$	stress-intensity factor range, $\text{MPa}\cdot\text{m}^{1/2}$
$\Delta K_{\text{eff}}$	effective stress-intensity factor range, $\text{MPa}\cdot\text{m}^{1/2}$
$\Delta K_{\text{th}}$	threshold stress-intensity factor range, $\text{MPa}\cdot\text{m}^{1/2}$
$\sigma_0$	flow stress (average between $\sigma_{ys}$ and $\sigma_u$ ), MPa
$\sigma_u$	ultimate tensile strength, MPa
$\sigma_{ys}$	yield stress (0.2 percent offset), MPa
$\phi$	parametric angle of ellipse

\* Kentron International, Inc., Hampton, Virginia

## INTRODUCTION

Numerous investigators [1-7] have observed that the growth characteristics of small fatigue cracks (less than about 1 mm in length) in plates and at notches differ from those of large cracks in the same material. On the basis of linear-elastic fracture mechanics, the small cracks were found to grow much faster than would be predicted from large crack data and to grow at stress-intensity factor levels well below the threshold for large cracks. Because crack growth from "small" pre-existing flaws in many engineering structures is a major portion of the component's fatigue life, the growth behavior of small fatigue cracks is important to the understanding of the total fatigue process.

The direct measurement of the growth of small cracks under fatigue loading has been accomplished in many alloys using a number of different techniques, notably optical microscopy [1,3,7], scanning electron microscopy (SEM) of replicas [2,4,5], in situ SEM observations [6], and cyclic-load changes to mark the fatigue surface [8]. The latter method, that of producing marker bands, has the advantages of delineating the crack front shape and of uninterrupted testing. These load changes, however, may alter the crack-growth rates. Forsyth and Powell [8] were successful in producing markings for small cracks (10  $\mu\text{m}$ ) but found that retardation occurred at low R-ratios (near zero). At high R-ratios, their results did not show a small-crack effect, that is, the crack-growth rates for the small and large cracks agreed.

Of the surface techniques, in situ observation in the SEM is perhaps the most elegant, yielding information on crack size, crack-opening loads, and mode of deformation at the crack tip. Periodic surface replication or optical microscopy interrupts testing but has the advantages of permitting analysis after completion of the test. Crack lengths are traced backwards in time from an easily located large crack to the small crack sizes. Crack lengths as small as 10  $\mu\text{m}$  have been commonly observed. Replica techniques permit recording data from a large area of interest, such as notch roots. The replicas are analyzed later under high magnification in the SEM.

The present paper describes measurements of crack-growth rates for small cracks emanating from semi-circular edge notches in 2024-T3 aluminum alloy sheet specimens. Two methods of crack measurement were used. One used a periodic load change, selected to mark the crack front while having minimal effect on crack growth (retardation and acceleration). The other method was surface replication. The effect of microstructure on the initiation and growth of small cracks is discussed. Experimentally determined crack-growth rates for small cracks are compared with data obtained for large cracks on this alloy stock by other investigators. Calculated values of crack-growth rates and crack shapes obtained from a crack-closure analysis are compared with experimentally determined values.

## MATERIAL, SPECIMEN, AND EXPERIMENTAL PROCEDURE

The specimen was a double-edge-notched tensile specimen made of 2024-T3 aluminum alloy (2.3 mm thick) as shown in Figure 1. This material has a yield stress ( $\sigma_{ys}$ ) of 359 MPa (52 ksi) and an ultimate tensile strength ( $\sigma_u$ ) of 496 MPa (72 ksi). The notches were semi-circular with 3.2 mm radius. The stress concentration factor was 3.18, based on gross-section stress. Typical microstructure perpendicular to the rolling direction and parallel to the nominal crack-growth plane is shown in Figure 2. Typical grain dimensions in the crack-growth directions, 2a and c, were 25  $\mu\text{m}$  and 55  $\mu\text{m}$ , respectively. The dimension in the rolling direction was typically 95  $\mu\text{m}$ . During the rolling process, the inclusion particles (black) are fragmented and form clusters.

The edges of the notches were deburred. The notch surfaces were mechanically polished with the final step using a 0.3  $\mu\text{m}$  diamond paste. Polishing motion was in the tangential direction of the notch to prevent scratches in the through-the-thickness direction. Prior to testing, the notch surfaces were lightly etched to reveal the microstructure and to remove a thin layer of metal which may have been cold worked during polishing. Guide plates lined with teflon sheets were loosely bolted on either side of the specimen to prevent buckling under compressive loads. The gross nominal stress,  $S_{max}$ , was 78.6 MPa (11.4 ksi) at a stress ratio of  $R = -1$  and a cyclic frequency of 15 Hz.

In addition to constant-amplitude loading, tests were also conducted under two variable-amplitude spectra (see Fig. 3). The spectra were chosen to produce fatigue-surface marker bands while having minimal effect on crack-growth rates under the primary loadings ( $S_{max} = 78.6$  MPa;  $R = -1$ ). For the high R-ratio marker load tests, each 2,000 cycles at  $R = -1$  were followed by 2,000 cycles at  $R = 0.5$  with  $S_{max}$  unchanged. The overload marker load tests consisted of 20 cycles at 1.3  $S_{max}$  after every 1,980 cycles at  $R = -1$  with  $S_{min}$  unchanged. These spectra are commonly used in conjunction with large crack studies.

The crack growth along the bore of the notches was monitored using the plastic replica method. While taking replicas, a specimen was loaded to about 0.8  $S_{max}$  so that any crack present would be open. Replicas were made every 5,000 cycles until a crack was observed on the notch surface with a low-power microscope. Some specimens were statically pulled to failure to allow measurement of the fatigue crack shape. Replicas were sputter-coated with a thin layer of Au-Pd alloy and examined in the scanning

electron microscope (SEM). The replicas taken at the highest number of cycles were analyzed first, as the cracks were large and easy to locate. By following, in sequence, from the last replica to the earlier replicas, the grain boundary and inclusion particle patterns could be used to locate the small cracks.

#### ANALYSIS

In the following sections, an approximate stress-intensity factor equation for a surface crack emanating from the center of a semi-circular edge notch is developed. This equation will be used later to compare crack-growth rates measured for small cracks with those measured for large cracks as a function of the stress-intensity factor range. A crack-closure model will be used to predict the crack-growth rates and crack shapes for small cracks growing from the notch using the baseline  $\Delta K$  - rate relationship obtained from large cracks. The closure model will also be used to evaluate the retardation and acceleration effects caused by the two types of marker-load spectra (high R-ratio and 1.3 overload) and to assess the reasonableness of using these spectra for the measurement of small cracks.

#### Stress Intensity Factor Equation

An approximate stress-intensity factor equation for a semi-elliptical surface crack located at the center of a semi-circular notch, as shown in Figure 4, subjected to uniform tension is developed herein. The equation was estimated from known solutions for similar crack problems. The equation is

$$K = S \sqrt{\pi \frac{a}{Q}} F_{sn} \left( \frac{a}{c}, \frac{a}{t}, \frac{r}{t}, \frac{r}{w}, \frac{c}{w}, \phi \right) \quad (1)$$

for  $0.2 < a/c < 2$ ,  $a/t < 1$ ,  $0.5 < r/t < 3$ ,  $(r+c)/w < 0.5$ ,  $r/w = 1/16$ , and  $-\pi/2 < \phi < \pi/2$ . (Note that Eq. (1) is valid for only one value of  $r/w$ ; that is the value used in this particular study.) Equations for  $Q$ , the shape factor, and  $F_{sn}$ , the boundary-correction factor, are given in the Appendix.

#### Crack-Growth Rates for Large Cracks

Center-crack tension specimens were used to obtain crack-growth rate data on large cracks ( $c > 2$  mm) in the 2024-T3 aluminum alloy sheet material used in this study. The data are shown in Figure 5. The solid symbols show  $\Delta K$  - rate data obtained by Hudson [9] at  $R = -1$ . Open symbols show the results of a load-reduction threshold test conducted by E. P. Phillips (NASA Langley Research Center). Instead of using an equation to relate crack-growth rates to  $\Delta K$ , a table-lookup procedure was used in this paper. The primary advantage in using a table is that the baseline data can be described more accurately than with a multi-parameter equation, especially in the transitional region (flat to slant crack growth). The table lookup is shown by the solid lines. The  $\Delta K_{th}$  value was not used herein because the reason for the development of the large crack threshold is unclear at present and the large crack threshold may not apply for small cracks. The baseline relation (solid lines) will be compared with crack-growth rates obtained from small cracks later.

#### Fatigue Crack-Closure Analysis

The analytical closure model developed in Reference 10, and applied to small cracks growing from holes in Reference 11, will be used herein to analyze crack growth under constant-amplitude loading and the two variable-amplitude spectra used to create marker bands.

Constant-Amplitude Loading. - Crack-opening stresses under constant-amplitude loading are a function of stress ratio, stress level, and the constraint factor ( $\alpha$ ) [10]. The constraint factor accounts for three-dimensional stress state effects on tensile yielding at the crack tip. The effective flow stress ( $\sigma_0$ ) under simulated plane-stress conditions was  $\sigma_0$  and under simulated plane-strain conditions was assumed to be  $2.5 \sigma_0$ . Plane-strain conditions were assumed to exist for crack-growth rates less than  $10^{-7}$  m/cycle. This corresponds closely with the rate at transition from flat-to-slant crack growth, as shown in Figure 5. Below this rate, the fatigue surface is flat, indicative of plane-strain conditions (small plastic-zone size to sheet thickness ratio). Above a rate  $7.5 \times 10^{-7}$  m/cycle, plane-stress conditions ( $\alpha = 1$ ) were assumed to exist. Here the crack is oriented at 45 degrees with respect to the load axis and the plastic-zone size is about one-half of the sheet thickness. Between these two rates, the constraint factor is assumed to vary linearly with log rate.

The constant-amplitude test results from Hudson [9] at various R-ratios ( $-1 < R < 0.7$ ) and Phillips' threshold test ( $R = -1$ ) were used to develop a relationship between the effective stress-intensity factor,  $\Delta K_{eff}$ , and crack-growth rate. The effective stress-intensity factor [12] is given by

$$\Delta K_{\text{eff}} = \left( \frac{S_{\text{max}} - S_0}{S_{\text{max}} - S_{\text{min}}} \right) \Delta K \quad (2)$$

As previously mentioned, a table-lookup procedure was used in this paper. The crack-growth table is

$\Delta K_{\text{eff}}$ MPa-m <sup>1/2</sup>	$\frac{dc}{dN}$ m/cycle
1.65	2.54E-10
2.75	2.54E-09
4.29	7.62E-09
5.71	2.54E-08
9.89	2.54E-07
16.5	2.29E-06
29.7	2.54E-05

The rates were selected so that straight lines between each adjacent data point would describe the  $\Delta K_{\text{eff}}$  - rate data using a visual fit, like that shown by the solid lines in Figure 5.

**Overload Marker Loading.**- The calculated crack-opening stresses normalized by the flow stress are shown in Figure 6 as a function of crack depth to specimen width ratio for the overload marker loading. The arrows at the top of the figure indicate the crack lengths over which the primary loading ( $S_{\text{max}}/\sigma_0 = 0.18$ ) and the secondary loading ( $S_{\text{max}}/\sigma_0 = 0.23$ ) were applied. The solid curve shows the calculated  $S_0$  values for overload marker loading and the dashed curve shows the  $S_0$  values under constant amplitude loading. Under the marker loading,  $S_0$  takes a sudden drop when the crack-tip region blunts due to the overload. Because  $S_0$  values are lower than the dashed curve when the primary loading is resumed, crack-growth rates are accelerated. As the crack grows into the overload plastic zone, the  $S_0$  values rapidly increase until they reach a maximum value at about one half of the overload plastic zone size. This is the point of minimum crack-growth rate. The  $S_0$  values then drop and approach the constant-amplitude crack-opening stress (dashed curve). The retardation effects ( $S_0$  greater than the dashed curve) are nearly eliminated when the crack has grown about one overload plastic-zone size. The process is repeated at the next overload. In the case of the 1.3-overload, the acceleration effects and retardation effects nearly cancel each other. For each 1980-cycle interval at the primary loading, the average calculated crack-growth rate is about 10 percent less than that for the constant-amplitude loading. Thus, according to the closure model, this overload marker spectrum appears to be a reasonable technique for studying small cracks.

**High R-Ratio Marker Loading.**- The calculated crack-opening stresses normalized by the flow stress are shown in Figure 7 as a function of crack depth to specimen width ratio for the high R-ratio marker loading. Again, the arrows at the top of the figure indicate the crack lengths over which the primary loading ( $R = -1$ ) and the high R-ratio loading ( $R = 0.5$ ) were applied. The maximum stress level was held constant at  $S_{\text{max}}/\sigma_0 = 0.18$ . The solid curve shows the calculated  $S_0$  values under high R-ratio marker loading. The dashed curve shows the constant amplitude results. During the high R-ratio loading, the crack-tip region was fully open. These results show that crack-growth retardation should occur when the primary loading is resumed just after the application of the  $R = 0.5$  loading. The  $S_0$  values very quickly decrease and approach the constant-amplitude results during the primary loading. Thus, for each 2000-cycle interval at the primary loading, the average calculated crack-growth rate is only about 5 percent less than the constant-amplitude value. This spectrum, too, should be useful for studying small cracks.

## RESULTS AND DISCUSSION

Typical fatigue surfaces for constant-amplitude loading and for each of the two types of marker-band loading are shown in Figure 8. In each case, cracks initiated at one or both notches along the bore of the notch rather than at the corners. Marker bands formed at the high R-ratio are visible as bright bands on the fatigue surface for the large through-the-thickness cracks (see Fig. 8(b)). In contrast, the overload cycles marked the surface with dark bands, Figure 8(c), which became more prominent toward the specimen edge in the regions of plane stress. Examination of the marker bands at high magnification in the SEM showed that the darker regions in Figures 8(b) and 8(c) contained more oxide debris and dimpled rupture (and less faceted fracture) than the neighboring lighter regions. These rough features tend to diffuse light making the region appear darker.

For the through cracks ( $c > 3$  mm), fatigue striations cannot be resolved over most of the fatigue surface because it is quite rough with dimpled rupture at inclusion particles. In the areas of smooth, faceted fracture, striations can be resolved with the SEM. Figure 9 shows such regions for an overload marker specimen and a high R-ratio marker specimen. The striations resulting from 20 cycles at  $1.3 S_{max}$  can be seen at the center of Figure 9(a). Figure 9(b) shows the boundary between crack growth under  $R = 0.5$  and  $-1$  loading. In the  $R = -1$  region, note the change in the orientation of the striations at the grain boundary. The striations on the high R-ratio portion of the fatigue surface are much more faint. The fatigue surface created at the  $R = 0.5$  loading is not as heavily deformed as it is for  $R = -1$  loading and, hence, the dark, rumpled portion of the striation does not form.

In the region of primary interest, that of a small crack less than 1 mm in length, the fatigue surface was not perceptively altered by the relatively mild marker loads. The lack of surface markings prevented measurement of small crack growth. It seemed unwise to resort to a more severe marker-load spectra which would produce marker bands during early crack growth. Data reported by Forsyth and Powell [8] showed that they were able to monitor crack growth for crack lengths down to  $10 \mu\text{m}$  using marker loads. However, they found crack growth rates to be only one-eighth of the constant-amplitude test rate in the  $R = 0.14$  low level blocks of 100 cycles, after applying high level blocks of 100 cycles at  $1.3 S_{max}$  with  $R = 0.3$ . Furthermore, they found that retardation effects were even more pronounced if the number of cycles in the low level blocks was increased to 2,000 cycles.

Figure 10(a) shows a typical fatigue crack initiation area created under constant-amplitude loading. The fatigue surface is predominantly faceted with river markings radiating from the region of initiation. There is some dimpled rupture, especially at inclusion particles. No striations could be resolved at this crack size. Of interest is the long narrow dimple feature at the region of initiation shown in Figure 10(b), an enlargement of Figure 10(a). Inclusion particles can be seen near the tip of the groove. The crack appears to have initiated from a defect caused by the separation of matrix material from an inclusion cluster. At this stress level ( $S_{max} = 78.6$  MPa), this type of initiation was common.

In Figure 11, the region of crack initiation on another constant-amplitude specimen is shown. The specimen was tilted 45 degrees from the load axis so that both the fatigue surface and notch surface are visible. Pits on the notch surface show where inclusion particles were removed from a large cluster by the polishing and etching process. An elongated dimple is present on the fatigue surface at the point of initiation. Here again, the crack nucleated by separation of matrix material from a cluster of inclusion particles. The crack exhibited Stage I growth through the neighboring surface grains along a plane of high shear stress (50 to 55 degrees from the load axis). Stage II crack growth began along the normal plane at a grain boundary. From the limited data available, it seems probable that the presence of large grains properly oriented for growth along a plane of high shear stress on either side of a large inclusion cluster is a most favorable condition for crack initiation.

Figure 12 shows a portion of a replica taken from the specimen shown in Figure 11. The crack length (2a) is about  $250 \mu\text{m}$ . Note that the replica is a mirror image of the notch surface. Pits on the notch surface appear as protrusions on the replica. Irregular surfaces emit more secondary electrons and, hence, are of higher intensity (light) than the smooth background (dark). A ridge is formed along the opened crack producing a bright trace of the crack pattern. Grain boundaries and polishing scratches (generally vertical) are also visible.

Figure 13 shows a replica of another notch surface where a crack has initiated at an inclusion cluster. The crack length (2a) is  $27 \mu\text{m}$  demonstrating the resolution obtainable using this method. In this study, data have been taken on crack lengths (2a) as small  $8 \mu\text{m}$  and as large as 1 mm (the upper limit is dictated by the specimen thickness). The length measurement was always taken as the projection on a plane perpendicular to the loading axis even though locally the crack might grow in an irregular pattern.

Crack initiation, in general, occurred at inclusion clusters and within the center half of the specimen thickness. The distribution of initiation sites along the bore of the notch is plotted in Figure 14. For the small cracks considered in the present work, modeling the crack as growing from a defect along the specimen centerline is a good assumption. Examination of the microstructure across the specimen thickness showed that the grain structure was uniform whereas the occurrence of inclusion clusters were less probable toward the specimen surfaces.

Figure 15 shows typical crack length measurements as a function of fatigue cycles taken from replicas of one crack. The slope of the curve is steep initially, then decreases to a minimum rate at a crack length (a) equal to about two grain diameters ( $50 \mu\text{m}$ ). This corresponds to about one grain diameter in the crack depth (c) direction. During further crack growth, the rate again increased. The crack length at which the minimum crack-growth rate occurs suggests that the presence of grain boundaries may depress the crack-growth rate. For large cracks, the crack front perimeter is much larger than the grain size and a more homogeneous material behavior may occur. Crack-growth rates and stress-intensity factor ranges were calculated from the replica data.

To calculate the stress-intensity factor range, the crack dimensions  $a$  and  $c$  must be known. To gain information about the growth of the crack in the depth direction ( $c$ ), some specimens were fatigue cycled to a specified number of cycles and then statically pulled to failure. An SEM photomicrograph of one of these specimens is shown in Figure 16. The initiation site at the notch edge is indicated by an arrow. The boundary between the dark region of primarily faceted fracture displaying river markings and the surrounding lighter region of dimpled rupture indicates the surface-crack shape. In Figure 16, the surface crack was nearly semi-circular ( $c/a$  was about unity). Figure 17 shows the variation of  $c/a$  with crack size ( $a/t$ ) for both naturally initiated cracks and those growing from a small machined starter notch. For both initial conditions, the cracks tended to grow more along the bore of the notch than away from the notch ( $c/a < 1$ ). At breakthrough ( $a/t = 1$ ), the  $c/a$  ratio was estimated to be about 0.7.

The curves in Figure 17 are predicted crack shapes using Eq. (1), evaluated at  $\phi = 0$  (point where crack intersects notch surface) and  $\pi/2$  (maximum depth point), and the baseline crack-growth rate relationship obtained for large cracks. The solid curve is predicted from an initial crack size of  $a_0 = 5 \mu\text{m}$  and of  $c_0 = 20 \mu\text{m}$ . This initial crack shape and size is about the same shape and size of the inclusion particle cluster shown in Figure 11. The dashed curve is predicted from an initial machined notch ( $a_0 = 0.127 \text{ mm}$ ;  $c_0 = 0.254 \text{ mm}$ ). These two predictions coincide for  $a/t$  ratios greater than 0.3. The predictions agree well with the experimental data.

Figure 18 shows a comparison of crack-growth rates against  $\Delta K$  for small and large cracks. To compare the small crack and large crack data, the rate  $da/dN$  is assumed to be equivalent to  $dc/dN$  for the same  $\Delta K$  value. The small cracks are growing in the  $a$ -direction, while the large cracks are growing in the  $c$ -direction. The solid lines show the  $\Delta K$  - rate relation for large cracks and the dashed-dot line shows  $\Delta K_{th}$  measured on large cracks (see Fig. 5). The crack-growth rates (symbols) measured for small cracks were faster than those measured for large cracks at the same  $\Delta K$  level. Small cracks also grew at  $\Delta K$  values below  $\Delta K_{th}$ . The  $\Delta K$  values for the small cracks were calculated using the predicted crack shapes for a crack growing from a natural defect as shown in Figure 17.

The dashed curve in Figure 18 is predicted from the closure model. The initial surface crack depth was assumed to be  $20 \mu\text{m}$  and the crack length ( $2a$ ) was assumed to be  $10 \mu\text{m}$ . This initial crack size was like the inclusion cluster shown in Figure 11. The high predicted rate at the lowest  $\Delta K$  value was due to the low initial crack-opening stress ( $S_0 = S_{min}$ ) and, hence, a high effective stress-intensity factor range ( $\Delta K_{eff}$ ). As the crack grew,  $S_0$  increased rapidly causing  $\Delta K_{eff}$  to decrease while  $\Delta K$  increased and, consequently, the crack-growth rate dropped. As the crack-opening stress began to stabilize, the  $\Delta K_{eff}$  values and the crack-growth rates began to increase, eventually blending into the large crack data.

#### CONCLUSIONS

1. The high R-ratio and overload marker loadings used in this study could not be used to monitor the growth of small cracks (less than about 2 mm in length) under constant-amplitude loading.
2. Surface replicas, although time consuming, could be used to measure the growth of small cracks ( $10 \mu\text{m}$  and greater) from material surface defects.
3. Experimental data showed that small cracks grew at stress-intensity factor ranges substantially less than the threshold stress-intensity factor range obtained from large cracks.
4. Cracks initiated at inclusion clusters along the bore of the notch, typically those with a depth to length ( $c/a$ ) ratio of about four.
5. At  $S_{max} = 78.6 \text{ MPa}$  and a stress ratio ( $R$ ) of  $-1$ , minimum crack-growth rates for small cracks tended to occur between one and two grain diameters from the initiation site along the notch surface and one grain diameter away from the notch surface.
6. The crack shape for the small cracks was nearly semi-circular ( $c/a$  about 1) and became more shallow ( $c/a$  approaches 0.7) as the crack length approached the specimen thickness.
7. The crack-closure model offered a plausible explanation of why small cracks grow faster than large cracks at the same stress-intensity factor range.

#### APPENDIX A--APPROXIMATE STRESS-INTENSITY FACTORS FOR A SURFACE CRACK LOCATED ALONG THE BORE OF A SEMI-CIRCULAR NOTCH

An approximate stress-intensity factor equation for a semi-elliptical surface crack located at the center of a semi-circular notch, as shown in Figure 19(a), subjected to uniform remote tension is developed herein. The equation was obtained by assuming that the ratio of stress-intensity factors for a surface crack at an edge notch (Fig. 19(a)) to that for surface cracks at a central hole (Fig. 19(b)) was the same as the ratio of

stress-intensity factors for a through crack at an edge notch (Fig. 19(c)) to that for through cracks at a central hole (Fig. 19(d)). In mathematical form

$$K_{sn} = K_{sh} \left( \frac{K_e}{K_b} \right) \quad (3)$$

An equation for the stress-intensity factors for semi-elliptical surface cracks at a central hole ( $K_{sh}$ ) was obtained from References 13 and 14.  $K_b$  is the stress-intensity factor for through cracks at a central hole [15] and  $K_e$  is the stress-intensity factor for a through crack at a semi-circular edge notch (Paul Tan, NASA Langley Research Center).

The stress-intensity factor equation for a semi-elliptical surface crack located at the center of a semi-circular edge notch, Figure 19(a), subjected to remote uniform stress is

$$K = S \sqrt{\pi \frac{a}{Q}} F_{sn} \quad (4)$$

for  $0.2 < a/c < 2$ ,  $a/t < 1$ ,  $0.5 < r/t < 3$ ,  $(r+c)/w < 0.5$ ,  $r/w = 1/16$ , and  $-\pi/2 < \phi < \pi/2$ . (Note that here  $t$  is defined as one-half of the full plate thickness.) The shape factor,  $Q$ , is given by

$$Q = 1 + 1.464 \left( \frac{a}{c} \right)^{1.65} \quad \text{for } \frac{a}{c} < 1 \quad (5a)$$

$$Q = 1 + 1.464 \left( \frac{c}{a} \right)^{1.65} \quad \text{for } \frac{a}{c} > 1 \quad (5b)$$

and

$$F_{sn} = \left[ M_1 + M_2 \left( \frac{a}{t} \right)^2 + M_3 \left( \frac{a}{t} \right)^4 \right] g_1 g_2 g_3 g_4 f_\phi f_w \quad (6)$$

For  $a/c < 1$ :

$$M_1 = 1 \quad (7)$$

$$M_2 = \frac{0.05}{0.11 + \left( \frac{a}{c} \right)^{3/2}} \quad (8)$$

$$M_3 = \frac{0.29}{0.23 + \left( \frac{a}{c} \right)^{3/2}} \quad (9)$$

$$g_1 = 1 - \frac{\left( \frac{a}{t} \right)^4 \left( 2.6 - 2 \frac{a}{t} \right)^{1/2}}{1 + 4 \left( \frac{a}{c} \right)} \cos \phi \quad (10)$$

$$g_2 = \frac{1 + 0.358\lambda + 1.425\lambda^2 - 1.578\lambda^3 + 2.156\lambda^4}{1 + 0.08\lambda^2} \quad (11)$$

$$\lambda = \frac{1}{1 + \frac{c}{t} \cos(0.9\phi)} \quad (12)$$

$$g_3 = 1 + 0.1(1 - \cos \phi)^2 \left( 1 - \frac{a}{t} \right)^{10} \quad (13)$$

$$g_4 = 1.14 - \frac{0.1}{\sqrt{1 + \frac{c}{r}}} \quad (14)$$

The finite-width correction,  $f_w$ , was

$$f_w = 1 - 0.2\gamma + 9.4\gamma^2 - 19.4\gamma^3 + 27.1\gamma^4 \quad (15)$$

where

$$\gamma = (c + 1)w$$

The function  $f_\phi$  is given by

$$f_\phi = \left[ \left( \frac{a}{c} \right)^2 \cos^2 \phi + \sin^2 \phi \right]^{1/4} \quad (16)$$

For  $a/c \gg 1$ :

$$M_1 = \sqrt{\frac{c}{a}} \quad (17)$$

The functions  $M_2$ ,  $M_3$ ,  $g_1$ ,  $g_2$ ,  $g_3$ ,  $g_4$ , and  $f_w$  are given by Eqs. (8) through (15), respectively, and  $f_\phi$  is given by

$$f_\phi = \left[ \left( \frac{c}{a} \right)^2 \sin^2 \phi + \cos^2 \phi \right]^{1/4} \quad (18)$$

#### REFERENCES

1. Pearson, S.: Initiation of Fatigue Cracks in Commercial Aluminum Alloys and the Subsequent Propagation of Very Short Cracks. Engineering Fracture Mechanics, Vol. 7, No. 2, 1975, pp. 235-247.
2. El Haddad, M. H.: A Study of the Growth of Short Fatigue Cracks Based on Fracture Mechanics. Ph.D. Thesis, University of Waterloo, Waterloo, Ontario, Canada, 1978.
3. Kung, C. Y.; and Fine, M. E.: Fatigue Crack Initiation and Microcrack Growth in 2024-T4 and 2124-T4 Aluminum Alloys. Metallurgical Transactions A, Vol. 10A, May 1979, pp. 603-610.
4. Taylor, D.; and Knott, J. F.: Fatigue Crack Propagation Behavior of Short Cracks--The Effects of Microstructure. Fatigue of Engineering Materials and Structures, Vol. 4, No. 2, 1981, pp. 147-155.
5. Lankford, J.: The Growth of Small Fatigue Cracks in 7075-T6 Aluminum. Fatigue of Engineering Materials and Structures, Vol. 5, No. 3, 1982, pp. 233-248.
6. Lankford, J.: The Effect of Environment on the Growth of Small Fatigue Cracks. Fatigue of Engineering Materials and Structures, Vol. 6, No. 1, pp. 15-31, 1983.
7. Sigler, D.; Montpetit, M. C.; and Haworth, W. L.: Metallography of Fatigue Crack Initiation in an Overaged High Strength Aluminum Alloy. Metallurgical Transactions A, Vol. 14A, May 1983, pp. 931-983.
8. Forsyth, P. J. E.; and Powell, P. M.: Fatigue Crack Growth Rates for Very Short Cracks Developing at Fastener Holes in 7075 and 7010 Aluminum Alloys Journal of Materials Science, Vol. 18, 1983, pp. 1852-1862.
9. Hudson, C. Michael: Effect of Stress Ratio on Fatigue-Crack Growth in 7075-T6 and 2024-T3 Aluminum-Alloy Specimens. NASA TND-5390, 1969.
10. Newman, J. C., Jr.: A Crack-Closure Model for Predicting Fatigue Crack Growth Under Aircraft Spectrum Loading. Methods and Models for Predicting Fatigue Crack Growth Under Random Loading, J. B. Chang and C. M. Hudson, eds., American Society for Testing and Materials, ASTM STP 748, 1981, pp. 53-84.

11. Newman, J. C., Jr.: A Nonlinear Fracture Mechanics Approach to the Growth of Small Cracks. Behavior of Short Cracks in Airframe Components, AGARD Conference Proceedings No. 328, 1982, pp. 6.1-6.26.
12. Elber, W.: The Significance of Fatigue Crack Closure. ASTM STP-486, American Society for Testing and Materials, 1971, pp. 230-242.
13. Newman, J. C., Jr.; and Raju, I. S.: Stress-Intensity Factor Equations for Cracks in Three-Dimensional Finite Bodies, ASTM STP-791, American Society for Testing and Materials, 1983, pp. I-238-I-265.
14. Newman, J. C., Jr.; and Raju, I. S.: Stress-Intensity Factor Equations for Cracks in Three-Dimensional Finite Bodies Subjected to Tension and Bending Loads. NASA TM-85793, National Aeronautics and Space Administration, April 1984.
15. Bowie, O. L.: Analysis of an Infinite Plate Containing Radial Cracks Originating at the Boundary of an Internal Circular Hole. Journal of Mathematics and Physics, Vol. XXXV, No. 1, 1956, pp. 60-71.

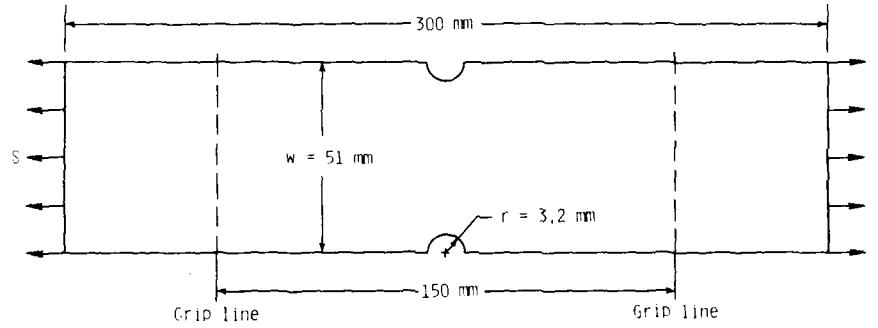


Figure 1.- Double-edge notched tension specimen.

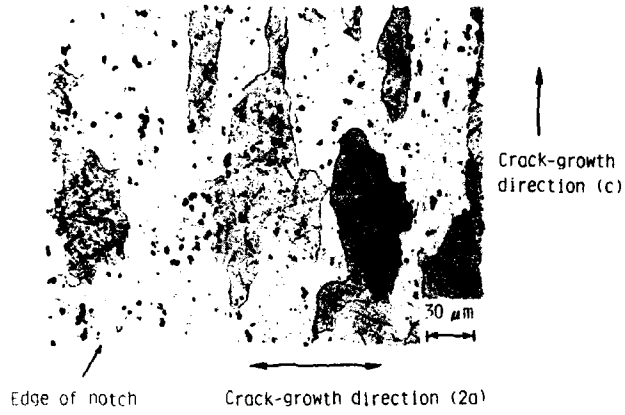
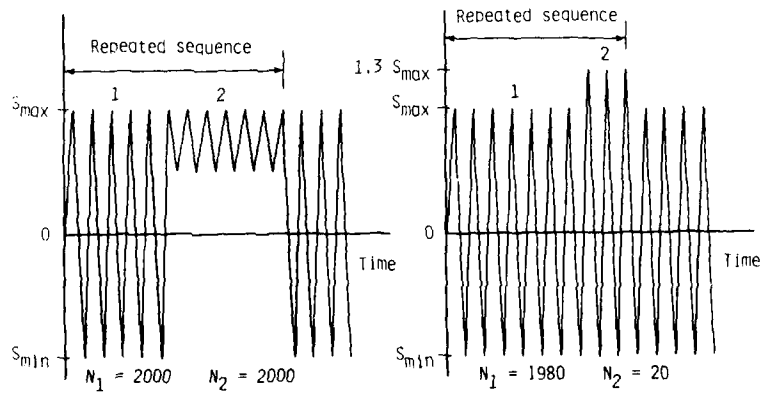


Figure 2.- Photomicrograph of etched crack-surface plane.



(a) High R-ratio marker loads. (b) Overload marker loads.

Figure 3.- Marker load sequences used in small crack growth study.

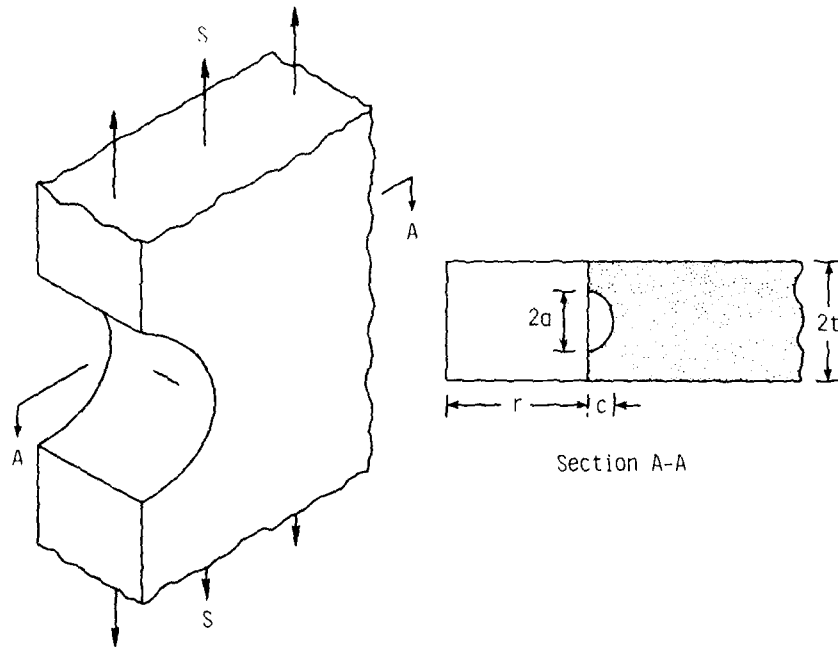


Figure 4.- Surface crack located at the center of a semi-circular notch.

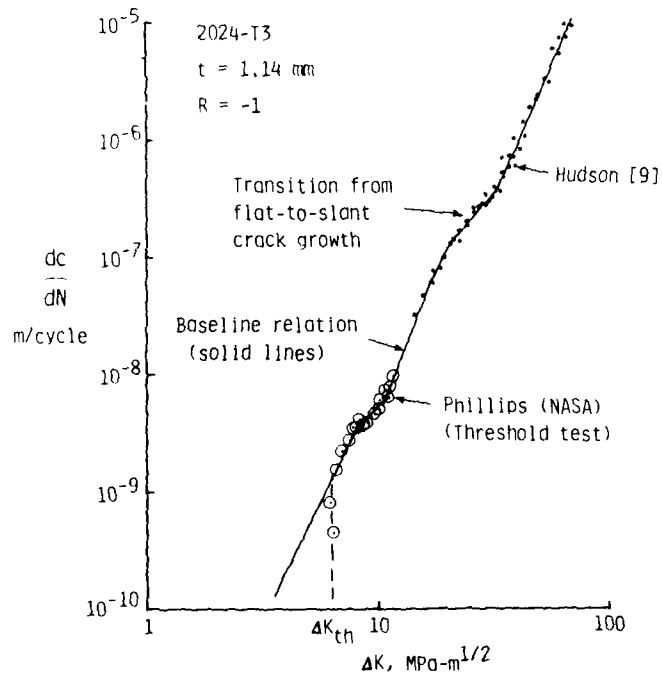


Figure 5.- Stress-intensity factor range against crack-growth rate for large through cracks ( $c$  greater than 2 mm).

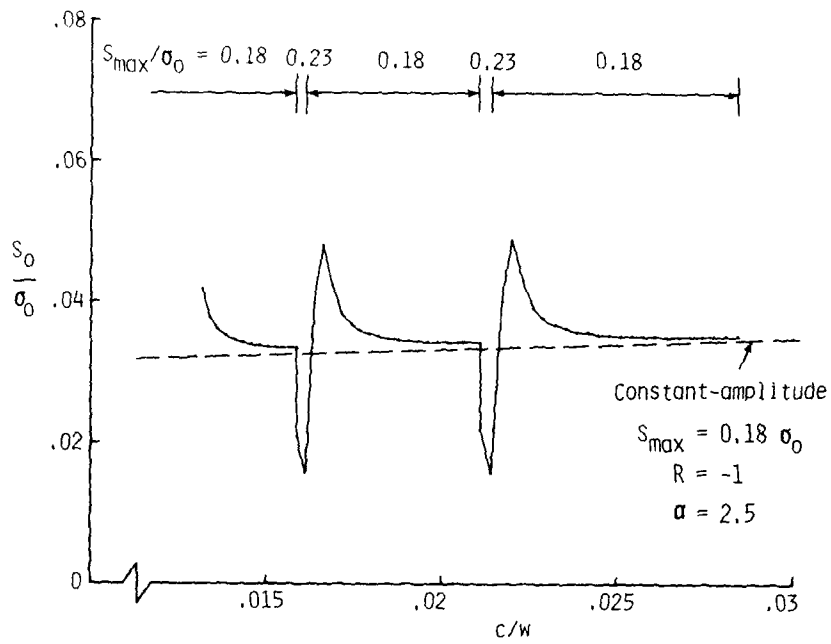


Figure 6.- Calculated crack-opening stresses under overload marker loading.

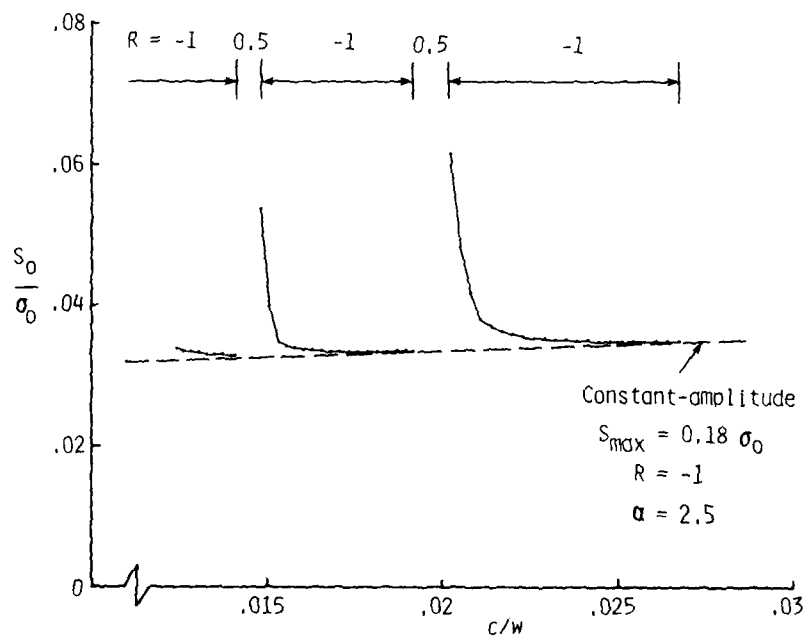


Figure 7.- Calculated crack-opening stresses under high R-ratio marker loading.

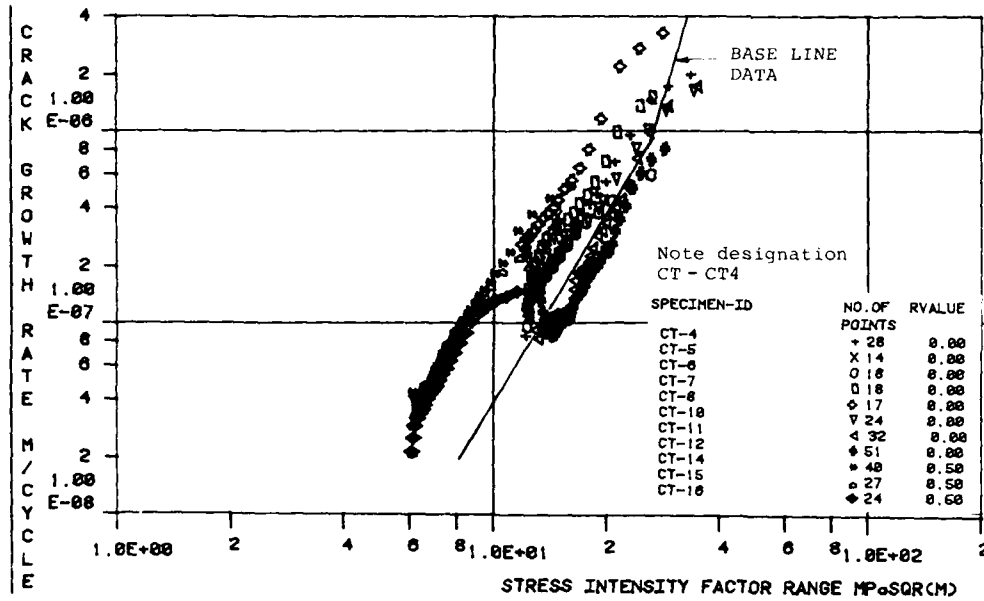


Fig. 4 Crack growth rate in 4 mm CT specimen  
Note: Designation CT - CT4

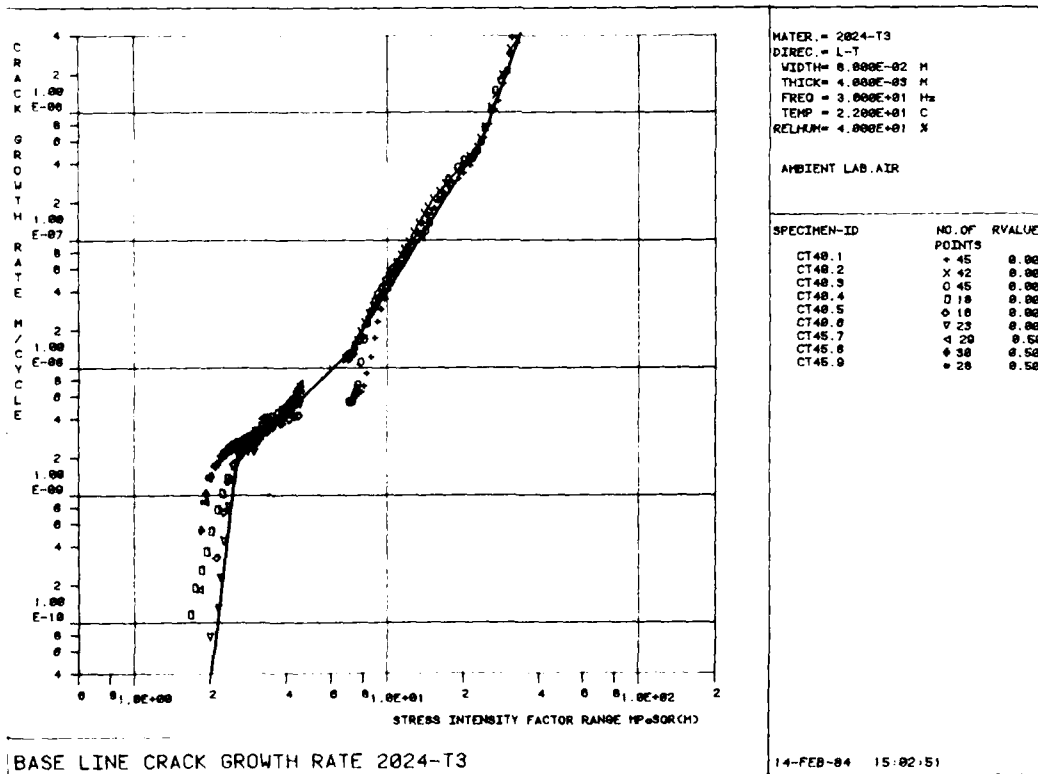


Fig. 5 Base line crack growth rate for sheet material 2024-T3

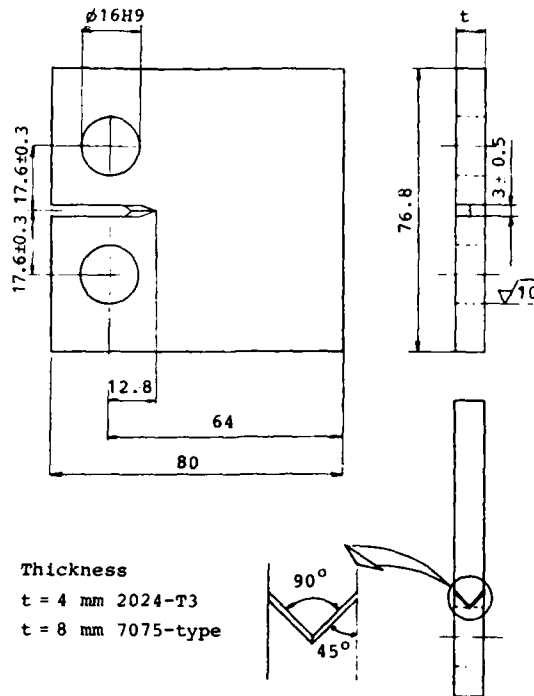


Fig. 1 Dimensions of CT-specimen used

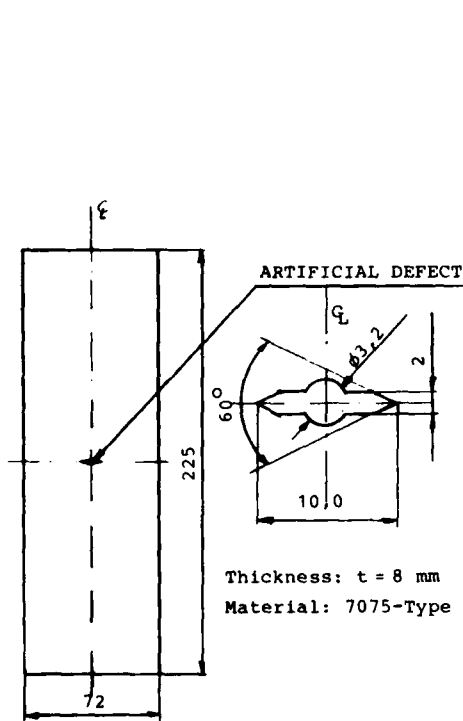


Fig. 2 Dimensions of 8 mm thick CC-specimen

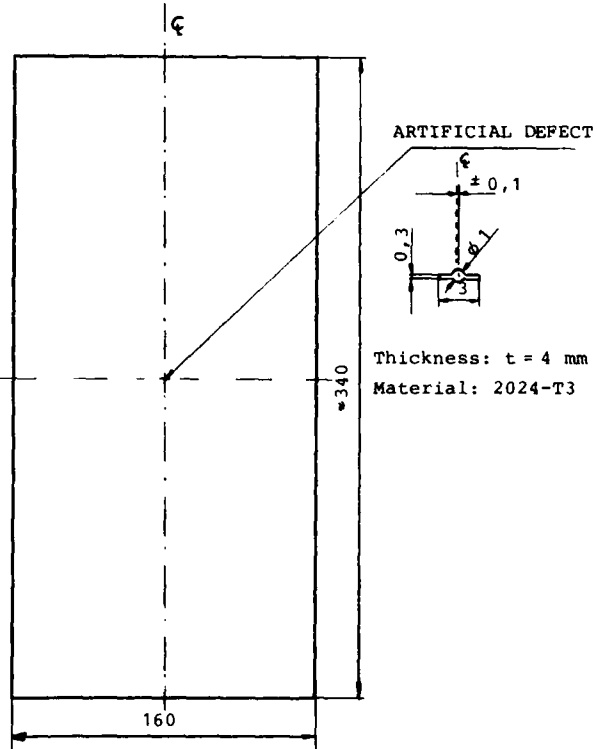


Fig. 3 Dimensions of 4 mm thick CC-specimen

SPECIMEN ID	SPECTRUM	MARKER LOAD PARAMETERS				EXPERIMENTAL RESULTS				
		$P_{max}$ [kN]	$\frac{P_{max,M}}{P_{max}}$	$R_M$	n [kcycles]	N [kflights]	FATIGUE LIFE $N_f$ [kflights]	NO OF MARKER BANDS	DETECT-ABILITY OF MARKER BANDS	MARKER BAND WIDTH $\Delta X$ [mm]
CC01	L1E5	51.0	1.0	0.9	5.0	0.2	34 794	173	2	-
CC02	"	"	"	"	10.0	"	14.788	73	3	0.34
CC03	"	"	"	"	5.0	1.0	11.550	11	2	-
CC04	"	"	"	"	10.0	"	9.613	9	2	-
CC05	L1E5	51.0	1.0	0.85	10.0	0.2	7.102	35	4	7.1
CC06	"	"	"	"	"	"	8.513	42	4	6.5
CC07	"	"	"	"	"	1.0	9.021	9	5	7.1
CC08	"	"	"	"	"	"	9.999	9	5	5.1
CC09	L1E5	51.0	0.69	0.75	10.0	0.2	6.024	30	5	8.0
CC10	"	"	"	"	"	"	6.810	34	4	8.2
CC11	"	"	"	"	"	1.0	6.725	6	5	0.34
CC12	"	"	"	"	"	"	5.958	5	5	5.0
CC13	L1E5	51.0	0.49	0.50	10.0	0.2	10.822	54	3	13.8
CC14	"	"	"	"	"	"	6.620	33	4	11.5
CC15	"	"	0.29	"	"	1.0	7.169	7	2	-
CC16	"	"	0.49	"	"	"	8.581	8	5	9.1
CC17	L1E5	51.0	-	-	-	-	8.902	-	-	-
CC18	"	"	-	-	-	-	6.995	-	-	-
CC19	"	"	0.24	0.55	10.0	1.0	17.540	17	2	-
CC20	"	"	-	-	-	-	12.281	-	-	-
C4B-10-1	TWIST	124.8	0.36	0.74	5.0	4.0	46.850	11	2	-
C4B-10-2	"	"	"	"	"	"	58.935	14	2	-
C4B-11-1	"	"	-	-	-	-	84.500	-	-	-
C4B-11-2	"	"	-	-	-	-	82.935	-	-	-
C4B-9-1	L25E2	99.84	0.78	0.85	5.0	79.224*	1702.500*	21	2	-
C4B-9-2	"	"	"	"	"	"	1773.640*	22	2	-
C4B-5-1	"	"	-	-	-	-	1713.460*	-	-	-
C4B-5-2	"	"	-	-	-	-	1492.550*	-	-	-

\* kcycles

Table 3 Experimental results for CC-specimens

SPECI- MEN ID	CONSTANT AMPLITUDE DATA		MARKER LOAD PARAMETERS					EXPERIMENTAL RESULTS					
	P <sub>max</sub> [kN]	R	$\frac{P_{max,M}}{P_{max}}$	R <sub>M</sub>	n [kcycles]	N [kcycles]	FATIGUE LIFE N <sub>f</sub> [kcycles]	NO OF MARKER BANDS	DETECT- ABILITY OF MARKER BANDS	SECOND LAST ΔK [MPa√m]	LAST ΔK [MPa√m]	SECOND LAST m <sub>w</sub> [mm]	LAST m <sub>w</sub> [mm]
CT8-1	3.57	0.0	0.7	0.45	5.0	5.0	97.372	19	4	7.0	9.7	0.22	0.88
CT8-2	"	"	"	"	"	"	65.000	13	5	6.4	21.3	0.35	2.27
CT8-3	"	"	"	"	"	2.0	55.403	27	4	7.8	9.3	0.45	0.84
CT8-4	"	"	"	"	"	"	44.000	22	5	8.2	10.8	0.70	1.26
CT8-5	3.57	0.0	1.0	0.70	0.0	5.0	66.033	13	5	5.8	9.1	0.54	1.51
CT8-6	"	"	"	"	5.0	"	65.000	13	3	5.9	11.9	0.22	1.30
CT8-7	"	"	"	"	"	2.0	64.586	32	4	6.9	9.4	0.28	0.96
CT8-8	"	"	"	"	"	"	54.969	27	4	7.0	9.3	0.34	0.76
CT8-9	3.57	0.0	1.3	0.80	5.0	5.0	74.687	14	3	4.5	5.7	0.09	0.24
CT8-10	"	"	"	"	"	"	114.000	22	2	4.8	5.7	0.10	0.32
CT8-11	"	"	"	"	"	2.0	64.716	32	4	5.7	6.6	0.15	0.26
CT8-12	"	"	"	"	"	"	80.000	40	4	5.9	7.3	0.21	0.30
CT8-13	3.57	0.5	1.0	0.70	5.0	5.0	319.484	63	4	6.5	7.4	0.63	0.74
CT8-14	"	"	"	"	"	"	292.575	58	4	7.9	10.0	0.64	1.20
CT8-15	"	"	"	"	"	5.0	259.059	17	5	1 5.3	6.6	0.23	0.48
CT8-16	"	"	"	"	"	"	345.030	23	5	5.2	6.2	0.16	0.53

Table 2 Experimental results for CT-specimens of 8 mm thickness and 7075 type of material

SPECI- MEN ID	CONSTANT AMPLITUDE DATA			MARKER LOAD PARAMETERS					EXPERIMENTAL RESULTS				
	P <sub>max</sub> [kN]	R	$\frac{P_{max,N}}{P_{max}}$	R <sub>M</sub>	n [kcycles]	N [kcycles]	FATIGUE LIFE N <sub>f</sub> [kcycles]	NO OF MARKER BANDS	DETECT- ABILITY OF MARKER BANDS	SECOND ΔK [MPa√m]	LAST m <sub>w</sub> [mm]	LAST ΔK [MPa√m]	LAST m <sub>w</sub> [mm]
CT4-1	2.60	0.0	0.69	0.55	5.0	5.0	56.476	11	1	-	-	-	-
CT4-2	"	"	"	"	10.0	"	21.863	4	1	-	-	-	-
CT4-3	"	"	"	"	"	2.0	*	-	-	-	-	-	-
CT4-4	"	"	"	"	"	"	60.694	30	3	-	10.5	0.34	-
CT4-5	2.60	0.0	1.0	0.80	10.0	5.0	22.059	4	2	-	-	-	-
CT4-6	"	"	"	"	"	"	75.045	15	2	-	-	-	-
CT4-7	"	"	"	"	"	2.0	40.479	20	3	-	-	5.9	0.35
CT4-8	"	"	"	"	"	"	29.601	14	2	-	-	3.8	0.08
CT4-9	2.60	0.0	1.3	0.87	10.0	5.0	15.000**	-	-	-	-	-	-
CT4-10	"	"	"	"	"	"	65.000	12	3	-	-	3.5	0.35
CT4-11	"	"	"	"	"	2.0	106.838	53	4	-	-	6.1	0.47
CT4-12	"	"	"	"	"	"	100.000	50	4	-	-	5.1	0.28
CT4-13	2.60	0.5	1.0	0.80	10.0	5.0	215.000**	-	-	-	-	-	-
CT4-14	"	"	"	"	"	"	197.272	39	3	-	-	6.9	0.4
CT4-15	"	"	"	"	"	15.0	214.616	14	4	-	-	5.3	0.3
CT4-16	"	"	"	"	"	"	253.421	16	3	-	-	-	-

\* Failure during precracking

\*\* Test stopped due to overload

Table 1 Experimental results for 2024-T3 CT-specimens of 4 mm thickness

crack growth rate for high R-ratios (at the time of testing) resulting in misjudgment of the marker load parameters  $P_{max,M}$  and  $R_M$ . Furthermore, in the case of CT-specimens, a high value of the maximum load  $P_{max}$  causing a shift in crack propagation mode. Finally, in the case of CC-specimens, load spectrum giving rise to coarse striations and lines of arrest which were difficult to separate from marker bands.

The scatter in fatigue lives is very large and thereby no real evidence of interaction effects caused by the marker loads can be recognized, except for the TWIST-loading case. The investigation does however not tell whether this scatter in fatigue life is caused by the marker loads or by material property scatter. Computations indicate that the effects of different marker load parameters may be small.

## REFERENCES

- [1] S.R. Murnane, L.F. Voorhees and O.B. Davenport, Northrop/United States Air Force Application of Failure Prediction to an Operational Aircraft Fracture Mechanics ed. by N. Perrone et al, The University Press of Virginia, 1978
- [2] B. Palmberg, Crack growth rates for two aluminum alloys AA7050-T73651 and 2024-T3 Investigation under progress at FFA, report due June 1984
- [3] B. Palmberg, A compilation of fracture mechanics data for the aluminum alloys 3627-48 and 3633-5 and for steel 1366-4 (In Swedish) FFAP-H-623 (FFA internal memo Dec 1982).
- [4] B. Palmberg, LIFE a computer program for crack growth evaluation. User guide. (FFA internal program manual).

## 5.2 Crack growth rates

The crack growth rates obtained for CT-specimens of 2024-T3 material, Fig 4, show rather large scatter compared to base line data, Fig 5, [2]. Four groups representing 4 different crack growth rates can be identified. The first group consisting of specimens CT4-4, CT4-6 and CT4-10 having a crack growth rate slightly above the base line data. The second group consisting of specimens CT4-5, CT4-7 and CT4-8 produced higher crack growth rates than the first group. The third group represented by specimens CT4-11 and CT4-12 showed initially decreasing crack growth rates with increasing stress intensity factor range. After reaching the lowest crack growth rate (well below the base line data) the growth rate increased with increasing stress intensity range to a rate close to the base line data. Finally, the fourth group represented by the specimens CT4-14, CT4-15 and CT4-16, which were tested using the load ratio  $R = 0.5$ , yielded crack growth rates well above the base line data for  $R = 0$  but close to results obtained for 2 mm thick CC-specimens of the same material tested with the load ratio  $R = 0.5$ , [2].

The constant amplitude testing of 8 mm thick CT-specimens of the 7075 type of material also resulted in rather large scatter in crack growth rates. The results have been plotted in Fig 6. Base line crack growth rates for 15 mm thick CT-specimens have been used for comparison, Fig 7, [3]. The highest crack growth rate was obtained for specimen CT8-4 and the lowest rates were found for specimens CT8-1 and CT8-10. If the two specimens with the lowest crack growth rates are excluded from the comparison the remaining specimens show crack growth rates close to or slightly below the base line data. The four specimens tested with a load ratio of 0.5 show crack growth rates well above the base line data for  $R = 0$  at low stress intensity ranges and approximately equal to the base line data for high stress intensity ranges.

The crack growth rates for the 4 mm thick CC-specimens of 2024-T3 material are shown in Figs 8-9. As can be seen in Fig 8 the differences in crack growth rate for specimens subjected to the Gauss-spectrum with and without marker loads are rather small except at high stress intensity "ranges" (the peak spectrum stress intensity factor is used as reference). Fig 9 shows that the crack growth rate for specimens subjected to the TWIST loading is altered considerably by introduction of marker loads. The characteristic dip in crack growth rate vanish for specimens tested with marker loads.

Crack growth rates for CC-specimens subjected to the LIE5 spectrum are shown in Fig 10. A line showing the mean crack growth rate for the three specimens (CC17, CC18 and CC20) tested without marker loads has been drawn in Fig. 10. The scatter is very large for specimens tested without marker loads and the marker load test results are within the scatter.

## 5.3 Marker band contribution to crack length

Generally, the produced marker bands are very small compared to the crack length. The marker band widths for the last applied marker block have been measured (when possible) and are presented in Tables 1-3 together with corresponding stress intensity ranges (for the 8 mm thick CT-specimens the second last marker bands are presented as well). The measuring accuracy is approximately 0.05 mm which means that the highest crack growth rate during any marker block is less than  $3 \cdot 10^{-7}$  m/cycle. This value is above the limit for producing "striation free" marker bands. However, for most of the marker bands the crack growth rate is well below the limit  $5 \cdot 10^{-8}$  m/cycle.

## 5.4 Predictions obtained by cycle-by-cycle computations

The fatigue life, the marker band width, number of applied marker blocks and total contribution to crack length from marker bands have been computed using the cycle-by-cycle crack growth program LIFE, [4]. The computations were based on the base line crack growth rates which were tabulated and stored in a table. Retardation and crack closure effects were not considered.

The computations indicate that differences in fatigue life should be very small due to different marker load parameters. Also, the contribution to the crack length from marker bands is small except when marker loads are applied immediately before the critical crack length is reached.

## 6 CONCLUSIONS

Marker bands detectable with the aid of an optical stereo microscope were produced in 48 tests where marker loads were applied. In 26 of these tests all marker bands could be detected and in 35 of the tests enough marker bands were detected to draw curves of crack length versus "time" and evaluate crack growth rates. Crack growth rates in specimens having too few detectable marker bands could be evaluated because some crack lengths were measured with a traveling microscope during testing. In the 7075 type of material marker bands were generally easy to detect and a maximum marker load  $P_{max,M} = 0.7 P_{max}$  gave the best results. In the 2024-T3 material marker bands were difficult to detect. The reason for this are assumed to be a poor knowledge of the near threshold

## 4 TEST PROCEDURE

The test procedure involved both constant amplitude testing and spectrum loading. CT-specimens were precracked and subjected to constant amplitude loading interrupted only by marker loads. The loading conditions and the marker load parameters used are shown in the Tables 1 and 2. The two prime variables were the maximum marker load and the periodic interval between marker blocks. The load ratio  $R$ , for the marker loads was determined on bases of the precrack length and the stress intensity threshold value.

It was assumed that different maximum marker loads would create different interaction effects. By using different intervals between marker loads the effects were assumed to be amplified. Thus, creating significantly different crack growth rates and cycles to failure. Also, by varying the periodic interval different contributions to the crack length were expected to arise.

The testing was carried out in a MTS 100 kN servo hydraulic testing machine controlled by a PDP 11/05 mini-computer.

The CC-specimens (2024-T3 material) were subjected to 2 different random loadings. The standard load sequence TWIST (Transport Wing Standard) and a load spectrum, L25E2, based on a Gaussian exceedence distribution were used. Only 4 of these test specimens (two for each load spectrum) were tested using marker loads.

The CC-specimens of 7075 type of material were, after precracking, subjected to a load spectrum called L1E5 representative for the lower wing of a fighter aircraft.

It should be pointed out that all 3 load spectrum used contain both tensional and compressive loads.

The loading conditions and the marker load parameters used are shown in Table 3. As for the CT-specimens the two prime variables were the maximum marker load and the periodic interval between marker blocks.

The CC-testing was carried out in a DOWTY 200 kN servo hydraulic testing machine also controlled by the PDP 05/11 mini-computer.

## 5 TEST RESULTS

5.1 Detectability of marker bands

The detectability of marker bands in the fracture surfaces by means of a stereo microscope has been studied. Five categories are used to classify, in a subjective manner, the detectability.

- 1 No marker bands can be detected at all
- 2 A few marker bands can be detected with difficulty
- 3 Practically all marker bands can be detected
- 4 All marker bands can be detected
- 5 All marker bands are easily detected

The results are presented in Tables 1-3. The specimens made of 2024-T3 material show less detectable marker bands than the specimens made from the 7075 type of material. In the case of CT-specimens this is particular pronounced for long cracks and seems to be caused by a change in crack propagation mode occurring in the 2024-T3 material. In both materials the crack growth started in a plane perpendicular to the plane of loading but in the 4 mm thick sheet material the crack growth shifted into a  $45^\circ$  plane. One reason for the shift in crack propagation mode is believed to be that the selected stress intensity range was 1.46 times larger for the 4 mm thick CT-specimens than for the 8 mm thick CT-specimens compared at the same crack length.

Futhermore, it can be noticed that in the 2024-T3 material marker bands produced by marker loads leading to overloads were the easiest to detect, while marker bands produced by marker loads having  $P_{max,M} < P_{max}$  were easiest detected in the 7075 type of material. For both materials marker bands in the fracture surfaces of CT-specimens subjected to constant amplitude loading with a load ratio  $R = 0.5$  were relatively easy to detect.

In the case of CC-specimens, difficulties in detecting marker bands in the 2024-T3 material were caused by the large number of coarse striations and lines of arrest that occurred in the crack surfaces due to the random loading. For the 7075-type of material marker bands were quite easy to detect particularly those produced by marker loads with load ratios of 0.75 and 0.85. This may be due to the fact that the stress intensity threshold value was known for  $R = 0.7$  and thereby the initial stress intensity range for the marker loads could be calculated with greater accuracy than for the other load ratios.

ON THE USE OF MARKER LOADS FOR FATIGUE CRACK GROWTH MEASUREMENTS

B. Palmberg

The Swedish Aeronautical Research Institute,  
Structures Department  
Box 11021, S-161 11 Bromma, Sweden

Abstract

An investigation of the possibility to use blocks of constant amplitude loading to produce macroscopic marks in the fracture surfaces is presented. The parameters to be selected are the maximum marker load, the marker load ratio, the number of marker load cycles and the periodic interval between marker blocks. An optical stereo microscope is used to detect marker bands in the fracture surface. The parameters are chosen in order to obtain marker bands which appear as striation free when observed through a scanning electron microscope. Marker loads have been added to both constant amplitude and spectrum loading during testing of two aluminum alloys. It has been found that detectable marker bands can be produced and that the interaction effects seems to be small except when TWIST loading spectrum is used.

1 INTRODUCTION

Difficulties in correlating marks in fracture surfaces with events in the load history are normally considerable and increasingly difficult with increasing complexity of the load spectrum. Deliberately introduced marks in fatigue fracture surfaces can, however, be used to obtain information on crack propagation characteristics.

The purpose of the present investigation was to study interaction effects caused by marker loads. Further, the detectability of marker bands by means of an optical stereo microscope in order to find optimum marker load parameters was investigated.

2 METHOD

The method used in this investigation for producing microscopic marks (striation marking) in the fracture surfaces has been suggested in [1]. Blocks of constant amplitude loading are included in the normal load sequence at regular intervals. Four parameters describe these marker blocks:

- 1) Maximum load  $P_{\max, M}$  in a marker load cycle
- 2) The load ratio  $R_M = P_{\min, M} / P_{\max, M}$
- 3) Number of load cycles  $n$ , within a marker block
- 4) Intervals  $N$ , between marker blocks.

Within a marker block the aim is normally to keep the crack growth rate below  $5 \cdot 10^{-8} \text{m/cycle}$ . The size of striations formed at such low rates are considered to be below the resolution limit of a scanning electron microscope (SEM). Thus, marker bands will appear as striation free zones on the fracture surface. However, if marker bands can be detected by means of an optical stereo microscope instead of a SEM the evaluation of crack growth characteristics would be simplified.

A systematic procedure for determining the marker load parameters is suggested. First the marker block interval  $N$  is determined from predictions of crack propagation. Secondly the maximum load  $P_{\max, M}$  is determined on bases of statistical information about the loading. The load ratio  $R_M$  is calculated using the stress intensity factor range  $\Delta K_M$  and the threshold value  $\Delta K_{TH}$ , where  $\Delta K_M$  is evaluated for the smallest crack to be marked and  $\Delta K_{TH} = \Delta K_{TH}(R_M)$ . Finally, the number of load cycles within a marker block is determined, using the crack growth rate for  $\Delta K_M$ , in such a way that the marker band width becomes large enough for detection.

3 TEST SPECIMENS

A total number of 62 test specimens have been manufactured from two different aluminium alloys, 2024-T3 4 mm sheet material and a 7075 type of forging with 0.25% Ag (O. Fuchs AZ74). Compact tension (CT) and centre cracked (CC) test specimens were cut out (LT-direction) from the sheet material. From the forging, a rejected main spar of the Viggen aircraft, 8 mm thick test specimens of the same types as for the sheet material were cut out mainly from the flanges. The dimensions of the 4 different test specimens are shown in Figs 1-3. The crack starter notches in the CC-specimens were made by drilling and electro discharge machining.

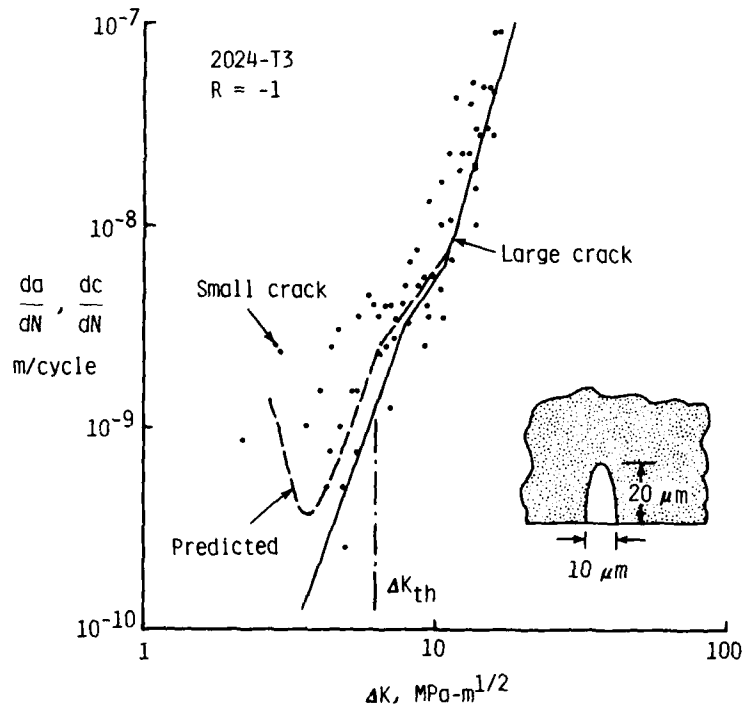


Figure 18.- Stress-intensity factor range against crack-growth rate for small and large cracks.

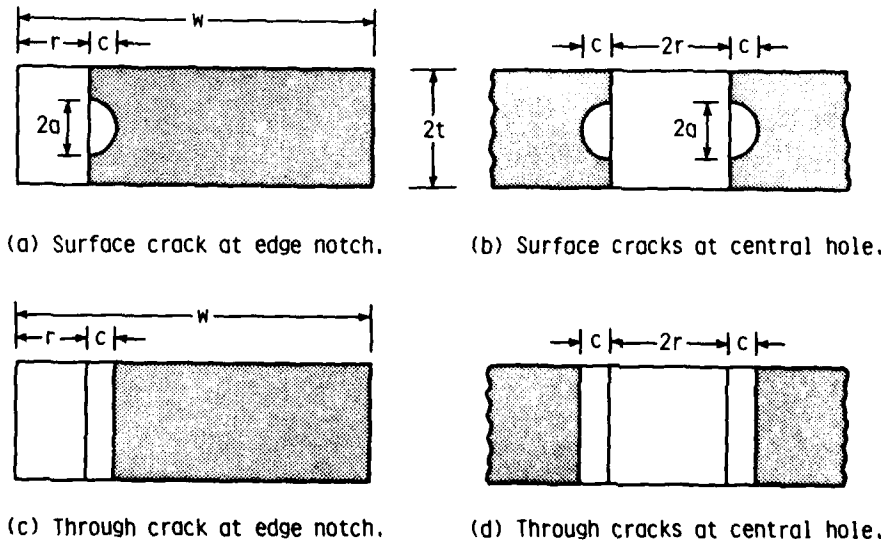


Figure 19.- Crack configurations used to estimate stress-intensity factors for surface crack located at the center of a semicircular edge notch.

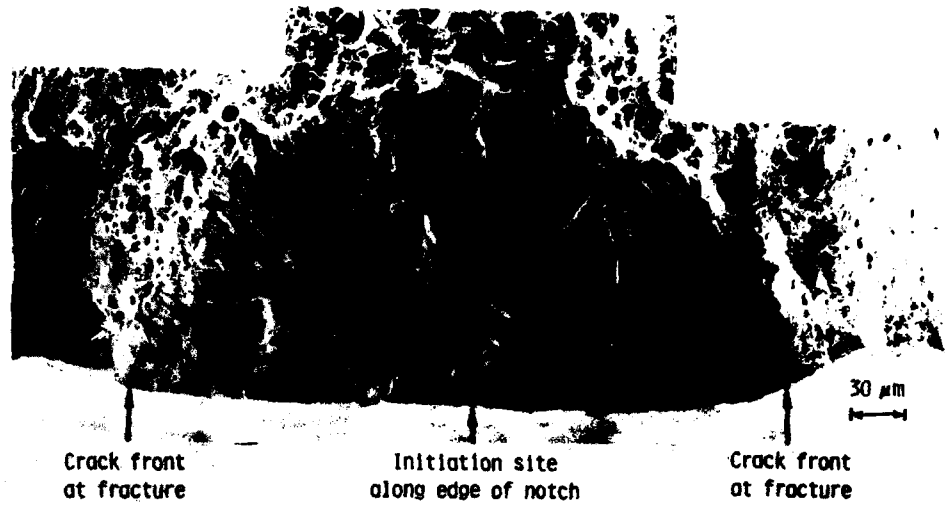


Figure 16.- Surface-crack shape early in fatigue life under constant-amplitude loading ( $R = -1$ ).

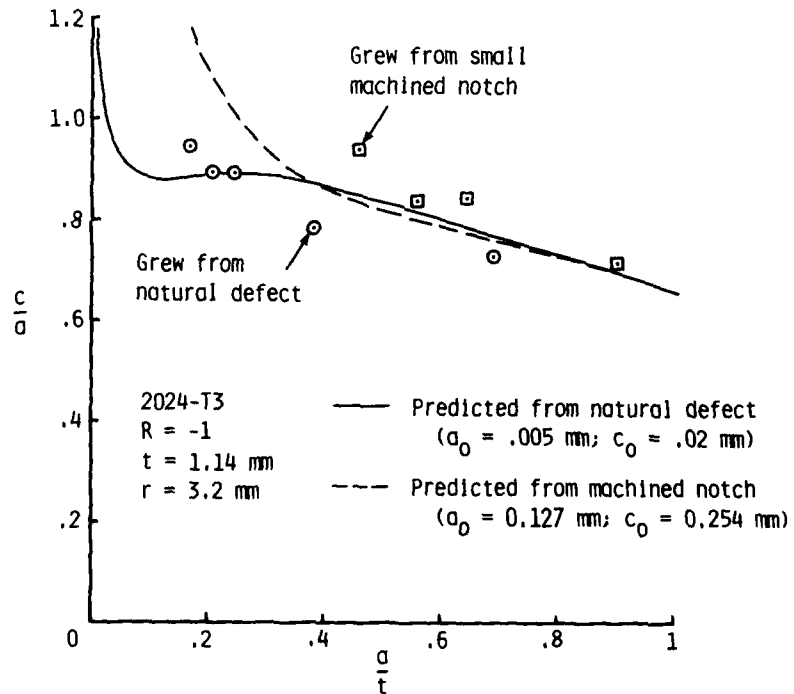


Figure 17.- Comparison of experimental and predicted surface-crack shapes under constant-amplitude loading ( $R = -1$ ).

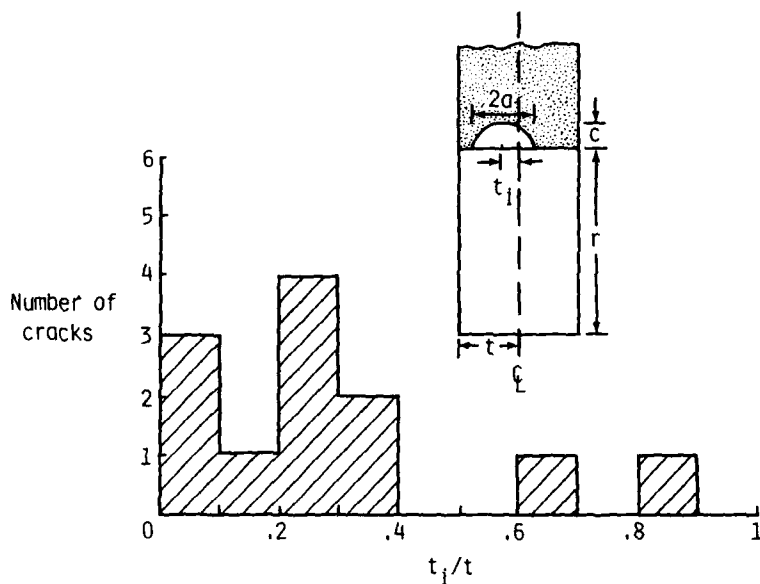


Figure 14.- Distribution of initiation sites along bore of notch.

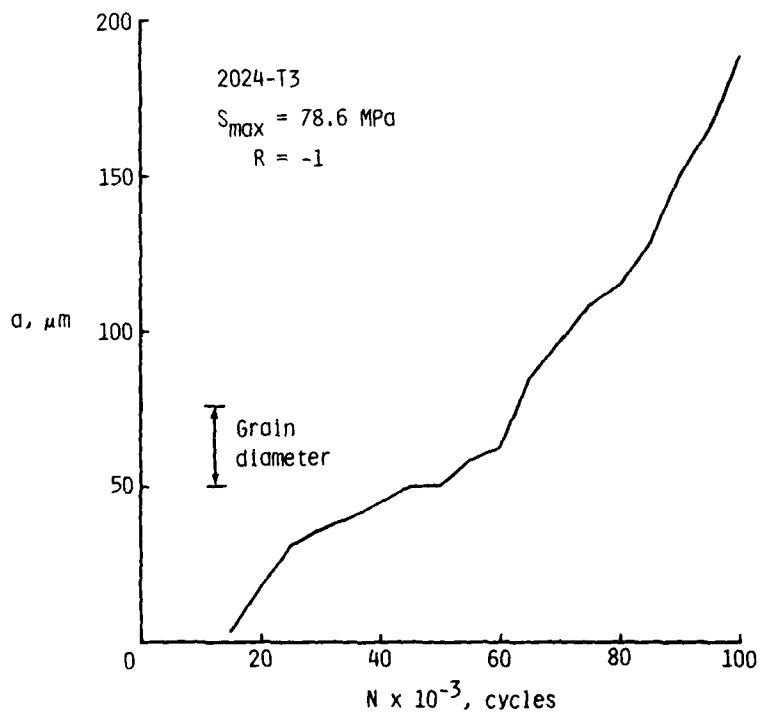


Figure 15.- Crack-length-against-cycles under constant-amplitude loading ( $R = -1$ ).

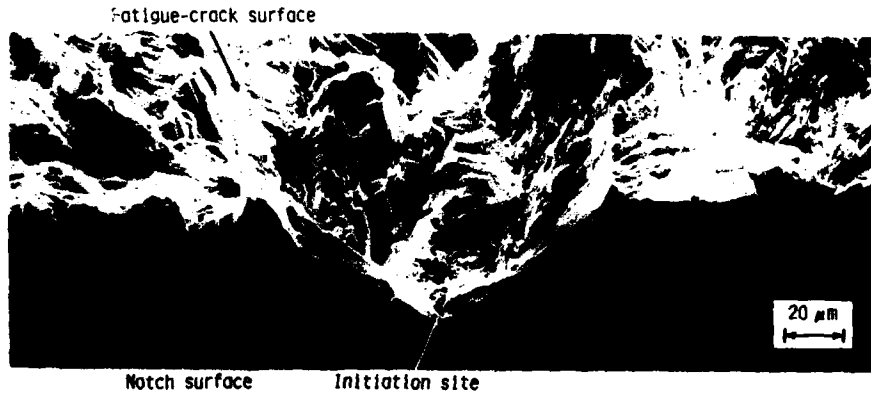


Figure 11.- Photomicrograph of initiation site at edge of notch under constant-amplitude loading ( $R = -1$ ; 45 degree tilt).

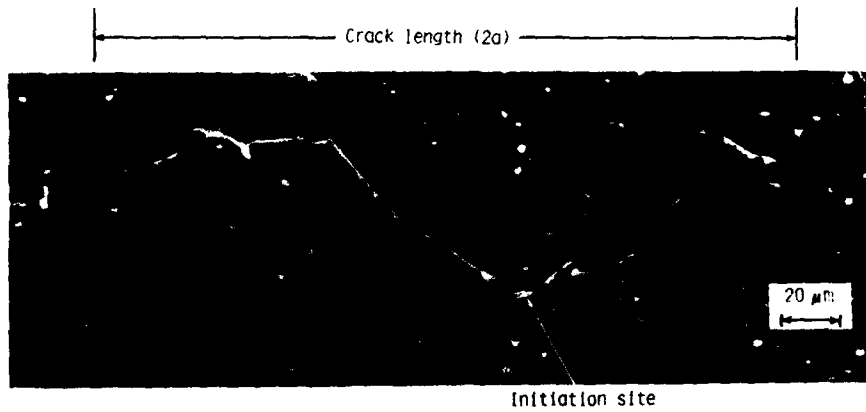


Figure 12.- Photomicrograph of surface replica of specimen shown in Figure 11.

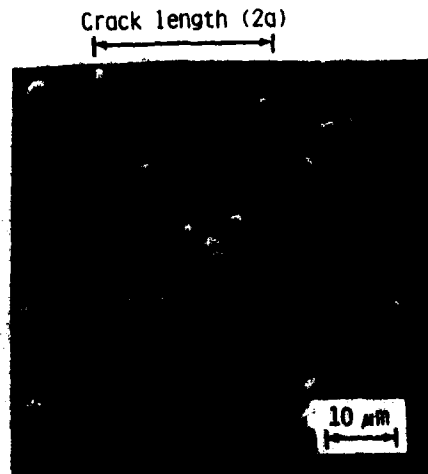


Figure 13.- Photomicrograph of surface replica with a small crack length.

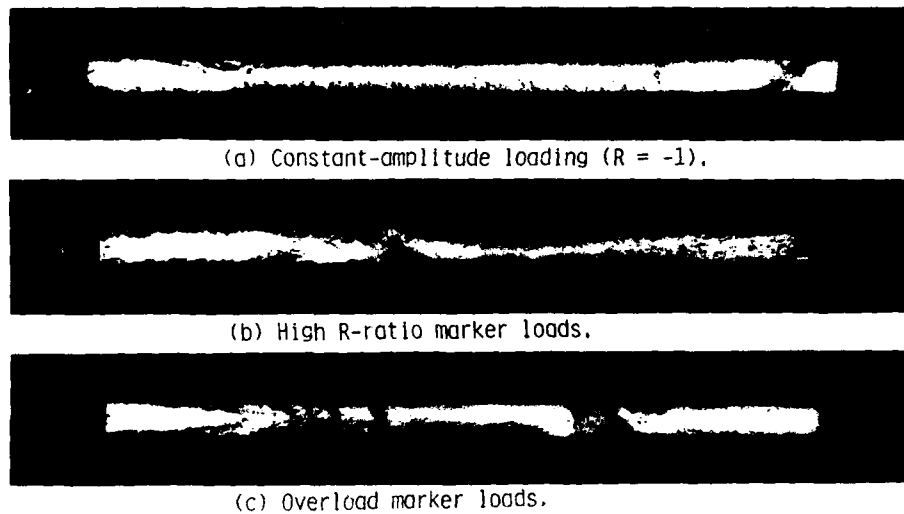


Figure 8.- Fatigue-crack growth surface markings under various loading.

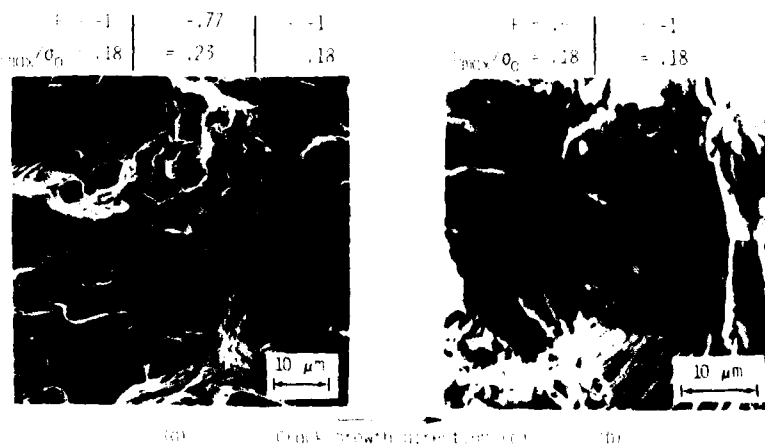


Figure 9.- Photomicrograph of fatigue surface features under (a) 1.3-overload conditions at  $c = 5.2$  mm and (b) high R-ratio conditions at  $c = 8$  mm.

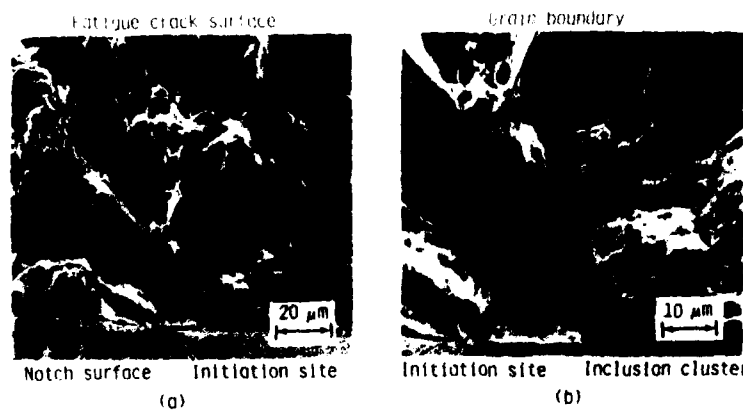


Figure 10.- Photomicrograph of (a) fatigue surface near initiation site and (b) separation of matrix from inclusion cluster under constant-amplitude loading ( $R = -1$ ; 0 degree tilt).

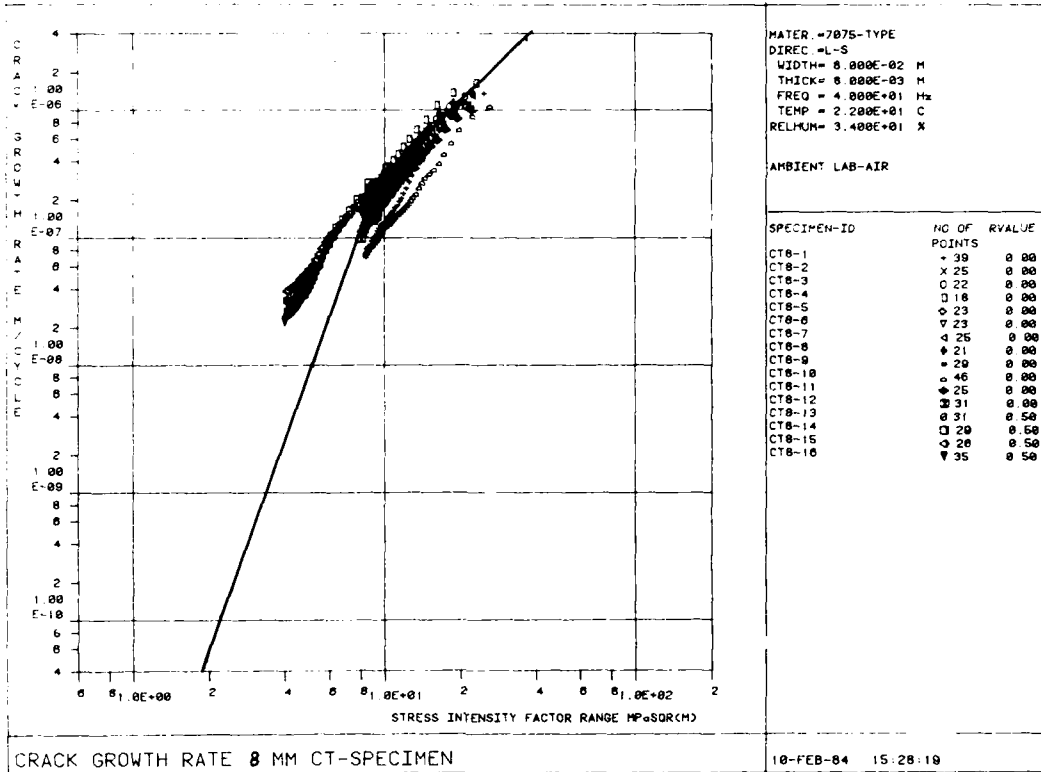


Fig. 6 Crack growth rate in 8 mm CT-specimen

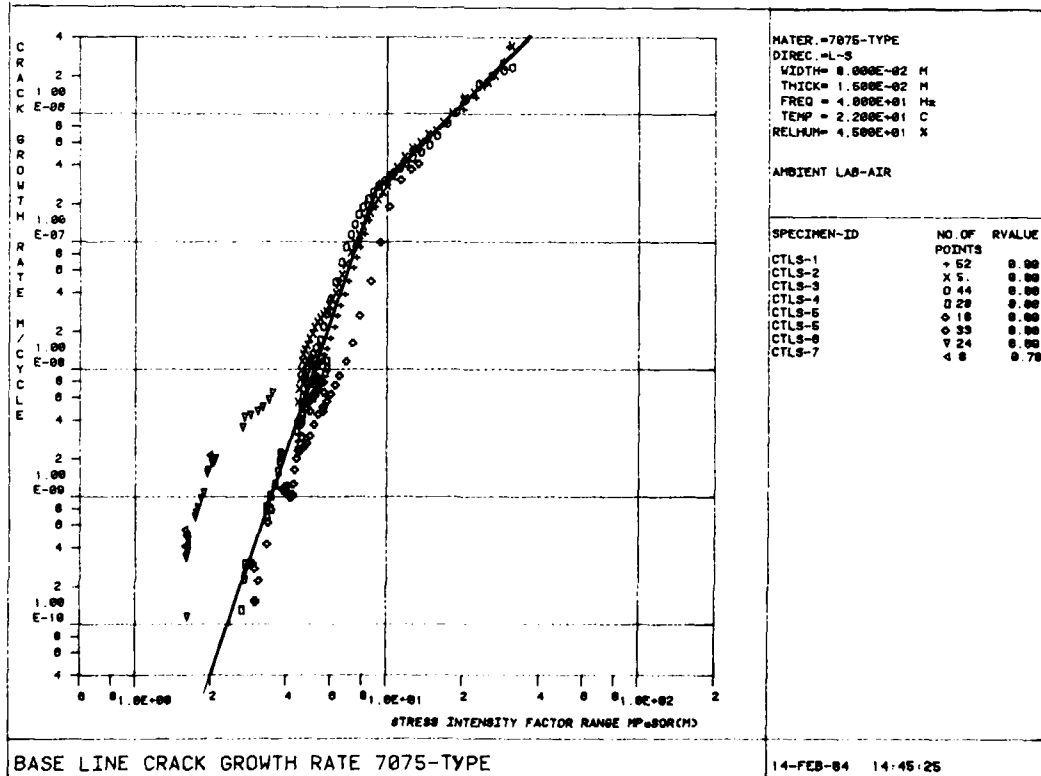


Fig. 7 Base line crack growth rate for forging material (7075-type)

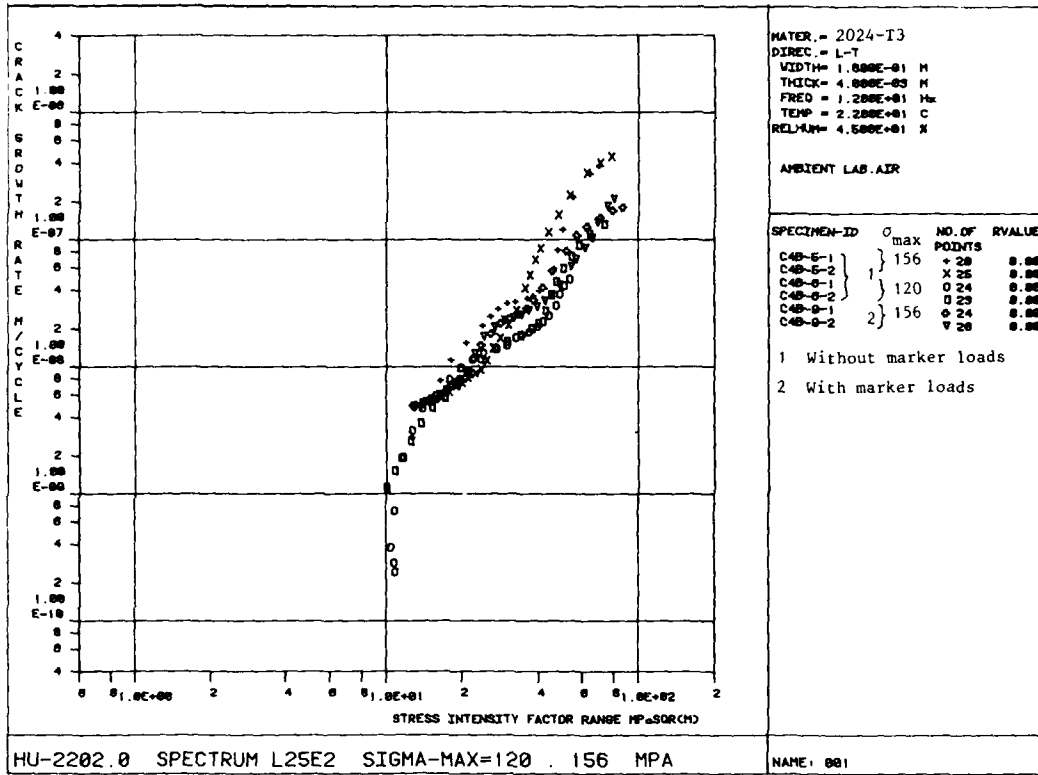


Fig. 8 Crack growth rate during spectrum loading of 4 mm sheet material

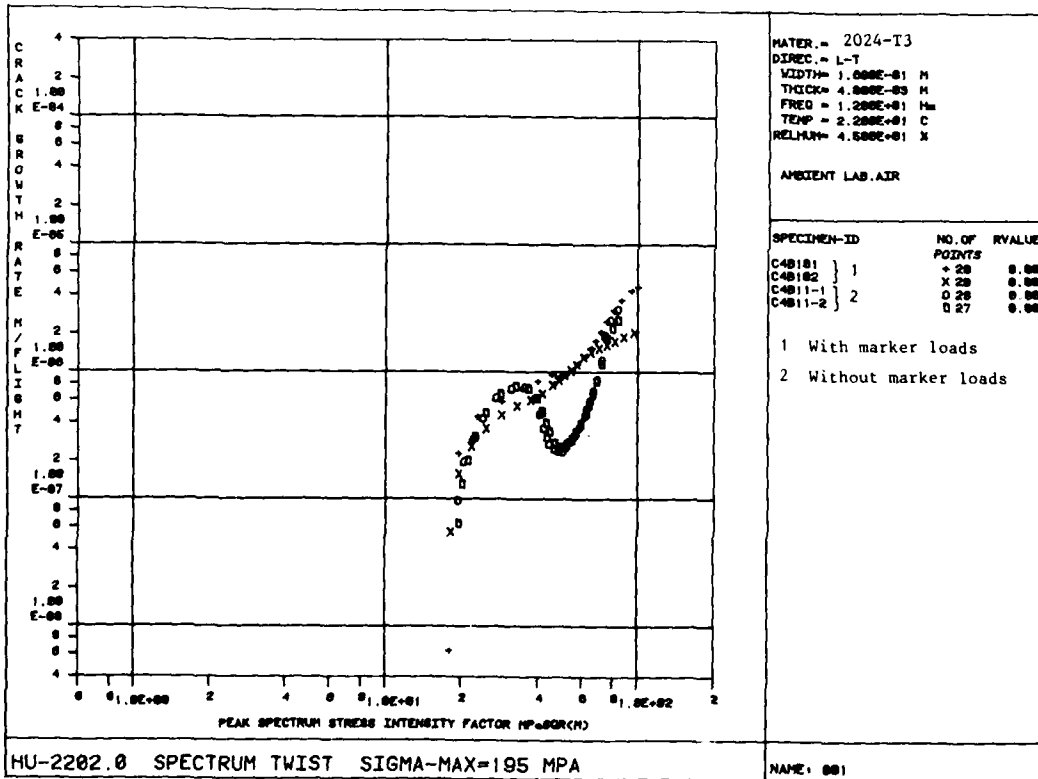


Fig. 9 Crack growth rate during spectrum loading of 4 mm sheet material

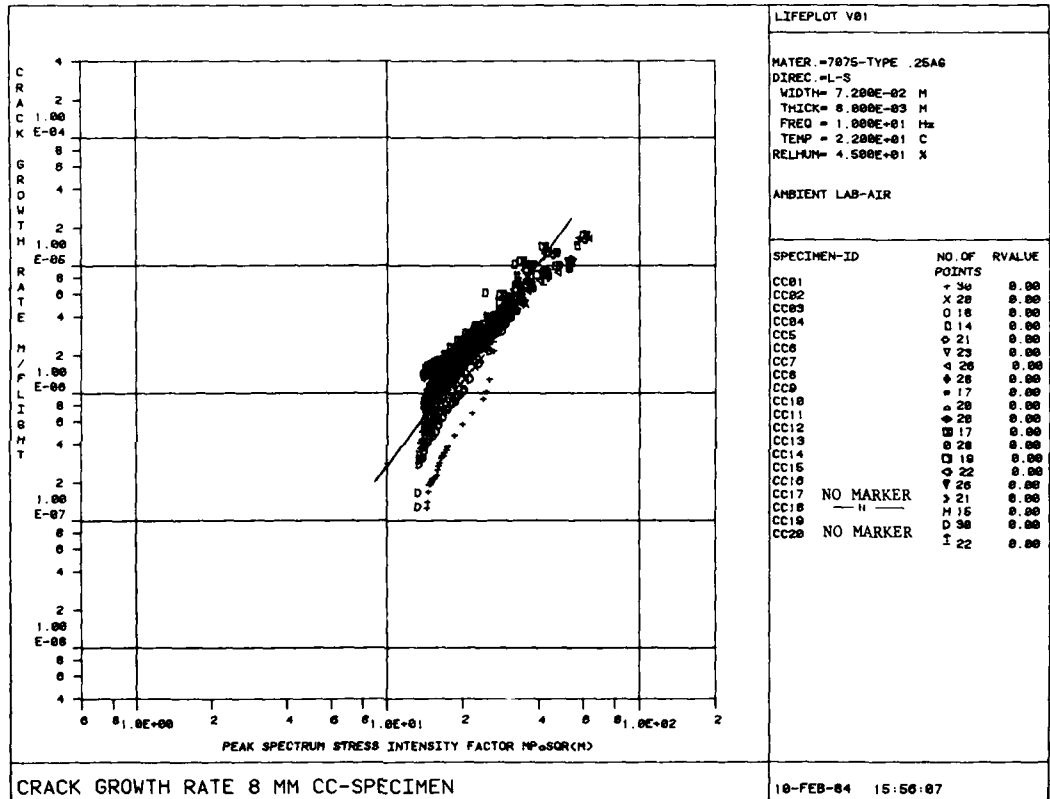


Fig. 10 Crack growth rate during spectrum loading (LIES) of 8 mm 7074-type of material

## FATIGUE CRACK TOPOLOGY AND CRACK GROWTH ANALYSIS

J. M. Potter  
AFWAL/FIBA

Air Force Wright Aeronautical Laboratories  
Wright Patterson Air Force Base, Ohio 45433  
USA

and

Dr. W. R. Garver, K. M. Koepsel, Dr. B. G. W. Yee  
Mail Zone 2680  
General Dynamics/Fort Worth Division  
P. O. Box 748  
Fort Worth, Texas 76101  
USA

### SUMMARY

Crack growth analysis and data collection via examination of fatigue fracture surfaces is presented. Stepped blocks, repeating tensile loads, and minimal compression loading are features of flight-by-flight load histories shown to be effective in providing distinguishable marks on crack surfaces during spectrum-fatigue loading. A reflected-light optical microscope equipped with stage micrometers is the basic equipment required to perform fractographic analysis. This can be used to trace crack growth histories in a variety of materials. The chief benefit of this method of data collection is low cost, which enables economical investigation of random variations in crack growth behavior and statistical characterization. The distribution of time for a crack population to reach a given size in wrought aluminum is found to be adequately modeled by the Weibull distribution. Crack growth rates are found to be log-normal. A method is presented to determine crack growth rate populations when fracture surface markings are fragmentary, as in aluminum castings. The crack growth histories for an entire population of structural details can then be predicted from sampled crack growth rate data. An example reliability calculation for cast aluminum structural details is shown to be consistent with test data.

### 1. INTRODUCTION

Current U. S. Air Force Structural Integrity (MIL-STD-1530A), [1] Damage Tolerance (MIL-A-83444), [2] and Durability (MIL-A-8866B) [3] design specifications require that metallic aircraft components be designed such that the presence of initial defects does not cause catastrophic failure nor widespread damage within one design service life. These specifications imply the use of fracture-based crack growth analysis in quantifying the structural performance (strength and remaining life) of aircraft designed for use by the U. S. Air Force.

Initial flaw sizes specified for analysis are presently based on the reliability of detection of crack-like flaws in the structure by nondestructive inspection (NDI) techniques. In research programs funded by the U. S. Air Force [4, 5, 6], the equivalent initial flaw size populations for several types of metallic structure have been inferred by examining crack growth behavior under complex spectrum loading conditions. Crack growth behavior has been analyzed by examining the fracture surfaces formed during subcritical flaw growth due to applied complex cyclic load histories. The purpose of this paper is to discuss crack growth measurement approaches which are successful in defining structural cracking behavior. These crack growth measurement approaches are based on the ability to discern changes in the fracture surface topology and relate these to specific loading events during a structural test. This method of data collection, called fractography, allows the collection of crack growth data from a number of structural test elements with minimal cost.

### 2. LOAD HISTORIES AND CRACK SURFACE TOPOGRAPHY

Certain types of complex load histories, representing flight-by-flight loading of aircraft structural control points, have been shown to provide excellent traceability in crack surfaces formed during fatigue crack growth. Figure 1 shows one such spectrum, designated NOR 1, which represents the loading at a control point in a wing carry-through box structure. This load history is repeated many times during one service life, with some variation. It contains several features which enhance its crack surface marking ability. These include regularly repeated high tensile loads, with minimal compressive loading.

Load histories which represent the intended application are often too random to provide distinctive marking features. These spectra can be modified to enhance the fractographic marking capabilities. Figure 2 illustrates a series of modifications to a complex spectrum which provide progressive improvements in marking characteristics.

- a. HUD 23 is a two-block F-16 fin-root bending-moment history which contains 80,714 load points per 1000 equivalent flight hours. This spectrum is highly random

and provides no distinctive crack surface features.

- b. FLA 2 is a modified version of HUD 23. Loads which are greater than 50% (maximum spectrum load) and which occur during the last 150 flight hours of each 1000-hour block are grouped together and arranged in ascending block sequence. This modification, added to the end of the 1000-hour block, increases the crack growth per block by about 15%. It provides a very heavy mark on the fracture surface every 1000 flight hours. However, only the last several marks before stopping the test are generally visible because the large compressive loads in the spectrum rub opposite faces of the crack together, obliterating marks formed early in the test.
- c. GAR 1 is a modified version of FLA 2. The heavy compressive loads are truncated and replaced by zero loads. This modification reveals crack growth history much earlier in the test. However, this modification is also the most radical departure from the actual load history for this application. Structural elements subjected to the load history shown in Figure 2c will not exhibit identical crack growth to the spectrum in Figure 2b. Crack growth rates in aluminum for these two spectra are in fact quite different. Therefore this type of spectrum modification is not suitable for load histories which will be used for structural verification testing. It is perhaps worth pointing out that the GAR 1 modification is consistent with many cycle-by-cycle crack growth analyses methods which ignore compressive loads by assuming that cracks close during compressive loads. Effective stress-intensity factor ranges are commonly computed from zero to the tensile peak for such compressive-tensile load cycles. Thus, a spectrum as in Figure 2b is often analyzed as if it were spectrum 2c, which would make the latter spectrum appropriate for comparison to analysis.
- d. GAR 2 is created by modifying GAR 1. The higher loads were grouped into frequent stepped blocks similar to the NOR 1 spectrum shown in Figure 1.

Load exceedance curves for these spectrum variations are shown in Figure 3. The additional high loads in FLA 2 which are in the stepped marker band represent about 15 percent of the high loads occurring in the original 1000 hour block. The crack growth which occurs during the stepped block is also equal to about 15 percent of the crack growth which occurs during the 1000 hour block. Therefore, crack growth from FLA 2 is about 15 percent more extensive than from HUD 23, which leads to conservative structural design. The extra high loads in FLA 2 are readily apparent in Figure 3. However, the number of extra cycles added to create FLA 2 is larger than necessary to produce clear fracture surface marks, so load exceedance variations for this type of spectrum modification could be reduced. Truncation of compressive loads, as in the GAR 1 spectrum, greatly changes the compressive exceedances, while leaving tensile exceedances unchanged. Rearrangement of loads, as in GAR 2, does not affect the load exceedance curve. The effect on crack growth is minimal in the situation which is illustrated, for which the original spectrum (HUD 23) is repeated several times during one service life.

One feature of the FLA 2 stepped marker loads is illustrated in Figure 4. The micrograph can be viewed through a stereo viewer to reveal the trough shape produced by the crack front during the progressive stepped marker band of the FLA 2 spectrum. High magnification examination in a scanning electron microscope reveals that each change in stress level within the block causes a change in crack plane, which produces the characteristic trough. This was not observed for other types of marker loads, such as constant amplitude blocks or single spike loads.

### 3. EQUIPMENT AND TECHNIQUES

An optical microscope was found to be most convenient in examining the fracture surfaces. Our system consists of a Zeiss Universal Microscope equipped with digital micrometers on an X-Y stage, and a high resolution T.V. camera and monitor. The micrometers allow convenient measuring of the locations of surface markings. The T.V. camera and monitor aid in the training of fractographers. They also give artificial contrast and brightness control which can aid in discerning surface markings and help relieve eye strain. Binary coded decimal (BCD) readout to a microprocessor is available to make data recording very easy. Fully trained personnel can read one crack about every half hour.

Special microscopic techniques may be used to aid in the observation of fractographic markings. This is illustrated by examining the same 400 hour load history on two different materials (Figure 5). A typical aerospace aluminum alloy, such as 7475, may be read most easily as a brightfield image. The very fine-grained 7091 powder metallurgy extrusion is best read as a darkfield image. A darkfield image gives very high contrast when compared to the conventional brightfield image. Aluminum castings, such as A357, also require enhancement of the contrast, but darkfield viewing is not suitable. This can be accomplished by using brightfield imaging and Nomarski differential interference contrast optics.

Random and semi-random load histories which contain from 40,000 to 100,000 load points are used at General Dynamics. Since the load histories represent only a few hundred hours of flight, they are repeated identically as many times as necessary to build-up one service life. A regular pattern, such as the 400 hour spectrum shown in Figure 5, allows an investigator to trace the crack growth backward from the terminal

crack front at the end of a test. The 400 hour spectrum has a sequence of several 93% loads followed shortly by a 100% load which gives a distinct double marking. The marking is helpful, since the fracture surface markings look quite different at large and small crack lengths. This difference is due to very different crack growth rates at different crack sizes. Using spectra such as the 400 hour spectrum or NOR 1, the crack growth history can be continuously traced from failure back to a small size (typically about 0.1 mm) of a given test element.

For some materials, such as aluminum castings or scrimmed adhesives, it is very difficult to trace the crack growth history continuously back from the end of the test. The technique of reading the fractographic surfaces then has to be modified. Test spectra with frequently repeating surface marking features are required. The fracture surface must be scanned and areas located which show a readable crack growth increment  $\Delta a$ . The time increment,  $\Delta t$ , or flight increment,  $\Delta f$ , represented by the crack growth increment must also be known. The location of these features can be measured. These locations represent the location of the crack front at the time of marking, and therefore, give the crack size,  $a$ , for each measurement of crack growth rate,  $\Delta a / \Delta f$ . Illustrative data for two A357 cast aluminum specimens tested with the NOR 1 spectrum are shown in Figure 6. Photographs show the fracture surfaces from which measurements were taken for each of the shaded data points. Open data points were obtained from other locations on the fracture surfaces, for which photos are not shown. The closest spaced marks in the photographs mark loads which occur once each flight sequence, while the heavier, more widely spaced lines mark loads occurring every tenth flight sequence.

#### 4. DATA ANALYSIS

When a group of tests are conducted identically, information can be obtained about the statistical distribution of crack growth. Data collected for 2024 plate tested under the NOR 1 spectrum load history, for example, is plotted as crack length vs. flight hours in Figure 7a. The time required for cracks to initiate and grow to a size of 5 mm is given by the intersection of each curve with the horizontal dashed line. This population of times is plotted in Figure 7b with a best fit two-parameter Weibull distribution shown as a solid line. This Weibull distribution can then be projected forward to the critical crack size using measured crack growth rates for reliability estimates if desired.

Similar analyses can be performed for A357 aluminum castings. Figure 8 presents a set of data for A357 similar to the data shown in Figure 7. Although the crack growth rate varies considerably for this material and load history, the crack growth is somewhat consistent for a given test specimen, as shown by shaded points for two of the specimens in the sample. Straight lines fitted to data points for a given test specimen represent a simple power law crack growth rate relationship. This relationship can then be easily integrated for each specimen to give crack growth ( $a$  vs.  $t$ ) curves as in the example of the 2024 plate shown in Figure 7a.

The statistical distribution of crack growth rate of the entire data set can also be determined for any crack size. For data shown in Figure 8, the best power law representation for crack growth rate has been determined for each test specimen in the sample. These straight line fits intersect 1 mm, for example, at the dashed vertical line shown in Figure 8. The population of all such intersections represents the population of crack growth rates at 1 mm crack size for this test condition. Figure 9 presents this population for A357 aluminum castings, tested using the NOR 1 spectrum at a maximum spectrum stress of 207 MPa. The solid line shown in Figure 9 is the best log-normal fit, which can be used in subsequent analyses.

Data such as these can be used for predictions of structural reliability. As an example, the distribution of crack growth rates shown in Figure 9 was used to predict the distribution of times to failure for a set of simulated components tested with an initial flaw of 1.21 mm (0.050 inch). The test elements, which simulate stress levels in a cast fin substructure for the F-16 aircraft, were predicted to have a failure rate of 7 percent when tested for four service lives (32,000 flight hours). Nine simulated components were actually tested with only one failing to reach 32,000 hours. It failed at 28,000 hours. Therefore, the failure rate was measured to be near 10 percent. Considering the scatter inherent in fatigue experiments, this is good agreement with the predicted failure rate. This gives some confidence that the functional representation for crack growth rate shown in Figure 9 is accurate and can be used for calculating the failure rate for other service times.

#### 5. CONCLUSIONS

Crack growth analysis can be accomplished using data from fracture surface examination of test specimens. Although the equipment needs are modest, time must be invested in training of personnel. Modification of load spectra is often necessary to allow ease in reading the fractographic surface.

The greatest benefit for this method is seen in the reduction in cost of testing and data collection. Time usually spent collecting data in spectrum fatigue is minimized which reduces the cost of testing large samples. This allows economical assessment of variations in crack growth behavior in critical airframe structural components.

6. REFERENCES

- [1] MIL-STD-1530A (USAF), "Aircraft Structural Integrity Program," 1975
- [2] MIL-A-83444 (USAF), "Airplane Damage Tolerance Requirements," 1974
- [3] MIL-A-8866B (USAF), "Airplane Strength and Rigidity Reliability Requirements, Repeated Loads and Fatigue," 1975.
- [4] P. J. Noronha, S. P. Henslee, D. E. Gordon, Z. R. Wolanski, and B. G. W. Yee, General Dynamics/Fort Worth Division, "Fastener Hole Quality," 1978, AFFDL-TR-78-206, Vol. I.
- [5] J. N. Yang, S. D. Manning, and W. R. Garver, General Dynamics/Fort Worth Division "Durability Methods Development," 1979, AFFDL-TR-79-3118, Volume V.
- [6] W. R. Garver, General Dynamics/Fort Worth Division, 1983, "Initial Quality of Advanced Joining Concepts," 1983, AFWAL-TR-83-3064, Phase I.

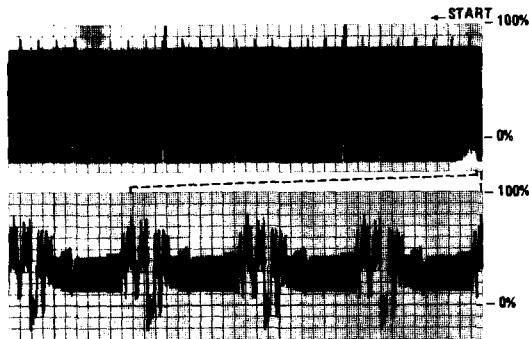


Figure 1 NDR 1 Wing Carry-Through Box Spectrum With Excellent Inherent Fracture Surface Marking Characteristics

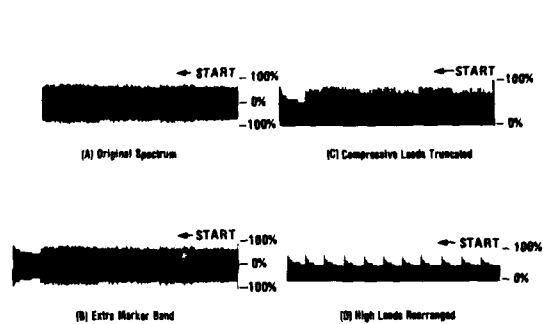


Figure 2 Fin Root Spectrum Modifications to Enhance Fracture Topology

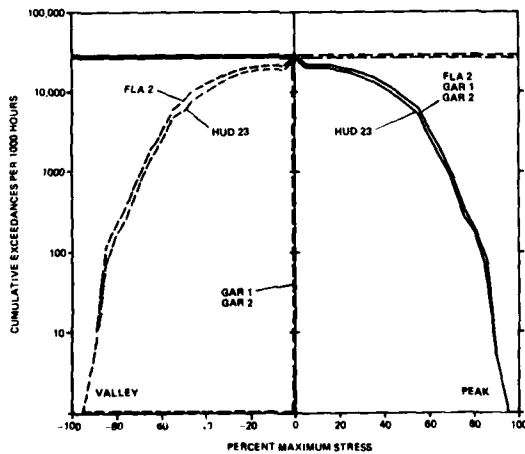


Figure 3 Stress Exceedances for F-18 Tail Root Spectra

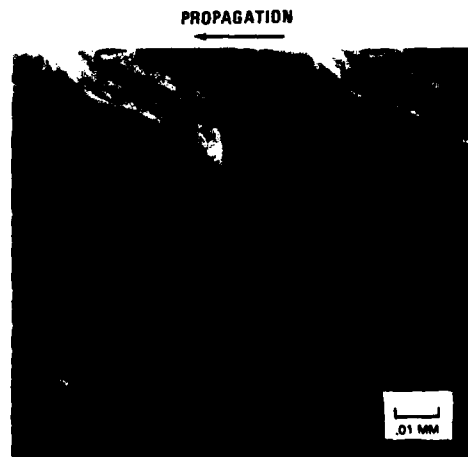


Figure 4 Stereomicrograph of Effect of FLA 2 Stopped Marker Bands on Fracture Surface

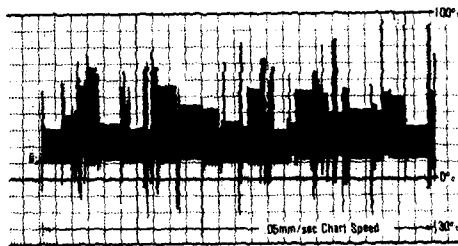
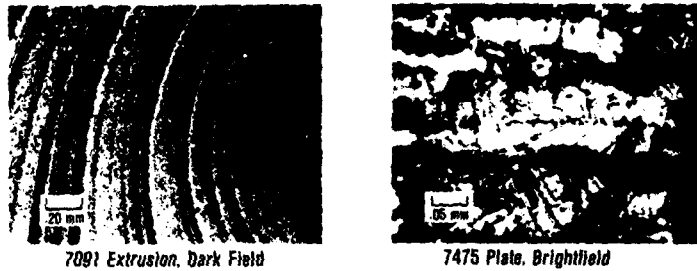


Figure 5 Fracture Surfaces for a Common Spectrum, Comparing Lighting Techniques in Two Aluminum Alloys (F-16 400 Hour Wing-Root Bending-Moment Spectrum)

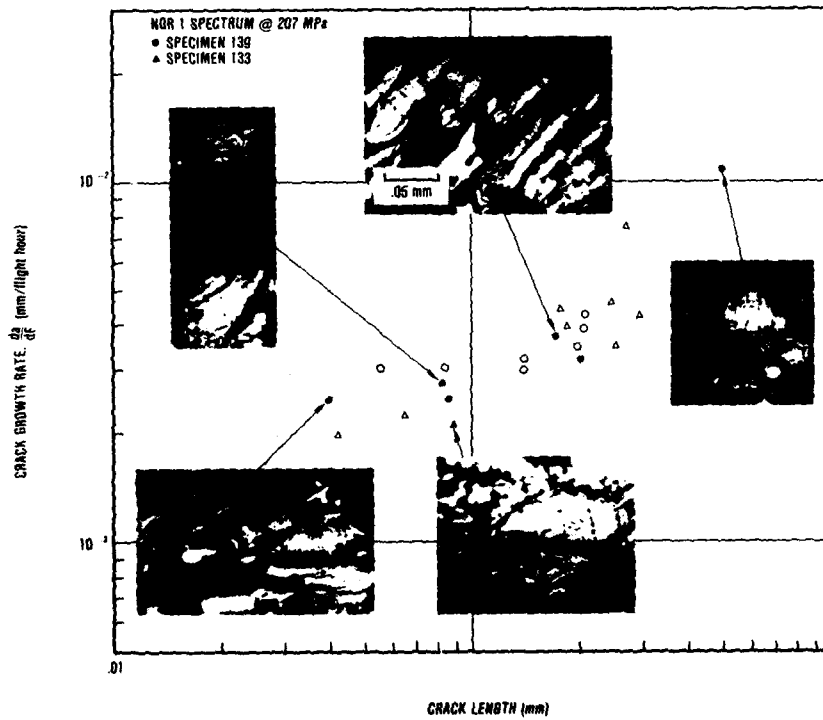


Figure 6 Crack Growth Rate Versus Crack Size in A367-T61 Aluminum Castings. Rates Were Determined From Markings Shown in Individual Photographs

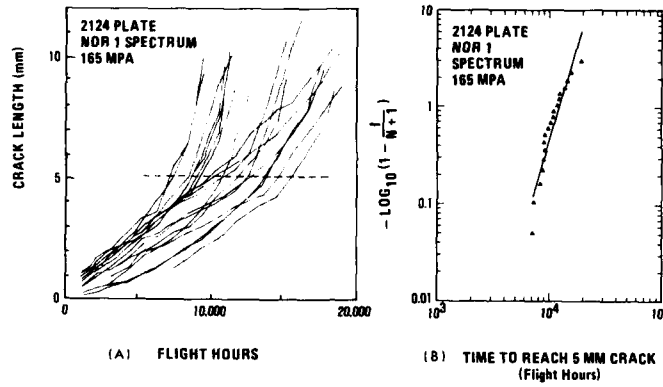


Figure 7 (a) Crack Growth Curves for a Set of Specimens Tested Identically, and (b) Time Distribution to Reach 5mm Crack Length in 2124 Aluminum

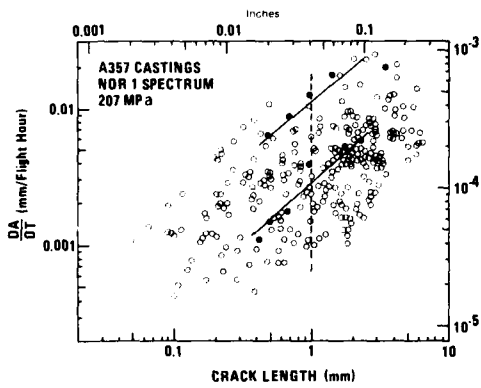


Figure 8 Crack Growth Rate Data for 50 A-357 Cast Aluminum Test Specimens

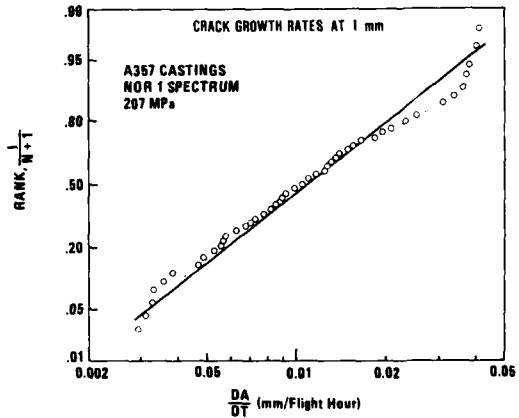


Figure 9 Distribution of Crack Growth Rates in A357 Castings

APPLICATION OF OPTICAL AND ELECTRON MICROSCOPIC TECHNIQUES  
IN THE FRACTOGRAPHIC DETERMINATION OF FATIGUE CRACK GROWTH RATES

R.V. Dainty  
Structures and Materials Laboratory  
National Aeronautical Establishment  
National Research Council  
Montreal Road, Ottawa, Ontario K1A 0R6 Canada

SUMMARY

The fractographic derivation of fatigue crack growth information is entirely dependent on the fractographer's ability to correlate accurately the striated fracture surface topography with the applied test or service loads. This paper will review some of the techniques that have been developed to acquire this type of quantitative information through the application of optical and electron microscopy. Fractographic analyses of fatigue specimens and components that have failed during laboratory and full-scale aircraft fatigue tests will be presented. These analyses will show how the identification and correlation of various fatigue load application formats, i.e. constant amplitude, programmed block, flight-by-flight and random loading, can be utilized to derive this type of experimental crack growth data.

1. INTRODUCTION

The use of damage tolerant design concepts depends critically on a knowledge of fatigue crack growth (FCG) rates so that for many applications, suitable service inspection intervals can be specified. These crack growth rates must often be determined experimentally from full-scale or component structural tests and it is therefore clear that the interpretation of these tests is very important.

For the many cases where visual crack growth measurements during a test are not available, interpretation of the test results often depends on the fractographer's ability to correlate accurately the striated fracture surface topography with the applied fatigue loads. The accuracy of this correlation is influenced by two factors: 1) the techniques that the fractographer employs, e.g. optical, scanning and/or transmission microscopy and 2) the manner in which the loads are applied and the test conducted. Clearly then, in order to obtain the maximum amount of information from the structural test, there must be close co-operation between the design-test engineers and the fractographer. In addition, the design-test engineers and managers should have some appreciation of the 'art' and 'science' of fractography. In particular it is important that they know, 1) how fatigue crack growth rates are derived by means of fractography, 2) the limitations of quantitative fatigue fracture surface analysis, and 3) what can be done in the test design stage to make the fracture surface topography more 'readable'.

This paper will attempt to provide some of this information by first reviewing some of the fractographic techniques that have been developed for acquiring FCG data through the application of optical and electron microscopy, and noting some of the major factors that influence the fractographer's ability to 'read' a fatigue fracture surface. Fractographic analyses of fatigue specimens and components that have failed during laboratory and full-scale aircraft fatigue tests will then be presented to illustrate and expand on some of these topics. The examples include the derivation of FCG information from various load application formats such as constant amplitude, programmed block, flight-by-flight and random loading.

2. FRACTOGRAPHIC TECHNIQUES

Originally, the fractographic determination of FCG information from laboratory tests was relatively straightforward since components and full-scale structures were tested under constant amplitude, Figure 1, or programmed block loading conditions, Figure 2. In the case of constant amplitude testing, where each fatigue striation represents the increment of crack growth that occurred during the application of one load cycle, numerical analysis of the fracture surface was accomplished by simply measuring the striation spacings either directly in the microscope or from fractographs. With programmed block loading, Figure 2, the load cycles at the various load levels can often be identified in the electron microscope by their respective fatigue striation spacings and an increment of crack growth due to each complete load block may contain several or possibly hundreds or thousands of individual striations. By determining an average 'striation spacing' for constant amplitude loading or an average 'load block spacing' for programmed block conditions at a number of 'representative areas' along the length of the fatigue crack, it is possible to relate crack growth rates to crack length and to estimate the time of crack initiation [1-6].

With the development of computer-controlled fatigue loading equipment, recent component and full-scale aircraft fatigue tests have utilized 'random' loading methods to simulate more closely actual service loading conditions. This randomization of the application of load cycles has, however, created new problems similar to those generally encountered in the quantitative analysis of fracture surfaces from service fatigue failures. These problems include the identification and correlation of the randomly spaced striations, Figure 3, with the specific loads that were applied during the test. This identification and correlation can be extremely difficult, particularly when a complex load spectrum consisting of a large number of cycles at various levels and amplitudes is involved. Generally with this type of load spectrum not all load cycles will create an increment of crack growth that can readily be resolved and accounted for, even at the relatively high magnifications of the electron microscope. In addition, load interaction effects may cause 'retardation' that may significantly arrest crack growth for several load cycles. Therefore, in order to acquire meaningful crack growth information from fracture surfaces generated by randomly applied fatigue loading it is usually necessary to incorporate 'marker loads' within the spectrum load block. These marker loads can consist of a single block of constant amplitude load cycles (see Case 6) or as a more complex block containing specific numbers of cycles at various load levels and amplitudes that may be applied at several locations within the repeating load block. In either case, the purpose of the 'marker loads' is to delineate fractographically the position of a propagating crack front at predetermined periodic intervals in the cyclic loading program so that this 'marker block' region can be readily detected by optical or electron microscopy. By measuring the spacing between successive 'marker bands' on the fracture surface it is possible to derive accurate crack growth data [7-11].

For these three general types of fatigue loading formats, i.e. constant amplitude, programmed block and random with 'marker loads', two basic fractographic techniques utilizing optical and electron microscopy are generally used for acquiring crack growth information. These are 'striation counting' and 'load block measuring'. Since the success and accuracy of an analysis using either method is dependent upon the inherent response of various engineering materials to delineate the position of a propagating crack front, some general comments on materials are warranted.

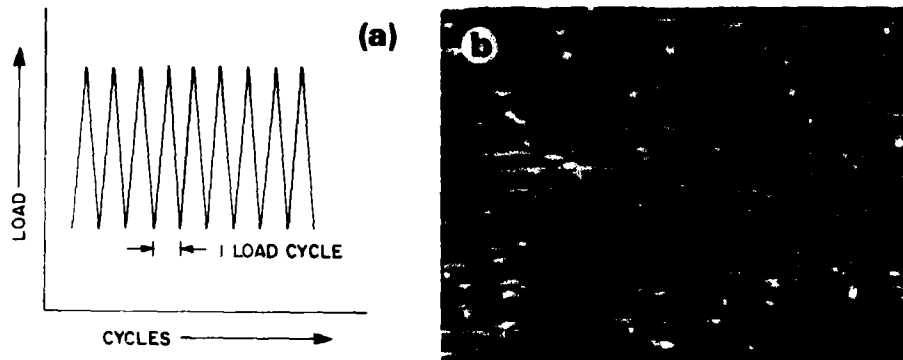


FIGURE 1: (a) CONSTANT AMPLITUDE FATIGUE LOADING, (b) SINGLE CYCLE STRIATIONS – ALUMINUM ALLOY

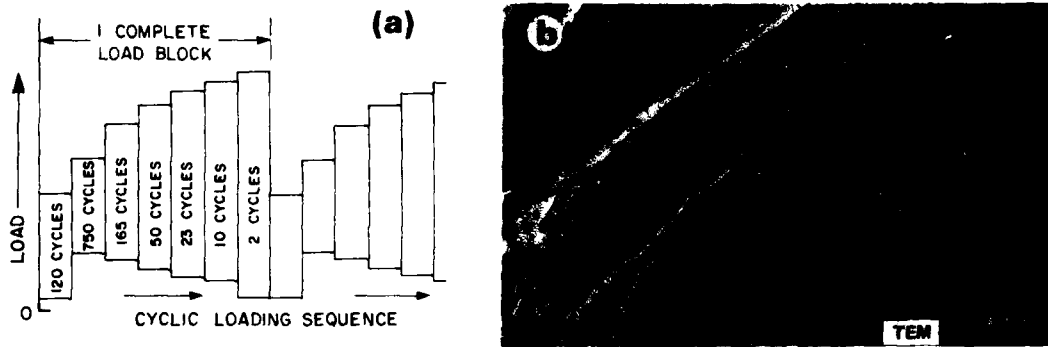


FIGURE 2: (a) PROGRAMMED BLOCK FATIGUE LOAD SPECTRUM, (b) DISTANCE BETWEEN ARROWS 'START' AND 'END' REPRESENTS CRACK GROWTH THAT OCCURRED DURING APPLICATION OF 'ONE COMPLETE LOAD BLOCK' – ALUMINUM ALLOY

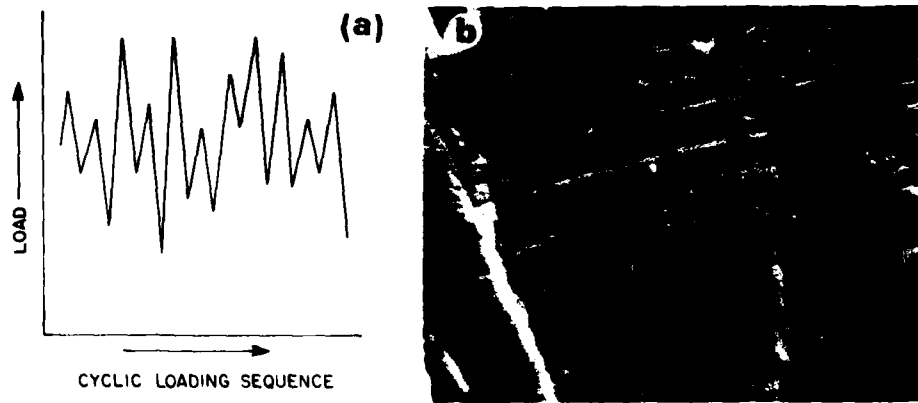


FIGURE 3: (a) RANDOM FATIGUE LOADING, (b) RANDOMLY SPACED STRIATIONS – ALUMINUM ALLOY

### 3. MATERIAL CONSIDERATIONS

It has been shown that under various fatigue loading conditions, many metals, alloys and polymeric materials [1-10, 12-28, 31-51] will form characteristic macroscopic and/or microscopic fracture surface markings, such as crack growth bands and striations. Although for the purpose of this paper it is not necessary to understand fully all of the factors involved in striation formation, various studies [16, 20-28, 33-48] have shown that striation formation is a function of stress intensity and localized plastic deformation at the fatigue crack tip and therefore is related to material properties, microstructure and environment. Since most engineering metals and alloys are polycrystalline with relatively complex microstructures it is not surprising that well defined striation formation is generally discontinuous and non-planar, particularly on the micro-scale [30]. As will be discussed later, these factors can present difficulties in acquiring accurate FCG data. A review of the literature indicates that most quantitative striation studies have involved aluminum alloys. Many structural aeronautical applications involve the use of 2XXX and 7XXX series aluminum alloys and in general these materials form reasonably well defined striations over a wide range of fatigue loading conditions [10, 16, 20, 21, 23, 27, 28, 37-43, 49-51]. On the other hand, most of the hardened and tempered steels generally do not form clearly defined striations [25, 26, 46] although under certain loading conditions they can exhibit well defined 'macroscopic' markings, Figure 4, that can be utilized for quantitative purposes (see Case 4) [3, 15].

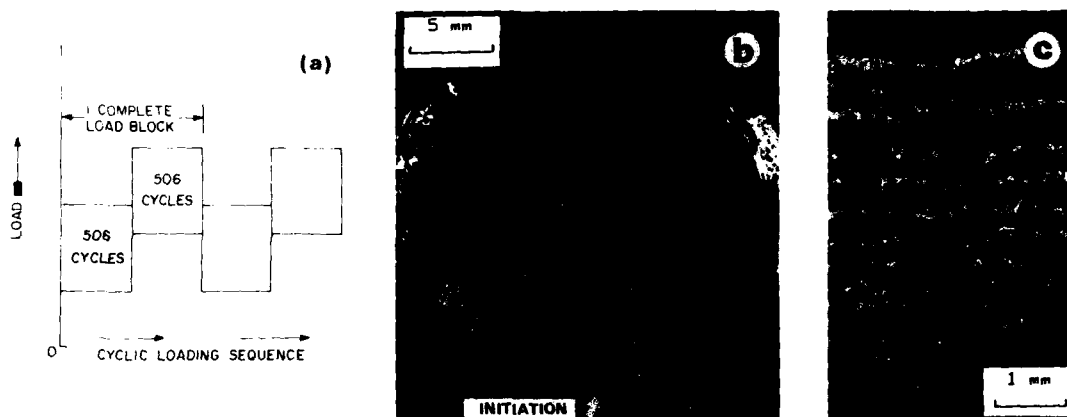


FIGURE 4: (a) BLOCK LOAD SPECTRUM, (b) MACROSCOPIC CRACK GROWTH BANDS — 4340 STEEL, (b) AND (c) DISTANCE 'A' REPRESENTS CRACK GROWTH THAT OCCURRED DURING APPLICATION OF 10 COMPLETE LOAD BLOCKS

### 4. STRIATION COUNTING

Using high magnification optical or electron microscopy, striation counting methods usually involve the direct measurement of single cycle striation spacings in the case of constant amplitude testing, or crack growth band spacings where the bands have been formed during the application of a repetitive sequence of load cycles. In both cases the striation ( $da/dN$  values) or crack growth band spacings are usually relatively small and would normally yield several hundreds or thousands of cycles or load blocks per mm of crack growth, particularly during the early stages of crack growth. While this method involves the straightforward determination of average striation or growth band spacings at numerous points along the entire crack length, the overall accuracy of an analysis is dependent on several factors. For any given fracture surface, striation spacings formed at the same nominal stress intensity can vary by at least a factor of two or three [21, 24, 26-29, 47]. During the early stages of crack growth the striations are often difficult or impossible to resolve, even at the higher magnifications of the transmission or scanning electron microscopes, and therefore fractographic derivation of initial crack growth rates may not be possible. In addition, since only the larger spaced striations would normally be observed in the initiation region, the spacings would not be truly representative of the average and would tend to suggest significantly larger crack growth rates than those that actually occurred [21-26]. Over the majority of the Stage II fatigue crack propagation region several areas of well resolved striations will generally be present and the main problem will be in the selection of representative areas from which to derive 'true' average striation spacing values. Even under the most ideal conditions striation formation is generally discontinuous and non-planar, occurring on isolated fracture planes or facets (see Case 1, Fig. 11). These facets may be inclined over relatively large angles that deviate from the general crack propagation direction (CPD) and macroscopic fracture plane. Various studies have shown that corrections for these angular deviations can be made in order to improve the accuracy of striation spacing measurements and hence crack growth rates [27, 29, 30]. These correction methods are laborious and time consuming and based on a limited number of investigations, do not significantly improve the overall accuracy of localized crack growth rates. During the latter stages of crack growth, striation formation can be associated with relatively large regions of rapid fracture usually in the form of ductile dimples. With this type of 'crack jumping' [16] it is not possible to use striation spacing measurements to derive crack growth rates for these mixed mode fracture regions since only a portion of the crack extension is attributable to striation formation. Any attempt to use striation spacing values in a mixed mode fatigue fracture region would yield lower crack growth rates than those that actually occurred [21-26]. The discrepancy between these growth rates would be related to the relative portions of striated fracture and rapid fracture.

In general the striated areas selected for spacing measurements should be, 1) oriented in the general CPD and 2) relatively flat with a tilt angle (with respect to the CPD) of less than  $\pm 30^\circ$  from the macroscopic fracture plane. This  $\pm 30^\circ$  condition would tend to limit localized striation spacing errors due to facet tilting deviations to approximately 15 percent. Each area should contain a minimum of 10 relatively uniformly spaced striations, and an evaluation of two to four areas per mm of crack length should yield sufficient data points to construct a representative fatigue crack growth curve.

Although a limited number of detailed studies [21, 22, 27] have been conducted to evaluate the accuracy of crack growth data derived by striation spacing measurements, an investigation by Cruickshanks-Boyd did conclude, "Striation spacings measured using the scanning electron microscope gave the best agreement with the optically-measured fatigue crack growth rate. This resulted in a reasonably accurate (i.e.  $\pm 30\%$ ) estimate of the number of fatigue cycles to failure." [27, pg 8].

## 5. LOAD BLOCK MEASURING

While 'striation counting' methods involve microscopic measurement of individual, relatively uniform closely spaced striations, 'load block measuring' methods involve the measurement of crack growth increments between relatively widely spaced recurring striation patterns. The load spectra involved in the formation of these types of fracture surfaces usually contain hundreds, or possibly thousands of load cycles at various levels and amplitudes that may be applied in a programmed block (Fig. 5(a)) or randomized format (see Cases 3 - 6). Generally the recurring striation pattern will contain a large number of well defined striations, although in the initiation region the major load(s) or load block(s) can produce what appear to be uniformly spaced, single cycle striations similar to those formed by constant amplitude testing, Figure 5(b). However, with increasing crack length and stress intensity, the less severe loads would tend to form additional striations that would continually change the detailed features of the striation pattern and make it evident that a loading format other than constant amplitude was involved, Figure 5(c). With programmed block or spectrum loading these changes are usually apparent since several of the various load levels can often be identified by their respective cycle counts and striation spacings, Figure 2, [17, pg 121].

With random loading the recurring nature of these topographical changes may not be readily apparent so that the use of 'marker loads' is usually necessary for acquiring FCG data [7-10]. Fracture surfaces produced by random or block loading methods generally result from damage tolerance investigations associated with component and full-scale testing. In these cases the Stage II fatigue crack propagation region will often involve relatively few complete load blocks, possibly only tens or hundreds (see Cases 3 to 6). Depending on the visual or macroscopic appearance of the recurring striation pattern these analyses can often be carried out relatively quickly using low power optical microscopy (see Cases 3 and 4), [5, 8]. However, in many cases the identification of the recurring striation pattern, or a specific segment of it, will require the higher magnification and increased resolution of the scanning or transmission electron microscopes whose use can be considerably more time consuming and expensive (see Cases 5 and 6), [7].

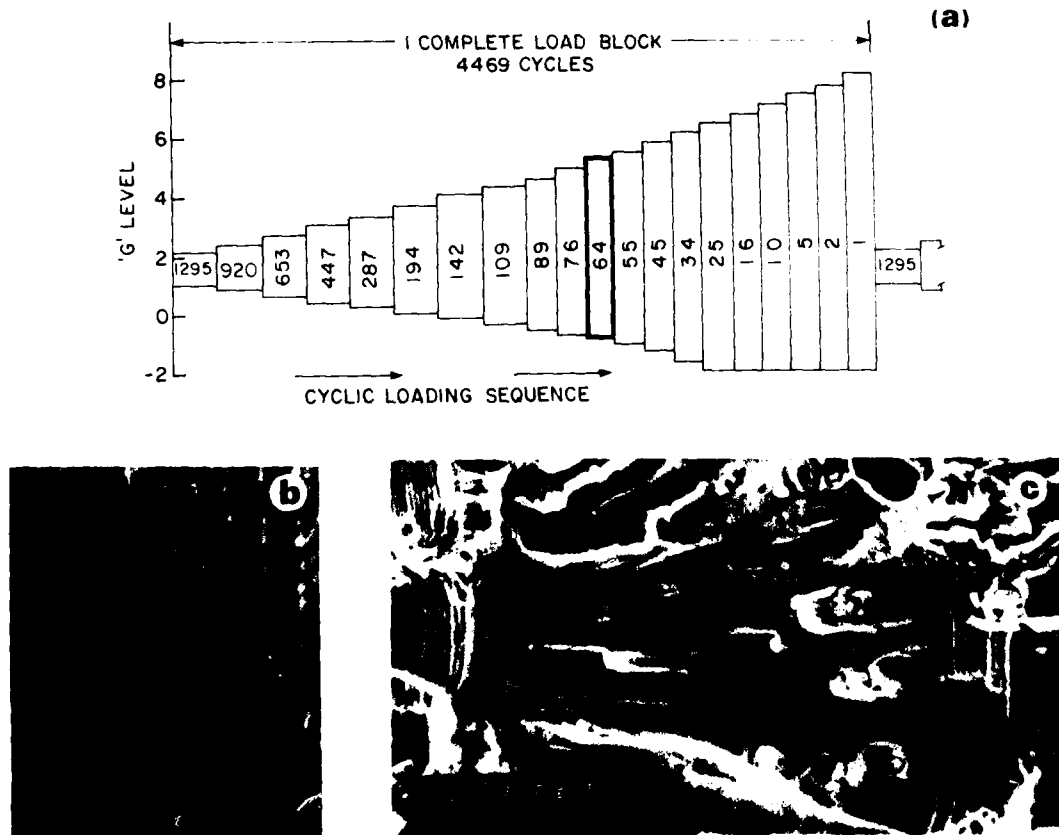


FIGURE 5: (a) 'LO-HI' BLOCK LOAD SPECTRUM, (b) LOW  $\Delta K$  CRACK GROWTH REGION, (c) HIGH  $\Delta K$  CRACK GROWTH REGION. (b) AND (c) DISTANCE 'A' REPRESENTS CRACK GROWTH THAT OCCURRED DURING APPLICATION OF 'ONE COMPLETE LOAD BLOCK' - ALUMINUM ALLOY

## 6. MICROSCOPIC EQUIPMENT AND TECHNIQUES

During the past 25 years the development and application of many optical and electron microscopic and specimen preparation techniques for acquiring FCG information have been well documented [12-14, 17, 19, 31, 52, 53]. Since it is not within the scope of this paper to describe fully all aspects of these techniques, the reader is advised to consult these references for the detailed information that will be essential to successfully carry out an analysis. Notwithstanding this, some of the general aspects, advantages and limitations of these techniques will be briefly outlined and their application to specific FCG analyses will be illustrated in the case studies in Section 8.

### 6.1 Optical Microscopy

Acquiring fractographic FCG data invariably begins with visual and low power (up to 100 times) optical examination and documentation of the fracture surface to determine the presence of macroscopic crack growth markings that could be readily correlated with the fatigue test load history. In programmed block loading the markings can appear as alternating bright and dark bands, Figures 4 and 6. (see Cases 3 and 4). In the early stages of crack growth, Figures 6(b) and 6(c), these bands represent alternate changes in the microscopic plane of fracture [41] that are generally associated with a significant change in stress intensity caused by cyclic load level changes. During the latter stages of crack growth, Figure 6(a), it has also been shown that the dark bands can consist of ductile dimples that are formed by the higher level fatigue loads [17, pg 120].

One of the most critical factors in low power optical microscopy is the illumination of the fracture surface in order to reveal and record significant topographical details. Various lighting techniques [17, pg 13] including circular, oblique and vertical illumination, in conjunction with various specimen tilting angles can be utilized to reveal any recurring crack growth patterns, Figure 7. In general, low power optical microscopic techniques can only be applied to fracture surfaces where the recurring increments of crack growth are relatively obvious (see Cases 3 and 4) [3, 5, 15, 16, 17 (pgs 31, 123)]. Examples include constant amplitude testing and programmed block loading where a particular segment of the load block forms a unique and optically detectable region that usually occurs once in each complete load block. It has also been shown that fracture surfaces formed primarily by random loading can be 'read' optically if a relatively severe 'marker load' sequence is utilized [8].

Depending on the obvious nature of any recurring striation pattern, further high power optical examination may be required at magnifications up to approximately 500 times, Figures 6(b) and 6(c), [16, 49]. In addition, examination of plastic (see Case 4) or metal carbon coated plastic replicas [12, 13, 17] using vertical or transmitted light can also reveal striation patterns at these magnifications, Figure 8, [50]. Utilization of replicas can be particularly useful when it is necessary that large components or fracture surfaces remain intact and therefore direct optical examination of the fracture surface, particularly at the higher magnifications, would be extremely difficult.

The major problems and limitations associated with optical microscopy are limited resolution and, at the higher magnifications, the relatively small depths of focus that are generally incompatible with the rough and irregular fatigue fracture surface topography. With these limitations it may not be possible to recognize the recurring striation pattern or to measure accurately the fine striation or load block spacings, particularly at the shorter crack lengths, thus necessitating the use of scanning or transmission electron microscopy.

### 6.2 Transmission Electron Microscopy (TEM)

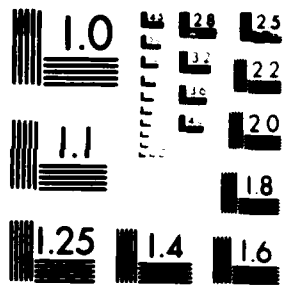
Initially the detailed studies of fatigue striation formation and crack growth were carried out at the high magnifications attainable in the TEM [1, 17-22]. The vast increase in useful magnification (up to approximately 100,000 times) and resolution, compared with optical microscopy, enabled researchers to examine and interpret the fine details of complex striation patterns [2, 37, 39] and resolve striation spacings as small as 175Å (17.5 nm) [43]. However, major drawbacks associated with the fabrication and examination of the two-stage plastic-carbon replicas did exist. The maximum replica area that could be examined in the TEM at any one time was limited to 3 mm dia. and approximately 25 percent of this area was totally obscured by the replica support grid. In addition, tearing of the extremely fragile carbon replica could preclude examination of large regions and folding or curling of the replica edge areas on the support grid made examination of fatigue crack initiation regions difficult. Although the TEM did provide a satisfactory method of carrying out crack growth studies at high magnifications, these limitations often made data acquisition laborious, time consuming and expensive.

### 6.3 Scanning Electron Microscopy (SEM)

The modern SEM [17, 31, 52] with its TV scanning rate and improved resolution is particularly well suited for fracture surface analysis with relatively few major drawbacks compared with high magnification optical and transmission electron microscopy. The SEM allows direct examination, with a useful magnification from approximately 25 to 50,000 times, of most fracture surfaces with little or no specimen preparation required for electrically conductive materials. Non-conductive materials are usually coated with a thin layer of a conducting material, such as carbon, aluminum, gold or gold-palladium alloy. These coating materials are generally applied to the specimen surface by high-temperature vacuum evaporation or by plasma discharge techniques [52, pgs 211-216]. The major disadvantage of the SEM is the limited size of sample (usually 2 cm to 5 cm) that can be accommodated in the specimen vacuum chamber and be conveniently traversed and manipulated in the specimen stage. This limitation often requires the cutting up of larger specimens, especially those usually associated with full-scale component tests. This does not have to be a serious limitation provided that proper documentation before sectioning and judicious care of the fracture surface during sectioning is undertaken.

When it is not possible to cut up large samples, replicas of the fracture surface can be prepared and, after coating, examined in the SEM in much the same manner as a small section of the specimen [12, pg 17]. However, coated plastic replicas will not yield the same clarity or resolution as direct examination of the fracture surface. In addition the relatively thin conducting coating may require lower accelerating voltages and filament/beam currents to minimize 'burn-through' that will cause localized destruction of the replica surface.





MICROCOPY RESOLUTION TEST CHART  
NATIONAL BUREAU OF STANDARDS 1963 A

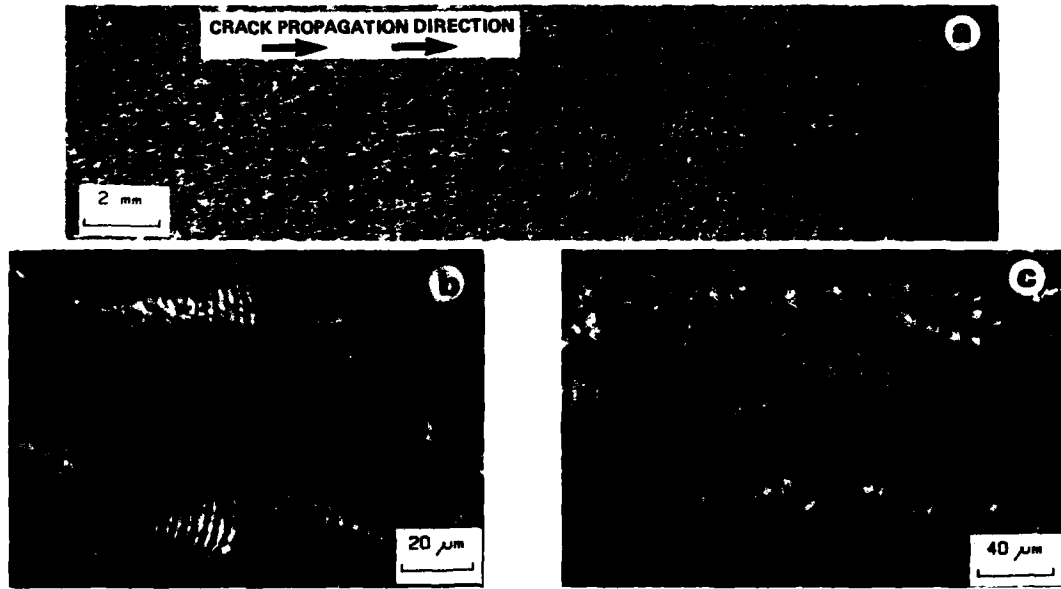


FIGURE 6: OPTICAL MICROSCOPY (BLOCK LOADING, SEE FIG. 5) - ALUMINUM ALLOY  
(b) AREA 'D', FIGURE 6(a), (c) AREA 'E', FIGURE 6(a)

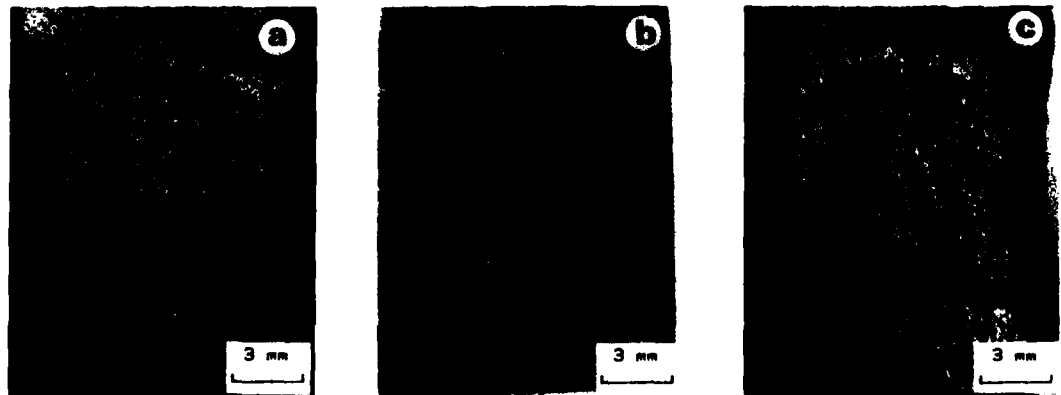


FIGURE 7: SURFACE ILLUMINATION IN LOW POWER OPTICAL MICROSCOPY, (a) VERTICAL, (b) CIRCULAR,  
(c) OBLIQUE (FRACTURE SURFACE TILTED 20° ABOUT AXIS PARALLEL TO CPD)

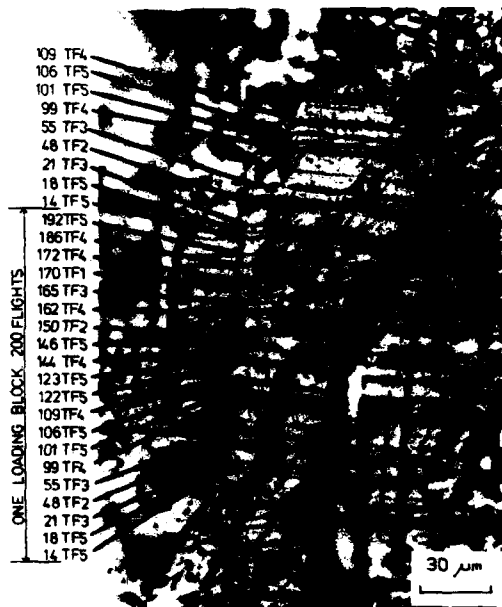


FIGURE 8: OPTICAL MICROSCOPY - SHADOWED PLASTIC REPLICA, VERTICAL ILLUMINATION - ALUMINUM ALLOY (ORIGINAL PHOTOGRAPH AND PERMISSION TO PUBLISH GENEROUSLY SUPPLIED BY MR. N.T. GOLDSMITH, DEPT. OF DEFENCE, AERONAUTICAL RESEARCH LABORATORIES, AUSTRALIA)

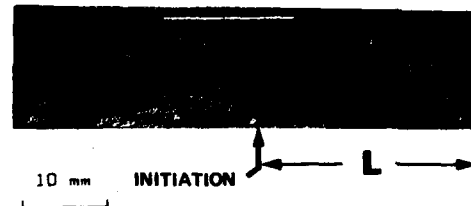


FIGURE 9: 'IRREGULARLY' SHAPED FATIGUE FRACTURE SURFACE WHERE HALF CRACK LENGTH 'L' IS TWO TIMES CRACK PENETRATION DISTANCE 'P'

## 7. SPECIMEN PREPARATION AND EXAMINATION PROCEDURES

It is sometimes necessary to remove the cracked portion of a large component and/or open up the crack in the laboratory in order to examine the fracture surfaces. After complete documentation [17, pgs 11-26] meticulous care must be taken during the handling and cutting of the component to ensure that the fracture surfaces and areas adjacent to them (e.g. initiation regions) are not damaged or altered [17, pgs 9, 10].

Component and full-scale structural fatigue tests conducted in normal laboratory atmospheric conditions form fracture surfaces that generally are free from the severe mechanical and corrosive damage that is often associated with service failures. Preparation of the fracture surfaces for microscopic examination [17, 31, 53] is therefore relatively straightforward and generally involves removal of surface oil films and debris caused by fretting or impacting of the mating fracture surfaces during crack growth or by dye penetrants that have seeped into the fatigue crack during inspection procedures. This debris can usually be removed by ultrasonic cleaning in suitable organic solvents such as acetone or alcohol. If the debris is extremely adherent, repeated 'replication' of the fracture surface (using 0.1-0.3 mm thick cellulose acetate tape) has been found to be an effective method of removal [53]. Particularly for SEM examination, replica cleaning is followed by thoroughly washing the fracture surface in acetone to remove any residual particles of plastic tape. Plastic, or any other electrically non-conducting debris remaining on the surface will 'charge up' in the electron beam and will hamper examination of the affected area in the SEM.

As mentioned previously, the size of specimen that can readily be examined in the SEM is usually limited to approximately 2 cm to 5 cm and this often requires the sectioning of larger components. As indicated in Case 6, (see Figs. 36 and 39) fracture surfaces with relatively long crack lengths should be carefully marked and sectioned to facilitate microscopic examination along the path of maximum crack growth. It has been found that placing an adhering tape, plastic replicas or plastic lacquer spray on the areas to be examined can provide good protection from minor mechanical damage during sectioning procedures. In order to preserve as much striated surface as possible it is also desirable to fracture, rather than cut, the fracture surface to be examined when the microscope cannot accommodate the complete fracture surface.

Specific fracture surface examination procedures for acquiring FCG information depend on several factors such as, 1) the nature of the recurring striation pattern, 2) total fatigue crack length and 3) the microscopic equipment used for the analysis. After an overall low power optical and/or SEM examination, it is preferable to begin the detailed high magnification examination toward the end of the Stage II fatigue crack region where striation formation is relatively continuous with no large rapid fracture areas. In this region the stress intensities are relatively large compared with those in the initiation region, and therefore the striation pattern details are generally more readily defined and easier to correlate with specific portions of the load spectrum (see Figs. 2 and 5). Once the recurring striation pattern and the appropriate crack growth spacings have been established for this region it is generally easier to recognize and interpret these features at shorter crack lengths. Crack lengths and striation or load block spacings are measured along a predetermined line generally coinciding with the path of maximum crack penetration or maximum crack length. For irregularly shaped fatigue fracture surfaces the maximum crack length may be considerably larger than the maximum depth of penetration, Figure 9, and FCG rates for both crack directions may be required. When the recurring crack growth spacings are relatively large and well defined, their values can be obtained directly using a travelling light microscope (low power optical microscopy) or by the micrometer specimen stage translation mechanism incorporated in optical and scanning electron microscopes. When the spacings are relatively small (in the order of 5 μm or less) their values are generally obtained from photographs. For direct crack length and incremental crack growth measurements, it is preferable to examine and photograph fracture surfaces or replicas that lie in a plane approximately normal to the direct incident light path or electron beam. However, it is sometimes necessary to tilt the fracture surface or replica to resolve or better define the striation pattern details. In these cases the fracture surface should be tilted, in either direction, about an axis normal to the crack propagation direction. Normally, tilt angles up to approximately 40° would be sufficient to enhance and observe these features. When measuring crack lengths and crack growth spacings directly or from photographs of tilted fracture surfaces it is necessary to correct these values since foreshortening of the projected images would yield values smaller than the true values.

## 8. CASE STUDIES

### 8.1 CASE 1 Striation Counting — SEM, TEM — Aluminum Alloy

Figure 10, shows the fracture surface of a 7075 aluminum alloy component that failed during a full-scale aircraft fatigue test after 55,508 equivalent flights. Three discrete levels of gust and manoeuvre loads were involved in the component failure, Table 1, and each block of 8460 load cycles was equivalent to 1000 flights. The 8460 cycles were randomly applied and the random sequence for the 1000-flight load block was repeated for the duration of the test, i.e. 55,508 blocks. As indicated in Figure 10, fatigue crack initiation of segments A, B and C occurred at the two fastener holes with the general direction of crack growth indicated by arrows A, B and C. Figure 11 clearly shows the faceted, discontinuous nature of striation formation. As demonstrated by the sequence of 85 striations, area B, Figure 11, SEM examination revealed that all three gust and manoeuvre load levels formed well defined single cycle striations over the majority of the fracture surface of all three segments. For this increment of crack growth, Figure 11(c), it was possible to correlate the 85 striations with the portion of the load program that had resulted in their formation. Examination of the load sequence print-out, Figure 11(c), established that this striation sequence, consisting of 77 cycles of level 1 load, 7 cycles of level 2 load and 1 cycle of level 3 load, corresponds precisely with cycles 7,428 to 7,512 of the 1000-flight load block. It was also established that this sequence of 85 cycles was unique in the 8460-cycle load block. As evident in Figure 11(c), the level 2 and 3 loads, in general, produced a significantly greater increment of crack growth than level 1 loads but the difference in growth increments between level 2 and 3 loads was generally not so apparent.

This sequence of 85 striations will also serve to demonstrate how striation spacings and crack growth rates were derived from fractographs obtained from the SEM. This increment of crack growth, located 7 mm from the point of crack nucleation, segment B, represented a crack advance of some 54  $\mu\text{m}$ . Since 8460 load cycles were contained in each load block of 1000 equivalent flights, it was possible to deduce that at this location, approximately 1587 load cycles or 188 flights would be required to advance the crack a distance of 1 mm. By repeating a similar procedure for various groups of striations at numerous points along the crack length, it was possible to derive the curves relating crack growth rates to fatigue crack length for all three segments. It should be noted that for segments A and B it was not possible to resolve the increments of crack growth formed by level 1 loads in the initiation regions. However, as shown in Figure 12, striations formed by levels 2 and 3 were clearly resolvable in this region, in the TEM. For the initial crack length of 12 mm and 1 mm for segments A and B respectively, growth rates were derived by considering only the 856 load cycles of level 2 and 3 that were applied in each 1000-flight load block. For Figure 12, this 18  $\mu\text{m}$  increment of crack growth, located 2.7 mm from the crack initiation site of segment A, indicated the presence of 49 striations formed by load levels 2 and 3. Based on 856 level 2 and 3 cycles per 1000-flight block, this yields 2723 cycles (levels 2 and 3 only) or 3180 flights to advance the crack 1 mm at this location. It is assumed that the spaces between the visible striations in Figure 12 represent crack growth due to the application of load cycles at level 1, and that the crack tip stress intensities due to level 1 loads were insufficient to form resolvable striations at this location. From the TEM and SEM derived data, the crack growth curve for segment A was established, Figure 13. Based on the assumption that final fracture of segment A occurred at 55,508 flights, Figure 14 shows the crack growth history relating flights to crack length. From this relationship crack initiation for segment A was estimated to have occurred at between 15,000 and 20,000 flights. The relative accuracy of this analysis was indicated by the correlation of two macroscopically visible crack growth bands, located some 5 mm and 10 mm from the crack initiation site, small arrows Figure 10, with a series of 'load dumps' that occurred at approximately 42,500 flights and again at 47,300 flights. If it is assumed these macroscopic arcs were formed by these load perturbations, an overall estimated accuracy within approximately 6% would be justified. Based on the assumptions that final fracture of segments A and C occurred simultaneously and that crack initiation of segment C immediately followed final fracture of segment B, similar analyses indicated that crack initiation of segments B and C occurred at approximately 44,000 and 55,200 flights respectively.

TABLE 1: GUST AND MANOEUVRE LOADS

LEVEL	NOMINAL COMPONENT STRESS LEVEL lb/in <sup>2</sup> (MPa)		CYCLES PER 1000 FLIGHT BLOCK
	MAXIMUM	MINIMUM	
1	5,604 (38.6)	-1,452 (-10.0)	7,604
2	7,248 (50.0)	-3,147 (-21.7)	746
3	8,240 (56.8)	-4,736 (-32.6)	110
TOTAL CYCLES PER LOAD BLOCK			8,460

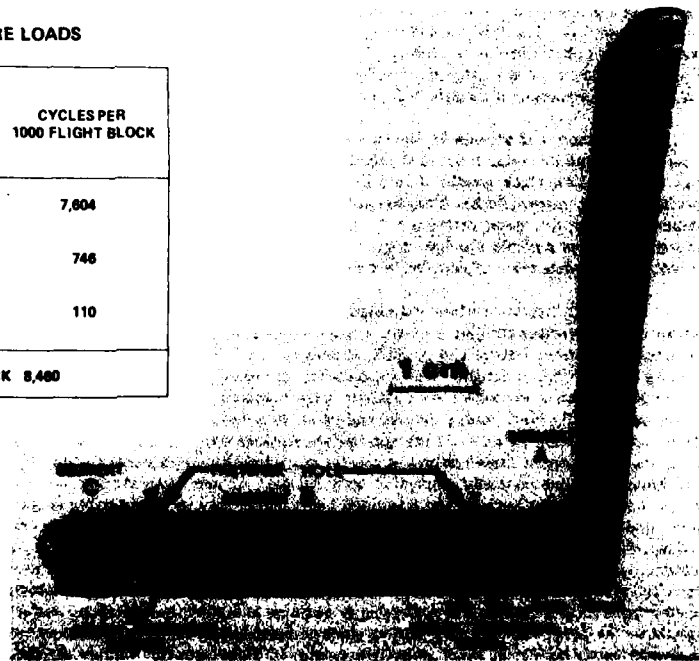


FIGURE 10: COMPONENT FRACTURE SURFACE — 7075 ALUMINUM



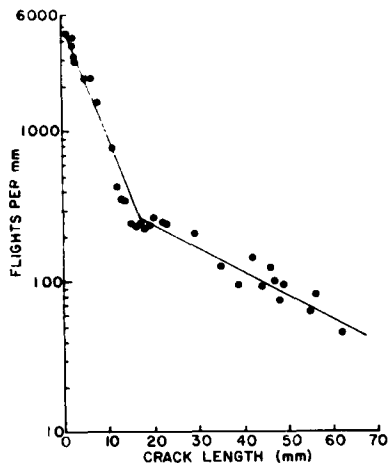


FIGURE 13: FATIGUE CRACK GROWTH RATE DATA AS DERIVED FROM GUST AND MANOEUVRE LOAD STRIATION SPACINGS

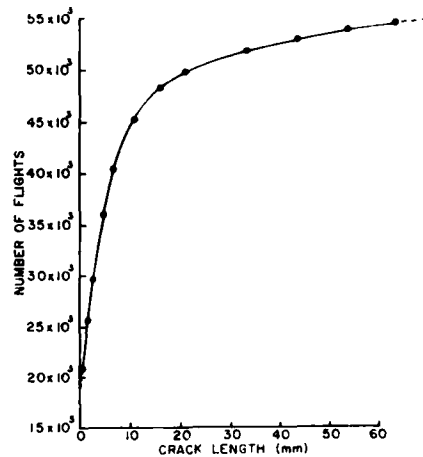


FIGURE 14: CRACK GROWTH HISTORY DERIVED FROM GROWTH RATE DATA

#### 8.2 CASE 2 Striation Counting — TEM — Low Alloy Steel

Figure 15 shows a steel alloy aircraft component that failed during a two-phase, constant amplitude fatigue test. The 4330 V MOD steel alloy (AMS 6411) had an ultimate tensile strength of 230 ksi (1590 MPa) and a hardness of 45 Rc. During the first phase of the test, 400,000 load cycles ranging between 12 ksi (83 MPa) and 45 ksi (310 MPa) were applied. In the second phase a total of 52,898 cycles ranging between 0.1 ksi (0.7 MPa) and 75 ksi (517 MPa) had been applied when final rapid fracture occurred. The fracture surface, Figure 16, revealed that crack initiation occurred independently in two bolt hole regions, arrows, Figures 15 and 16, and merged after onset of final rapid fracture. Crack growth rates for the 8.4 mm crack length A, Figure 16, were derived from over 200 fractographs used in this analysis, Figure 17. By numerical integration of this curve it was possible to derive the crack growth history, Figure 18, relating cycles to crack length. This curve indicates that some 42,000 cycles (phase two) were involved in the growth of crack A and based on final fracture at 52,898 cycles, crack initiation occurred after the application of approximately 11,000 cycles. Since no macroscopic or microscopic evidence of a load level change was observed on the fracture surface, this would further substantiate the conclusion that the crack did not initiate prior to the application of the more severe phase two load cycles.

Figure 19 shows three TEM fractographs (using two stage carbon-plastic replicas) taken at various crack lengths along the path indicated by arrow A, Figure 16. Although these areas exhibited reasonably well defined striations it must be remembered that they were among the best selected from over 200 fractographs. A comparison of these three striated areas with Figure 11, Case 1, clearly shows the significant difference in the general appearance (at the higher magnifications) of single cycle striations formed in aluminum alloys and medium strength low alloy steels. For medium and high strength steels the striations are generally more poorly defined and discontinuous, and those regions suitable for quantitative evaluation appear in relatively few areas (estimated to be as small as 1% of the total stage II fatigue fracture region). Although reasonably accurate crack growth rates for these materials can be derived from fracture surfaces formed by constant amplitude loading [25, 26, 46, 48] or simple programmed block loading (see Case 4), these factors make it difficult or impossible to acquire this information when more complex or random load application formats are used.

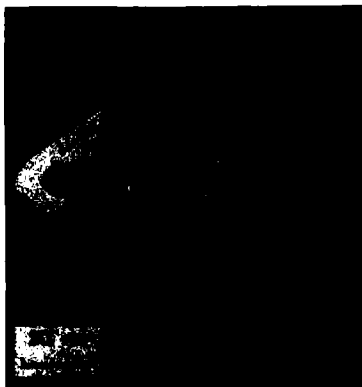


FIGURE 15: FAILED COMPONENT — 4330 STEEL

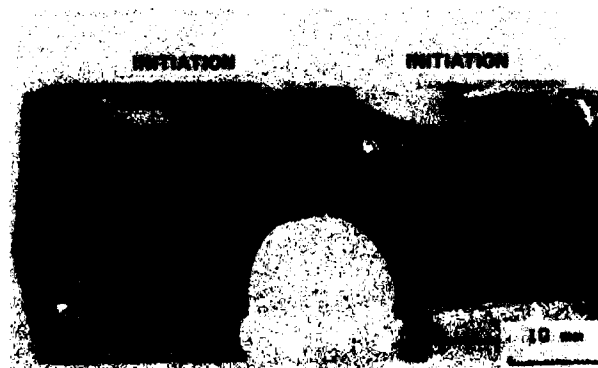


FIGURE 16: FRACTURE SURFACE

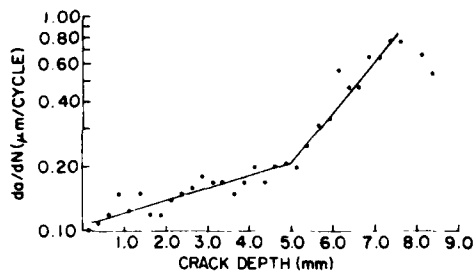


FIGURE 17: FATIGUE CRACK GROWTH RATE DATA DERIVED FROM STRIATION SPACINGS

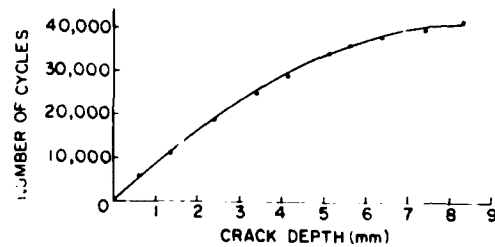


FIGURE 18: CRACK GROWTH HISTORY DERIVED FROM GROWTH RATE DATA

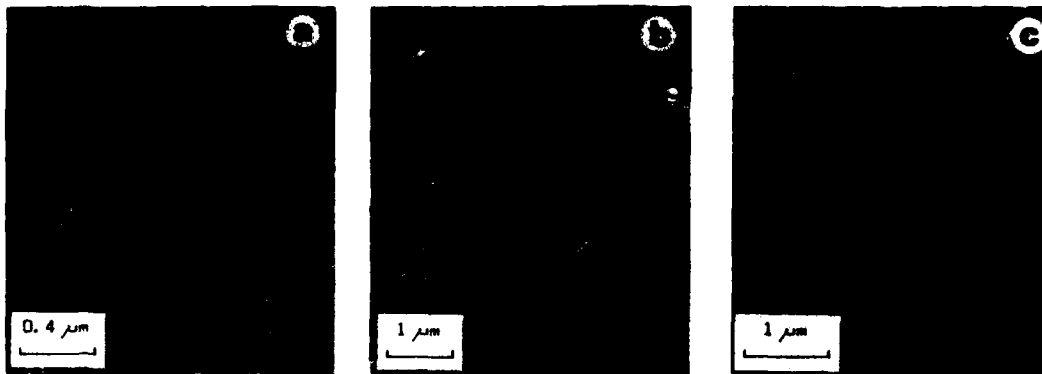


FIGURE 19: TEM FRACTOGRAPHS (CRACK SEGMENT 'A', FIG. 16)  
 (a) CRACK DEPTH 0.2 mm,  $da/dN$  0.08  $\mu\text{m}$ , (b) CRACK DEPTH 3.2 mm,  $da/dN$  0.21  $\mu\text{m}$ , (c) CRACK DEPTH 8.4 mm,  $da/dN$  0.54  $\mu\text{m}$

### 8.3 CASE 3 Load Block Measuring — Optical — Aluminum Alloy

**NOTE** The specimen, test information and optical crack growth data were generously supplied by Dr. J.M. Potter, Air Force Wright Aeronautical Laboratories (AFSC), Wright-Patterson Air Force Base.

Figure 20(a), shows a typical fatigue crack that was formed during a fastener hole quality test. Apparently the testing of six hundred, 7475-T7651 aluminum specimens necessitated the development of an accurate, but relatively quick, convenient and inexpensive method to evaluate 1200 'short' fatigue cracks [5]. Since this material formed well defined crack growth bands under the load spectrum used, it was possible to use low power optical microscopy, (10 to 30 magnification) using oblique illumination, to acquire FCG information over relatively short crack lengths. The load spectrum applied was a blocked, flight-by-flight history that was repeated every 400 equivalent flight hours. Each 400-hour block contained 240 discrete load blocks with a total of 18,915 cycles. For the subject specimen the fatigue test was terminated before final fracture after the application of 40 load blocks (16,000 flight hours).

As indicated by arrows A, Figures 20 and 21, the fatigue crack was initiated in the bore of the hole and penetrated a total of 2.3 mm. Figures 20(b) and 20(c) show several well resolved crack growth bands (striations) located within 0.3 mm of initiation. The first resolvable increment of crack growth, attributed to the application of one complete load block, was identified within 20  $\mu\text{m}$  of the crack initiation site, Figure 20(c). Figure 21 shows the general appearance and spacings of the crack growth bands during the latter stages of crack growth. The crack growth curve, Figure 22, was derived from the optical microscope measurements.

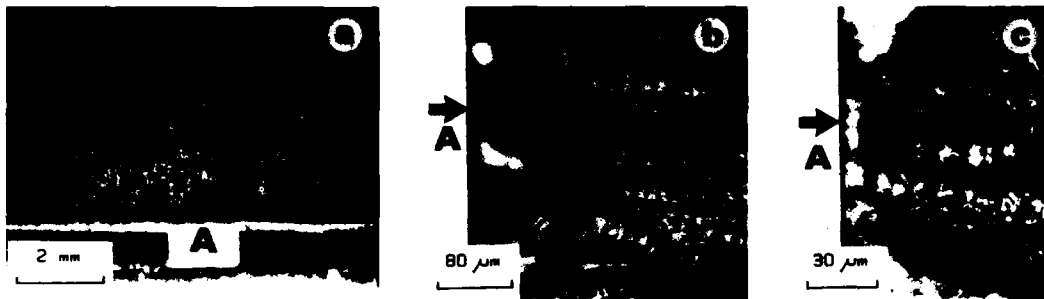


FIGURE 20: ARROWS 'A' INDICATE FATIGUE CRACK INITIATION SITE (a) FRACTURE SURFACE — 7475-T7651 ALUMINUM, (b) AND (c) CRACK GROWTH BANDS (STRIATIONS) IN INITIATION REGION, (c) DISTANCE BETWEEN SMALL ARROWS REPRESENTS CRACK GROWTH THAT OCCURRED DURING THE APPLICATION OF THREE COMPLETE LOAD BLOCKS (1200 EFH)

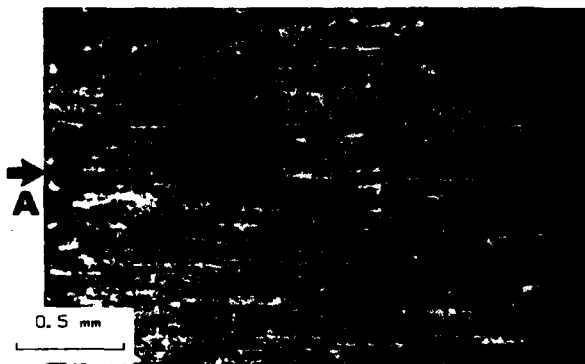


FIGURE 21: CRACK GROWTH BANDS IN LATTER STAGES OF FATIGUE CRACK GROWTH. LONG ARROW INDICATES CRACK GROWTH THAT OCCURRED DURING APPLICATION OF LOAD BLOCKS 26 TO 40 (6000 EFH)

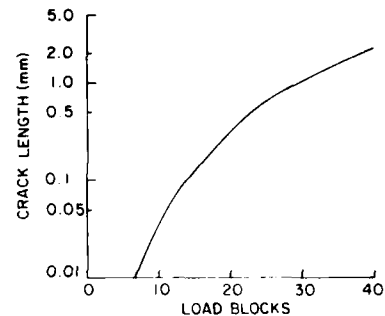


FIGURE 22: CRACK GROWTH HISTORY DERIVED FROM GROWTH BAND SPACINGS

#### 8.4 CASE 4 Load Block Measuring — Optical (transmitted light-replica) — Steel Alloy

The fracture surface of a 4340 steel transport joint (Fig. 23) that failed during a full-scale aircraft fatigue test is shown in Figure 24. The fatigue crack was initiated in the region indicated by arrows A, Figures 24 and 26(a), and propagated to a length of 45 mm when, during the application of the maximum load in block 483, final rapid fracture occurred. Each load block of 50 equivalent flight hours consisted of 461 cycles that were applied in a lo-hi-lo format over a range of 1.0 'G' to 6.0 'G', Figure 25.

Examination of plastic replicas of the fracture surface using transmitted light revealed the presence of well defined crack growth bands (striations), Figure 26, over a crack length from 1.2 mm to 45 mm from the crack initiation site. Based on the assumption that each striation represents the increment of crack growth that occurred during the application of one complete load block, it was possible to derive the crack growth curve shown in Figure 27. Striation spacing measurements were taken along the path indicated by arrow B, Figure 24. As indicated in Figure 27, approximately 200 load blocks were accounted for over the crack length from 1.2 mm to 45 mm and approximately 10 blocks accounted for the final 30 mm of fatigue crack growth. Extrapolation of the curve also indicated that at a crack length of approximately 0.2 mm, an estimated 150 load blocks had been applied.

Figure 26(c) shows an area of 4 relatively coarse striations (corresponding approximately to load blocks 440 to 443, Fig. 27) that was observed some 9 mm from the initiation site, arrows C, Figures 24 and 26(a). Since these striation spacings were considerably larger than the spacings immediately preceding or following them, it was speculated that loading perturbations caused a significant increase in the transport joint stress level during load application in blocks 440 to 443. Unfortunately, no test evidence could account for this apparent increase in stress and, therefore, it was not possible to use this 'abnormal marker band' as an indication of the overall accuracy of the analysis.

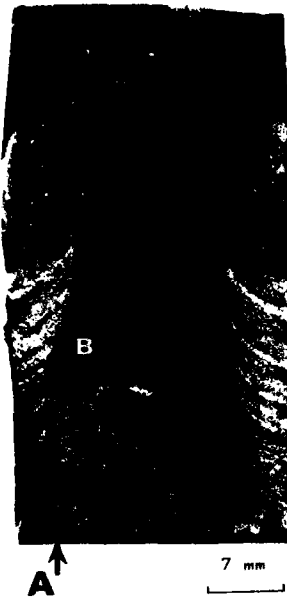


FIGURE 24: FRACTURE SURFACE

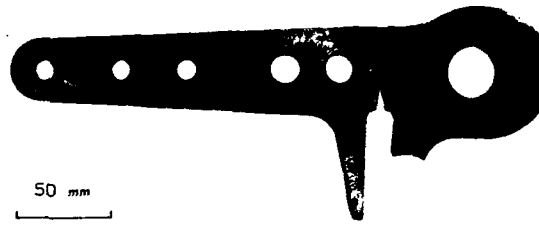


FIGURE 23: FAILED TRANSPORT JOINT - 4340 STEEL

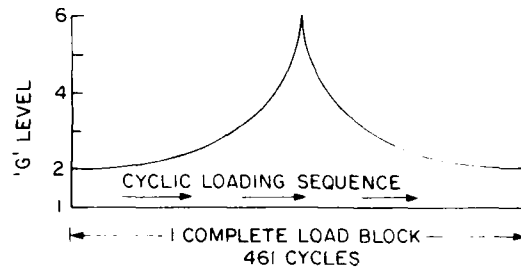


FIGURE 25: LO-HI-LO LOAD SPECTRUM

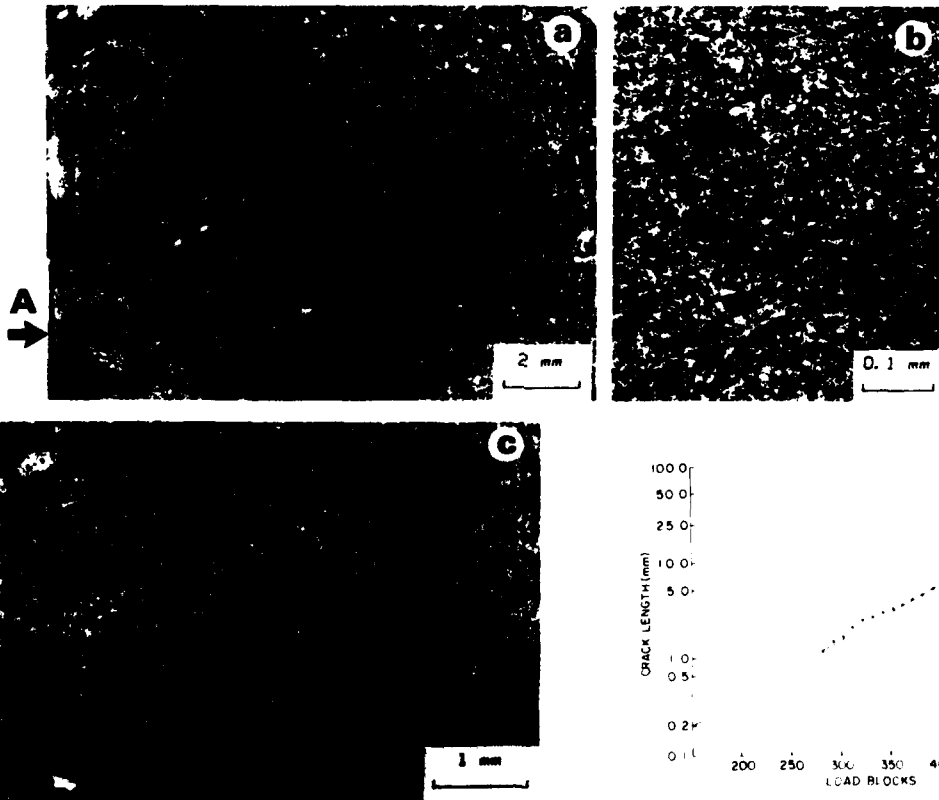


FIGURE 26: CRACK GROWTH BANDS (TRANSMITTED LIGHT-REPLICA)  
 (b) 1.5 mm FROM CRACK INITIATION SITE. DISTANCE BETWEEN ARROWS INDICATES CRACK GROWTH THAT OCCURRED DURING APPLICATION OF 10 COMPLETE LOAD BLOCKS, (c) LOADING PERTURBATION AREA

FIGURE 27: CRACK GROWTH HISTORY DERIVED FROM GROWTH BAND SPACINGS

### 8.5 CASE 5 Load Block Measuring — SEM — Aluminum Alloy

The fracture surface of a 7075 aluminum alloy extrusion that failed during a full-scale aircraft fatigue test is shown in Figure 28. The component failure was found during a routine visual inspection after 12 complete load blocks (36,000 equivalent flying hours (EFH)) of the fatigue program had been applied. The gust and manoeuvre loads involved in the component failure were applied in a block type format, Figure 29. Each complete load block of 3,000 EFH contained 304,710 cycles.

As indicated by arrows A and B, Figure 28, crack initiation occurred on either side of the fastener hole. The fatigue cracks propagated through the 4 mm wall thickness and then proceeded in the direction indicated by arrows A and B, Figure 28, for a distance of 130 mm and 10 mm respectively. Crack growth data was determined for crack length A only.

SEM examination of the initiation region, Figure 30, revealed 6 bands of relatively coarse, similarly spaced striations located within 7.3 mm of the initiation site, Figure 31. Figures 30(b) and (c) show a portion of the first and fourth of these bands located 1.0 mm and 2.2 mm respectively from the initiation site. Each of these bands contained approximately 42 striations and, as expected, was readily correlated with the most severe segment of the load block, i.e. the 42 E-A load cycles. For the initial 3 mm of crack growth containing the 5 E-A striation bands, Figure 31, it was not possible to identify any other crack growth regions formed by the less severe load levels. However, with increasing stress intensities at the longer crack lengths it was possible to identify striation bands formed by both the D-A and C-A load levels. Figure 32(a) shows the transition region of the C-A to D-A load level located 0.5 mm before the 6th E-A band, Figure 32(b). While the D-A striations are clearly resolved (Fig. 32(a)) the stress intensities due to the C-A loads are still insufficient to form well resolved striations at this location. As indicated in Figure 33, at a crack length between 15 mm and 25 mm (area C, Fig. 28) it was possible to identify (in the SEM) the 5 crack growth bands formed by the C-A, D-A and E-A load levels. A similar final crack growth band region, area D, Figure 28, was also identified between 50 mm and 59 mm from the crack initiation site. Arrows E and F, Figure 28, show the location of the E-A fracture region in areas C and D respectively. By identifying and measuring the successive locations of the 42 striation E-A regions, and based on the assumption that final fracture occurred during load block 12 before the application of the E-A load cycles, it was possible to derive the crack growth curve shown in Figure 34. Extrapolation of the curve indicates that crack initiation occurred relatively early in the test, probably during the application of load block 1 or 2.

Figure 35 shows an area of the third E-A crack growth region (Fig. 31) that contained an obvious distortion in the otherwise evenly spaced striation pattern. This distortion of 6 striations, area D, Figure 35(b), was attributed to a series of load dumps and restarts that apparently had occurred during the application of one of the early E-A load blocks. Although this loading perturbation could have been utilized to correlate a particular load block with a precise location of the propagating crack front, and therefore would have provided a check on the accuracy of the analysis, the lack of detailed test information negated this possibility. Although visual inspection of the component area was reported to have been carried out following every 2nd load block application, it would appear that the crack was not detected during the load block 10 inspection at which time it apparently had propagated to a length of at least 25 mm, Figures 28, 33 and 34.

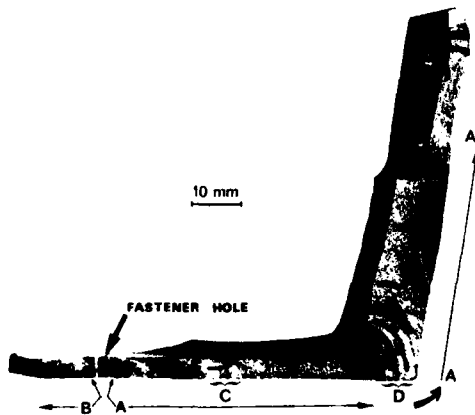


FIGURE 28: FRACTURE SURFACE — 7075 ALUMINUM

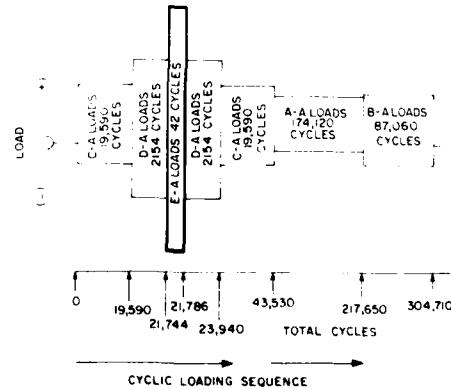


FIGURE 29: GUST AND MANOEUVRE LOAD SPECTRUM

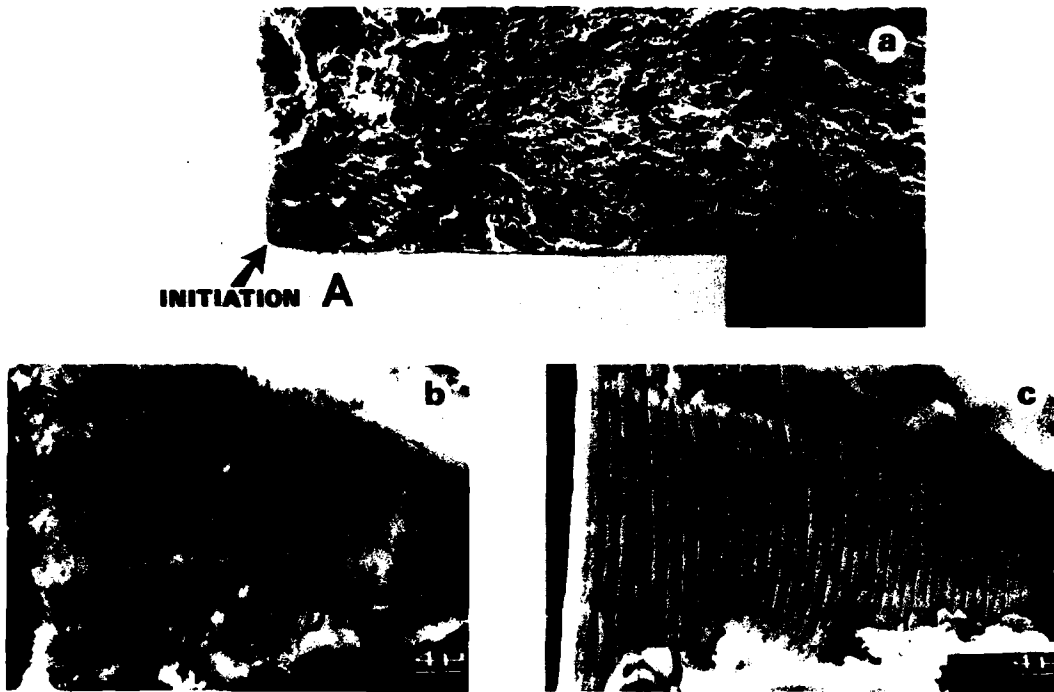


FIGURE 30: 42 CYCLE E-A LOAD LEVEL STRIATION BANDS IN SECTION 'A' INITIATION REGION  
 (b) NO. 1 E-A BAND - 1.0 mm FROM INITIATION SITE, (c) NO. 4 E-A BAND - 2.2 mm FROM INITIATION SITE

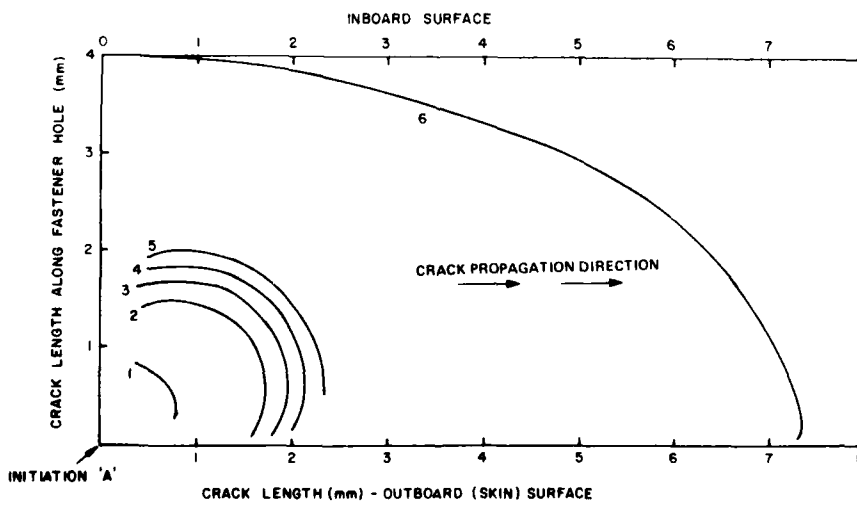


FIGURE 31: 42 CYCLE E-A LOAD LEVEL STRIATION BAND LOCATIONS IN SECTION 'A' INITIATION AREA

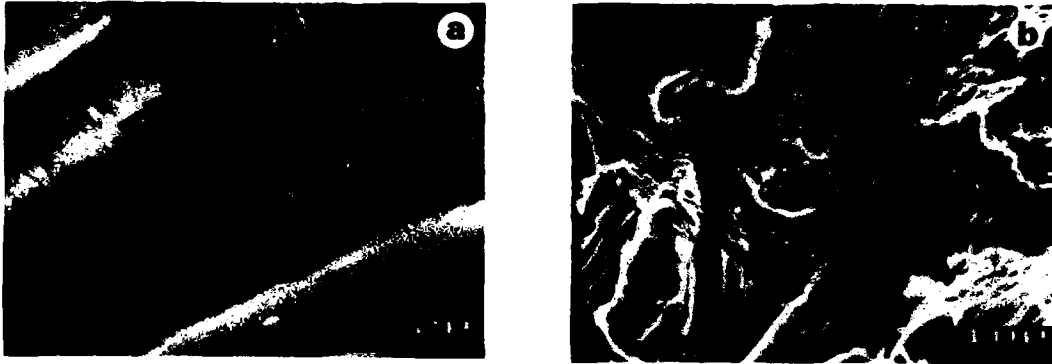


FIGURE 32: (a) C-A TO D-A LOAD LEVEL TRANSITION REGION, (b) D-A TO E-A LOAD LEVEL TRANSITION REGION

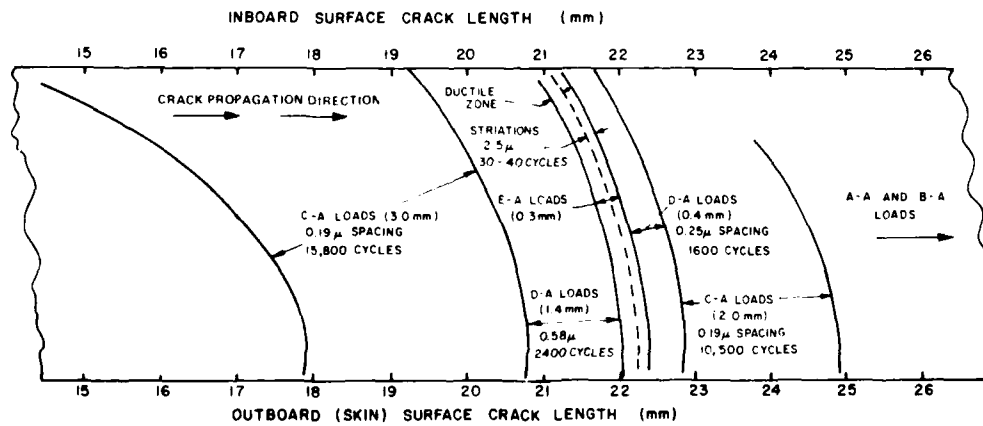


FIGURE 33: FRACTURE REGION SHOWING DISCRETE CRACK GROWTH INCREMENTS AND AVERAGE STRIATION SPACINGS BY C-A, D-A, E-A, D-A AND C-A LOAD SEQUENCE (AREA 'C', FIG. 28). NOTE RETARDATION EFFECTS IN D-A AND C-A CRACK GROWTH REGIONS FOLLOWING APPLICATION OF E-A LOADS

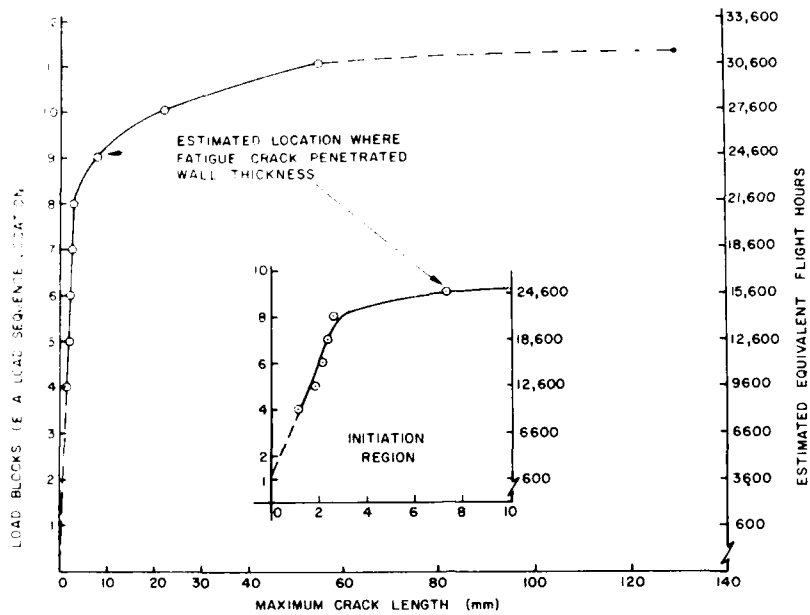


FIGURE 34: CRACK GROWTH HISTORY DERIVED FROM E-A LOAD LEVEL STRIATION BAND SPACINGS



FIGURE 35: (a) NO. 3 E-A STRIATION BAND LOCATED 2.0 mm FROM CRACK INITIATION SITE — SECTION 'A', (a) AND (b) LOAD DUMPING STRIATION SEQUENCE, AREA 'D'

- [11] D.W. Cameron, D.W. Hoepfner, A servohydraulic-controlled load frame for SEM fatigue studies, *Int. J. of Fatigue* 5 (1983) pp. 225-229.
- [12] J. Woodtli-Folprecht, I. Rady, Ein REM-Zusatz für die in situ Beobachtung von Oberflächen deformationen während Ermüdung, *Deutscher Verband für Materialprüfung*, 9. Sitzung Arbeitskreis Rastermikroskopie, 8.-9. Oct. 1982, Stuttgart, W.Germany.
- [13] D. Klaffke, Beobachtung der Orientierungsbestimmung der Oberflächenkristallite polykristalliner 99,999 % Al-Proben bei Biegewechselbeanspruchung, *Bundesanstalt für Materialprüfung (BAM) Berlin* (1978) Forschungsbericht 55.
- [14] W. Kromp, B. Weiss, R. Stickler, Direct observation of surface fatigue damage in the SEM, *Metallurgical Transactions* 4 A (1973) pp. 1167-1169.
- [15] K. Schulte, H. Nowack, K.-H. Trautmann, Beiträge der Rasterelektronenmikroskopie zur Analyse des Betriebsfestigkeitsverhaltens hochfester Leichtbauwerkstoffe, *Proceeding 9. Sitzung des Arbeitskreises Rastermikroskopie, Deutscher Verband für Materialprüfung (DVM), Stuttgart* 8./9. 10. 1979, pp. 71-82.
- [16] K. Schulte, Reihenfolgeeffekte auf die Ermüdungsrißausbreitung an hochfesten Aluminiumlegierungen, *Ph.D.Thesis, Ruhr-Universität Bochum* (1979), W.-Germany.
- [17] H.F.J. von Euw, R.W. Herzberg, R. Roberts, Delay effects in fatigue crack propagation, *ASTM-STP 513* (1972) pp. 230-259.
- [18] S. Jacoby, H. Nowack, H.T.M. van Lipzig, Experimental results and a hypothesis for fatigue crack propagation under variable amplitude loading, *ASTM-STP 595* (1976) pp. 172-183.
- [19] R.W. Herzberg, On the relationship between fatigue striation spacings and stretched zone width, *Int. Journ. of Fracture* 15 (1979) pp. R69-R72.
- [20] Y. Katz, A. Bussiba, H. Mathias, Micromechanisms of fatigue crack growth exposed to load transient effects, *Metal Science* 15 (1981) pp. 317-319.

#### 6. FIGURES

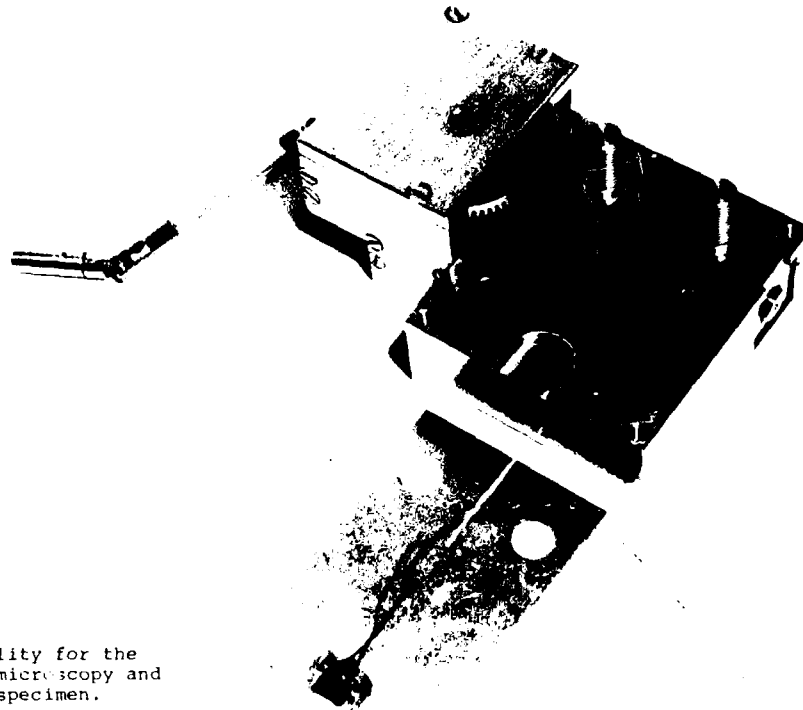


Fig. 1: Loading facility for the SEM in situ microscopy and modified CT-specimen.

### 3.3 Crack Propagation under a High-Low Sequence

In Fig. 2b was shown the fatigue crack propagation behavior after a high-low loading sequence. A significant crack retardation occurs followed up by a gradual increase in the crack propagation rates until the stable conditions corresponding to the low loading level are reached. This behavior becomes visible on the fracture surfaces in Fig. 11. (Fig. 11 stems from the same specimen, where the previous micrographs for the low-high transitions in Figs. 5, 7 and 10 were also taken from.) After the drop in the loading level the striations first disappear due to the significant decrease in the crack propagation rates. As the crack rates increase again, the striation spacings also gradually increase. The crack growth retardation is a result of the crack closure, as it has already been discussed together with the Figs. 9 and 10.

### 4. CONCLUSIONS

- In situ SEM analyses of the fatigue crack propagation are a useful tool to investigate the mechanical and physical contributions to the crack propagation. They enable a further insight into the widely unknown near surface processes of the fatigue crack propagation. However, because of the high expenses of in situ SEM analyses this cannot be seen as a general tool for engineering purposes.
- On the basis of in situ analyses together with SEM micrographs of the fracture surfaces the following investigation results were achieved:
  - The crack closure behavior becomes clearly visible. During loading the crack opening begins at some distance from the crack tip and approaches the crack tip as the load is further increased. This coincides with continuum mechanics analyses which terminate a triangular shape of the residual plastic displacements along the crack contour.
  - The fracture surface morphology influences the crack opening level.
  - Under a low-high loading sequence a stretched zone is formed during the first increase in load. The stretched zone consists of two parts. A reason may be that the crack first penetrates into material regions, which are cyclically plastically hardened from the low loading level period. After the crack reaches material, which is not yet cyclically hardened, the crack tilts.

Especially at the high loading level significant differences in the crack propagation at the specimen surface and in the interior of the specimen were observed. During the cycles at the high loading level (except the first half cycle) crack closure occurred only along that part of the crack which was formed during the high loading period.

- The crack retardation after a high loading sequence could clearly be identified on the SEM micrographs of the fracture surface.

### 5. REFERENCES

- [1] W. Elber, The significance of fatigue crack closure, ASTM-STP 486 (1971) pp. 230-242.
- [2] H. Führung, Berechnung von elastisch-plastischen Beanspruchungsabläufen in Dugdale-Rißscheiben mit RiBuferkontakt auf der Grundlage nichtlinearer Schwingbruchmechanik, Heft 30, Institut für Statik und Stahlbau der TH Darmstadt (1977).
- [3] H. Nowack, K.-H. Trautmann, K. Schulte, G. Lütjering, Sequence effects on fatigue crack propagation: Mechanical and microstructural contributions, ASTM-STP 677 (1979) pp. 35-43.
- [4] G. Marci, P.F. Packmann, Einfluß der Bruchflächenschließung auf die Struktur der Bruchflächen, Z. Metallkde. 68 (1977) pp. 47-51.
- [5] H.L. Ewalds, R.T. Furnee, Crack closure measurements along the fatigue crack front of center cracked specimens, Int. Journal of Fracture, 14 (1978) R53-R55.
- [6] Q. Bowles, The role of environment, frequency and wave shape during fatigue crack growth in aluminum alloys, Delft University of Technology, Report LR-270, Delft, The Netherlands (1978).
- [7] N. Walker, C.J. Beevers, A fatigue crack closure mechanism in titanium, Fatigue of Eng. Mat. and Struct. 1 (1979) pp. 135-148.
- [8] S. Suresh, R.O. Ritchie, A geometric model for fatigue crack closure induced by fracture surface roughness, Metallurgical Transactions, 13 A (1982) pp. 1627-1631.
- [9] R.O. Ritchie, S. Suresh, C.M. Moss, Near threshold fatigue crack growth in 2 1/4 Cr-1Mo pressure vessel steel in air and hydrogen, J. Eng. Mat. Tech., Trans. ASME Series H., 1980, vol. 102, pp. 293-299.
- [10] I. Lankford, D.L. Davidson, The effect of overloads upon fatigue crack tip opening displacement and crack tip opening/closing loads in aluminum loads (ICF 5), Advances in Fracture Research, Editor D. Francois, Cannes 1981, pp. 899-906.

yet available.

### 3.2.1 Crack Behavior at the Specimen Surface and on the Fracture Surfaces

In the previous sections various in situ SEM micrographs of the specimen surface were shown. In the following the essential question, how far surface observations of the crack behavior correlate to the behavior in the interior of the specimen, will be considered in more detail, and it will be shown that in situ observations represent a useful tool to get a better insight into the correlation (especially in the near surface areas).

In Fig. 7 SEM micrographs of the fracture surface are shown which were taken from the same crack tip area as the in situ micrographs in the Figs. 5a-d. In the micrograph three different stages a) - c) can be distinguished: Region a) represents the range with crack propagation at the low loading level and region c) the range with the crack propagation at the high loading level. Region b) was formed during the transition from the low to the high loading level. Region b) shall be considered in more detail in the following: During the increase in the load the crack propagation mechanism and the crack propagation rates in the interior of the specimen and at the specimen surface change. A predominant reason for this observation may be that the stress states change from the interior of the specimen with a predominantly plain strain condition to a predominantly plain stress condition in the near surface range of the specimen. A plain stress situation favours the formation of shear lips (which are actually present in the near surface range of the specimen) and the plain strain condition is responsible for the formation of the stretched zone and also the formation of the step within the stretched zone.

As it was already mentioned before, the formation of the step in the interior of the specimen is not adequately reproduced at the specimen surface. The crack advance at the specimen surface (where the shear lips are present) is greater. From these microscopical observations it has to be concluded that the surface behavior is not representative for the crack behavior in the interior of the specimens. This conclusion is further substantiated, if Fig. 2a is considered. The crack propagation measurements from the specimen surface give the impression that due to the transition from the low to the high loading level an acceleration of the crack growth occurs with a subsequent gradual decrease in the fatigue crack propagation rates (open circles in Fig. 2a). However, Fig. 8 shows that in the interior of the specimen a significantly higher crack growth rate is only observed for the first cycle after the transition to the high loading level. During the following cycles the striations exhibit approximately the same distances indicating that the fatigue crack propagation rate is already nearly stable.

The situation can become even more complicated than described before. The formation of a step during a low-high load transition may not be accompanied by a crack advance on the specimen surface at all. The Figs. 3 and 6 which are again taken from the same specimen show a situation where a crack with a branched crack tip was present in the low loading period. Figure 9 gives a sequence of pictures which were taken during the transition from the low to the high loading level. Only very small crack propagation can be observed for the upper crack branch, where a hook is formed (compare Fig. 9b). However, in the interior of the specimen a significant crack advance occurred. Furtheron, in the interior of the specimen no signs of the crack branching were found at all.

In conclusion, the correlation between the specimen surface effects and the behavior in the interior of the specimen is very weak.

### 3.2.2 Crack Propagation Mechanism

SEM in situ observations give further insight into the physical basis of the crack propagation. In this context the CTOD behavior is of special interest, which can be evaluated from the in situ micrographs. The Figs. 9a and 9c show micrographs for a same loading level before and after the low-high transition. It can be seen that the opening of the crack in Fig. 9c is larger. Even if the load is reduced to the minimum load of the loading period on the higher level, the crack opening is still larger than in Fig. 9a. In all cases no blunting of the crack tip was observed. This differs from the behavior in the interior of the specimen and also from the observations which are reported in the literature [6,10].

Another important phenomenon has to be mentioned: After the transition to the high loading period the crack remains open. As the main reason for that is seen the generation of high elastic plastic deformations in the plastic zone area ahead of the crack tip due to the increase in the load onto the high loading level, and the presence of large residual deformations upon unloading (compare also section 3.2.1).

In Fig. 10 the same crack tip area as in Fig. 5 is shown, after about 40 cycles were applied at the specimen at the high loading level. During the first cycle at the high loading level the crack propagated up to the vertical marker line. During the following cycles the crack further propagated up to the position as shown in Fig. 9c. The in situ SEM micrograph was taken at the minimum load in the cycle and it can be seen that crack closure occurred only along that part of the crack length, which was newly formed during the cycles applied after the first cycle of the high loading level. This result coincides with the above mentioned observations.

eration is measured at the high loading cycles (compare Fig. 2a). Under a high-low sequence the crack propagation rates quickly decrease down to a minimum value and then gradually increase again until values are reached, which correspond to the behavior under stable low loading constant amplitude loading (Fig. 2b). The constant amplitude crack propagation behavior is also shown in the figures as dotted lines.

### 3.1 Crack Propagation under Constant Amplitude Loading

As already mentioned before, the crack propagation is significantly influenced by the crack closure behavior. The existence of the crack closure was analytically shown by analyses which are mainly based on the Dugdale-Barenblatt model [2] and experimentally due to the measurements of the plastic displacements in front of and behind the crack tip [3]. In the Figs. 3a-d the in situ SEM observations of the crack behavior are given. The crack tip area at minimum load in a cycle is shown in Fig. 3a. The crack is completely closed. If the load is increased even up to about 30 % of the maximum load in the cycle, the crack surfaces still remain in contact (compare Fig. 3b). At some distance from the crack tip, however, the onset of the opening of the crack can be observed. The fact that the opening of the crack occurs apart from the crack tip is attributed to the residual deformations which are left behind the propagating crack on the upper and lower fracture surfaces and which exhibit an approximately triangular shape [2,3]. At 45 % of the maximum load in the cycle the opening of the crack approaches the crack tip area. At 60 % of the maximum load it is observed that the crack starts to open also at the crack tip (compare Fig. 3c). At maximum load the crack is fully open. All these observations are in a good agreement to the already mentioned analytical and experimental results in the literature. Walker and Beevers [7] investigated the crack opening behavior of the Ti-6Al-4V alloy using a replication technique. They observed that the crack closure process does not occur as a simple contact of the upper and lower crack surfaces, but that discrete points of the fracture surfaces come into contact. The preferred locations of contacts are those, where a misfit of the upper and lower surface due to the surface roughness was present. Lateron, Suresh and Ritchie [8] proposed a geometrical model for the consideration of the surface roughness induced crack closure. In the present study a similar behavior was also observed. This is shown in Fig. 4. Because of the unsteady crack morphology a crack contact occurs at discrete points, together with an abrasion of the material and deformations due to a peeling off process.

The microstructural appearance of the crack surface is one contribution to the crack closure besides others, as the mechanical environment, the local stress-strain response of the material and the instantaneous crack propagation mechanism [3].

### 3.2 Crack Propagation under a Low-High Sequence

The crack propagation behavior during a low-high loading sequence was shown in Fig. 2a. After the increase in the load the crack rates became rapidly larger. The results of the optical crack propagation measurements are indicated in the figure by open circles. The crack propagation was also determined on the basis of the striation spacings in the middle of the fracture surface of the specimen. These results are indicated by solid circles. In Fig. 5 in situ micrographs for the low-high sequence are shown. Figure 5a gives an overview of the crack tip region at 60 % of the maximum load at the low loading level. Figure 5b shows the closed crack at the minimum load. At the maximum load at the low loading level the crack is fully open (compare Fig. 5c). The crack advance during the first increase in the load onto the maximum load of the high loading period is shown in Fig. 5b. In order to find out how the specimen surface phenomena and the fracture surface morphology correlate, both types of micrographs were compared. In Fig. 6a it can be seen that during the increase in the loading level a step was formed, which is present over the entire width of the specimen. At the specimen surface the step contour becomes less pronounced. A higher magnification of the shape of the step is given in Fig. 6b. In the figure the striations, which were formed during the last cycles before the loading level was increased, become clearly visible. During the first increase onto the maximum load at the high loading level a stretched zone is formed, whereby two ranges of the stretched zone can be distinguished. At first the crack advance occurred perpendicular to the loading direction followed by the formation of a ramp. In Fig. 6c the behavior is schematically shown. The following reason may be especially important for the formation of the step: At the increase of the load up to the maximum load at the high loading level the stress intensity considerably increases, and with that the size of the plastic zone in front of the crack tip. The plastic displacements within the plastic zone are considerably larger as during the low loading period. This has also an important effect on all following load cycles. Along with the formation of the large plastic zone during the first increase in the load, the crack first advances deeply into material regions, which were intensively cyclically hardened during the loading period at the low loading level. After penetration through the cyclically hardened region the crack enters material regions which are less cyclically deformed. This may be the reason for the tilt in the crack propagation direction within the stretched zone in Fig. 6c.

The formation of stretched zones, which exhibit two stages during the application of overloads, has been also discussed by Herzberg [19] and Katz et al. [20]. They suggest that the width of the stretched zone and the step formation depend on the effective stress intensity value during the first high load maximum on the high loading level, and, probably, on the  $K_{IC}$ -value of the alloy. Katz et al. further assumed that the previous loading period has an influence, as well. A fully satisfactory explanation of the process is not

NEW ANALYSIS ASPECTS OF THE FATIGUE CRACK PROPAGATION  
BEHAVIOR BY SEM-IN SITU MICROSCOPY

by  
K. Schulte, K.-H. Trautmann, H. Nowack  
DFVLR - Institut für Werkstoff-Forschung  
D 5000 Köln 90  
West-Germany

SUMMARY

In situ analyses of fatigue crack propagation in a SEM enable a more detailed observation of the fatigue process. This is of special value for variable amplitude loading conditions, where pronounced crack accelerating and decelerating effects occur. Results of the in situ observation are shown and are compared to the fracture surface morphology in the interior of the specimen and in the vicinity of the specimen surface.

1. INTRODUCTION

After several decades of research in the field of fatigue crack propagation there are numerous questions, which still need answers. In situ scanning electron microscope (SEM) investigations enable a cycle by cycle observation of the crack propagation. The crack tip morphology and the crack advance during the increase and during the decrease of the load in a cycle can be studied. Analyses of this type are of special importance, if variations in the loading conditions occur. Under such circumstances an interaction of mechanical and microstructural contributions to the crack propagation occurs in such a manner that accelerations or decelerations of the crack propagation are observed. These nonlinearities of the crack propagation (sequence effects) cannot sufficiently be explained until now. One important contribution is the crack closure mechanism [1]. Analytical [2] and experimental [3] studies have shown that the crack closure process begins in the vicinity of the crack tip after the maximum load in a cycle has been passed. With the further decrease of the load an increasing portion of the upper and the lower crack surface come into contact. Regarding the crack closure process different interpretations are given in the literature. In [4,5] it is reported that the crack closure predominantly occurs close to the specimen surface. In [3,6-8] it is stated that the roughness of the fracture surface and deposits of corrosion products [9] increase the crack closure level, indicating that the crack closure occurs over the whole fracture surface.

In situ analysis techniques have been used already by several investigators. Davidson and Lankford [10] directly observed the crack tip opening displacement (CTOD). Cameron and Hoepfner [11], Woodtli - Folprecht and Rady [12], Klaffke et al. [13] and Kromp, Weiss and Stickler [14] used this technique for the analysis of the response of materials (surface roughness, formation of slip steps, initiation of cracks, short crack behavior) in the course of a fatigue loading. It has to be pointed out, however, that the in situ investigations can only monitor the behavior in the near surface range of the material. That is the reason why the possibilities to investigate the complete crack propagation process are limited. This limitation can be overcome by the use of special techniques, as for example by Bowles' replication methods [6]. In the present investigation another procedure was applied. Besides the in situ surface observations, SEM micrographs of the fracture surface were made, and both were compared for the interpretation of the crack propagation phenomena.

2. EXPERIMENTAL INVESTIGATIONS

For the in situ investigations a special loading facility was constructed (compare Fig. 1), which is mounted on a commercial specimen holder for scanning electron microscopes. The load is applied to the specimen by moving the two bolts of the loading facility via the z-drive of the specimen holder of the SEM [15].

For the in situ studies a modified CT-specimen (thickness: 1 mm) was used. This specimen was precracked in fatigue on a servohydraulic testing machine. During the loading in the servohydraulic machine the strain in the ligament of the specimen was measured and registered by a strain gauge. Later on, the same strain as it was observed during the precracking procedure was applied by the loading facility in the SEM.

The alloy investigated was the pure version of the high strength 7075 aluminum alloy, where no Cr, Fe and Si was present. With this alloy well defined striations could be observed on the fracture surfaces.

The loading histories, which were applied in the tests, were constant amplitude loading at stress ratios of 0.05 and of 0.33 and low-high and high-low block loading sequences again with the R-ratios of 0.05 and 0.33 for the individual block stages.

3. RESULTS AND DISCUSSION

The crack growth behavior which was observed in the tests is similar to that reported in the literature [16-18]. Under a low-high loading sequence an initial crack accel-

41. Forsyth, P.J.E.  
Powell, P.M.      Fatigue Crack Growth Rates for Very Short Cracks Developing at Fastener Holes in 7075 and 7010 Aluminum Alloys.  
Journal of Materials Science, Vol. 18, 1983, pp. 1852-1862.
42. McMillan, J.C.  
Pelloux, R.M.      Fatigue Crack Propagation Under Programmed Loads and Crack Tip Opening Displacements.  
Engineering Fracture Mechanics, Vol. 2, 1970, pp. 81-84.
43. Hertzberg, R.W.      Application of Electron Fractography and Fracture Mechanics to Fatigue Crack Propagation in High Strength Aluminum Alloys.  
Ph.D. dissertation, Lehigh University, Bethlehem, Pa., June 1965.
44. Hertzberg, R.W.  
Skibo, M.D.  
Manson, J.A.      Fatigue Fracture Micromechanisms in Engineering Plastics.  
Fatigue Mechanisms, Proceedings of an ASTM-NBS-NSF symposium, Kansas City, Mo., May 1978, J.T. Fong, Ed., ASTM STP 675, American Society for Testing and Materials, 1979, pp. 471-500.
45. Ruppen, J.A.  
McEvily, A.J.      Influence of Microstructure and Environment on the Fatigue Crack Growth Fracture Topography of Ti-6Al-2Sn-4Zr-2Mo-0.1Si.  
Fractography and Materials Science, ASTM STP 733, L.N. Gilbertson and R.D. Zipp, Eds., American Society for Testing and Materials, 1981, pp. 32-50.
46. Ritter, J.C.      Use of Fractography and Fracture Mechanics in Analysing Fatigue Cracks.  
Metals Forum, Vol. 5, No. 1, 1982, pp. 65-73.
47. Hertzberg, R.W.      Deformation and Fracture Mechanics of Engineering Materials.  
Wiley, New York, 1976, pp. 533-540, 598-615.
48. Masuda, C.  
Nishijima, S.      Quantitative Analysis of Fatigue Fractographs for Some Heat Treated Steels.  
Transactions of National Research Institute for Metals, Vol. 24, No. 3, 1982, pp. 22-27.
49. Darts, J.      Determination of Crack Growth Rates Under Flight-by-Flight Loading from Fracture Surface Markings.  
RAE Technical Report 78023, 1978, Royal Aircraft Establishment, Farnborough, Hampshire, England.
50. Goldsmith, N.T.      Fractographic Examinations Relevant to the F & W Mirage Fatigue Test.  
ARL-Mat-Tech-Memo-371, AR-001-295, Defence Science and Technology Organisation, Aeronautical Research Laboratories, Melbourne, Victoria, Australia, August 1978.
51. Roberts, E.C.      Integration of Optical and Electron Fractography Methods in the Study of Fatigue.  
Microstructural Science, Vol. 6, 1978, pp. 131-141.
52.      Practical Scanning Microscopy.  
J.I. Goldstein and H. Yakowitz, Eds., Plenum, New York, 1975.
53. Dahlberg, E.P.  
Zipp, R.D.      Preservation and Cleaning of Fractures for Fractography - Update.  
Scanning Electron Microscopy/1981/I, pp. 423-429.
54. Jost, G.S.      A Review of Australian Investigations on Aeronautical Fatigue During the Period April 1981 to March 1983.  
Structures Technical Memorandum 359, Dept. of Defence, Aeronautical Research Laboratories, 1983, p. 9/29.

21. Broek, D.  
van der Vet, W.J.                    Systematic Electron Fractography of Fatigue in Aluminum Alloys.  
NLR-TR 68002U, National Aerospace Laboratory NLR, The Netherlands, November 1967.
22. Whiteson, B.V.  
Phillips, A.  
Kerlins, V.  
Rawe, R.A.                            Special Fractographic Techniques for Failure Analysis.  
Electron Fractography, ASTM STP 436, American Society for Testing and Materials, 1968, pp. 151-178.
23. Albertin, L.  
Hudak, S.J., Jr.                      Effect of Compressive Loading on Fatigue Crack Growth Rate and Striation Spacing in Type 2219-T851 Aluminum Alloy.  
Fractography and Material Science, ASTM STP 733, L.N. Gilbertson and R.D. Zipp, Eds., American Society for Testing and Materials, 1981, pp. 187-201.
24. Bates, R.C.  
Clark, W.G.                            Fractography and Fracture Mechanics.  
Transactions American Society for Metals, Vol. 62, 1969, pp. 380-389.
25. Au, J.J.  
Ke, J.S.                                Correlation Between Fatigue Crack Growth Rate and Fatigue Striation Spacing in AISI 9310 (AMS 6265) Steel.  
Fractography and Materials Science, ASTM STP 733, L.N. Gilbertson and R.D. Zipp, Eds., American Society for Testing and Materials, 1981, pp. 202-221.
26. Hinton, B.R.W.  
Proctor, R.P.M.                      Quantitative Fractography of Fatigue Cracking of X-65 Pipeline Steel in Air and Sodium Chloride Solutions.  
Metals Forum, Vol. 5, No. 1, 1982, pp. 80-91.
27. Cruickshanks-Boyd,  
D.W.                                  A Comparison of Fatigue Crack Growth Rates as Determined by Striation Measurements and by Observations of Crack Length on the Specimen Surface During the Test.  
TR 76012, Royal Aircraft Establishment, Farnborough, U.K., January 1976.
28. Peel, C.J.  
Forsyth, P.J.E.                        The Quantitative Analysis of Fatigue Cracking Under Programmed Loading.  
TR 80073, Royal Aircraft Establishment, Farnborough, U.K., May 1980.
29. Stofanak, R.J.  
Hertzberg, R.W.                      The Effect of Replica Tilt on Striation Spacing Measurements.  
International Journal of Fracture, Vol. 20, 1982, pp. R-145 to R-149.
30. Underwood, E.E.  
Starke, E.A., Jr.                      Quantitative Stereological Methods for Analyzing Important Microstructural Features in Fatigue of Metals and Alloys.  
Fatigue Mechanisms, Proceedings of an ASTM-NBS-NSF symposium, Kansas City, Mo., May 1978, J.T. Fong, Ed., ASTM STP 675, American Society for Testing and Materials, 1979, pp. 633-682.
31.    Failure Analysis of Metallic Materials by Scanning Electron Microscopy.  
Eds., S. Bhattacharyya, V.E. Johnson, S. Agarwal and M.A.H. Howes, IIT Research Institute, January 1979.
32. Kershaw, J.  
Liu, H.W.                              Electron Fractography and Fatigue Crack Propagation in 7075-T6 Aluminum Sheet.  
International Journal of Fracture Mechanics, Vol. 7, No. 3, 1971, pp. 269-276.
33. Hertzberg, R.W.                      Fatigue Fracture Surface Appearance.  
Fatigue Crack Propagation, ASTM STP 415, Am. Soc. Testing Mats., 1967, p. 205.
34. Takemori, M.T.                        Fatigue Fracture of Polycarbonate.  
Polymer Engineering and Science, Vol. 22, No. 15, 1982, pp. 937-945.
35. Takemori, M.T.                        On a Fatigue Crack-Front Marking Technique for Polymers.  
Journal of Materials Science, Vol. 17, No. 9, 1982, pp. 2547-2552.
36. Rimnac, C.M.  
Hertzberg, R.W.  
Manson, J.A.                            Fatigue Fracture Surface Micromorphology in Poly(vinyl chloride).  
Fractography and Materials Science, ASTM STP 733, L.N. Gilbertson and R.D. Zipp, Eds., American Society for Testing and Materials, 1981, pp. 291-313.
37. McMillan, J.C.  
Pelloux, R.M.N.                        Fatigue Crack Propagation Under Program and Random Loads.  
Fatigue Crack Propagation, ASTM STP 415, Am. Soc. Testing Mats., 1967, p. 505.
38. Hertzberg, R.W.  
Mills, W.J.                              Character of Fatigue Fracture Surface Micromorphology in the Ultra-Low Growth Rate Regime.  
Fractography-Microscopic Cracking Processes, ASTM STP 600, C.D. Beachem and W.R. Warke, Eds., American Society for Testing and Materials, 1976, pp. 220-234.
39. Abelkis, P.R.                         Use of Microfractography in the Study of Fatigue Crack Propagation under Spectrum Loading.  
Fractography in Failure Analysis, ASTM STP 645, B.M. Strauss and W.H. Cullen, Jr., Eds., American Society for Testing and Materials, 1978, pp. 213-234.
40. Pelloux, R.M.  
Faral, M.  
McGee, W.M.                            Assessment of Crack Tip Closure in an Aluminum Alloy by Electronfractography.  
Fatigue of Engineering Materials and Structures, Vol. 1, 1979, pp. 21-35.

## REFERENCES

1. Wiebe, W. Quantitative Fatigue Crack Propagation Analysis by Means of Electron Fractography. Aeronautical Report LR-450, National Research Council Canada, National Aeronautical Establishment, March 1966, 17 pages.
2. Wiebe, W. Fracture Surface Analysis by Means of Electron Fractography. Canadian Aeronautics and Space Journal, Vol. 13, No. 3, March 1967, pp. 135-140.
3. Wiebe, W.  
Dainty, R.V. Notes on the Value of Fractography in Failure Analysis. NRC NAE LTR-ST-591, National Research Council Canada, National Aeronautical Establishment, Ottawa, Ontario, January 1973, 41 pages.
4. Wiebe, W.  
Dainty, R.V. Fractographic Determination of Fatigue Crack Growth Rates in Aircraft Components. Canadian Aeronautics and Space Journal, Vol. 27, No. 2, 1981, pp. 107-117.
5. Potter, J.M.  
Yee, B.G.W. Use of Small Crack Data to Bring About and Quantify Improvements to Aircraft Structural Integrity. AGARD-CP-328, Behaviour of Short Cracks in Airframe Components, Advisory Group for Aerospace Research and Development, NATO, April 1983, pp. 4-1 to 4-13.
6. Wang, D.Y. A Study of Small Crack Growth Under Transport Spectrum Loading. AGARD-CP-328, Behaviour of Short Cracks in Airframe Components, Advisory Group for Aerospace Research and Development, NATO, April 1983, pp. 14-1 to 14-15.
7. Dainty, R.V. Use of 'Marker Blocks' as an Aid in Quantitative Fractography in Full-Scale Aircraft Fatigue Testing: A Case Study. Fractography of Ceramics and Metal Failures, ASTM STP 827, J.J. Mecholsky and S.R. Powell, Jr., Eds., American Society for Testing and Materials, 1984, pp. 285-308.
8. Dimmig, W. Marker Band Evaluation Analysis and Results. Report SA160R9416, Fairchild Republic Company, Farmingdale, L.I., New York, 1979.
9. Shewmaker, A.P.  
Russ, J.L.  
Hopkins, J.L. Design for Maximum Durability and Damage Tolerance in the Manufacture of a Heavy Transport Wing. Presented at the 12th International Committee on Aircraft Fatigue Symposium, Toulouse, France, 24-30 May 1983.
10. Friedrich, S.  
Schijve, J. Fatigue Crack Growth of Corner Cracks in Lug Specimens. Report LR-375, Department of Aerospace Engineering, Delft University of Technology, The Netherlands, January 1983.
11. Wanhill, R.J.H.  
Schra, L. A Pilot Programme for Fatigue Marker Loads. Memorandum SM-83-018U, National Aerospace Laboratory, NRL, The Netherlands, March 1983.
12. Pittinato, G.F.  
Kerlins, V.  
Phillips, A.  
Russo, M.A. SEM/TEM Fractography Handbook. MCIC-HB-06, Metals and Ceramics Information Center, Battelle, Columbus, Ohio, December 1975.
13. Phillips, A.  
Kerlins, V.  
Whiteson, B.V. Electron Fractography Handbook. Technical Report ML-TDR-64-416, Wright-Patterson Air Force Base, Ohio, January 31, 1965.
14. Ryder, D.A. Elements of Fractography. Agardograph 155, NATO, Advisory Group for Aerospace Research and Development, November 1971.
15. Wiebe, W. A Fractographic Study of the Fatigue Failure of Aircraft Wheels. NRC NAE LR-541, National Research Council Canada, National Aeronautical Establishment, Ottawa, Ontario, November 1970, 26 pages.
16. Forsyth, P.J.E. The Determination of Fatigue Crack History from Fracture Surface Analysis, Advances in Crack Length Measurement, C.J. Beevers, Ed., Chameleon, London, 1982, pp. 3-40.
17. Fractography and Atlas of Fractographs. Metals Handbook, 8th Edition, Vol. 9, H.E. Boyer, Editor, American Society for Metals, Metals Park, Ohio, August 1974.
18. Beachem, C.D.  
Pelloux, R.M.N. Electron Fractography - A Tool for the Study of Micromechanisms of Fracturing Processes. Fracture Toughness Testing and its Applications, STP 381, American Society for Testing and Materials, 1965, pp. 210-244.
19. Phillips, A.  
Kerlins, V.  
Rawe, R.A.  
Whiteson, B.V. Electron Fractography Handbook - Specific Applications of Electron Fractography. Technical Report AFML-TR-64-416, Supplement II, Wright-Patterson Air Force Base, Ohio, March 1968.
20. McMillan, J.C.  
Hertzberg, R.W. Application of Electron Fractography to Fatigue Studies. Electron Fractography ASTM STP 436, American Society for Testing and Materials, 1968, pp. 89-123.



FIGURE 45: SECOND OBSERVED MARKER BAND, SURFACE A1, RIVET 1 (0.63 mm FROM CRACK INITIATION SITE), (b) MARKER BAND WIDTH:  $9.2 \mu\text{m}$ ; AVERAGE STRIATION SPACING SPACING:  $0.14 \mu\text{m}$

## 9. CONCLUDING REMARKS

Through the application of optical and electron microscopy, the case studies have shown that accurate FCG information can be acquired from fracture surfaces that have been formed by several types of load spectra and fatigue load application methods. In general the recurring striation pattern will be better defined and easier to identify if an 'ordered' load spectrum and load application method (for example blocked load levels applied in a lo-hi manner) is used. In some cases it may be necessary to alter the proposed spectrum, for example to include the use of 'marker loads', in an attempt to provide the means for acquiring this information. In these cases it is essential that the design-test engineers, in collaboration with the fractographer, ensure that the test parameters will provide 'readable' fracture surfaces. In full-scale tests, where extensive costs and testing times are involved, it may be necessary to pre-determine the 'readability' of fracture surfaces with an appropriate specimen testing program [7, 8]. However, for some materials and/or fatigue loading conditions, it may not be possible to derive FCG information by currently available fractographic means.

In several of the case studies involving full-scale aircraft testing, 'irregular' fracture surface topography, usually in the form of abrupt changes in striation spacing, was occasionally observed. In some cases these areas were identified and correlated with known loading perturbations and therefore provided an unexpected indication of the accuracy of the fractographic analysis. Unfortunately in other cases a lack of detailed test information did not permit similar irregularities to assist in deriving more accurate growth curves and crack initiation times. It should be emphasized to the test operators that this type of information should be accurately recorded since it could be fractographically significant even though fatigue cracks may not have been 'detected' at the time of an abnormal loading condition.

The selection of the appropriate microscopic equipment and techniques for acquiring FCG information will basically depend on the level of resolution and magnification that will be required to identify and measure the spacings of the recurring striation pattern. It is apparent that most quantitative analyses are currently being carried out using optical and/or scanning electron microscopy. In recent years significant improvements in resolution and the general operating characteristics of the SEM have provided an invaluable facility for use in quantitative fractography. Current developments involve the application of 'image analysis' systems that, when interfaced directly with the optical [54] and scanning microscopes, can provide a semi-automatic quantitative fractographic facility. The system basically consists of digital micrometers and co-ordinate counters on the specimen stage translation mechanism that are interfaced to a computer and digital plotter. The fractographer simply stores the topographical information as it is being acquired and on completion of the analysis the computer can process the data to derive 'instant' crack growth rates and can plot crack growth curves and crack front profiles. However, to justify the extensive costs of these systems, and to realize the potential time savings, compared to handling and processing the data manually, there would have to be a relatively heavy involvement in quantitative fractography. The use of these semi-automated procedures would still depend on the fractographer's ability to identify the recurring striation pattern.

Although it may appear to those with limited fractographic experience that all quantitative analyses are accomplished in a relatively quick and straightforward manner, this is not always the case. For tests involving 'complex' spectra and 'randomized' loading, the striation patterns are generally similar to those formed in service and they present similar analytical problems. For these cases the analyses will often involve many hours or perhaps days of tedious and laborious microscopic examination, by an experienced fractographer, in the 'attempt' to identify and correlate the recurring striation pattern with the load spectrum.

## ACKNOWLEDGEMENTS

The author wishes to express his sincere appreciation to Mr. W. Wiebe and Dr. R.L. Hewitt of this laboratory for their ideas and assistance associated with the preparation of this paper and to Mr. Wiebe for providing the material contained in some of the case studies.



FIGURE 42: (a) FIRST OBSERVED MARKER BAND ON SPAR CAP FRACTURE SURFACE (2.6 mm FROM CRACK INITIATION SITE), (b) MARKER BAND WIDTH: 10.3  $\mu\text{m}$ ; AVERAGE STRIATION SPACING: 0.16  $\mu\text{m}$

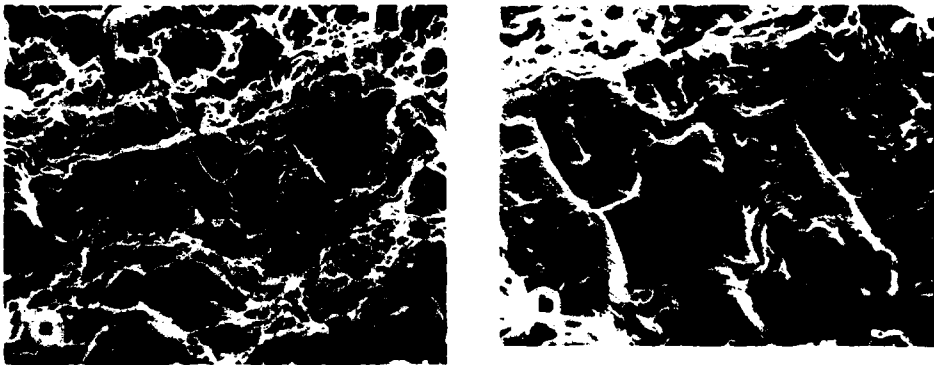


FIGURE 43: (a) LAST OBSERVED MARKER BAND ON SPAR CAP FRACTURE SURFACE (42 mm FROM CRACK INITIATION SITE), (b) MARKER BAND WIDTH: 76  $\mu\text{m}$ ; AVERAGE STRIATION SPACING: 1.2  $\mu\text{m}$

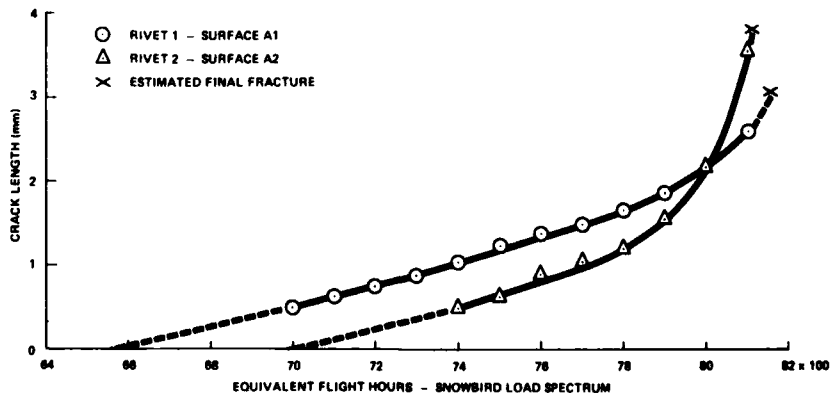
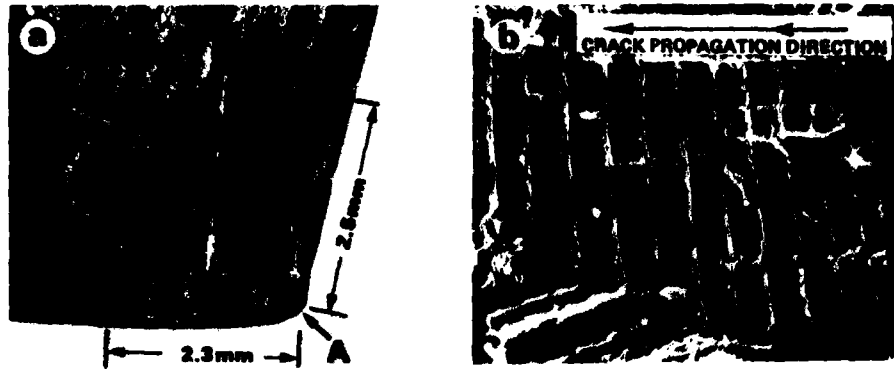
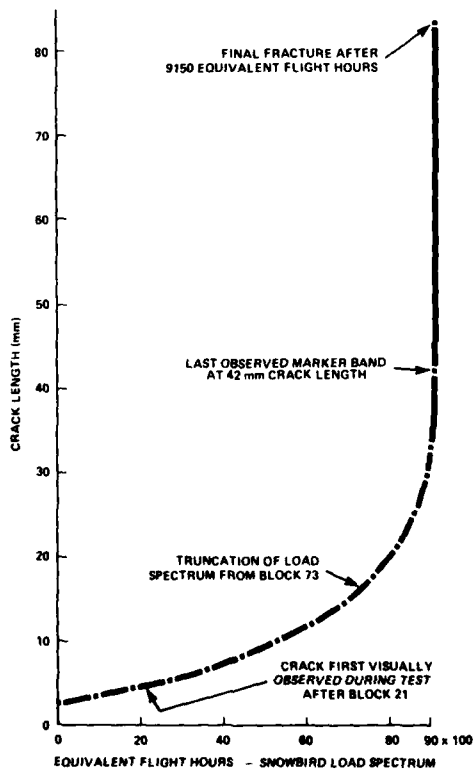


FIGURE 44: RIVET CRACK GROWTH HISTORY DERIVED FROM MARKER BAND SPACINGS



**FIGURE 40: SPAR CAP CRACK INITIATION REGION**  
 (a) INCIPIENT CRACK FORMED DURING INITIAL PHASE OF FULL-SCALE TEST, (b) INCIPIENT CRACK FRACTURE TOPOGRAPHY (BLOCK LOADING) 2.4 mm FROM CRACK INITIATION SITE



**TABLE 3: SPAR CAP MARKER BAND LOCATIONS**

Marker Band	Distance From Crack Initiation Site (mm)	Marker Band	Distance From Crack Initiation Site (mm)
*	2.5	62	12.8
5	3.3	64	13.5
10	4.0	66	14.2
15	4.6	68	14.9
		70	15.7
20	5.1	72	16.6
25	5.6	74	17.6
30	6.2	76	18.7
35	7.0	78	20.1
40	7.8	80	21.8
42	8.2	81	22.7
44	8.6	82	23.5
46	9.0	83	24.6
48	9.4	84	25.8
50	9.9	85	27.0
52	10.3	86	28.4
54	10.8	87	30.2
56	11.2	88	33.0
58	11.8	89	42.0
60	12.3	**	83.0

\* Initial crack length prior to random loading  
 \*\* Total fatigue crack length

**FIGURE 41: SPAR CAP CRACK GROWTH HISTORY DERIVED FROM MARKER BAND SPACINGS**

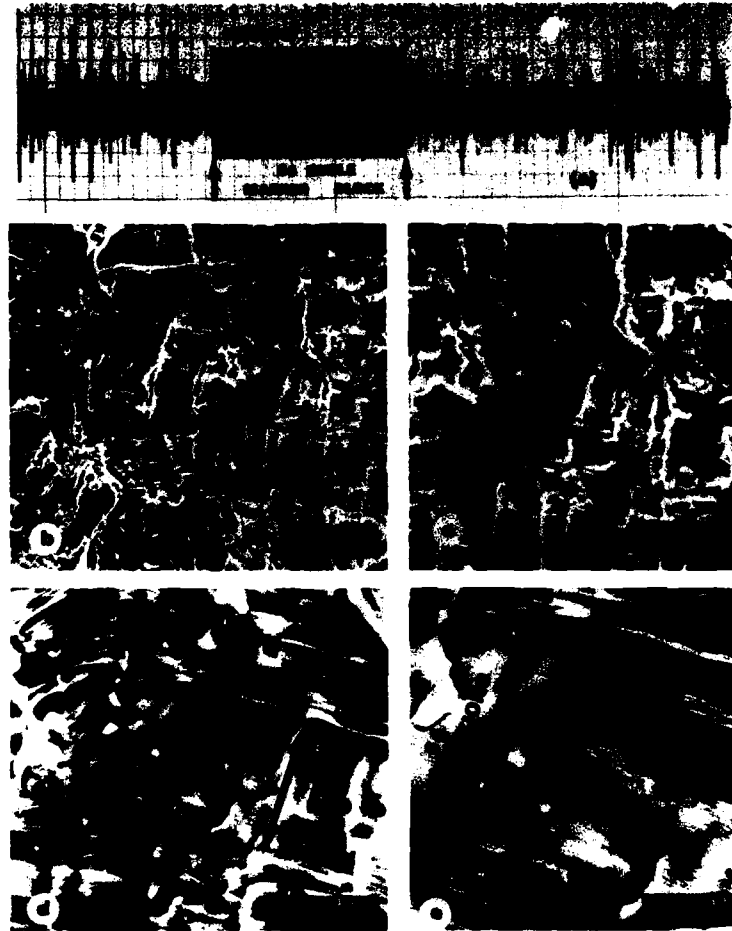


FIGURE 38: (a) RANDOM LOAD SPECTRUM WITH 'MARKER BLOCK', (b) TO (e) MARKER BAND AS VIEWED ON FRACTURE SURFACE (ARROWS INDICATE MARKER BAND)



FIGURE 39: FRACTURE SURFACE PREPARED FOR SEM EXAMINATION

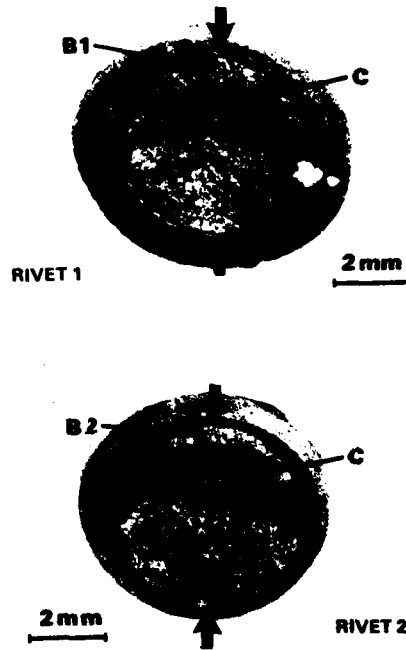


FIGURE 37: WING SKIN RIVET FRACTURE SURFACES – 2024-T31 ALUMINUM. ARROWS INDICATE CRACK INITIATION SITES. AREAS 'C' INDICATE OVER-LOAD REGIONS

TABLE 2: RANDOM TEST LOAD SPECTRUM

TOTAL CYCLES PER BLOCK 4469  
 EQUIVALENT FLIGHT HOURS PER BLOCK 100  
 ESTIMATED SPAR CAP STRESS 18.8 MPa (2.727 KSI) PER G

Interval	G Load Max.	G Load Min.	Cycles Per Block	Miner's Rule Estimate of Fatigue Damage (% Per Block)
1	8.231	-2.000	1	0.8
2	7.798	-2.000	2	1.3
3	7.461	-2.000	5	2.8
4	7.123	-2.000	10	4.8
5	6.802	-2.000	16	6.5
6	6.491	-1.983	26	8.7
7	6.182	-1.902	34	9.1
8	5.873	-1.766	45	9.1
9	5.561	-1.034	55	8.4
10	5.252	-0.810	64	7.3
11	4.943	-0.815	76	6.4
12	4.632	0.437	89	5.4
13	4.323	0.269	109	4.8
14	4.013	-0.102	142	4.4
15	3.703	0.074	194	4.0
16	3.394	0.267	287	3.9
17	3.084	0.488	447	3.8
18	2.774	0.734	653	3.3
19	2.465	0.981	920	2.7
20	2.155	1.000	1295	2.5

### 8.6 CASE 6 Load Block Measuring — SEM — Aluminum Alloy

The fracture surfaces of a 2024-T4 aluminum extrusion spar cap and two 2024-T31 aluminum rivets that failed during a full-scale aircraft fatigue test [7] are shown in Figures 36 and 37. The test used a random load application method and in anticipation of the difficulties that would be encountered in acquiring FCG information, a block of constant amplitude 'marker loads' was incorporated into the load spectrum. Table 2 lists the load spectrum details with the 20 intervals of 4469 cycles representing 100 equivalent flying hours. For each 100-hour load block, 4405 cycles were computer generated in a random sequence (on a draw without replacement basis). The remaining 64 load cycles (interval 10, Table 2) were utilized as a constant amplitude 'marker load block' that was applied as the concluding segment of each 100-hour load block. Figure 38 shows the command signal for a portion of the test spectrum, including the 64-cycle marker load sequence, and a portion of a typical well defined 'marker band' as observed in the SEM. It is clear from this series of fractographs that at the lower magnifications the marker band appeared as a relatively flat featureless increment of crack growth among the randomly spaced striations. At the higher magnifications the presence of some 64 uniformly spaced striations unequivocally established that this band was formed during the application of the 'marker block' interval of 64 constant amplitude load cycles. The spar cap failed after 91 completed 100-hour load blocks plus approximately 1000 cycles of block 92. It should be noted that from block 73 to the conclusion of the test, the 2215 cycles of interval 19 and 20, Table 2, were eliminated from the spectrum in order to expedite the test. Also, for equipment calibration purposes, the fatigue loads for the first 100-hour block were not applied in a random sequence.

To facilitate examination in the SEM the spar cap was sectioned and marked along the 83 mm path of maximum crack penetration as shown in Figure 39. Examination of the initiation area, arrows A, Figures 36 and 39, revealed that an undetected incipient crack had been initiated and had propagated to a length of 2.5 mm, Figure 40, during a previous phase of the full-scale test. Since this previous test had utilized a lo-hi-lo programmed block loading spectrum, (similar in form to that shown in Fig. 25) the initial 2.5 mm of fracture was readily distinguishable (Fig. 40(b)) from the major portion of the fracture formed by the random load spectrum (see Fig. 38). By identifying the marker bands and measuring their successive spacings (summarized in Table 3), and based on a final fracture time of 9150 hours, it was possible to derive the crack growth curve for the 80.5 mm crack length portion of the fracture surface formed by the random load spectrum, Figure 41. A total of 89 of the 90 marker blocks applied were accounted for. The first observed marker band, Figure 42, was located 2.6 mm from the crack initiation site. As shown in Figure 43, the final marker band identified (Figs. 36 and 39) was located 42 mm from the crack initiation site indicating that the final 41 mm of fracture occurred during the application of the 1000 cycles of load block 92. Test log records substantiate this conclusion since they state that the crack had propagated approximately halfway through the spar cap at the conclusion of load block 91.

SEM examination of the rivets, Figure 37, indicated that failure (during load block 82) occurred as a result of reverse bending fatigue. The first marker bands identified on fracture surfaces A1 and A2 were located approximately 0.5 mm from the initiation sites. The crack growth curves, Figure 44, indicate the number and location of the respective marker bands for surfaces A1 and A2. Extrapolation of the growth curves indicated that approximately 4 to 5 load blocks were involved in the initial 0.5 mm of rivet crack growth. The 'marker load' stress intensities were apparently insufficient in this region to form resolvable striations thus precluding marker band identification. Figure 45 shows a well defined region of marker band 2 located 0.63 mm from the initiation site of surface A1. Since crack initiation of the spar cap did not occur during the application of the random load spectrum, it was not possible to determine a similar minimum crack length where the marker blocks could be identified. However, since the initial marker bands identified for both the spar cap and the rivets have similar striation spacings, (see Figs. 42 and 45) this does suggest that the minimum crack length for marker band identification for the spar cap may not have been significantly less than 2.6 mm.

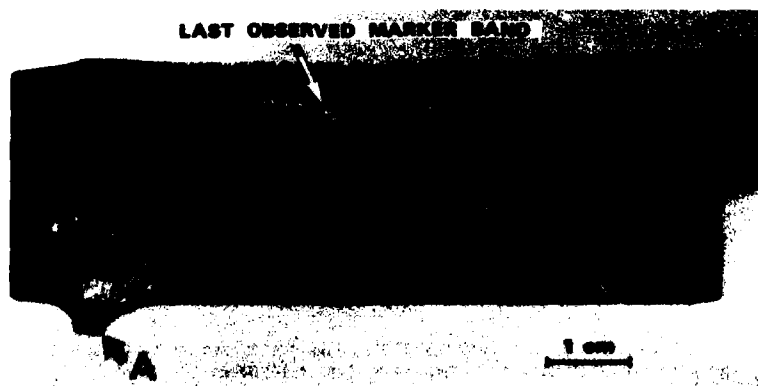


FIGURE 36: SPAR CAP FRACTURE SURFACE — 2024-T4 ALUMINUM EXTRUSION  
(ARROW 'A' INDICATES CRACK INITIATION SITE)

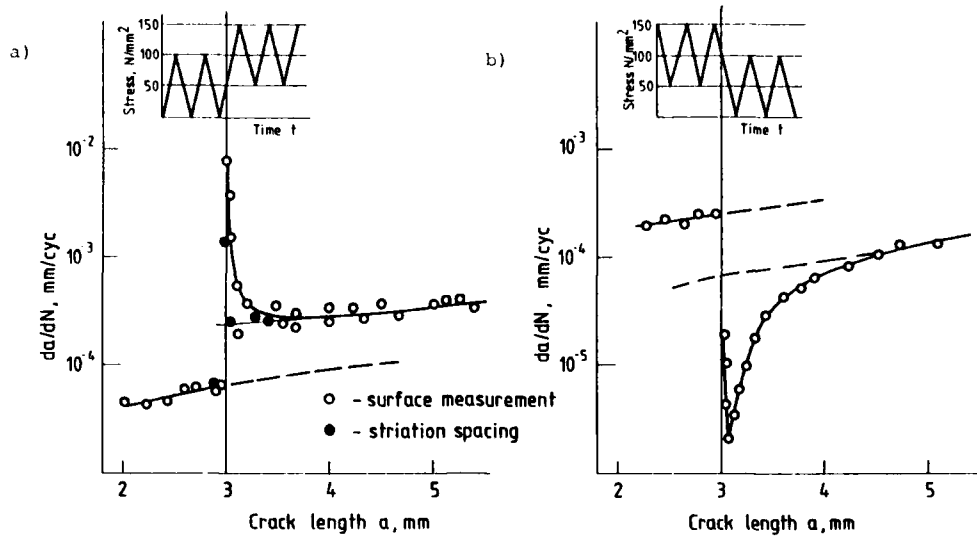


Fig. 2: Fatigue crack propagation behavior  
 a) low-high loading sequence  
 b) high-low loading sequence

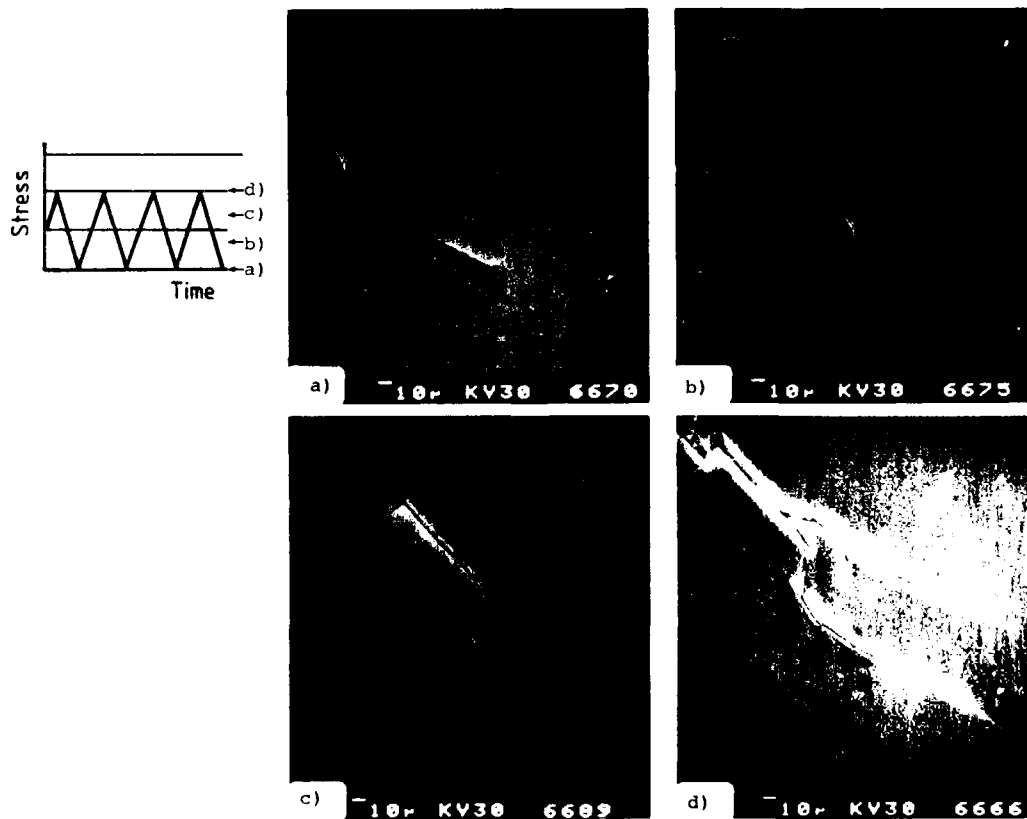


Fig. 3: SEM-micrographs of the crack tip (Al X-7075 24 h 100 °C); crack opening behavior under constant amplitude loading: a) at minimum load in a cycle, b) at 30 % of the maximum load in a cycle, c) at 60 % of the maximum load in a cycle, d) at maximum load in a cycle.  $R = 0.05$ .

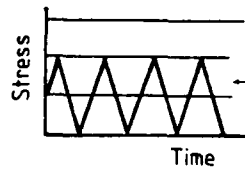


Fig. 4: SEM-micrograph of the crack contour (Al X-7075 24 h 100 °C); at 65 % of the maximum load in a cycle.

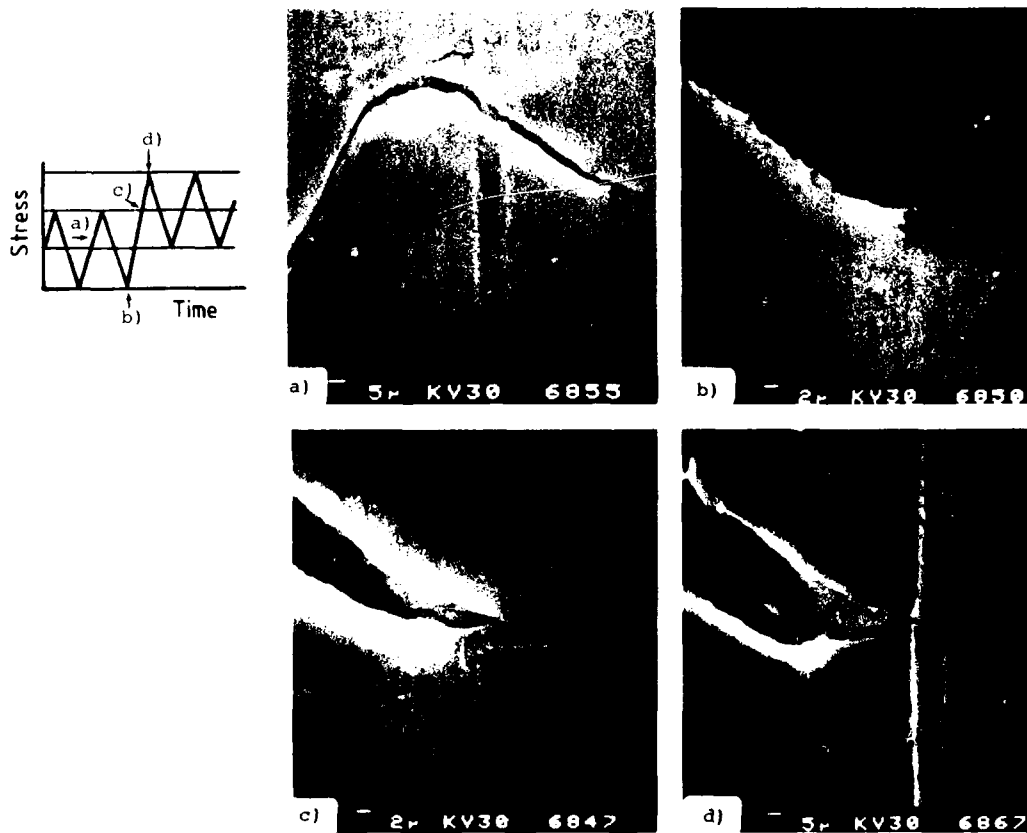


Fig. 5: In situ SEM-micrographs of the crack tip (Al X-7075 48 h 180 °C); behavior under a low-high; sequence. a) Crack tip area at 60 % of the maximum load in the cycle (overview); b) closed crack tip at minimum load in the cycle; c) crack fully open at maximum load in the cycle (photo taken prior to transition to the high loading level); d) crack advance after the transition to the high loading level which is 150 % of the previous maximum load.

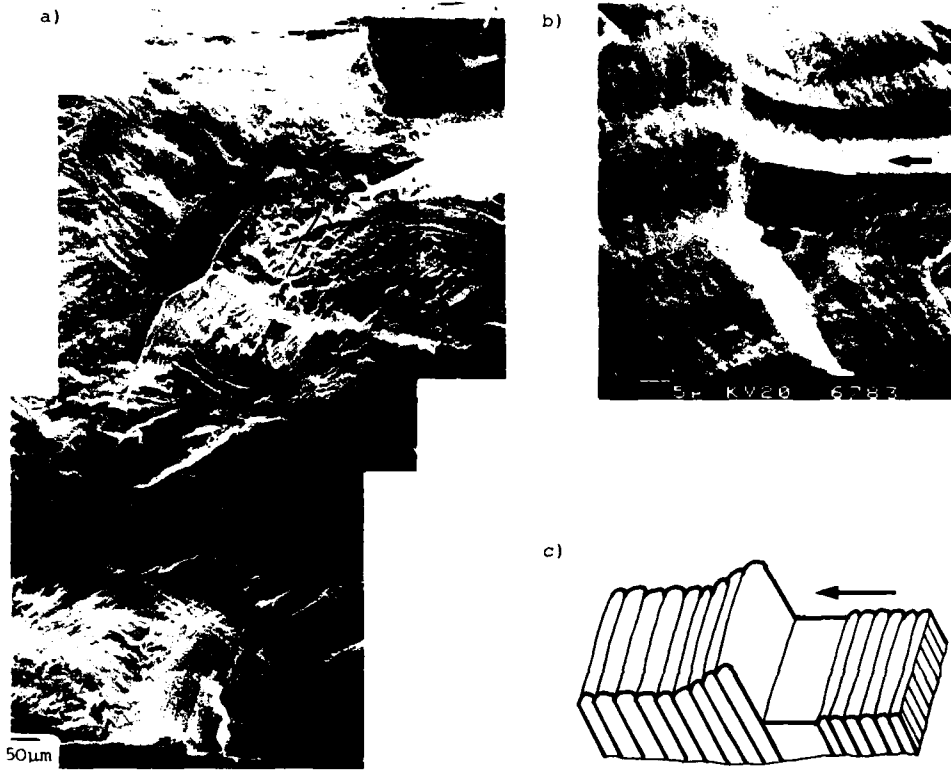


Fig. 6: SEM-micrograph of the fracture surface (Al X-7075 24 h 100 °C); crack propagation during a low-high sequence: a) transition from the low to the high loading level (whole cross section of the specimen), b) formation of a step at the transition from the low to the high loading level (section of a), c) step formation, schematically. Crack propagation direction ←.

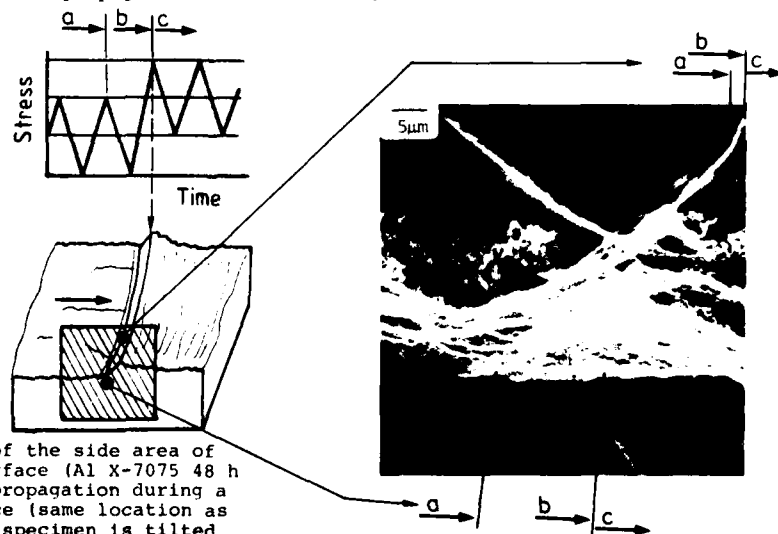


Fig. 7: SEM-micrograph of the side area of the fracture surface (Al X-7075 48 h 180 °C); crack propagation during a low-high sequence (same location as in Fig. 5). The specimen is tilted by about 15° in the SEM.

Fig. 8: SEM-micrograph of the fracture surface (Al 7475 24 h 100 °C); crack propagation during a low-high sequence; striation and step formation during the transition from the low to the high loading level [16].

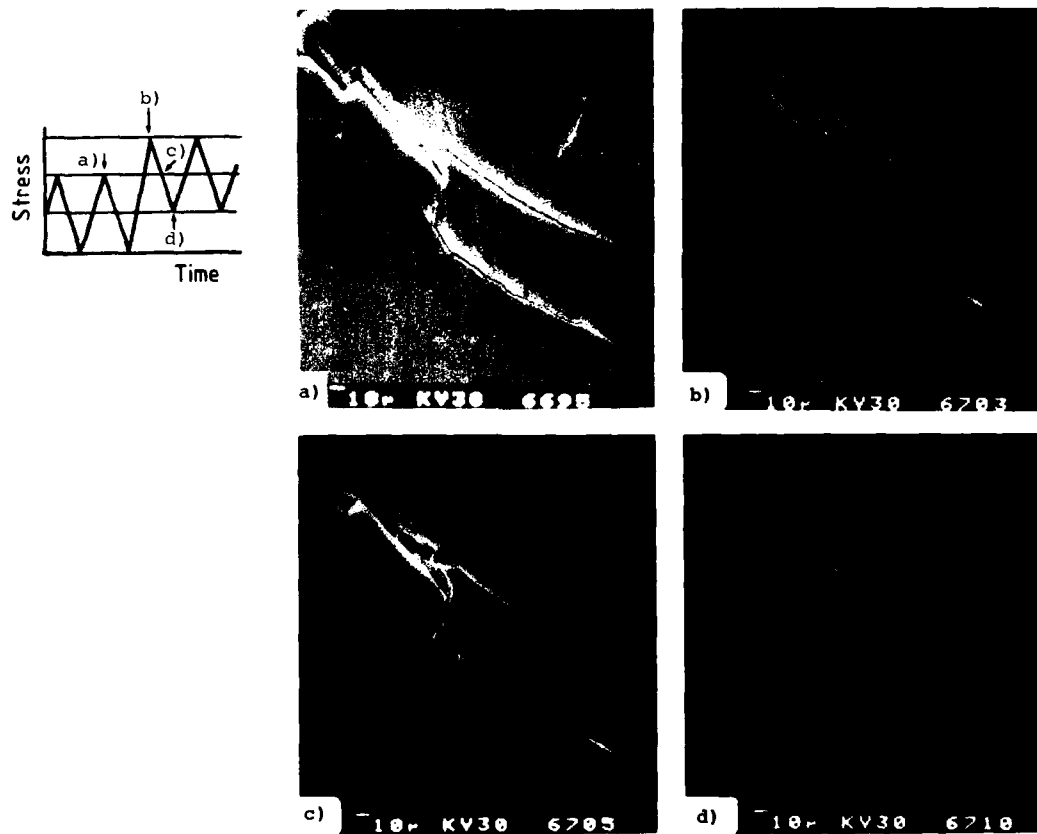
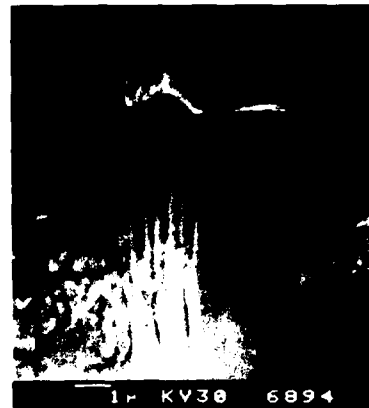


Fig. 9: SEM-micrographs of the crack tip and of the crack opening under a low-high loading sequence (Al 7075 24 h 100 °C); a) maximum load at the low loading level, b) maximum load during the first cycle at the high loading level, c) at a medium load level after the first high load maximum at the high loading level (same loading level as in a), d) at minimum load after the first maximum load at the high loading level.



Fig. 10: SEM-micrograph of the crack tip (Al X-7075 48 h 180 °C); crack propagation after a low-high sequence with 40 cycles applied at the high loading level; micrograph taken at minimum load in the cycle.

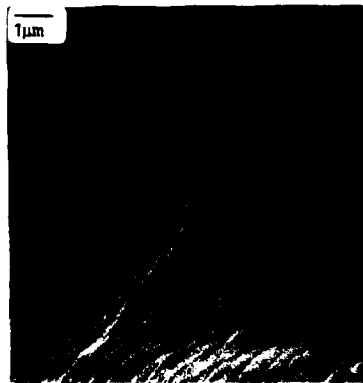


Fig. 11: SEM-micrograph of the fracture surface (Al X-7075 48 h 180 °C); crack propagation during a high-low sequence and variation of the striation spacing.

CRACK PROPAGATION UNDER CONSTANT AND VARIABLE STRESS  
AMPLITUDES : A COMPARISON OF CALCULATIONS BASED ON  
THE STRIATION SPACING AND TESTS

by

Dr.-Ing. Joachim Foth and Dr.-Ing. Walter Schütz

Industrieanlagen-Betriebsgesellschaft mbH  
Einsteinstraße, 8012 Ottobrunn, Germany

## 1. INTRODUCTION

As our knowledge and understanding of fracture phenomena improves, so does the amount of information which we can obtain from a failure analysis of metallic components. In the past, an investigator usually was satisfied with identifying the type of failure (i.e. static failure, fatigue failure, corrosion failure etc.), locating the fracture origin, determining the material composition, microstructure and properties and providing a general explanation for the failure / 1 /.

In the meantime, however, it was realized that there is a definite relation between the fatigue fracture surface appearance and the crack growth rate due to the loading history. The cyclic opening and closing of a fatigue crack will develop a typical pattern of ripples, which are called fatigue striations. These striations are the result of the plastic deformation at the crack tip and represent successive positions of the crack front during crack propagation.

So the fracture surface is a fingerprint or a record of the loading experienced by the specimen or test structure in service. Observations of the fracture surface on a microscopic level can give detailed information about cycle-by-cycle crack propagation rates and load interaction effects by striation counting and striation spacing measurement / 2 - 5 /.

Where striations are found it is generally true that each striation was produced by one load cycle. On the contrary, it is not generally true that every load cycle produces a striation. The strong correlation of striation spacing and crack growth rate per cycle is only valid at medium crack growth rates / 6 - 9 /. However, if the relation between striation spacing and macroscopic crack growth rate is known, one can calculate the stresses having acted in the relevant cycle, provided the crack length, a formula for the stress intensity factor  $K$  and the functional dependency of macroscopic crack growth rate on the stress intensity range is given. The problem is rather straightforward for constant amplitude loading. However, it becomes a complex and difficult one for variable amplitude loadings. Nevertheless, this knowledge of the stresses, would have obvious advantages, for example in the case of a full scale fatigue test, if cracks were accidentally discovered long after they had occurred and their cause were not clear. Another, and much bigger advantage, would be the possibility of calculating the stresses which had acted on a component which had failed unexpectedly and unexplainably in service. The objective of the present test program was to investigate these possibilities.

## 2. EXPERIMENTAL PROGRAM

The materials under investigation were typical commercial aircraft alloys as the titanium alloy Ti6Al4V, aluminium alloys 2024-T3 and 7075-T7351, the silver containing aluminium alloy AZ 74.61, a high-strength, high toughness steel HP 9-4-30 and a superalloy for turbine discs, INCONEL 718 / 10 - 12 /. The chemical compositions are given in Tab. 1.

Fatigue crack propagation tests were carried out on flat sheet specimens containing a central hole with two saw-cuts as crack starters (CCT-specimen). The crack growth was observed with a travelling light-optical microscope. All experiments were done at room temperature except the constant amplitude tests with INCONEL 718 at 620°C.

The variable loads applied corresponded to a flight by flight tactical aircraft load sequence, consisting of 17 different flight types, a short section of which is shown in Fig. 1 / 13 /. After the fatigue tests the fracture surfaces were observed with a scanning electron microscope to determine the striation spacing and fracture surface topography.

## 3. RESULTS AND DISCUSSION

### 3.1 CONSTANT AMPLITUDE LOADING

The simplest cyclic loading is of constant amplitude with constant mean stress. The crack propagation rates were obtained by measuring the crack length on the side of the specimen by means of a light-optical microscope while the test is running. The crack propagation rates  $da/dN$  under constant amplitude loading are usually plotted vs. the stress intensity range  $\Delta K$  for a given stress ratio  $R$ . Since the stress intensity range  $\Delta K$  depends both on the range of the applied stress  $\Delta \sigma$  and the crack length  $l$ , for a comparison of the observed macroscopic crack growth rate and the crack propagation on a microscopic scale SEM-pictures were taken at certain distances from the crack starter notch. Therefore several SEM-pictures were

taken at identical lengths in order to obtain details about the scatter of striation spacing and the resulting uncertainties in the prediction of stresses in the case of service loading.

Fig. 2 shows a typical example of a fracture surface of a Ti6Al4V alloy revealing excellent fatigue striations. The length of the fatigue crack was 2,3 mm leading to a stress intensity range of  $25 \text{ MN}\cdot\text{m}^{-3/2}$ . For the determination of the striation spacing the distance between two striation profiles perpendicular to their flanks has to be taken. In most cases this direction differs slightly from the macroscopic crack growth direction, which may be one reason for the observed large scatter. Another reason can be derived directly from Fig. 2: The striation spacing varies even at two individual striations under consideration. Moreover, for different striation pairs at nearly the same crack length the obtained striation spacing varies from  $1,9 \times 10^{-4} \text{ mm}$  to  $5,7 \times 10^{-4} \text{ mm}$ . So it is appropriate to integrate over several striations leading to an average striation spacing of  $4,6 \times 10^{-4} \text{ mm}$  in the present case. From other SEM-pictures at the same crack length this average striation spacing ranged between  $3,8 \times 10^{-4} \text{ mm}$  and  $6,8 \times 10^{-4} \text{ mm}$ . The main reason for the observed differences are microstructural features like grain boundaries, inclusions, dislocation pile up, residual stresses or crystallographic slip plane orientation which may sometimes hinder and sometimes favour the local crack growth behaviour with respect to the integrating macroscopic crack growth rate.

In Fig. 3 the macroscopic crack growth rate  $da/dN$  is plotted vs. the stress intensity range  $\Delta K$  as a straight line for constant amplitude loading with the Ti6Al4V alloy. The open circle symbols denote the macroscopically observed striation spacings. Here it is assumed that each striation was produced by one cycle, and the units on the ordinate give the amount of striation spacing in mm. For Ti6Al4V striations were detectable for stress intensity ranges between  $24 \text{ MN}\cdot\text{m}^{-3/2}$  and  $64 \text{ MN}\cdot\text{m}^{-3/2}$  and striation spacings from  $3,6 \times 10^{-4} \text{ mm}$  to  $2,5 \times 10^{-3} \text{ mm}$ , respectively. For higher crack growth rates and larger stress intensity ranges the mechanism of fatigue crack propagation changes: The mechanism of dimple production overrules the striation formation. In the crack growth region of about  $5 \times 10^{-3} \text{ mm/cycle}$  there is a very close correlation between average striation spacing and crack growth rate, as shown in Fig. 3, whereas for larger crack lengths (i.e. higher crack growth rates) the striation spacing is found to be much smaller than the macroscopic crack growth rate. This may be due to the fact that for higher growth rates the dimple formation is the governing mechanism and only small fractions of the fracture surface show striations with relatively small spacings as compared to the global crack growth rate.

The scatter of the striation spacing for a certain crack length (that means at a certain stress intensity range) was about 1:3 for all crack lengths. Fig. 4 shows the results of the constant amplitude tests for the 7075-T7351 aluminium alloy. As already discussed for the Ti6Al4V alloy, striations can only be found within certain ranges of the crack growth rate and the stress intensity range respectively. For stress intensity ranges  $\Delta K$  below  $10 \text{ MN}\cdot\text{m}^{-3/2}$  and crack growth rates below  $2,5 \times 10^{-4} \text{ mm/cycle}$  no striations were found. The same holds true for stress intensity ranges above  $20 \text{ MN}\cdot\text{m}^{-3/2}$  and crack growth rates above  $1,2 \times 10^{-3} \text{ mm/cycle}$ . Within these boundaries a fairly good correlation was observed between striation spacing and crack growth rate, while the striation spacing exhibited about the same scatter as in the case of the Ti6Al4V alloy.

For small crack lengths (i.e. low  $\Delta K$ -values) there was a slight tendency of the striations to exceed the observed crack propagation rate. One reason for this behaviour may be as follows: It has been proved by experiments (e.g. / 6 /) that at low crack growth rates the crack advances step by step, the crack opens and closes for a certain number of cycles, but does not propagate. Then it jumps, leaving one striation. So the macroscopic crack growth rate is lower than the spacing between the striations.

In Fig. 5 the results of fracture surface examinations for 5 different materials are given. The measured striation spacing is plotted vs. the macroscopic crack growth rate. The straight line gives the strict 1:1 correlation, whereas the dashed line represents a best fit regression for all materials examined. It turns out that the close correlation between striation spacing and crack growth rate is only present in a limited region of crack growth rate (i.e. in a limited region of the stress intensity range). In general it can be stated that at relatively small crack growth rates the striation spacing exceeds the growth rate while at relatively high crack growth rates the spacings fall below the observed macroscopic crack growth rates. In the limited region where striations were observed (i.e. crack growth rates of about  $10^{-4} \text{ mm/cycle}$  up to rates of about  $4 \times 10^{-2} \text{ mm/cycle}$ ) the relation between striation spacing and crack growth rate can be expressed by

$$s = 1,5 \times 10^{-2} \times (da/dN)^{0,47}$$

(Striation spacing  $s$  in mm, when  $da/dN$  in mm/cycle),

which refers to the dashed straight line in the log-log plot (see Fig. 5).

Using Bates and Clark's equation / 9 / which expresses striation spacing as a function of the stress intensity range  $\Delta K$  normalized over Young's modulus  $E$ , leads finally to nearly the same expression if one considers the different  $da/dN$ - $\Delta K$  behaviour for the different materials. This gives the opportunity to calculate the crack growth rate from fractographic striation measurements for constant amplitude loading, and, moreover, the possibility of assessing the stresses having acted, provided the functional dependency of stress intensity upon crack length can be obtained.

### 3.2 VARIABLE AMPLITUDE LOADING

In Fig. 6 an example of a fracture surface with striations from the flight by flight loading sequence mentioned before is shown. The material is Ti6Al4V. As expected, the striation spacing varies due to the different load levels in the load sequence. However, it was not possible to recognize definite sections of the load sequence from the SEM-pictures. This may be due to the fact that the load sequence under consideration does not contain consecutive blocks of loads which reveal recognizable patterns on the fracture surface. In other cases where the waveform of the load sequence is repeated frequently (e.g. FALSTAFF

/ 14 /) a typical pattern of striations can be observed on the fracture surface / 15 /. The same was found for simple block programs / 2 - 5, 16 /, but even in those case some of the load cycles of the blocks did not produce detectable striations.

This may explain some of the difficulties which arise when comparing the striation spacing and the macroscopic crack growth rate in the case of the rather complicated variable load sequence. Other reasons are the uncertainties in crack length and crack growth rate measurements which lead to further errors in recognition of sections of the loading sequence. Under variable amplitudes, a plot of the crack growth rate  $da/dN$  vs. stress intensity range  $\Delta K$  is not possible because the stress range and therefore  $\Delta K$  changes with every cycle. So for a comparison of striation spacing and crack growth rate the expected crack growth rates for the different loading levels have to be calculated for each crack length using the material's crack growth data from constant amplitude tests as a basic input, disregarding any interaction effects. Together with the relation between striation spacing and macroscopic crack growth rate under constant amplitude loading (see section 3.1 and Fig. 5) it is now possible to assess the striation spacing due to the different stress ranges in the load sequence at certain crack lengths.

In Fig. 7 the calculated striation spacing is plotted as solid lines vs. crack length for the Ti6Al4V alloy for the 5 most frequent stress ranges of the loading sequence. The observed striation spacings at different crack lengths are given as open circles. The observed striation spacings cover the area in a kind of "shot gun" pattern and only with considerable optimism and phantasy it can be agreed that these points belong to that curve and so on. In the case of the aluminium alloy 2024-T3 (comp. Fig. 8) not as many striation spacings were observed as with the Ti6Al4V alloy, so only the 4 most frequent stress ranges of the loading sequence are considered, see Fig. 8. Here a slightly better correlation between observed and expected striation spacing resulted. However, a correlation of data points is still not possible, because it cannot be proved that a certain point, even if lying on the calculated curve, corresponds to that curve.

#### 4. CONCLUSIONS

The striation spacing was determined from fractographic examinations and compared to the crack growth rates in experiments both for constant amplitude and variable amplitude loadings for 6 different typical commercial aircraft alloys (Ti6Al4V, 7075-T7351, 2024-T3, AZ 74.61, HP 9-4-30, INCONEL 718). The following conclusions can be drawn:

- Under constant amplitude loadings striations are observed only in a limited region of crack growth rate and stress intensity range, respectively, depending upon the material.
- For constant amplitude loading the striation spacing follows a straight line when plotted vs. crack growth rate (log-log plot) for all materials under consideration.
- The crack growth behaviour is inhomogeneous over the entire fracture surface for a given crack length leading to considerable scatter of the striation spacing, which has to be taken into account when assessing the crack growth rate from striation spacing measurements.
- For a tactical aircraft flight-by-flight loading sequence a correspondence of striation patterns on the fracture surface and "typical" sections of the loading sequence could not be achieved.
- An assessment of the stresses having acted from fractographic striation spacing measurements leads to good to fair results for constant amplitude but not for variable amplitude loading.

#### 5. REFERENCES

- / 1 / Madeyski, A. and L. Albertin: "Fractographic Method of Evaluation of the Cyclic Stress Amplitude in Fatigue Failure Analysis". Fractography in Failure Analysis, ASTM-STP-645, Am.Soc.Test.Mat., 1978, S. 73
- / 2 / Abelkis, P.R.: "Use of Microfractography in the Study of Fatigue Crack Propagation under Spectrum Loading". Fract. in Failure Analysis, ASTM-STP-645, Am.Soc.Test.Mat., 1978, S. 213
- / 3 / McMillan, J.C. and R.M.N. Pelloux: "Fatigue Crack Propagation under Program and Random Loads". Fat. Crack Prop., ASTM-STP-415, Am.Soc.Test.Mat., 1967, S. 505
- / 4 / Hertzberg, R.W.: "Fatigue Fracture Surface Appearance". Fat. Crack Prop., ASTM-STP-415, Am.Soc. Test.Mat., 1967, S. 205
- / 5 / Broek, D.: "Elementary Engineering Fracture Mechanics". Noordhoff Int.Publ., Leyden, 1974
- / 6 / Schwalbe, K.H.: "Mechanik und Mechanismen des stabilen Rißwachstums in metallischen Werkstoffen". Fortschr.-Ber.d. VDI-Z., Rh. 18, 1977, Nr. 3
- / 7 / Edwards, P.R.: "Methods of Obtaining Crack Growth Data in Metals". AGARD Lecture Series, LS 118, 1981, 9.1
- / 8 / Miller, G.A.: "Fatigue Fracture Appearance and the Kinetics of Striation Formation in some High-Strength Steels". Trans. ASM-62, 1969, S. 651
- / 9 / Bates, R.C. and W.G. Clark, jun.: "Fractography and Fracture Mechanics". Trans. ASM-62, 1969, S.380

- / 10 / Kratzer, H. und W. Scharfenberger: "Vergleich von gerechneter und mikroskopisch gemessener Rißfortschrittsgeschwindigkeit zur Beurteilung von Betriebsbrüchen". IABG-Bericht Nr. TF-659, 1977
- / 11 / Oberparleiter, W. und W. Zeitler: "Bauteilspezifische Werkstoffuntersuchungen an Gesenkschmiedestücken der silberhaltigen Aluminiumlegierung 3.4354.7 (Fuchs AZ 74.61)". IABG-Bericht Nr. TF-861, 1979
- / 12 / Oberparleiter, W. und W. Scharfenberger: "Bauteilspezifische Werkstoffuntersuchungen an Triebwerkscheiben aus INCONEL 718". IABG-Bericht Nr. TF-874, 1979
- / 13 / Oberparleiter, W. und W. Schütz: "Rißfortschrittsversuche an 7075-T7351, 2024-T3 und Ti6Al4V (geglüht) unter Einzelflug- und Einstufenbelastung". IABG-Bericht Nr. TF-483, 1975
- / 14 / Lowack, H., D. Schütz, M. Hück and W. Schütz: "Standardisiertes Einzelflugprogramm für Kampfflugzeuge-FALSTAFF". IABG-LBF-Report Nr. TF-568/3045, IABG/LBF, 1976
- / 15 / Darts, J.: "Determination of Crack Growth Rates under Flight Simulation Loading from Fracture Surface Markings". Proc. 10th ICAF-Symposium, Brussels, 1979, S. 3.4/1
- / 16 / Pelloux, R.M. and M. Faral: "Assessment of Crack Tip Closure in an Aluminium Alloy by Electronfractography". Fat.Eng.Mats.Structs., Vol. 1, 1979, S. 21 .

### Chemical Composition

<b>Ti 6Al 4V</b>										
Al 6.2	V 4.0	Fe 0.1	O <sub>2</sub> 0.2	Ti Balance						(Weight-%)
<b>2024-T3</b>										
Cu 4.4	Mg 1.6	Mn 0.6	Zn 0.25	Cr 0.1	Ti 0.15	Fe 0.5	Si 0.5	Al Balance		
<b>7075-T7351</b>										
Zn 5.6	Mg 2.5	Cu 1.8	Mn 0.3	Fe 0.5	Si 0.4	Cr 0.25	Ti 0.2	Al Balance		
<b>AZ 74.61</b>										
Zn 5.8	Mg 2.4	Cu 1.0	Ag 0.25	Cr 0.17	Mn 0.1	Fe 0.15	Si 0.1	Al Balance		
<b>HP 9-4-30</b>										
Ni 8.5	Co 4.0	Cr 1.0	Mo 1.0	C 0.3	V 0.1	Mn 0.25	Fe Balance			
<b>INCONEL 718</b>										
Cr 18.2	Mo 3.0	Ni 52.8	Al 0.5	Co 0.2	Cu 0.3	Nb+Ta 5.0	Ti 0.9	Fe Balance		

Table 1 : Chemical composition

### Tactical Aircraft Load Sequence



Fig. 1 : Section of variable load sequence



Fig. 2 : Fracture surface of Ti6Al4V: Fatigue striations for constant amplitude loading

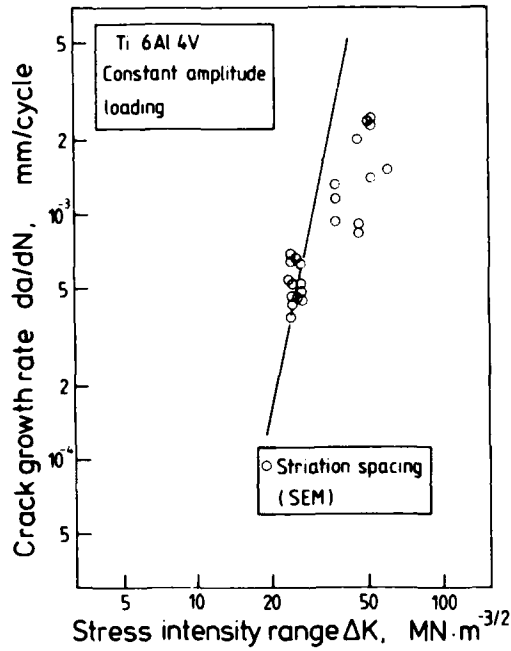


Fig. 3 : Comparison of actual crack growth rate and striation spacing for Ti6Al4V for constant amplitude loading

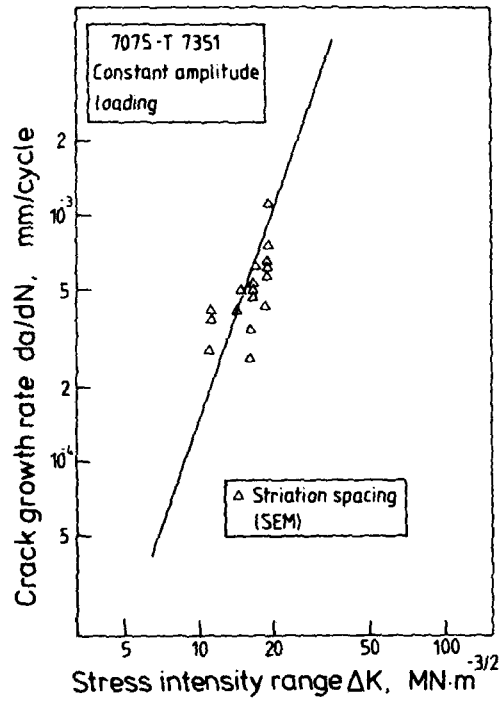


Fig. 4 : Comparison of actual crack growth rate and striation spacing for 7075-T7351 for constant amplitude loading

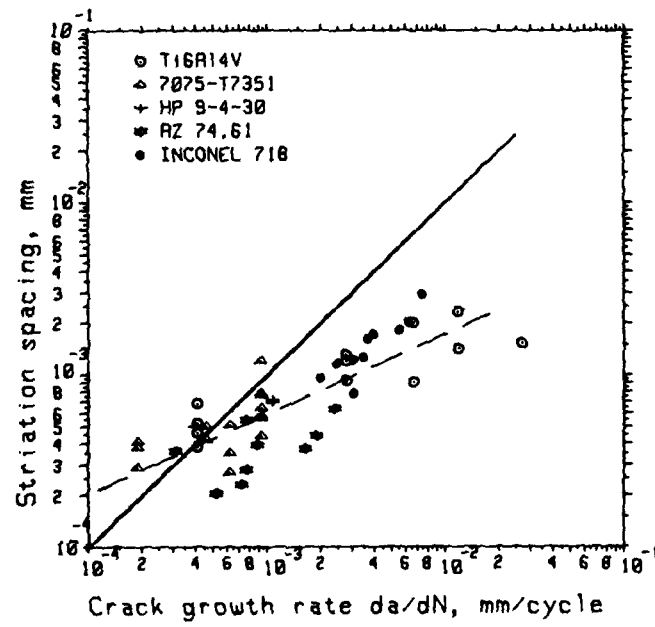


Fig. 5 : Comparison of striation spacing and macroscopic crack growth rate for several materials



Fig. 6 : Fracture surface of Ti6Al4V: Fatigue striations for flight-by-flight loading (MRCA)

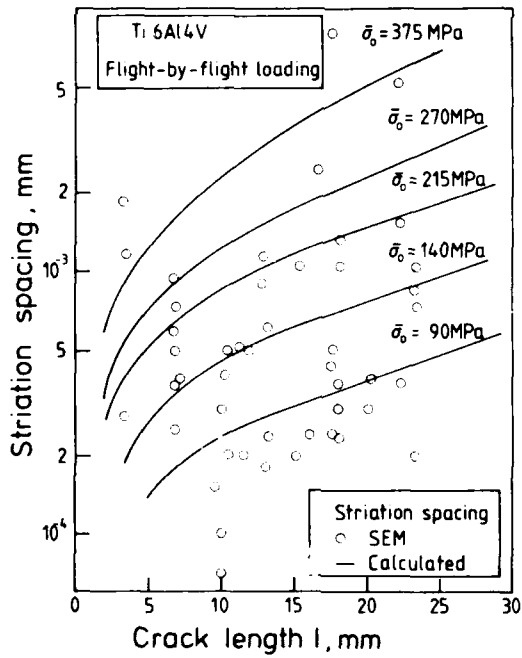


Fig. 7 : Comparison of expected and observed striation spacing for Ti6Al4V for flight-by-flight loading (MRCA)

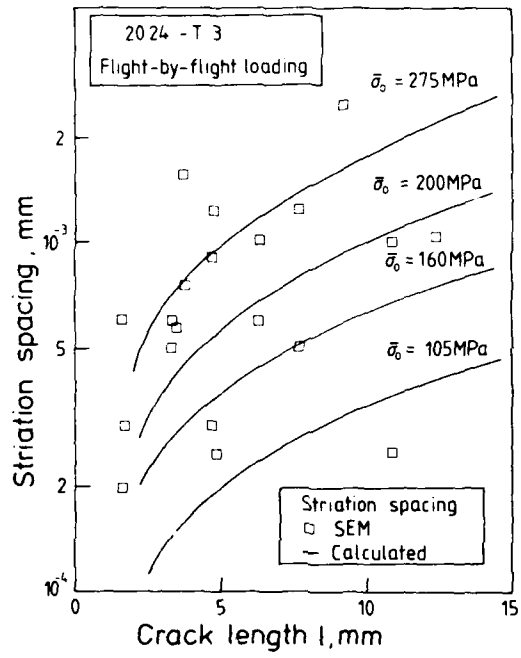


Fig. 8 : Comparison of expected and observed striation spacing for 7075-T7351 for flight-by-flight loading (MRCA)

Review of Session IV: General Discussion  
 Compiled by J.B. de Jonge and J. Schijve

The General Discussion was introduced by the discussion leader, Prof. J. Schijve.

With the aid of a set of viewgraphs (see Fig. 1) he summarized the main aspects of crack front marking as they had come up during the various presentations and he formulated a set of questions as a framework for the ensuing discussion.

With regard to the purpose of crack front marking (viewgraph 1) one can distinguish between the case where we want to have crack growth data for cracks that were found too late, e.g. in a full scale fatigue test, and situations where the crack cannot be observed, e.g. cracks in boltholes.

In the latter case, the crack size of interest may be very small, and the crack will often be a part-through crack. For such cracks the shape of the crack front may be of interest; purpose of crack front marking may then specifically be the monitoring of the crack shape development, e.g. for checking fracture mechanics prediction methods.

A number of papers presented dealt with marker loads in C.A. tests. Three marker load methods applied are shown in viewgraph 2. The 1st and 2nd method introduce additional small load cycles, giving small crack growth increments and producing visible marker bands. In the third method, large cycles are introduced, replacing basic cycles on an "equal damage" basis.

Undoubtedly crack front marking in C.A. tests is of interest for research programs and prediction problems. However, it was agreed that in the present discussion the attention should be concentrated on crack front marking in Flight simulation tests.

Viewgraph 3 summarizes methods ranked in what might be called an order of decreasing artificiality. The inclusion of blocks of C.A. cycles is considered in this context as the most artificial method. In the presentations there were various examples of this.

Sometimes, these blocks are simply added to the original load sequence. In other cases, the C.A. cycles were extracted from the original variable amplitude sequence.

There was also an example presented where parts of the original sequence had been replaced on an "equal damage" basis by a C.A. cycle block.

The addition of peak loads is also considered as artificial. In the presentations, good marking of peak loads was reported, but also a considerable retarding effect on crack growth was observed. In view of this, peak load markers appear to be unacceptable.

Changing the sequence of flights may be considered as a less artificial possibility to get crack front marking.

Again, many examples were presented. In general, the replacement of a "random" service load history by a completely programmed sequence is not attractive because of incorrect crack growth simulation.

In several test series, the location of severe flights at constant intervals was reported as useful. The clustering of severe flights appeared to be questionable in view of significant effects on crack growth.

Finally, the "non-artificial" markings, such as associated with g.a.g. cycles or a "most severe flight" were reported in a number of cases as very useful. However, it was agreed that they will not offer a general solution for all cases.

The applicability of a marking technique is associated with the criteria that we will set for acceptability (viewgraph 4).

Do we accept an effect of the marker loads on the crack growth and/or the crack initiation life and if so how much?

Viewgraph 5 summarizes visibility aspects. Macroscopic bands can be observed with the unaided eye or simple means. However, for small cracks, say from 2 to 10 mm, no successful macro-marking has been reported and microscopical means appear to be essential.

Prof. Schijve concluded his introduction with the formulation of a set of questions (viewgraph 6) that were used as a basis for the general discussion.

A lively discussion developed with regard to question 1 on Acceptability criteria. It was generally recognized that the contribution of the marker bands to the total crack growth should remain small. Some people considered 10 percent as perhaps a too large value. Examples were reported where good marking was obtained with considerably less than 10 % band width. However, some strong opinions why 10 percent is quite acceptable were also heard. The main argument then was that there is already so much uncertainty about other aspects like e.g. the load spectrum that 10 percent is negligible compared to the very important advantage of being able to trace back the growth of cracks that are detected too late.

The replacement on basis of "equal damage" was not received with great enthusiasm.

It was generally agreed that the main criterion must be that the marker loads should not interact with the original loads by changing their damaging effect, such as may be the case with peak-marker loads. In other words, the marker loads should not change the crack growth mechanism.

In the same context, the problems of marker loads in load sequences containing heavy compressive loads were discussed. It is known that compressive loads tend to destroy the markings. Yet it was the general feeling that it is definitely unacceptable to leave out the compressive loads, just for the benefit of getting a visible marking.

Everybody agreed that when planning a large scale fatigue/damage tolerance test it is highly advisable to evaluate the effectiveness and the influence on crack growth and initiation of marker loads in explanatory tests.

Question 2: Agreement about the fact that the right moment of application of a marker block is after a period of relatively quiet or smooth flights, shortly before a severe flight. If the markers are applied after or during a severe flight, the fracture surface is very rough and the marker bands are not or hardly visible.

It was noted that this necessitates prior knowledge of the location of the severe flights and hence excludes a "real time" random load program generation.

Question 3: led to very little discussion as everybody agreed that application of different marker blocks may provide very useful information, especially in those cases where for some reason one or more marker bands have been lost. Also, the use of "different" markers for small and large cracks was generally con-

sidered as potentially useful. An example was presented of marker blocks consisting of 30 relatively small load cycles followed by thirty larger ones. At small crack length, the larger cycles produced a recognizable marking, whereas at large cracks the small cycles gave a visible marker band.

Question 4: , dealing with the acceptability and usefulness of marking by means of systematic variations in flight sequences, led to a lively discussion. One discussor felt that sometimes we are overdoing in our desire to randomize our sequences. In fact, quite often he had noticed in service-failure surfaces a regularity in loading pattern, considerably less "random" than applied in the test.

In his experience, related to transport-type loading sequences, a judicious programming of flights could lead to retrievable markings, without a noticeable effect on the crack growth.

Another discussor formulated his opinion with regard to variation of flight sequences in the following way:

- In any randomised sequence of flights, or loads, the sequence used is only one of a very large number of sequences that might occur in service. Hence, so long as the sequences do not depart markedly from those possible in service some minor adjustment of the position of severe, marker flights should be acceptable within the usual factors used to allow for variability. By placing these flights in a slightly irregular pattern within the main body of the sequence it should be possible to achieve an identifiable sequence without destroying the essentially realistic nature of the flight-by-flight test.

During the discussion, the following aspects came up:

- Useful markings caused by severe flights are found if the crack length is relatively large.
- Clustering of severe flights may give good marking, but can considerably influence the crack growth.
- Different materials will mark differently.

Again, it was emphasized that exploratory tests are required to assess the effects of programmed changes in flight sequence.

Question 5: , dealing with the visibility and associated observation techniques, gave rise to little discussion.

For large cracks, easily observable macrobands can be created, but for smaller cracks microscopical means appear to be essential, with the use of small cycle blocks as marker appearing as the most promising solution.

Having thus covered the "question list", the remaining time was then passed in a general and lively discussion, in which the following aspects came forward:

- The majority of examples discussed dealt with aluminium alloys; it appears that marker load research for other metals, especially in steels is needed. It must be expected, however, that aluminium alloys offer the optimum with regard to marking possibilities.
- The possibility of marking by means of other changes of the crack front than striations only was mentioned. Periods of very severe loading could be traced back from pronounced crack "jumps".
- The possibility of marking by means of deposition of specific elements, or the colouring or "staining" of the fracture surface was questioned. One discussor mentioned a experiment he had made in this area using dye penetrant, with completely negative result.

The Chairman closed the Meeting at the scheduled time.

He expressed as his opinion that the Meeting had been a highly informative one and he directed a special word of thanks to Prof. Schijve, who had led the General Discussion in such an excellent way.

## VIEWGRAPH 1

PURPOSE OF MARKER LOADS

obtain crack growth data if:

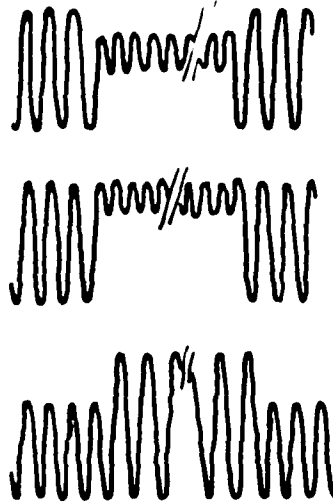
- (1) crack found too late
- (2) crack cannot be observed

(e.g. corner crack at hole)  
crack front shapes

TYPE OF CRACK

- through crack
- part-through crack (may be small)

## VIEWGRAPH 2      MARKER LOADS IN CA-TEST



## VIEWGRAPH 3

MARKER LOADS IN FLIGHT-SIMULATION TESTS

- Artificial: - Blocks of CA-cycles
  1. extracted from spectrum
  2. added
  3. replacement  
(equal damage)
- Peak loads
- Less artificial: - Change sequence of flights
  1. Programmed sequence
  2. Severe flights at constant intervals
- Non artificial: No-marker loads  
Analysis based on:
  1. GAG cycle
  2. Most severe flight

## VIEWGRAPH 4

CRITERIA FOR ACCEPTABILITY

- same crack growth curve ?
- same crack initiation life ?
- marker load cycles with almost  
*no contribution to crack growth*
- marker load cycles as a replacement  
of other cycles (same damage ?)

## VIEWGRAPH 5

VISIBILITY

- macroscopic bands - unaided eye
  - other simple means  
(pictures  
projections)
- microscopical means
  - stereo microscope
  - optical microscope
  - SEM
  - TEM

## VIEWGRAPH 6

QUESTIONS

1. Criteria.
  - band width 1-5 % acceptable ?
  - 10 % too much ?
  - "equal damage" bands
2. Marker block.
  - shortly before severe flight ?
3. Should we know which band we see ?
  - 3a. different marker blocks each time
  - 3b. different marker blocks for small and large cracks
4. Programmed load sequences
  - 4a. Block program FST acceptable      macro bands
  - 4b. Periodic severe flights
5. Preference for - macro bands ?
  - micro bands
 Preference for
  - optical microscope
  - SEM
  - TEM

**REPORT DOCUMENTATION PAGE**

<b>1. Recipient's Reference</b>	<b>2. Originator's Reference</b>	<b>3. Further Reference</b>	<b>4. Security Classification of Document</b>		
	AGARD-CP-376	ISBN 92-835-1480-7	UNCLASSIFIED		
<b>5. Originator</b>	Advisory Group for Aerospace Research and Development North Atlantic Treaty Organization 7 rue Ancelle, 92200 Neuilly sur Seine, France				
<b>6. Title</b>	FATIGUE CRACK TOPOGRAPHY				
<b>7. Presented at</b>	the 58th Meeting of the Structures and Materials Panel in Sienna, Italy, on 1-6 April 1984.				
<b>8. Author(s)/Editor(s)</b>	Various		<b>9. Date</b> November 1984		
<b>10. Author's/Editor's Address</b>	Various		<b>11. Pages</b> 244		
<b>12. Distribution Statement</b>	This document is distributed in accordance with AGARD policies and regulations, which are outlined on the Outside Back Covers of all AGARD publications.				
<b>13. Keywords/Descriptors</b>	<table border="0"> <tr> <td>                     Airframes                      Crack propagation                      Cracking (fracturing)                 </td> <td>                     Fatigue (materials)                      Tolerances (materials)                      Surface defects                 </td> </tr> </table>			Airframes Crack propagation Cracking (fracturing)	Fatigue (materials) Tolerances (materials) Surface defects
Airframes Crack propagation Cracking (fracturing)	Fatigue (materials) Tolerances (materials) Surface defects				
<b>14. Abstract</b>	<p>In recent years the concept of Damage Tolerance for Aircraft Structures has become widely accepted in the aerospace industry. For the application of this concept, knowledge of crack growth rates has become of primary importance.</p> <p>This meeting brought together specialists in the field of fracture surface analysis and structural test engineering with the aims of:</p> <ul style="list-style-type: none"> <li>- reviewing available methods for determining the growth rate of cracks from their topography</li> <li>- noting any shortcomings in these methods and recommending further research and development.</li> </ul> <p>The four sessions of the meeting were devoted to 'Phenomenological Aspects of Fatigue Fractures', 'Methods and Means of Crack Front Marking', 'Fracture Surface Analysis Techniques', and to a general discussion. <i>Originator supplied keywords include:</i></p>				

D-4

<ul style="list-style-type: none"> <li>— reviewing available methods for determining the growth rate of cracks from their topography</li> <li>— noting any shortcomings in these methods and recommending further research and development.</li> </ul> <p>The four sessions of the meeting were devoted to 'Phenomenological Aspects of Fatigue Fractures', 'Methods and Means of Crack Front Marking', 'Fracture Surface Analysis Techniques', and to a general discussion.</p> <p>ISBN 92-835-1480-7</p>	<ul style="list-style-type: none"> <li>— reviewing available methods for determining the growth rate of cracks from their topography</li> <li>— noting any shortcomings in these methods and recommending further research and development.</li> </ul> <p>The four sessions of the meeting were devoted to 'Phenomenological Aspects of Fatigue Fractures', 'Methods and Means of Crack Front Marking', 'Fracture Surface Analysis Techniques', and to a general discussion.</p> <p>ISBN 92-835-1480-7</p>
<ul style="list-style-type: none"> <li>— reviewing available methods for determining the growth rate of cracks from their topography</li> <li>— noting any shortcomings in these methods and recommending further research and development.</li> </ul> <p>The four sessions of the meeting were devoted to 'Phenomenological Aspects of Fatigue Fractures', 'Methods and Means of Crack Front Marking', 'Fracture Surface Analysis Techniques', and to a general discussion.</p> <p>ISBN 92-835-1480-7</p>	<ul style="list-style-type: none"> <li>— reviewing available methods for determining the growth rate of cracks from their topography</li> <li>— noting any shortcomings in these methods and recommending further research and development.</li> </ul> <p>The four sessions of the meeting were devoted to 'Phenomenological Aspects of Fatigue Fractures', 'Methods and Means of Crack Front Marking', 'Fracture Surface Analysis Techniques', and to a general discussion.</p> <p>ISBN 92-835-1480-7</p>

<p>AGARD Conference Proceedings No.376 Advisory Group for Aerospace Research and Development, NATO FATIGUE CRACK TOPOGRAPHY Published November 1984 244 pages</p> <p>In recent years the concept of Damage Tolerance for Aircraft Structures has become widely accepted in the aerospace industry. For the application of this concept, knowledge of crack growth rates has become of primary importance.</p> <p>This meeting brought together specialists in the field of fracture surface analysis and structural test engineering with the aims of:</p> <p>P.T.O</p>	<p>AGARD-CP-376</p> <p>Airframes Crack propagation Cracking (fracturing) Fatigue (materials) Tolerances (materials) Surface defects</p>	<p>AGARD Conference Proceedings No.376 Advisory Group for Aerospace Research and Development, NATO FATIGUE CRACK TOPOGRAPHY Published November 1984 244 pages</p> <p>In recent years the concept of Damage Tolerance for Aircraft Structures has become widely accepted in the aerospace industry. For the application of this concept, knowledge of crack growth rates has become of primary importance.</p> <p>This meeting brought together specialists in the field of fracture surface analysis and structural test engineering with the aims of:</p> <p>P.T.O</p>	<p>AGARD-CP-376</p> <p>Airframes Crack propagation Cracking (fracturing) Fatigue (materials) Tolerances (materials) Surface defects</p>
<p>AGARD Conference Proceedings No.376 Advisory Group for Aerospace Research and Development, NATO FATIGUE CRACK TOPOGRAPHY Published November 1984 244 pages</p> <p>In recent years the concept of Damage Tolerance for Aircraft Structures has become widely accepted in the aerospace industry. For the application of this concept, knowledge of crack growth rates has become of primary importance.</p> <p>This meeting brought together specialists in the field of fracture surface analysis and structural test engineering with the aims of:</p> <p>P.T.O</p>	<p>AGARD-CP-376</p> <p>Airframes Crack propagation Cracking (fracturing) Fatigue (materials) Tolerances (materials) Surface defects</p>	<p>AGARD Conference Proceedings No.376 Advisory Group for Aerospace Research and Development, NATO FATIGUE CRACK TOPOGRAPHY Published November 1984 244 pages</p> <p>In recent years the concept of Damage Tolerance for Aircraft Structures has become widely accepted in the aerospace industry. For the application of this concept, knowledge of crack growth rates has become of primary importance.</p> <p>This meeting brought together specialists in the field of fracture surface analysis and structural test engineering with the aims of:</p> <p>P.T.O</p>	<p>AGARD-CP-376</p> <p>Airframes Crack propagation Cracking (fracturing) Fatigue (materials) Tolerances (materials) Surface defects</p>

**AGARD**

NATO  OTAN  
7 RUE ANCELLE · 92200 NEUILLY-SUR-SEINE  
FRANCE

Telephone 745.08.10 · Telex 610176

**DISTRIBUTION OF UNCLASSIFIED  
AGARD PUBLICATIONS**

AGARD does NOT hold stocks of AGARD publications at the above address for general distribution. Initial distribution of AGARD publications is made to AGARD Member Nations through the following National Distribution Centres. Further copies are sometimes available from these Centres, but if not may be purchased in Microfiche or Photocopy form from the Purchase Agencies listed below.

NATIONAL DISTRIBUTION CENTRES

**BELGIUM**

Coordonnateur AGARD - VSL  
Etat-Major de la Force Aerienne  
Quartier Reine Elisabeth  
Rue d'Ev

**ITALY**

Aeronautica Militare  
Ufficio del Delegato Nazionale all'AGARD  
3 Piazzale Adenauer  
00144 Roma/EUR

**CANADA**

Defence  
Dept of  
Ottawa.



National Aeronautics and  
Space Administration

Washington, D.C.  
20546

**SPECIAL FOURTH CLASS MAIL  
BOOK**

Postage and Fees Paid  
National Aeronautics and  
Space Administration  
NASA-451

Official Business  
Penalty for Private Use \$300



**DENMARK**

Danish I  
Ved Idr.  
2100 C

**FRANCE**

O.N.E.F.  
29 Ave  
92320 C

DEPT OF DEFENSE  
DEFENSE TECH. INFO. CENTER  
ATTN: DDC-DDA-2  
CAMERON STATION BLDG 5  
ALEXANDRIA VA 22314

shment

AGARD

**GERMANY**

Fachinf  
Physik.  
Kernfor  
D-7514

**GREECE**

Helleni  
Research and Development Directorate  
Holargos, Athens

ment (ARGE)  
a

**ICELAND**

Director of Aviation  
c/o Flugrad  
Reykjavik

**UNITED KINGDOM**

Defence Research Information Centre  
Station Square House  
St Mary Cray  
Orpington, Kent BR5 3RE

**UNITED STATES**

National Aeronautics and Space Administration (NASA)  
Langley Field, Virginia 23365  
Attn: Report Distribution and Storage Unit

THE UNITED STATES NATIONAL DISTRIBUTION CENTRE (NASA) DOES NOT HOLD STOCKS OF AGARD PUBLICATIONS, AND APPLICATIONS FOR COPIES SHOULD BE MADE DIRECT TO THE NATIONAL TECHNICAL INFORMATION SERVICE (NTIS) AT THE ADDRESS BELOW.

PURCHASE AGENCIES

*Microfiche or Photocopy*

National Technical  
Information Service (NTIS)  
5285 Port Royal Road  
Springfield  
Virginia 22161, USA

*Microfiche*

ESA/Information Retrieval Service  
European Space Agency  
10, rue Mario Nikis  
75015 Paris, France

*Microfiche or Photocopy*

British Library Lending  
Division  
Boston Spa, Wetherby  
West Yorkshire LS23 7BQ  
England

Requests for microfiche or photocopies of AGARD documents should include the AGARD serial number, title, author or editor, and publication date. Requests to NTIS should include the NASA accession report number. Full bibliographical references and abstracts of AGARD publications are given in the following journals:

Scientific and Technical Aerospace Reports (STAR)  
published by NASA Scientific and Technical  
Information Branch  
NASA Headquarters (NIT-40)  
Washington D.C. 20546, USA

Government Reports Announcements (GRA)  
published by the National Technical  
Information Services, Springfield  
Virginia 22161, USA



Printed by Specialised Printing Services Limited  
40 Chigwell Lane, Loughton, Essex IG10 3TZ

ISBN 92-835-1480-7

5-8